57/2/2025
ISSN 1338-3523
ISSN 0369-2086

# Mineralia Slovaca

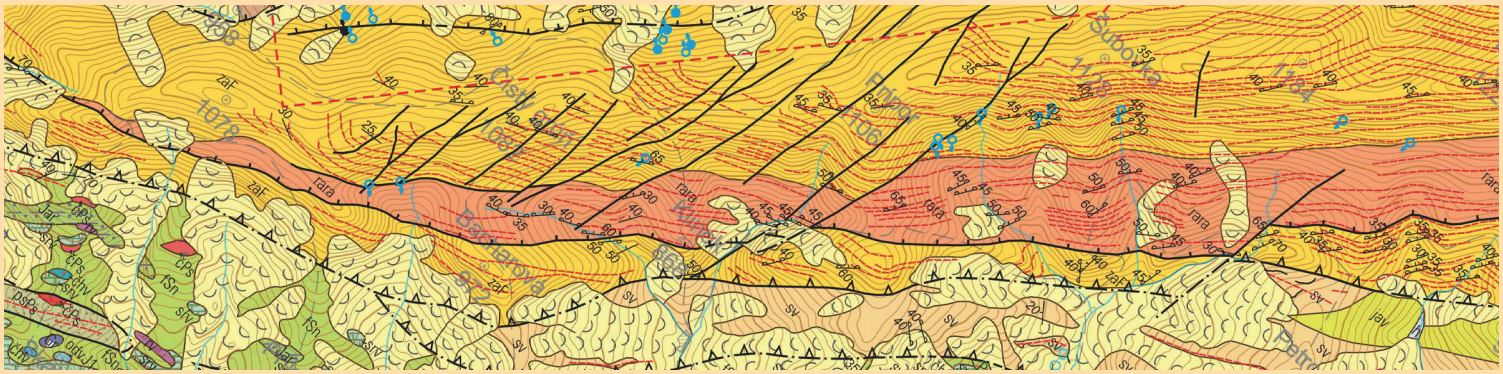

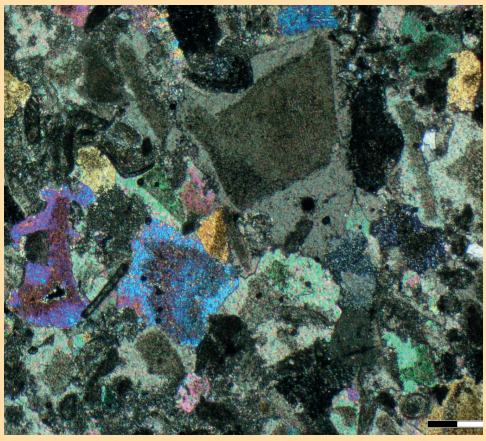

Štátny geologický ústav Dionýza Štúra Bratislava

**Mineralia Slovaca**

Časopis pre základné a aplikované vedy o Zemi

Journal of Basic and Applied Earth Sciences



Mineralia Slovaca (Web ISSN 1338-3523, ISSN 0369-2086), EV 3534/09, vychádza dvakrát ročne. Vydavateľ a tlač: Štátny geologický ústav Dionýza Štúra, Mlynská dolina 1, 817 04 Bratislava, IČO 31 753 604. Dátum vydania čísla 57/2/2025: marec 2026.
Predplatné v roku 2025 vrátane DPH, poštovného a balného pre jednotlivcov 22,00 €, pre členov SGS a geologických asociácií 20,90 €, pre organizácie v SR 31,90 €, pre organizácie v ČR 55,00 €. Cena jednotlivého čísla pri nákupe cez e-shop alebo pri osobnom nákupe v predajni ŠGÚDŠ v RGS Košice je 6,05 € vrátane DPH. Časopis možno objednať v redakcii a v knižnici regionálnej geologickej služby v Košiciach.

Adresa redakcie:
Štátny geologický ústav D. Štúra, Mlynská dolina 1, 817 04 Bratislava. Telefón: 02/59 375 257; e-mail: mineralia.slovaca@geology.sk, e-mail knižnica: secretary.ke@geology.sk

Mineralia Slovaca (Web ISSN 1338-3523, ISSN 0369-2086) is published twice a year by the State Geological Institute of Dionýz Štúr Bratislava, Slovak Republic. The date of issuing of the number 57/2/2025: March 2026.
Subscription for the whole 2025 calendar year (two numbers of the journal): 66.00 € (Europe), 77.00 € (besides Europe), including VAT, postage and packing cost. Claims for nonreceipt of any issue will be filled gratis.
Order of the Editorial Office: Štátny geologický ústav D. Štúra – RC Košice (Library), Jesenského 8, SK-040 01 Košice, Slovak Republic. Phone: +421/55/625 00 43; fax: +421/55/625 00 44, e-mail: mineralia.slovaca@geology.sk, library: secretary.ke@geology.sk

PÔVODNÉ ČLÁNKY – ORIGINAL PAPERS



**COVER:**

**Top:** A section of the geological map of the Oravská Magura Mts. SE of Babín and Lokca villages.

**Center:** Left: A thin section of Middle Jurassic gray crinoidal limestone from the Babín Klippen area. Center: Outcrop of crinoidal (Smolegowa) limestone at the Rúbane locallity. Right: Slide body (pebbly mudstone) with in the cut of the Skalnatý potok Stream. (Photos: O. Pelech)

**Below:** Panoramic view from the Hruštínske podolie with Babín village in the centre. Line of the Babín Klippen stretching roughly along the forest edge above the power line between the Malcov Fm (meadows to the left) and Zábava Fm (ridge of the Oravská Magura Mts.). View to the NE. (Photo: F. Teťák)

**OBÁLKA:**

**Hore:** Výrez geologickej mapy Oravskej Magury v úseku Babínskych bradiel v oblasti jv. od Babína a Lokce.

**Stred:** Vľavo: Výbrus sivého krinoidového vápenca strednej jury, oblasť babínskych bradiel. Uprostred: Odkryv krinoidového (smolegowského) vápenca v lokalite Rúbane. Vpravo: Sklzové teleso (obliakovitý ílovec) v koryte Skalnatého potoka.

**Dole:** Panoramatický pohľad do Hruštínskeho podolia s Babínom v strede. Línia babínskych bradiel prechádza približne na hranici lesa nad líniou elektrického vedenia medzi malcovským súvrstvím (lúky poniže vľavo) a zábavským súvrsvím (hrebeň Oravskej Magury). Pohľad smerom na SV. (Foto: F. Teťák)

*Mineralia Slovaca, Web ISSN 1338-3523, ISSN 0369-2086, https://doi.org/10.56623/ms.2025.57.2.1*
*57, 2 (2025), 97 – 110, © Authors 2025. CC BY 4.0*

# The Babín Klippen – a peculiar branch of the Orava sector of the Pieniny Klippen Belt (Slovakia)

FRANTIŠEK TEŤÁK[1]*, ONDREJ PELECH[1] and † MICHAL POTFAJ[1]

[1] State Geological Institute of Dionýz Štúr, Mlynská dolina 1, SK-81704, Bratislava 1, Slovak Republic,
* corresponding author, frantisek.tetak@geology.sk

**Abstract:** The Pieniny Klippen Belt (PKB) is a narrow, approx. 5 – 8 km wide zone at the boundary of the External and Internal Western Carpathians. The zone of the Babín Klippen, which is the main subject of this study, represents northerly situated branch of the PKB located at the NW slopes of the Oravská Magura Mts. SE of Babín and Lokca villages (Námestovo district) in the northern Slovakia. The paper presents the results of geological mapping and lithostratigraphic investigation of the area. The PKB rocks are surrounded by sandstones of the Zábava Fm. and claystone-rich Malcov and Racibor fms. belonging to the Krynica Unit of the Flysch Belt. The soft matrix between the rigid klippen is represented mainly by the quartz-carbonate sandstones of the Snežnica and Sromowce fms. and red marls or shales of the Púchov Fm. Locally also red Malinowa-type shales of the Pavláškova skala Fm. were identified. The klippen rocks represented mainly by the limestones of the Pieniny Fm., locally also radiolarites of the Czajakowa Fm. and spotted limestones of the Allgäu Fm. are correlated with the Orava succession. The Jurassic crinoidal limestones of the Smolegowa and Krupianka fms. and red nodular limestones of the Czorsztyn Fm. are part of the Czorsztyn succession. The whole zone is intensively deformed and brecciated. The additional deformation can be interpreted as a consequence of backthrust and incorporation of the PKB successions inbetween the thrust sheets of the Krynica Unit, which is consistent with some older opinions.

**Key words:** Western Carpathians, Orava succession, Czorsztyn succession, Šariš succession, Backthrust

**Graphical abstract**

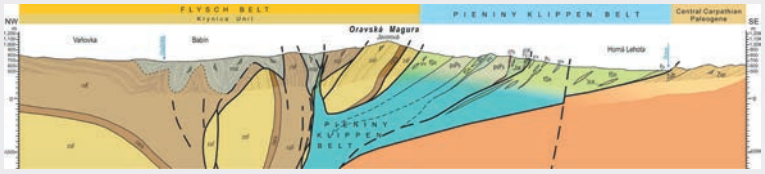


**Highlights**

- The Babín Klippen is approx. 8 km long and 200 m wide and extremely deformed zone of the Pieniny Klippen Belt (PKB) on the northern slopes of the Oravská Magura Mts.
- The studied area is composed of the Orava, Czorsztyn and Šariš successions of the Oravic units.
- The Babín Klippen Zone formed due to SE-vergent backthrust of the Krynica Unit of the Flysch Belt.

## Introduction

The Pieniny Klippen Belt (PKB) is a narrow tectonic unit, approximately 0.5–8 km wide, located at the boundary between the External and Internal Western Carpathians (Andrusov, 1938; Andrusov & Scheibner, 1960; Scheibner, 1967; Mišík, 1997; Bezák et al., 2008; Plašienka, 2018). The PKB is characterized by its "klippen" structure, which consists of rigid limestone lenses (traditionally termed klippen), usually of Jurassic to Early Cretaceous age, located within a less competent formations composed of Upper Cretaceous flysch or marlstones (Andrusov, 1938; Plašienka, 2018). The internal structure of the PKB is highly complicated due the considerable lithofacies diversity and intensive compressional and transpressional deformation, related to the extreme convergence of lithotectonic units. Additionally, the interpretation of the PKB structure is hampered by insufficient exposures.

Despite the internally complicated structure, the PKB is confined to a coherent fault bounded zone, without significant outliers. The well-known exceptions are the Čakanov Klippen in the Vlára river Valley NW of Nemšová town, Mestečko Klippen NW of Považská Bystrica town and Mariková klippen in the western sector of the PKB (Mello et al., 2005; Plašienka et al., 2010; Pešková et al., 2021; Teťák, 2024).

A similar isolated structure formed by the PKB rocks surrounded by flysch sequences of the Krynica Unit of the Magura group of nappes of the Flysch Belt occurs in a narrow zone on the northern slopes of the Oravská Magura Mts. The PKB rock sequences form an independent strip on the NW slopes of the Prípor Hill (1,105.8 m), SE of

Babín and Lokca villages (Námestovo district, Fig. 1). The occurrences were discovered already by Andrusov (1931) and are also shown on later geological maps (Potfaj et al., 1981; Potfaj, 1979, 1983; Bezák et al., 2008; Káčer et al., 2024). Although some authors take these occurrences into account in regional interpretations (e.g., Marschalko, 1986; Vozár et al., 1999), the more detailed description and analysis of this PKB zone have not been available in English, especially for the international audience.

The zone of klippen south of Babín and Lokca villages was originally termed the Babín sector of the PKB (in Slovak: *babínsky úsek bradlového pásma;* Potfaj, 1983). A shorter name the Babín Klippen (in Slovak: *babínske bradlá*) is proposed for the zone after the nearby Babín village.

The earliest reference to the PKB rocks in this area is a pre-WW II 1:25,000 geological map by Andrusov (1931), who marked the occurrence of limestones of the Pieniny Fm. surrounded by the marlstones of the Púchov Fm. in the Skalnatý potok Stream and further north on the ridge. Other occurrence of the Pieniny Fm. has been shown further to the northeast, on the slope of the Rúbane locality. In the northeast, in the stream north of Šubovka Hill, another occurrence of the Púchov and Pieniny fms. is indicated. The PKB rocks are surrounded by the Paleogene formations of the Krynica Unit of the Carpathian Flysch Belt.

Potfaj et al. (1981) extended the known occurrences of the PKB facies in the unpublished manuscript of 1:25,000 map sheet Trstená to the Stodoly area, the right branch of

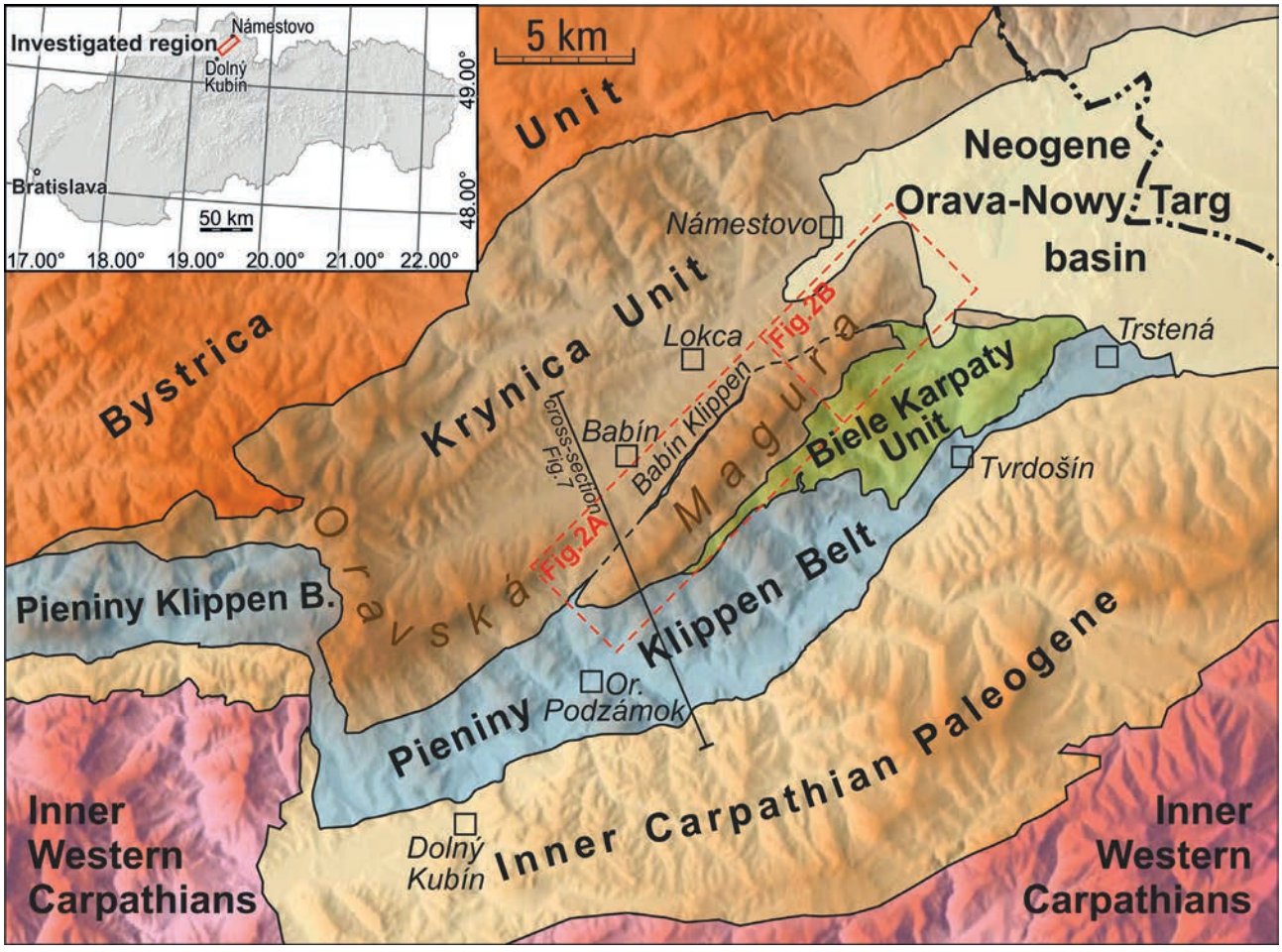


**Fig. 1.** Location of the investigated region within Slovakia marked by the red polygon

**Fig. 2.** Geological map of the Babín Klippen and their surroundings (Geological map of Oravská Magura: Teťák et al., in press)

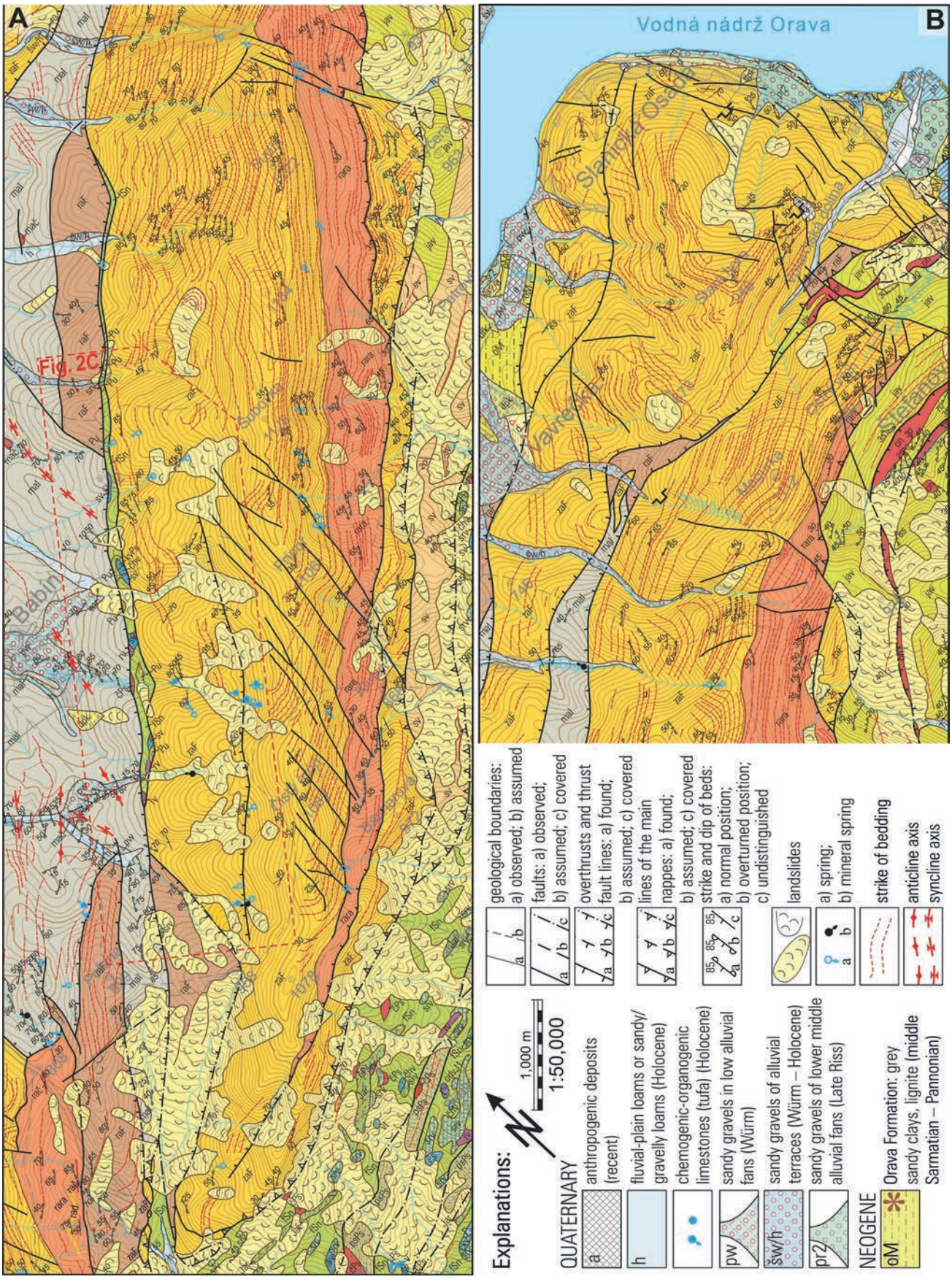
A
B
Fig. 2C
Vodná nádrž Orava
Babín
Slanická Osada
Vavrečka
Stefanov
Explanations:
1,000 m
1:50,000
QUATERNARY
a anthropogenic deposits (recent)
h fluvial-plain loams or sandy/gravelly loams (Holocene)
chemogenic-organogenic limestones (tufa) (Holocene)
pw sandy gravels in low alluvial fans (Würm)
šw/h sandy gravels of alluvial terraces (Würm – Holocene)
pr2 sandy gravels of lower middle alluvial fans (Late Riss)
NEOGENE
oM Orava Formation: grey sandy clays, lignite (middle Sarmatian – Pannonian)
geological boundaries: a) observed; b) assumed
faults: a) observed; b) assumed; c) covered
overthrusts and thrust fault lines: a) found; b) assumed; c) covered
lines of the main nappes: a) found; b) assumed; c) covered
strike and dip of beds: a) normal position; b) overturned position; c) undistinguished
landslides
a) spring; b) mineral spring
strike of bedding
anticline axis
syncline axis

## FLYSCH BELT – KRYNICA UNIT

- mal mač — Malcov Formation: light claystones, chaotically bedded sandstones to claystones; mač – layer of red claystones (Latest Eocene – Oligocene)
- raF — Racibor Formation: thick grey claystones and thin beds of sandstones, thick Magura type greywacke sandstones (Middle Eocene – Early Oligocene)
- rara — Racibor Formation – Račová Member: thick grey claystones, thin beds of laminated sandstones (Middle Eocene)
- zaF — Zábava Formation: thick Magura type greywacke sandstones and thin-bedded flysch (Late Paleocene – Middle Eocene)

## BIELE KARPATY UNIT – Štefanov Nappe

- sv — Svodnice Formation: massive calcareous claystones, quartz-carbonate sandstones (Paleocene – Early Eocene)
- svp — Svodnice Formation: thick-bedded massive greywacke sandstones
- jav — Lopeník Formation – Javorina Member: quartz-carbonate sandstones: thin-bedded flysch deposits (Late Campanian – Maastrichtian)
- on — Lopeník Formation – Ondrášovec Member: thin-bedded flysch, red and grey-green claystones (Middle Campanian – Late Maastrichtian)

## KLIPPEN BELT

- Jar — Jarmuta-Proč Formation: quartzy-carbonate sandstones, conglomerates, organodetritic and reef limestones (Campanian? – Maastrichtian – Early Eocene?)
- psPs — Pavláškova skala Formation: massive quartzy-wacke sandstones (Turonian – Campanian)
- čPs — Pavláškova skala Formation: thin-bedded flysch: red claystones, grey-green quartzy-carbonate sandstones
- Pu — Púchov Formation: Púchov-type marlstones: red, green and grey marlstones to limestones with intercalations of sandstones (Cenomanian – Maastrichtian)
- fSn — Snežnica-Sromowce Formation: quartzy-carbonate sandstones, claystones, sporadically conglomerates (Turonian – Santonian)
- čhv — Czorsztyn and Niedzica limestones: red nodular limestone of "ammonitico rosso" facies (Toarcian, Bathonian – Callovian, Kimmeridgian – Tithonian)
- srv — Pieniny Formation: grey to white locally spotted thin-bedded limestones with cherts (Tithonian – Barremian)
- rv — Czajakowa Formation: red and green radiolarites and radiolarian limestones (Oxfordian)
- Ps — Posidonia and Supra-Posidonia mbs.: dark-grey shales, dark-grey limestones (Aalenian – Bajocian)
- odvJ1 — Lúty potok Formation: sandy, sandy-crinoidal limestones and quartzy conglomerates (Sinemurian – Pliensbachian)
- sv — Allgäu and Dolný mlyn Formation: black calcareous silty shales, spotty calcareous shales (Flacenmergel), spotty and grainy limestones (Fleckenkalk), intercalations of crinoidal limestones (Sinemurian – Pliensbachian)
- Gr — "Gresten Beds": grey to brown quartzy sandstones, locally grey claystones (Sinemurian)

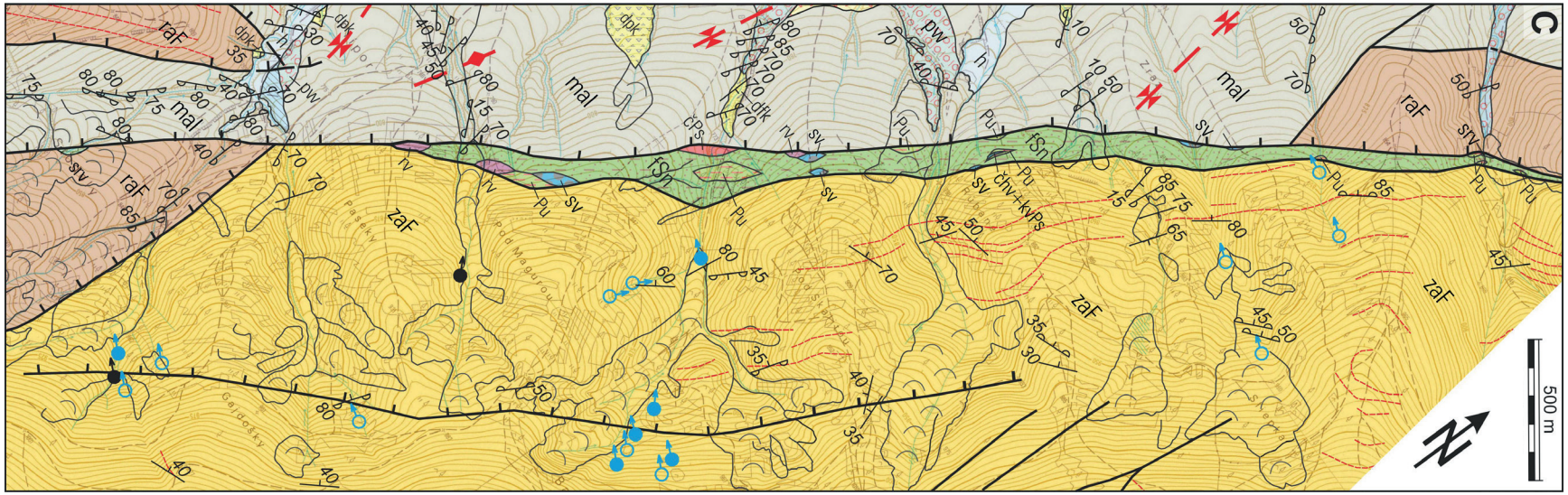

the Bučníkový potok Stream, and above the Zraz locality. In addition to the spotted siliceous limestones with cherts and red marlstones of the Púchov Fm., already described in the previous work (Andrusov, 1931), new occurrences of Jurassic radiolarites and Upper Cretaceous PKB flysch formations were reported. At the documentation point D-365 (approx. at the locality Pod Magurou, N 49.3160398°, E 19.3909382°) a rich foraminifera assemblage from red marlstones of the Púchov Fm. indicated the Coniacian age (Gašpariková in Potfaj et al., 1981).

Potfaj (1979) described the occurrence of the PKB rocks along the line Príslop saddle (808 m) – Kubička locality – Vavrečka village as: *"strongly crushed belt with tectonic breccia up to 80 m thick. Apart from the Paleogene sandstones and claystones, breccia contains fragments of Tithonian clayey limestones, green radiolarites, 'exotic' conglomerates with similar pebble composition as conglomerates near Krivá village, tectono-sedimentary breccias of 'Záskalie-type' with Campanian – Maastrichtian age and brick-red claystones with Turonian microfauna. Based on the field measurements the line is dipping 80–85° to the SE"*. Potfaj (1983) stated that *"the Magura sandstone complex is tectonically separated from the Malcov Formation at the northern foot of the Oravská Magura and meets the Malcov Formation through a 20 to 200 m wide tectonic zone, along which fragments, lenses, and breccias of rocks from the sedimentary sequences of the Pieniny Klippen Belt are brought to the surface"*.

Apart from the cited works, the Babín Klippen area has not been studied or properly discussed. During the new geological mapping, it was possible to verify and accurately locate most of the known sites and several new sites were discovered. The present paper is aimed on a revision and description of the geological structure of the Babín Klippen.

## Methods

The area was mapped using the standard methods of geological mapping according to the *Directive of the Ministry of Environment of the Slovak Republic No. 4/1996-3.1. for the compilation of basic geological maps and explanatory notes at the scale 1:25,000 and regional geological maps at the scale 1:50,000*. Additionally, the standard geological mapping was enhanced thanks to LiDAR assisted base maps using DTM 5.0 with accuracy of ~0,2 m (Liščák et al., 2022; Leitmannová & Gálová, 2023). The accuracy of the GNSS devices used for field navigation was within 5 m. The mapping was based mainly on the occurrence of rock fragments in a scree. Better outcrops were found only in the Skalnatý potok Stream and in the Rúbane section after the riverbed was washed out by an extreme storm in April 2025.

## Results

The Babín Klippen form a 20 to 250 m wide and about 8 km long continuous zone, consisting mainly of the Upper Cretaceous Snežnica and Sromowce flysch formations composed of claystones and quartz-carbonate sandstones. Structurally, we can follow the Babín Klippen Zone south-westward to the spur of the PKB in the Račová Stream valley, and north-eastward to the spur of the Biele Karpaty Unit, although rocks of the PKB are not exposed in the area (Fig. 2). The Babín Klippen structure follows the morphological break of the slope at a distinct

**Tab. 1**

Important studied localities with WGS coordinates mentioned in the text

| Number | Locality | WGS X (N) [°] | WGS Y (E) [°] | Description |
|---|---|---|---|---|
| 1.1 | Skalnatý potok Stream, SE of Babín village | 49.3218442 | 19.3951113 | cut of the stream, contact of Malinowa-type shales with grey shaly mélange |
| 1.2 | | 49.3213092 | 19.3951895 | cut of the stream, Pavláškova skala Fm. |
| 1.3 | | 49.3215107 | 19.3965051 | dirt road cut, Púchov, Allgäu and Czajakowa fms. |
| 1.4 | | 49.3211137 | 19.3958103 | cut of the stream, brecciated Pieniny Lmst. |
| 2.1 | Šubovka, ESE of Vasiľov village | 49.3414387 | 19.4171408 | cut of the stream, toe of the landslide, Púchov Fm. |
| 2.2 | | 49.3409803 | 19.4177868 | debris in the stream, Pieniny Fm. |
| 2.3 | | 49.3414679 | 19.4172501 | debris in the stream, Pieniny Fm. |
| 3 | Rúbane section, E of Babín village | 49.3286451 | 19.4037086 | outcrop in dirt road and its surroundings, Púchov Fm. with Smolegowa and Czorsztyn fms. klippen |

tectonic contact between the sandstone-rich Zábava Fm. (Ypresian – Lutetian) and the claystone-rich Malcov or Racibor formations (middle Eocene – Oligocene) of the Flysch Belt. The Flysch Belt formations are strongly tectonically reworked and often brecciated at the contact with the Babín Klippen (locality no. 1.1, N 49.3218442°, E 19.3951113°). The area is poorly exposed, covered by Quaternary deluvial sediments and soils with sandstone debris from the topographically higher exposed Zábava Fm. The continuation of the Babín Klippen to the SW and NE is manifested by distinct tectonic jointing and even brecciation of the rocks of the Flysch Belt. In the Skalnatý potok Stream valley (locality no. 1.1, Tab. 1), a tectonic mélange was observed, consisting mainly of debris of the Snežnica and Sromowce fms. The klippen cover rocks are broken into blocks and breccia of grey claystones, laminated fine-grained sandstones, massive medium-grained sandstones, and grey claystones (Fig. 4A, B, and 4F). The sandstones are fine-grained quartz-carbonate and well-sorted. The limestone material can be found as cm to dm clasts and boulders either in-situ in outcrops or as alluvial deposits in the stream (Figs. 4G and 4H).

Especially in the northern margin of the section red clays accompanied by green laminated fine-grained Malinowa-type sandstones with biotite and muscovite occur (locality no. 1.2, N 49.3213092°, E 19.3951895°). They are interpreted as the part of the Pavláškova skala Fm. The Pavláškova skala Fm., a name originally proposed by Potfaj in Bezák et al. (2009) as an informal name for occurrences of flysch strata with red claystones in the Zázrivá area, whose age was not satisfactorily determined at that time. Plašienka et al. (2021) have correlated this lithostratigraphic unit with the Turonian – Campanian Malinowa and Haluszowa formations and assigned them to the Grajcarek or Šariš successions, which should represent the structurally lowermost Šariš Unit of the PKB in the Orava sector of the PKB. The lithostratigraphic classification of the Pavláškova skala Fm. is, however, beyond the scope of this paper. For further discussion see Teťák et al. (2025).

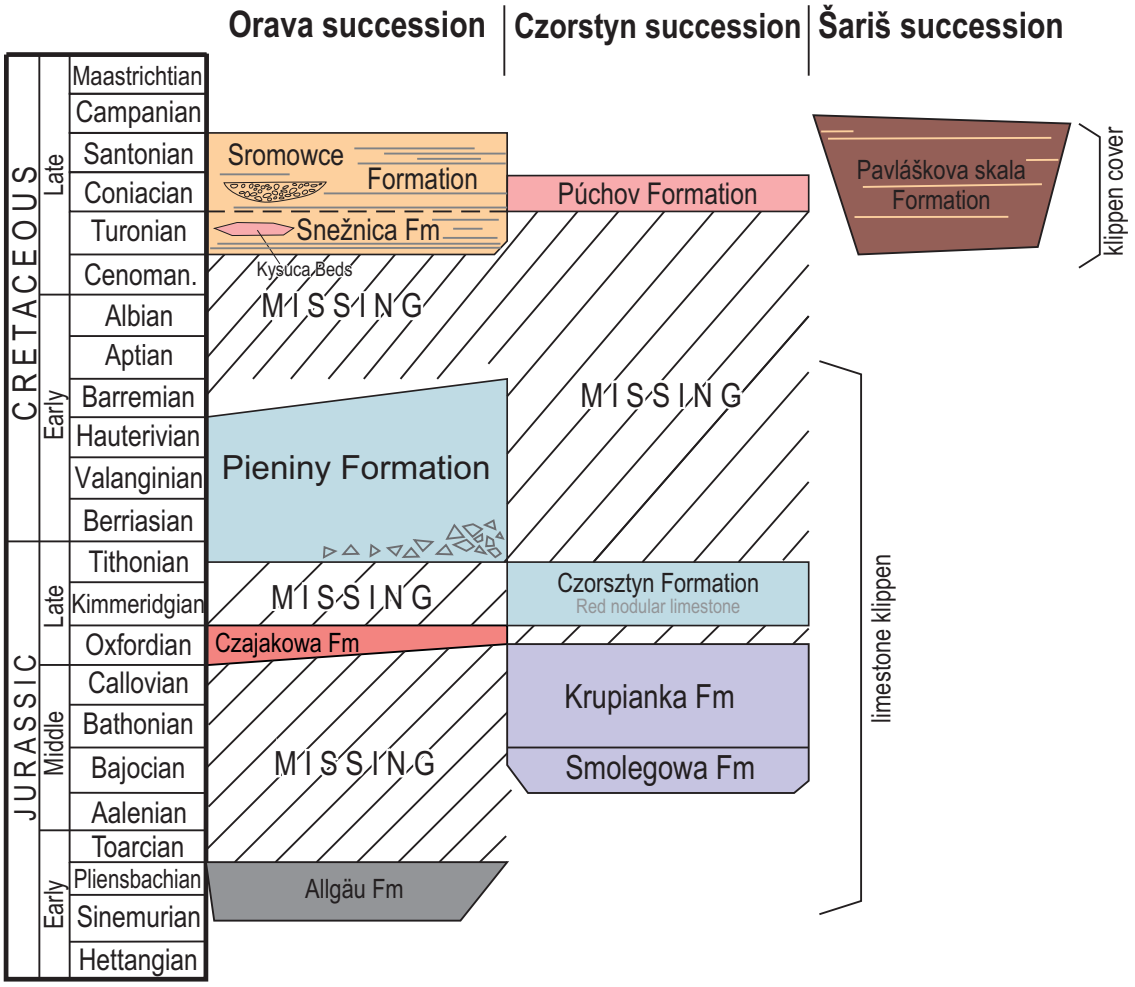


**Fig. 3.** Lithostratigraphic scheme of the PKB successions in the studied area of the Babín Klippen


**Fig. 4.** A – Fleckenkalk-type limestone with *Teichichnus* isp. from the right slope of the Skalnatý potok Stream valley, locality 1.3; B – Grey spotted radiolarite, SE of the Babín village; C – Grey brecciated limestone of the Pieniny Fm., SE of Vasiľov village; D – Detail of the limestone breccia from the same locality; E – Outcrop of grey and pink crinoidal limestone of the Smolegowa Fm., the Rúbane section, loc. 3; F – Red nodular limestone of the Czorsztyn Fm., the Rúbane section, loc. 3; G – Block of grey quartz-carbonate sandstone of the Snežnica or Sromowce Fm.; H – Pebbly mudstone with exotic blocks and pebbles at the Skalnatý potok Stream locality.

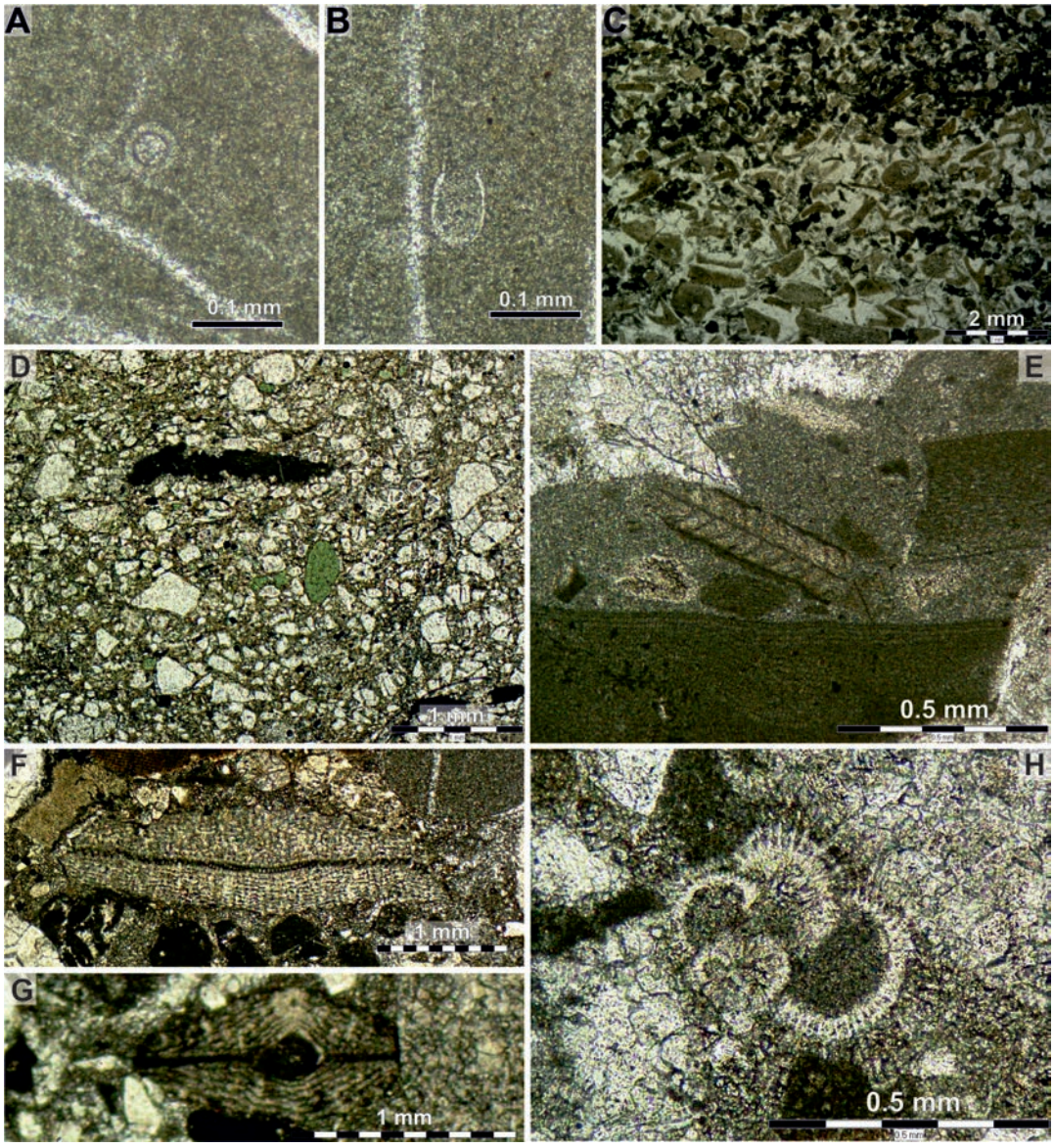


**Fig. 5.** A–B – Pieniny Formation, locality 1.4, sample OP1234OMa. A – *Colomisphaera minutissima* Nowak. B – *Calpionella elliptica* (Cadisch). C – Crinoidal grainstone microfacies of the Smolegowa Fm. (sample OP1239OM). D – Glauconitic sandstone with angular quartz clasts (sample OP1241OM); E–H – Organodetritic quartz-carbonate sandstone of the Eocene age (sample OP1234OMb). E – Feather-shaped algae *Districhoplax biserialis* (Dietrich). F–G – Fragments of larger benthic foraminifera *Discocyclina* sp. H – Planktonic foraminifera *Subbotina* cf. *yeguanensis* (Weinzierl & Applin).

The other klippen material represented by red and green radiolarites to radiolarian limestones of the Czajakowa Fm., white Biancone-type limestones of Pieniny Fm., brecciated Pieniny limestone with a dark matrix, and exotic polymictic conglomerates were observed in a tectonic mélange (Fig. 4H; locality no. 1.4, N 49.3211137°, E 19.3958103°). The mélange contains also grey crinoidal limestone blocks.

On the right slope of the Skalnatý potok Stream valley (locality no. 1.3, N 49.3215107°, E 19.3965051°), in the road track, numerous red claystones of the Púchov Fm. and spotted limestones of the Fleckenmergel-Fleckenkalk facies (Allgäu Fm.) accompanied with fine-grained quartz-carbonate sandstones occur as a debris in a scree (Fig. 4G). The Allgäu Fm. as well as the Czajakowa Fm. radiolarites occur to the south and north. The surrounding deluvium is rich in fragments of fine-grained (rarely coarse-grained) quartz-carbonate sandstones representing most likely flysch deposits of the Snežnica and Sromowce formations with red claystone interbeds, probably belonging to the

Púchov Fm. The klippen composed of Allgäu, Czajakowa, Pieniny, Snežnica and Sromowce formations could be correlated with the Orava or Kysuca successions (Fig. 3).

Apart from the quartz-carbonate sandstones of the klippen cover, sandstones clearly derived from the surrounding Flysch Belt also occur. These are represented by glauconitic sandstones (Fig. 5D) and organodetritic sandstones (locality no. 2, Šubovka ESE of Vasiľov village, N 49.3414387°, E 19.4171408°) with fragments of algae, larger benthic foraminifera and planktonic foraminifera (Figs. 5E–H).

In the Šubovka stream (ESE of Vasiľov, Tab. 1), red clays and fragments of red shales with calcite veins typical for the Púchov Fm., a tectonic breccia of Pieniny limestones with cherts (Fig. 4C, and 4D; locality no. 2.1, N 49.3409803°, E 19.4177868°), followed by fine-grained conglomerates with carbonate pebbles up to 15 mm (rarely up to 15 cm) and predominantly strongly tectonically brecciated laminated fine-grained quartz-carbonate sandstones, apparently from the accompanying flysch formations, were observed. The Pieniny limestone was transported with the toe of landslide (locality no. 2.2, N 49.3414679°, E 19.4172501°). The brecciated white Pieniny limestones occurring at this locality represent mudstone to wackestone with radiolarians. The limestones contain *Colomisphaera minutissima* Nowak and *Calpionella elliptica* (Cadisch) indicating early to middle Berriasian age (according to Reháková, 2000 and Reháková & Michalík, 1997; Figs. 5A and B). The studied limestone represents a lower part of the Pieniny Fm.

The only more-or-less geomorphologically manifested klippe can be found in the Rúbane section (locality no. 3, N 49.3286451°, E 19.4037086°). The Rúbane section is up to 70 m long sequence exposed in a dirt road, which consists of grey and pink crinoidal limestones of the Bajocian Smolegowa and Krupianka fms. The crinoidal Smolegowa limestones are coarse-grained and massive (Fig. 4E). Microstructurally the crinoidal limestones represent packstones to grainstones (Fig. 5D). The overall thickness of the grey and pink crinoidal limestone is approx. 10 m. The overlying thin-bedded red nodular limestones of the Czorsztyn Fm. contain sporadic ammonite and belemnite fragments (Fig. 4F). Their thickness is up to 5 m. The crinoidal and red nodular limestone klippe is surrounded by red claystones and marlstones of the Púchov Fm. The whole sequence at this locality could be correlated with the Czorsztyn succession (Fig. 3). The wider area is formed by klippen cover flysch formations, represented predominantly by darker grey claystones and fine- to medium-grained laminated quartz-carbonate sandstones, sporadically interbedded with red claystones or marlstones.

## Discussion

In his 1938 geological cross-sections, Andrusov (1938, Tabs. XIII and XIV) had already shown the PKB extending into the footwall of the Oravská Magura Mts. in the Hruštínka valley. However, he interpreted the whole structure as inclined to the south, which is no longer the case, although numerous evidences of the south-vergent backthrust were provided already at the time (Andrusov, 1938). The presence of the PKB rocks in this area was mentioned by Marschalko (1986, p. 16) in the same context.

The contact between the Flysch Belt and the Pieniny Klippen Belt at greater depths was discussed by Potfaj (1983), who stated that *"The fold-and-thrust-belt style can be mapped along the aforementioned tectonic line on the northern slope of the Oravská Magura Mts. (i.e., the Babín sector of the PKB) and probably extends to the line of Námestovo-Žilina gravimetric minimum. From a structural point of view, we can shift the northern boundary of the PKB that far"*. This opinion can still be considered valid today.

The new mapping confirmed the lithology and precise location of the klippen mapped by Andrusov (1931). It has been found that the klippen mapped by Potfaj et al. (1981) are located up to 200 m further to the south. The presence of several klippen could not be confirmed due to poor exposure conditions, so we assume that there are more small broken blocks than Jurassic klippen shown on the map in Fig. 2. However, the extent of the Babín Klippen structure is reliably delineated by the occurrence of quartz-carbonate sandstones in Quaternary slope debris, as these are otherwise rare in this portion of the Krynica Unit.

The study of the Babín Klippen is important due to the fact, that the area is transected by the seismic profile 2T (Vozár et al., 1999; Tomek et al., 1989; Tomek, 1993). The interpretation of this profile, suggesting a north-dipping geometry of the PKB and a backthrust of the Flysch Belt, is supported by the recent geological investigations (Teťák et al., 2025). In contrast, the interpretation of the seismic profile 512/86 (Vozár et al., 1999), located slightly farther east, shows significant differences in the geometry of the PKB and the accretionary wedge of the External Western Carpathians. The main difference can be considered to be the absence of backthrust of the PKB. We would interpret the subsurface extent of the Internal Western Carpathian units (i.e. units south of the PKB) significantly further north, similar to profile 2T (Fig. 6).

The successions of the PKB are generally strongly tectonically deformed. However, the deformation in the Babín Klippen Zone is exceptionally intense. Approximately 1 km south of the Babín Klippen Zone, changes in the bedding dip of the Zábava Fm., together with a distinct change in morphology, are interpreted to reflect an additional (back-)thrust. This structure is further expressed by a high concentration of springs, several of which precipitate tufa, forming the most extensive accumulation of tufa-bearing springs in the region (N 49.314853°, E 19.403826°). Within this zone and in the Babín Klippen Zone, three

mineral springs enriched in $H_2S$ occur. The association of tufas and mineral springs suggests deep groundwater circulation, likely facilitated by tectonic structures. In the PKB and the Biele Karpaty Unit of the Považie region, more than 100 tufa-forming springs have been documented (Pešková et al., 2021), many of which show a clear relationship to underlying fault systems.

Several issues in the examined area remain unsolved. Firstly, there is the unusual pebbly mudstone body that passes to the tectonic mélange in the Skalnatý potok Stream. Although not studied in detail, based on our field observations, we correlate it with the polymict conglomerate bodies of the Upper Cretaceous Sromowce Fm. (Fig. 4H). Secondly, we also draw attention to the occurrences of organodetritic sandstones ESE of the Vasiľov village (Fig. 5E–H), which cannot be correlated with any of the surrounding formations. The organodetritic sandstones with fragments of algae and foraminifera resemble organodetritic limestones from the Malcov Fm. of the Flysch Belt described by Potfaj (1983, p. 127), or possibly part of the Proč Fm. of the PKB.

extremely deformed exposure related to the backthrust of the External Western Carpathian accretionary wedge to the SE.

**Acknowledgements**

Authors FT and OP dedicate this paper to the memory of Dr. Michal Potfaj, who mapped the Babín Klippen in 1980-ies. Michal unexpectedly passed away at the end of 2025, before finalizing the manuscript.

The study was financially supported by the Ministry of Environment of the Slovak Republic project no. 02 20 Geological map of the Oravská Magura Mts. at scale 1:50,000. The authors are also grateful to handling editor Klement Fordinál, and reviewers Jozef Hók and Jozef Madzin for their constructive comments which helped to improve the manuscript. For the identification of foraminifera microfauna, authors would like to thank Assoc. Prof. Ján Soták, and Prof. Daniela Reháková for review of our determination of calpionellids and dinoflagellates.

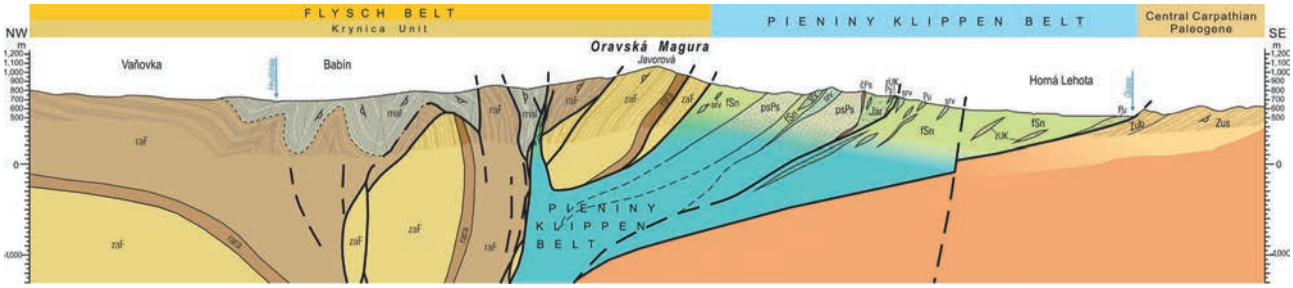


**Fig. 6.** The cross-section extending into the foothills of the Oravská Magura Mts. oriented approximately parallel to the line of the 2T seismic profile (based on Teťák et al., in press). For location of the profile see Fig. 1.

## Conclusions

The narrow zone of the Pieniny Klippen Belt sandwiched inbetween the thrust sheets of the Krynica Unit of the Flysch Belt on the northern slopes of Oravská Magura Mts. is known as the Babín Klippen (Figs. 1, 2 and 6). The Babín Klippen form approximately 200 m thick and 8 km long strongly disintegrated zone of the PKB rocks SE of the Babín and Vasiľov villages (Námestovo district). The Babín Klippen Zone consists of the three different PKB sedimentary successions. From the paleogeographic point of view the Orava (or Kysuca) succession was the southernmost one (in present coordinates) and is represented by rocks of the Allgäu, Czajakowa, Pieniny, Snežnica and Sromowce fms. The second one is the Czorsztyn succession represented by rocks of Krupianka, Smolegowa, Czorsztyn and Púchov fms. The most northerly situated was the Šariš succession formed by the Pavláškova skala Fm. is represented to a lesser extent. The studied Babín Klippen represent unique

## References

Andrusov, D., 1931: Geologická mapa útesového pásma v údolí Oravy 1 : 25 000. Díl východní. In: Matějka, A. & Andrusov, D. (eds.): Guide des excursions dans les Carpathes occidentales. *Praha, Státní geologický ústav Československé republiky*, 397 pp.

Andrusov, D., 1938: Geologický výzkum vnitřního bradlového pásma v Západních Karpatech, část III.: Tektonika. *Rozpravy Státního geologického ústavu Československé republiky, IX, 1 – 136* (in Czech, French summary).

Andrusov, D. & Scheibner, E., 1960: Prehľad súčasného stavu poznatkov o geológii bradlového pásma medzi Vlárou a Tvrdošínom. *Geologický sborník Slovenskej akadémie vied*, 11, 2, 239–279 (in Slovak).

Bezák, V. (ed.), Elečko, M., Fordinál, K., Ivanička, J., Kaličiak, M., Konečný, V., Kováčik, M. (Košice), Maglay, J., Mello, J., Nagy, A., Polák, M., Potfaj, M., Biely, A., Bóna, J., Broska, I., Buček, S., Filo, I., Gazdačko, Ľ., Grecula, P., Gross, P., Havrila, M., Hók, J., Hraško, Ľ., Jacko, S. ml., Jacko, S. st., Janočko, J., Kobulský, J.,

Kohút, M., Kováčik, M., Lexa, J., Madarás, J., Németh, Z., Olšavský, M., Plašienka, D., Pristaš, J., Rakús, M., Salaj, J., Siman, P., Šimon, L., Teťák, F., Vass, D., Vozár, J., Vozárová, A. & Žec, B., 2008: Prehľadná geologická mapa Slovenskej republiky 1 : 200 000. *Bratislava, Ministerstvo životného prostredia SR – Štátny geologický ústav Dionýza Štúra.*

Bezák, V. (ed.), Elečko, M., Fordinál, K., Ivanička, J., Kaličiak, M., Konečný, V., Maglay, J., Mello, J., Nagy, A., Polák, M., Potfaj, M., Šimon, L., Biely, A., Broska, I., Buček, S., Filo, I., Grecula, P., Hraško, Ľ., Jacko, S., Kobulský, J., Kohút, M., Kováčik, M., Lexa, J., Olšavský, M., Plašienka, D., Pristaš, J., Teťák, F., Vass, D. & Vozárová, A., 2009: Vysvetlivky k Prehľadnej geologickej mape Slovenskej republiky 1 : 200 000. *Bratislava, Štátny geologický ústav Dionýza Štúra*, 534 pp. (in Slovak).

Káčer, Š., Antalík, M., Lexa, J., Zvara, I., Fritzman, R., Vlachovič, J., Bystrická, G., Potfaj, M., Madarás, J., Nagy, A., Maglay, J., Ivanička, J., Gross, P., Rakús, M., Vozárová, A., Buček, S., Boorová, D., Šimon, L., Mello, J., Polák, M., Bezák, V., Hók, J., Teťák, F., Konečný, V., Kučera, M., Žec, B., Elečko, M., Hraško, Ľ., Kováčik, M. & Pristaš, J., 2024: Geologická mapa Slovenska M 1 : 50 000. *Bratislava, Štátny geologický ústav Dionýza Štúra*. Online: http://apl.geology.sk/gm50js.

Leitmannová, K. & Gálová, L., 2023: Slovensko už má digitálny model reliéfu z celého územia. *Geodetický a kartografický obzor*, 69, 111, 12, 265–273 (in Slovak).

Liščák, P., Pauditš, P., Bystrická, G., Teťák, F., Maglay, J., Dananaj, I., Ondrus, P., Mašlár, E., Mašlárová, I., Olšavský, M., Pelech, O., Vitovič, L., Leitmannová, K., Fraštia, M. & Papčo, J., 2022: Využitie DMR 5.0 z leteckého laserového skenovania pri riešení geologických úloh ŠGÚDŠ. *Geodetický a kartografický obzor*, 68, 110, 8, 149–159 (in Slovak).

Marschalko, R., 1986: Vývoj a geotektonický význam kriedového flyšu bradlového pásma. *Bratislava, Veda, Vydavateľstvo SAV*, 140 pp. (in Slovak, English summary).

Mello, J. (ed.), Potfaj, M., Teťák, F., Havrila, M., Rakús, M., Buček, S., Filo, I., Nagy, A., Salaj, J., Maglay, J., Pristaš, J. & Fordinál, K., 2005: Geological map of the Middle Váh Valley 1 : 50 000. *Bratislava, Ministerstvo životného prostredia SR – Štátny geologický ústav Dionýza Štúra.*

Mišík, M., 1997: The Slovak part of the Pieniny Klippen Belt after the pioneering works of D. Andrusov. *Geologica Carpathica*, 48, 4, 209–220.

Pešková, I., Teťák, F. (eds.), Pelech, O., Sentpetery, M., Olšavský, M., Kováčik, M., Maglay, J. & Vlačiky, M., 2021: Geological map of the Biele Karpaty Mts. (Northern part) 1 : 50 000. *Bratislava, Štátny geologický ústav Dionýza Štúra.*

Plašienka, D., 2018: The Carpathian Klippen Belt and types of its klippen – an attempt at a genetic classification. *Mineralia Slovaca*, 50, 1, 1–24.

Plašienka, D., Sýkora, M., Aubrecht, R., Krobicki, M. & Józsa, Š., 2010: Reinterpretation of the lithostratigraphy and tectonic position of the Mariková Klippen (Middle Váh Valley, western Slovakia). *Acta Geologica Slovaca*, 2, 1, 1–9.

Plašienka, D., Aubrecht, R., Bezák, V., Bielik, M., Broska, I., Bučová, J., Fekete, K., Gaži, P., Gedl, P., Golej, M., Halásová, E., Hók, J., Jamrich, M., Józsa, Š., Klanica, R., Konečný, P., Kubiš, M., Madarás, J., Majcin, D., Marko, F., Molčan Matejová, M., Potočný, T., Schlögl, J., Soták, J., Suan, G., Šamajová, L., Šimonová, V., Teťák, F. & Vozár, J., 2021: Structure, composition and tectonic evolution of the Pieniny Klippen Belt – Central Western Carpathians contiguous zone (Kysuce and Orava regions, NW Slovakia). *Bratislava, Comenius University*, 150 pp.

Potfaj, M., 1979: Tektonický profil styku bradlového pásma a magurskej jednotky v priestore Oravskej Magury. In: Maheľ, M. (ed.): Tektonické profily Západných Karpát. *Bratislava, Geologický ústav Dionýza Štúra*, 37–40 (in Slovak).

Potfaj, M., 1983: Postavenie magurských pieskovcov a malcovské vrstvy na Orave. *Geologické práce, Správy*, 79, 117–140 (in Slovak).

Potfaj, M., Haško, J., Gašpariková, V., Snopková, P. & Samuel, O., 1981: Vysvetlivky ku geologickej mape 1 : 25 000, list 26-411 (Trstená). Čiastková záverečná správa za rok 1977 – 1981. *Manuscript. Bratislava, Archive of St. Geol. Inst. of D. Štúr* (arch. no. 50488), 47 pp. (in Slovak).

Reháková, D., 2000: Evolution and distribution of the Late Jurassic and Early Cretaceous calcareous dinoflagellates recorded in the Western Carpathian pelagic carbonate facies. *Mineralia Slovaca*, 32, 79–88.

Reháková, D. & Michalík, J., 1997: Evolution and distribution of calpionellids the most characteristic constituents of Lower Cretaceous Tethyan microplankton. *Cretaceous Research*, 18, 493–504. https://doi.org/10.1006/cres.1997.0067.

Scheibner, E., 1967: Karpatské pásmo bradlové. In: Buday, T. (ed.), Cicha, I., Hanzlíková, E., Chmelík, F., Koráb, T., Kuthan, M., Nemčok, J., Pícha, F., Roth, Z., Seneš, J., Scheibner, E., Stráník, Z., Vaškovský I. & Žebera, K., 1967: Regionální geologie ČSSR, Díl II Západní Karpaty, svazek 2. *Praha, Ústřední ústav geologický, Academia*, 7–105 (in Czech).

Teťák, F., 2024: Revízia geologickej mapy západného úseku flyšového pásma Západných Karpát s diskusiou k vybraným geologickým problémom. *Geologické práce, Správy*, 140, 75 – 106 (in Slovak, English summary). https://doi.org/10.56623/gps.140.3.

Teťák, F., Pelech, O., Laurinc, D., Olšavský, M., Fekete, K., Vitovič, L., Maglay, J., Demko, R. & Korábová, K., 2025: Geologická mapa Oravskej Magury v mierke 1 : 25 000 (východná časť). Čiastková záverečná správa geologickej úlohy. *Manuscript. Bratislava, Archive of St. Geol. Inst. of D. Štúr*, 150 pp.

Teťák, F. (ed.), Pelech, O., Laurinc, D., Olšavský, M., Vitovič, L., Maglay, J., Fekete, K., Nagy, A., Madzin, J. & Dananaj, I., *in press*: Geological map of the Oravská Magura Mts. *Bratislava, State Geol. Inst. of Dionýz Štúr.*

Tomek, C., Ibrmajer, I., Koráb, T., Biely, A., Dvořáková, L., Lexa, J. & Zbořil, A., 1989: Korové struktury Západních

Karpat na hlubinném seizmickém profilu 2T. *Mineralia Slovaca*, 21, 1, 3–26.

Tomek, Č., 1993: Deep crustal structure beneath the central and inner West Carpathians. *Tectonophysics*, 226, 417–431.

Vozár, J., Šantavý, J. (eds.), Potfaj, M., Szalaiová, V., Scholtz, P., Tomek, Č., Šefara, J., Machková, N., Gnojek, I., Šály, B., Pereszlényi, M., Hrušecký, I., Hlavatý, I., Jureňa, V., Rudinec, R., Magyar, J. & Slávik, M., 1999: Atlas of deep reflection seismic profiles of the Western Carpathians and its interpretation. *Bratislava, Ministry of Environment of the Slovak Republic*, 76 pp.

# Babínske bradlá – osobitý výbežok oravského úseku pieninského bradlového pásma (Slovensko)

Na viacerých starších geologických mapách je zobrazené vystupovanie bradlového pásma v úzkej zóne na severnom svahu Oravskej Magury nad Babínom (Andrusov, 1931; Potfaj et al., 1981; Potfaj, 1983). Potfaj (1979) charakterizuje babínske bradlá ako *„silne drvené pásmo s tektonickými brekciami o hrúbke až do 80 m. Okrem paleogénnych pieskovcov a ílovcov sú v brekcii aj úlomky titónskych kalových vápencov, zelených rádiolaritov, ‚exotické' zlepence s obdobným zložením valúnového materiálu, ako majú zlepence pri Krivej, tektonicko-sedimentárne brekcie ‚záskalského typu' s vekovým zaradením do kampánu až maastrichtu a tehlovočervené slieňovce s turónskou mikrofaunou. Podľa priebehu v teréne má línia 80-85° sklon k JV"*. Potfaj (1983) udáva, že *„komplex magurských pieskovcov je na sz. úpätí Oravskej Magury tektonicky odrezaný od malcovského súvrstvia a stýka sa cez 20 až 200 m širokú tektonickú zónu, pozdĺž ktorej sú na povrch vyvlečené útržky, šošovky a brekcie hornín z vrstevných sledov bradlového pásma"*.

Andrusov (1931) nad Babínom zaznamenal na mape viaceré výskyty titónsko-spodnokriedových pieninských vápencov pieninskej sukcesie, miestami obklopené púchovskými vrstvami. Bradlové pásmo na mape a v reze zobrazuje ako izolované vystupovanie hornín bradlového pásma, obklopené paleogénnym súvrstvím Oravskej Magury. Lokalizácia uvedených výskytov je presná a overili sme ju.

Potfaj et al. (1981) na mape listu Trstená rozšírili známe výskyty fácií bradlového pásma na časť Stodoly, pravú vetvu Bučníkového potoka a nad Zraz. Okrem škvrnitých slienitých vápencov s rohovcami a červených slieňov gbelianskych vrstiev, ktoré uvádza už Andrusov (1931), sa na viacerých miestach nachádzali aj výskyty rádiolaritov a flyšových súvrství bradlového pásma.

Okrem uvedených dvoch prác úsek babínskych bradiel nebol skúmaný a do novších prác boli informácie prevzaté. Pri novom geologickom mapovaní sa nám podarilo overiť a presne lokalizovať väčšinu známych lokalít. Zistili sme niekoľko nových lokalít (tab. 1, obr. 2). Nepodarilo sa overiť napr. vystupovanie v Bučníkovom potoku, no kvôli úplnosti preberáme aj neoverené výskyty.

Babínske bradlá tvorí súvislá, len 20 až 250 m široká a asi 8 km dlhá zóna tvorená prevažne flyšovým súvrstvím s ílovcami a kremenno-karbonátovými pieskovcami. Je lokalizovaná pod morfologickým lomom svahu na výraznom tektonickom kontakte zábavského súvrstvia s malcovským, prípadne raciborským súvrstvím. Spomínaný úsek je značne prekrytý sutinou z pieskovcov zábavského súvrstvia. Predmetom štúdia boli len výskyty horninových úlomkov, in-situ odkryvy boli pozorované len výnimočne. Výnimkou bolo jediné morfologicky vystupujúce bradlo v časti Rúbane.

V doline Skalnatého potoka bola pozorovaná tektonická melanž, ktorú tvoria flyšové sedimenty bradlového obalu rozbité na bloky až brekcie sivých ílovcov, laminované jemnozrnné pieskovce s patinou, masívne strednozrnné pieskovce a tenko vrstvený flyš so sivými ílovcami. Pieskovce sú jemnozrnné, kremenno-karbonátové. Bradlový materiál sa nachádza v podobe balvanov a úlomkov v potoku. Výrazné boli červené hliny, hojne sprevádzané zelenými laminovanými jemnozrnnými pieskovcami s biotitom a muskovitom, ktoré zaraďujeme do súvrstvia Pavláškovej skaly. V melanži sme pozorovali blok rádioláriového vápenca, bloky slienitého vápenca (aj škvrnité), početnú sutinu pieninského vápenca fácie biancone v brekcii s tmavým matrixom a množstvo obliakov exotických polymiktných zlepencov sromowského súvrstvia. V pravom svahu doliny v koľaji cesty je veľa červených slieňovcov a na pár metroch sú úlomky allgäuského súvrstvia s patinou, doplnené jemnozrnnými kremenno-karbonátovými pieskovcami. Aj vyššie na hrebienku vystupuje na dvoch miestach allgäuské súvrstvie. V okolí sú hojné jemnozrnné (vzácne až hrubozrnné) kremenno-karbonátové pieskovce reprezentujúce snežnické a sromowské súvrstvie a šmuhy červených hlín.

Najvýraznejšie bradlo vystupuje v časti Rúbane (lokalita č. 3, tab. 1). Je dlhé až 70 m. Na západnom konci ho tvoria hľuznaté čorštynské biomikritické vápence s amo-

nitmi aj belemnitmi, ktoré smerom na sever prechádzajú do ružových krinoidových vápencov. Bradlo sa končí v poľnej ceste sivými hrubozrnnými krinoidovými vápencami smolegowského súvrstvia. Je obklopené červenými slieňovcami púchovského súvrstvia a v širšom okruhu bradlovým flyšom snežnického a sromowského súvrstvia. Sú to prevažne tmavšie sivé ílovce sprevádzané jemno- až strednozrnnými laminovanými kremenno-karbonátovými pieskovcami, miestami s patinou, zriedka doplnenými šmuhou červených hlín/slieňovcov.

V potoku sz. od k. Šubovka v čele zosuvu vystupujú premiestnené červené hliny s úlomkami červených slieňovcov púchovského typu s množstvom kalcitových žiliek, pieninské vápence fácie biancone, miestami s rohovcami vo forme tektonickej brekcie, ale aj celistvý až béžový, miestami škvrnitý vápenec, drobnozrnné zlepence s obliačikmi karbonátov s veľkosťou do 15 mm (vzácne do 15 cm) a prevažne silno tektonicky drvené laminované jemnozrnné kremenno-karbonátové pieskovce, zrejme zo sprievodného bradlového flyšu.

V zóne babínskych bradiel môžeme vyčleniť tri sedimentárne sekvencie bradlového pásma. Z paleogeografického hľadiska bola oravská (resp. kysucká) sukcesia najjužnejšia (v súčasných súradniciach). Tvoria ju horniny allgäuského, čajakovského, pieninského, snežnického a sromowského súvrstvia. Druhou je čorštynská sukcesia reprezentovaná horninami krupianskeho, smolegowského, čorštynského a púchovského súvrstvia. Najsevernejšie sa nachádza šarišská sukcesia tvorená súvrstvím Pavláškovej skaly, ktoré vystupuje iba v plošne obmedzenej miere. Študované babínske bradlá predstavujú jedinečný, extrémne deformovaný výstup bradlového pásma súvisiaci so spätným prešmykom akrečného klina Vonkajších Západných Karpát smerom na juhovýchod.

Tento článok je venovaný pamiatke RNDr. Michala Potfaja, PhD., ktorý v minulosti pracoval v oblasti babínskych bradiel a v decembri 2025 nás nečakane opustil.

Doručené / Recieved: 2. 1. 2026
Prijaté na publikovanie / Accepted: 10. 3. 2026

*Mineralia Slovaca, Web ISSN 1338-3523, ISSN 0369-2086, https://doi.org/10.56623/ms.2025.57.2.2*
*57, 2 (2025), 111 – 144, © Authors 2025. CC BY 4.0*

# Heavy mineral analysis of the Upper Cretaceous to Lower Eocene synorogenic formations of the Pieniny Klippen Belt (Šariš Unit, eastern Slovakia): new data from the Jar-2 borehole (Jarmuta-Proč Fm.) and outcrops (Malinowa Fm.)

JOZEF MADZIN [1]* and DUŠAN PLAŠIENKA [2]

[1] Earth Science Institute, Slovak Academy of Sciences, Ďumbierska 1, 974 01 Banská Bystrica, Slovak Republic;
* corresponding author, jozef.madzin@savba.sk
[2] Comenius University, Faculty of Natural Sciences, Department of Geology and Palaeontology, Ilkovičova 6, 842 15 Bratislava, Slovak Republic; dusan.plasienka@uniba.sk

**Abstract:** The study presents new results of heavy mineral analyses including detrital garnet, tourmaline and Cr-rich spinel chemical compositions from the synorogenic Maastrichtian-Ypresian Jarmuta-Proč Fm. of the Šariš Unit of the Pieniny Klippen Belt, penetrated by the structural borehole Jar-2 in eastern Slovakia. For comparison, outcropped fine-grained sandstones of the hemipelagic Turonian-Campanian Malinowa Fm. of the Šariš Unit were analysed. The heavy mineral assemblages of both formations are dominated by garnet with variable amounts of apatite, rutile, tourmaline, zircon and subordinate Cr-rich spinel. Almandine-rich garnets with variable grossular, pyrope, and spessartine proportions prevail in both formations. Unusual complex-zoned X-vacant magnesio-foititic to foititic and schorlitic-dravitic tourmaline grains with fine intergrowth with quartz and abundant inclusions were revealed. Cr-rich spinels show chemistry typical for supra-subduction zone peridotites. The chemistry of the Cr-rich spinels and complex-zoned tourmalines supports their common provenance in the Meliata ophiolite-bearing complexes of the internal Western Carpathian zones. Decreasing-upward Cr-rich spinel contents in the Upper Cretaceous to Lower Eocene flysch deposits of the PKB is evident. A multiple recycling model in which flysch formations of the Klape Unit, situated in a false accretionary wedge position, formed the "proximal" source of the ophiolitic debris recycled to the younger clastic formations of the foreland basins is advocated.

**Key words:** Western Carpathians, Pieniny Klippen Belt, synorogenic deposits, garnet, tourmaline, Cr-rich spinel, geochemistry, provenance

**Graphical abstract**

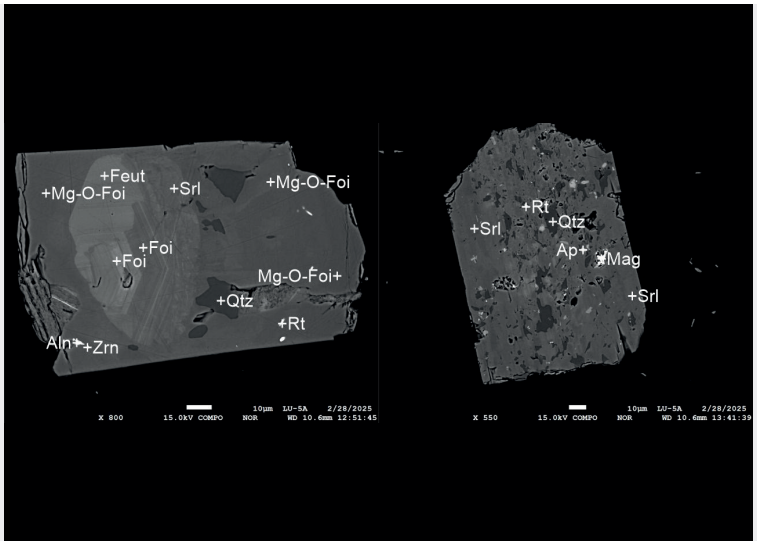


**Highlights**

- Unusual complex-zoned X-vacant magnesio-foititic to foititic and schorlitic-dravitic tourmaline grains with fine intergrowth with quartz and abundant inclusions revealed.
- Chemistry of the Cr-rich spinels and complex-zoned tourmalines supports their provenance in the Meliata ophiolite-bearing complexes of the internal Western Carpathian zones.
- Albian-Cenomanian flysch formations of the Klape Unit in a false accretionary wedge position shed ophiolitic debris to the Upper Cretaceous to Lower Eocene clastic formations of the foreland basins.

## Introduction

The external and internal zones of the Western Carpathians are sharply separated by a more than 600 km long but exceptionally narrow zone with an unusually complicated structure, known as the Pieniny Klippen Belt (PKB). Its complex polyphase structural deformation dominated by the Paleocene to Eocene nappe thrusting resulted in the superposition and juxtaposition of numerous lithologically and palaeogeographically distinct tectonic units (e.g., Birkenmajer, 1977, 1986; Mišík, 1997; Jurewicz, 2005, 2018; Plašienka & Mikuš, 2010; Plašienka, 2012a). Subsequent wrench deformations obliterated original fold-and-thrust

structures resulting in the peculiar "klippen" structure (e.g., Ratschbacher et al., 1993; Kováč & Hók, 1996; Plašienka et al., 2020). Therefore, the PKB is often characterized as a block-in-matrix structure or mélange formed by isolated rigid blocks "klippens" composed of competent Middle Jurassic to Lower Cretaceous carbonates surrounded by a soft matrix of the "klippen cover" consisting of Lower Jurassic and Upper Cretaceous to Palaeogene shales, marls and flysch formations (e.g., Birkenmajer, 1977; Plašienka & Mikuš, 2010; Jurewicz, 2018; Plašienka, 2018). The main tectonic units of the PKB s.s., were derived from an independent palaeogeographic domain known as the Oravic domain or Oravicum (Maheľ, 1986). It is thought that the Oravic domain represents the continental crustal fragment in the Middle Penninic position (analogous to the Briançonnais microcontinent, Tomek, 1993) surrounded by North Penninic (Valais-Rhenodanubian-Magura) and South Penninic (Ligurian-Piemont-Vahic) oceanic domains as a continuation of the oceanic tract of the Alpine Tethys to the Carpathian realm (e.g., Schmid et al., 2008; Plašienka, 2012a). The suture-like structure of the PKB is related to the collision of the Oravic continental fragment with the frontal parts of the Central Western Carpathian block after the closure and subduction of the Vahic oceanic domain (Plašienka, 2012a; Plašienka et al., 2020). The sedimentary record of the contractional tectonic processes is preserved in the Upper Cretaceous to Lower Eocene synorogenic flysch or wildflysch deposits including huge olistostromatic bodies and bodies of polymict "exotic" conglomerates (Mišík & Marschalko, 1988; Plašienka & Mikuš, 2010; Plašienka, 2012a; Plašienka et al., 2012; Golonka et al., 2015). In addition to the diverse pebble material of the conglomerates, the heavy mineral associations of psammitic deposits of the synorogenic formations also provide valuable information about provenance and composition of completely eroded or subducted source terrains (Salata, 2004; Aubrecht et al., 2009, 2021; Bellová et al., 2018; Bónová et al., 2018; Madzin et al., 2019). This study presents new results of heavy mineral analyses including detrital garnet, tourmaline and Cr-rich spinel chemical compositions from the synorogenic Maastrichtian-Ypresian Jarmuta-Proč Fm. of the Šariš Unit of the Pieniny Klippen Belt, penetrated by the structural borehole Jar-2 in eastern Slovakia. For comparison and revealing potential difference in composition and abundance of heavy mineral associations, outcropped fine-grained sandstones of the hemipelagic Turonian-Campanian Malinowa Fm. of the Šariš Unit were analysed as well.

## Geological settings

The eastern branch of the PKB in eastern Slovakia forms almost straight NW-SE trending 3–5 km narrow zone, which is distinctly fault-bounded against the Paleogene flysch complexes of the Krynica Unit of the Magura nappe system toward the NE, as well as against the flysch deposits of the Central Carpathian Paleogene Basin (CCPB) towards the SW (Fig. 1) (Oszczypko et al., 2005; Jurewicz, 2018; Plašienka et al., 2020). The bounding faults are steeply NE-dipping up to vertical and show a complex kinematic history (e.g., Plašienka & Mikuš, 2010; Plašienka et al., 2013; Ludwiniak, 2018). The studied part of the PKB is dominantly composed of the Oravic units with relatively well-preserved original nappe edifice (Jurewicz, 1997, 2005, 2018; Plašienka & Mikuš, 2010; Plašienka, 2012b; Plašienka et al., 2020). In places, the original nappe structure was strongly modified by superimposed transpressional and transtensional deformations (e.g., Ratschbacher et al., 1993; Nemčok & Nemčok, 1994; Plašienka, 2012b; Plašienka et al., 2020). The completely detached Jurassic to Lower Eocene Oravic sedimentary successions have been assigned to the three main superposed and/or juxtaposed tectonic units (Figs. 1, 2) (Plašienka & Mikuš, 2010; Plašienka et al., 2012). These are from bottom to top and from the external to internal position the Šariš Unit and the Subpieniny and Pieniny thrust sheets. All three units are characterized by a thickening and coarsening upward clastic sedimentary successions (Fig. 2), manifesting the basin tectonic inversion and contractional tectonic regime due to the closure of the South Penninic Vahic Ocean and ensuing collision of the Oravic ribbon continent with the Central Western Carpathian block during the latest Cretaceous and Paleogene (Jurewicz, 2005; Plašienka, 2012a; Plašienka et al., 2020). In the topmost Pieniny thrust sheet, the youngest sediments are distal turbidites of the Turonian Snežnica Fm., passing to the thick-bedded sandstones with huge exotics-bearing conglomerates of the Coniacian-Santonian Sromowce Fm. (Starek et al., 2010; Plašienka, 2012a). The sedimentary succession of the Subpieniny thrust sheet is terminated by calcareous turbidites of the Maastrichtian-Danian Jarmuta Fm., with olistostromatic bodies known as the Gregorianka Breccia (Nemčok et al., 1989; redefined by Plašienka & Mikuš, 2010). The Jarmuta Fm. often occurs in an overturned position or is tectonically reduced and missing. In that case, the sedimentary succession of the Subpieniny nappe is terminated by variegated calcareous hemipelagites, with thin beds of fine- to medium-grained sandstones of the Jaworki Fm. (Birkenmajer, 1977, equivalent to the Púchov marls). The Šariš sedimentary succession is terminated by deepwater, poorly or completely non-calcareous, variegated hemipelagites with thin beds of siltstones to fine-grained sandstones of the Turonian-Campanian Malinowa Fm. (Birkenmajer, 1977). The Malinowa Fm. passes to thick clastic deposits of the Maastrichtian-Ypresian Jarmuta-Proč Fm. The Jarmuta-Proč Fm. involves deep-water turbidites with bodies of mass-flow deposits (Milpoš Breccia) (Plašienka & Mikuš, 2010), that consist of variegated

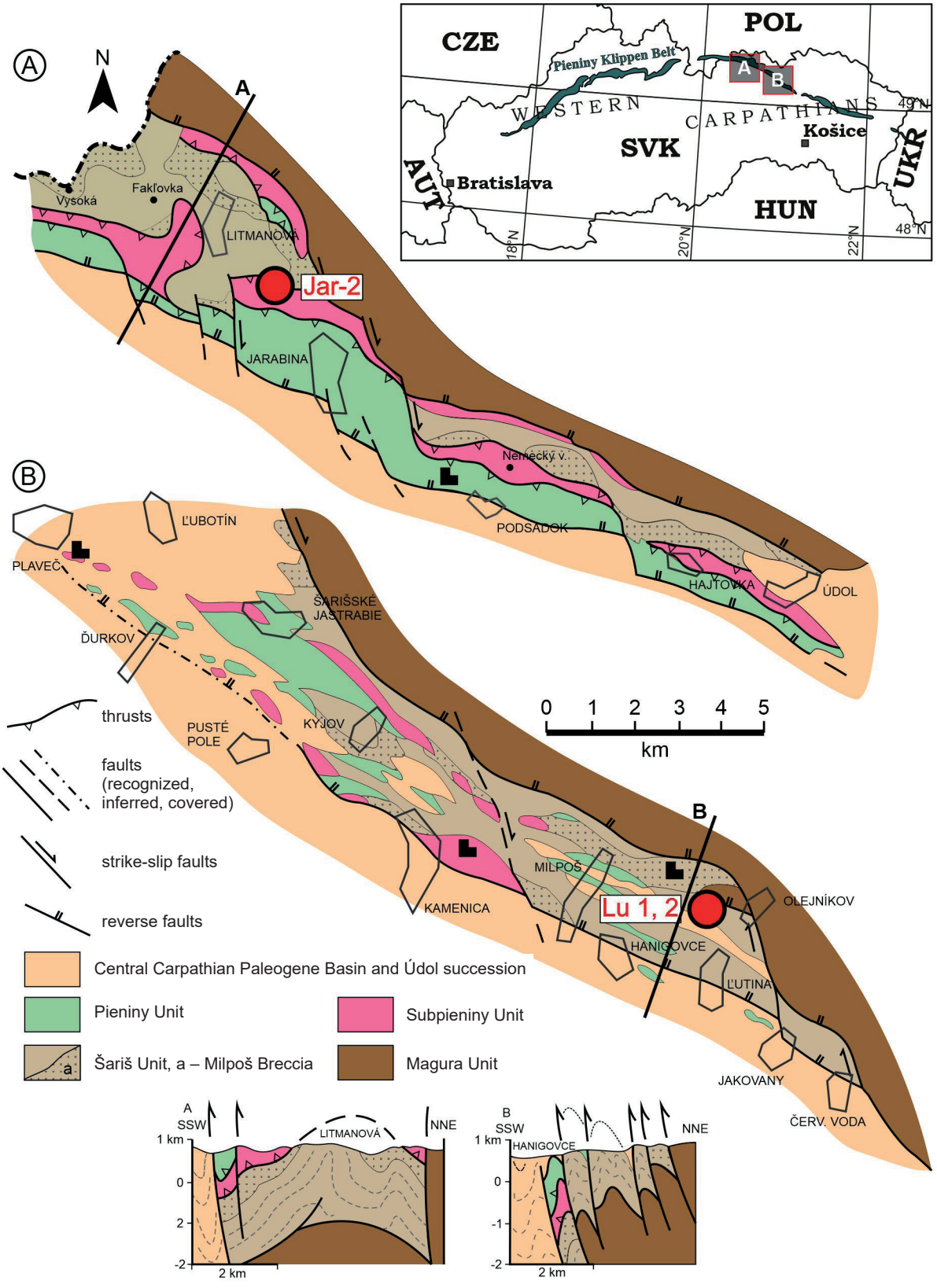


**Fig. 1.** Schematic tectonic maps of the eastern sector of the PKB between Litmanová and Červená Voda villages in eastern Slovakia with marked positions of the structural borehole Jar-2 and the studied outcrop near the village of Ľutina (modified according to Plašienka & Mikuš, 2010)

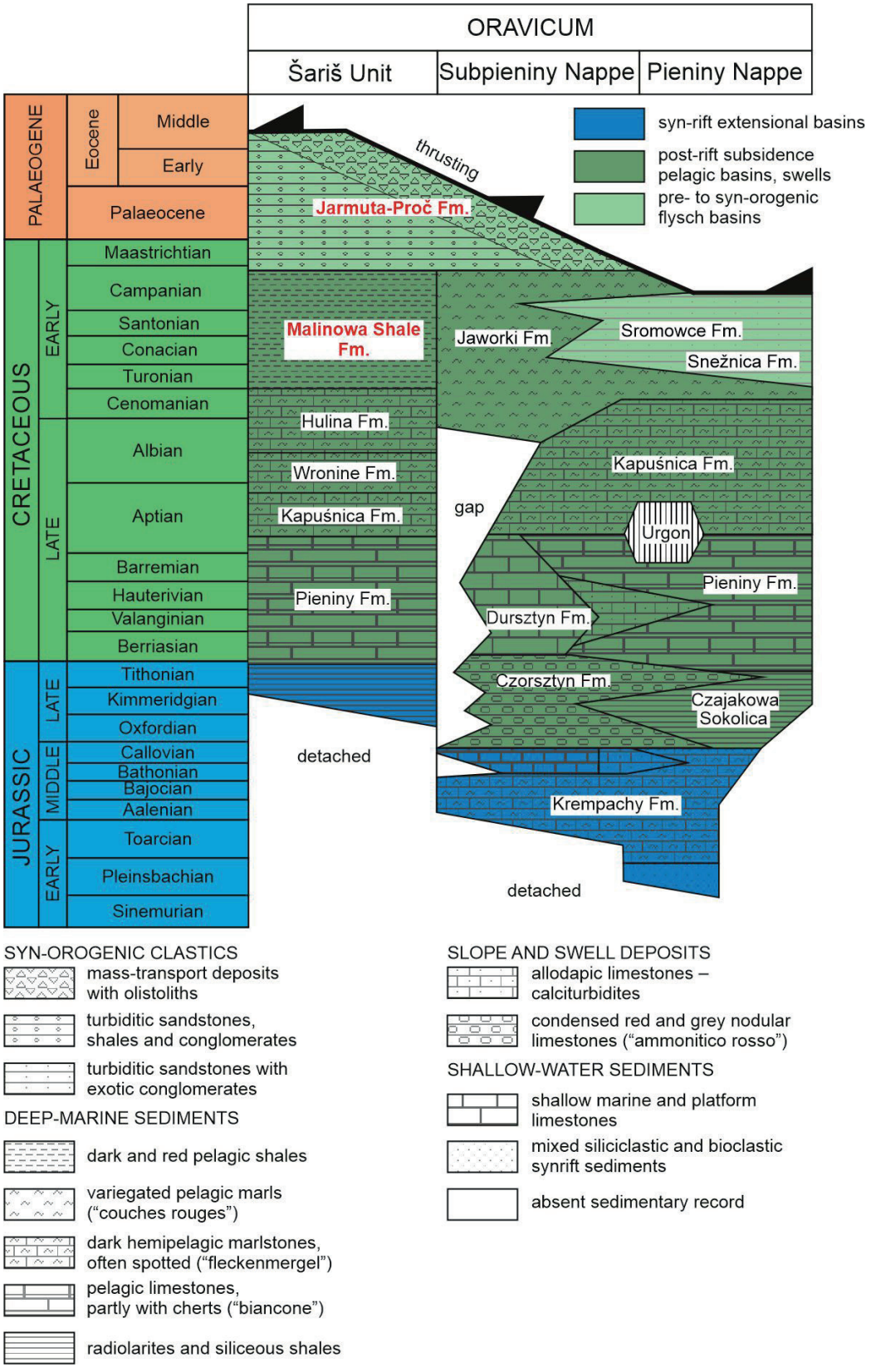


**Fig. 2.** Simplified lithostratigraphic column of the principal Oravic units of the Pieniny Klippen Belt (according to Plašienka, 2012a)

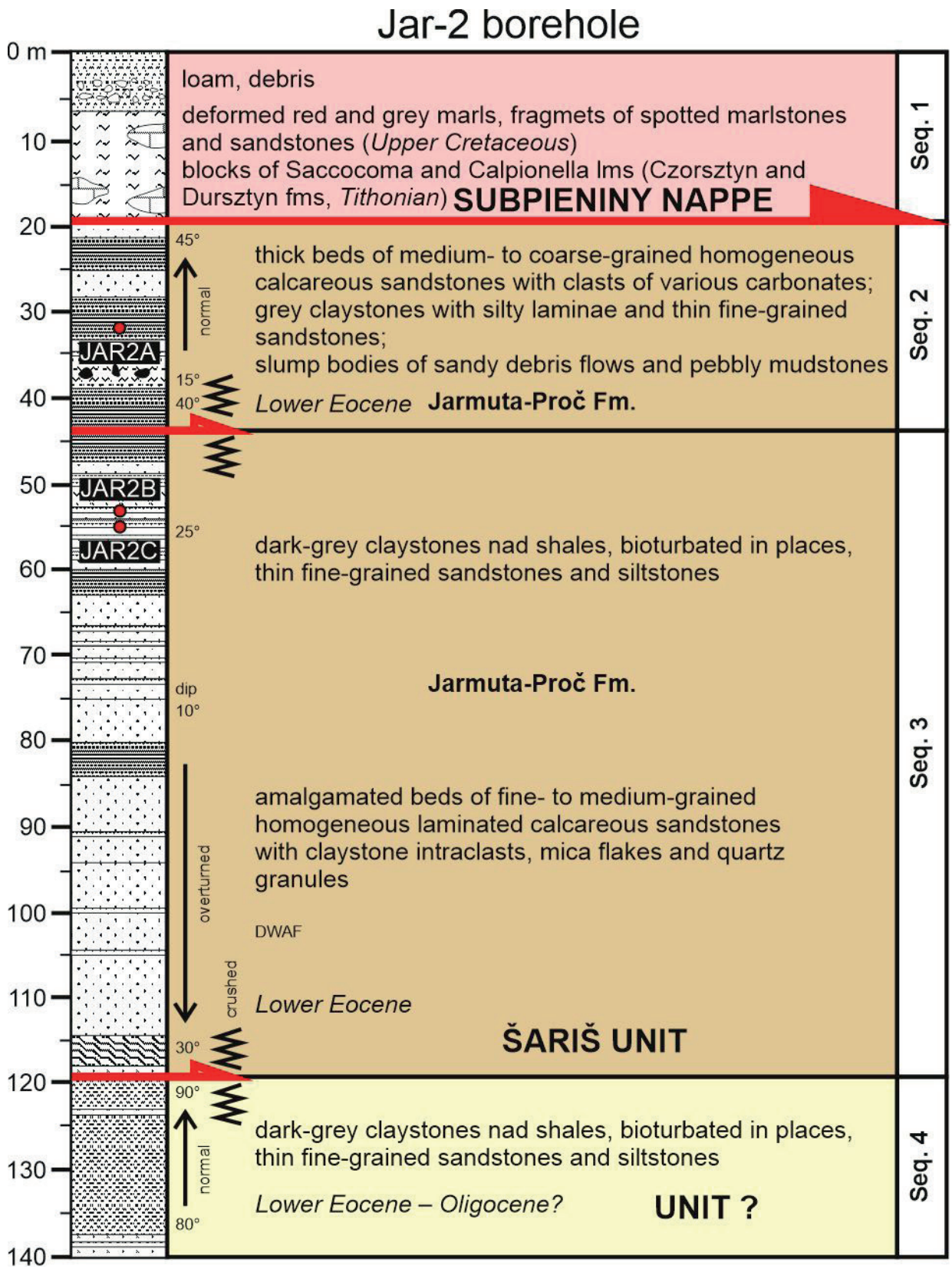


**Fig. 3.** Lithostratigraphic profile of the Jar-2 borehole, with the position of the samples taken for the heavy mineral analysis (modified after Plašienka et al., 2012)

clastic material derived dominantly from destroyed fronts of the advanced nappe stack (the Subpieniny and Pieniny thrust sheets).

## Sampling and Methods

The studied material comes from a natural outcrop of thin-bedded fine-grained sandstones of the hemipelagic Turonian-Campanian Malinowa Fm. (Fig. 1, Tab. 1) and from thin-bedded siltstones to fine- to medium-grained sandstones of the core material of the structural borehole Jar-2 (Tab. 1, Figs. 1, 3), that penetrated a turbiditic sequence of the Maastrichtian-Ypresian Jarmuta-Proč Fm. of the Šariš Unit (Plašienka et al., 2012). Two boreholes Jar-1 and Jar-2 were drilled in winter 2009 near the village of Jarabina in the Pieniny sector of the PKB in eastern Slovakia (Figs. 1, 3). The Jar-2 borehole, with a core diameter of 4 cm, was continuously drilled to the final depth of 140 m. The borehole penetrated strongly deformed and overturned imbrications of the sedimentary successions of the Subpieniny nappe and several sequences of the Middle to Upper Cretaceous-Lower Eocene synorogenic sediments of the Šariš Unit (Fig. 3) (for more details, see Plašienka et al., 2012). The core material is stored at the Geological repository and borehole core collections of the State Geological Institute of Dionýz Štúr in Bratislava (Slovakia).

The sandstone samples for heavy mineral analyses (at least 1 kg each, due to availability of the core material) were cleaned, crushed and sieved under 250 μm. Then the 63–125 μm fraction was soaked in 10 % diluted cold acetic acid for at least 24 hours to dissolve carbonate content. After acidic treatment the fraction was cleaned in an ultrasonic bath and dried in an oven. Such prepared fraction was ready for the heavy liquid separation in LST heavy liquid (2.85 g/cm$^3$) using a separating funnel. Associations of heavy minerals were studied under a petrographic microscope Zeiss Axiom Scope A.1 and a stereomicroscope Olympus SZ-61 in both transmitted and reflected light. At least 200 grains were counted using the ribbon counting method (Galehouse, 1971) and shown as number percentages (Tab. 2).

**Tab. 1**

List of samples for heavy mineral analysis, with their geographic coordinates, lithostratigraphy and position in the borehole Jar-2

| Sample | Locality | Lithostratigraphy | Lat | Lon | Note |
|---|---|---|---|---|---|
| **Jar-2a** | Jarabina, borehole Jar-2 | Jarmuta-Proč Fm. | 49.356583 | 20.638367 | depth 33.0–33.4 m |
| **Jar-2b** | Jarabina, borehole Jar-2 | Jarmuta-Proč Fm. | 49.356583 | 20.638367 | depth 52.5–52.7 m |
| **Jar-2c** | Jarabina, borehole Jar-2 | Jarmuta-Proč Fm. | 49.356583 | 20.638367 | depth 55.3 m |
| **Lu-5a** | Ľutina | Malinowa Fm. | 49.180861 | 21.042472 | outcrop |
| **Lu-5b** | Ľutina | Malinowa Fm. | 49.180861 | 21.042472 | outcrop |

**Tab. 2**

Frequencies of individual heavy minerals in the sandstones studied. Abbreviations of minerals (Whitney & Evans, 2010): Zrn – zircon, Tur – tourmaline, Rt – rutile, Grt – garnet, Spl – spinel, Ap – apatite, Cld – chloritoid, Ep – epidote, ZTR – zircon-tourmaline-rutile index, proportion of ultra-stable minerals (Hubert, 1962)

| Sample | Zrn | Tur | Rt | Grt | Spl | Ap | Cld | Ep | ZTR |
|---|---|---|---|---|---|---|---|---|---|
| **Jar-2A** | 1.0 | 26.9 | 8.5 | 36.3 | 0.5 | 24.9 | 1.0 | 1.0 | 36.3 |
| **Jar-2B** | 5.0 | 7.5 | 5.5 | 64.0 | 1.0 | 17.0 | 0.0 | 0.0 | 18.0 |
| **Jar-2C** | 5.4 | 5.9 | 7.9 | 69.0 | 1.0 | 10.8 | 0.0 | 0.0 | 19.2 |
| **Lu-5A** | 10.3 | 8.3 | 34.3 | 40.7 | 2.9 | 3.4 | 0.0 | 0.0 | 52.9 |
| **Lu-5B** | 12.5 | 2.5 | 22.5 | 59.0 | 3.0 | 0.5 | 0.0 | 0.0 | 37.5 |

Selected minerals including garnets, tourmalines and Cr-rich spinels were hand-picked, placed in an epoxy resin, polished and carbon coated for microprobe analyses. Chemical compositions of the selected minerals were analysed using a JEOL JXA-8530FE microprobe (Earth Science Institute of the Slovak Academy of Sciences, Banská Bystrica, Slovakia) under the following conditions: accelerating voltage 15 kV, sample current 20 nA, probe diameter 2–5 μm, counting time 10 s – peak and 5 s for background, ZAF correction. The standards used, including lines and detection limits (in ppm) were: Ca (Kα, 19–21) – diopside, Mn (Kα, 49–62) – rhodonite, Si (Kα, 45–50) – quartz, Mg (Kα, 35–37) – olivine, F (Kα, 112–294) – fluorite, Na (Kα, 31–36) – jadeite, Al (Kα, 38–40) – kyanite, K (Kα, 29–38) – orthoclase, Fe (Kα, 43–57) – hematite, Ti (Kα, 35–38) – rutile, Cr – (Kα, 71–130) – $Cr_2O_3$, Cl (Kα, 27–34) – tugtupite. The analyses of detrital garnets were normalized to 12 oxygens. The $Fe^{2+}/Fe^{3+}$ was calculated assuming full occupancy. The chemical formulae of detrital tourmalines were calculated based on 15 Y + Z + T cations, $^{W}O^{2-}$ was obtained from the charge-balanced formula and OH was calculated as OH = 4 – Cl – $^{W}$O apfu. $B_2O_3$ was calculated assuming 3.0 B apfu and $H_2O$ was calculated by considering OH + O + F + Cl apfu. The analyses of detrital Cr-rich spinels were calculated based on 3 cations and $Fe^{2+}$ and $Fe^{3+}$ were allocated according to the ideal stoichiometry.

## Results

### *Heavy mineral assemblages*

The dominant heavy mineral in the JAR-2A, B, C samples is garnet (36–69 %) followed by apatite (11–25 %), tourmaline (6–27 %), rutile (6–9 %) and zircon (1–5 %). Subordinate is Cr-rich spinel, epidote and chloritoid (~1 %). In the samples from the Malinowa Fm. garnet (41–59 %) and rutile (23–34 %) are dominant heavy minerals with lesser amount of ultra-stable zircon (10–13 %) and tourmaline (3–8 %). Compared to the samples of the Jarmuta-Proč Fm. the amount of Cr-rich spinel is slightly higher ~3 %, while apatite is much less present (1–3 %). The ZTR index (Hubert, 1962) indicates moderate maturity and is slightly higher in the samples from the Malinowa Fm. (Tab. 2).

Garnets occur mostly as subangular to subrounded grains showing extensive signs of corrosion. Corrosive features include etched facets and etch-pits. Ultra-stable zircon, tourmaline and rutile occur as angular to subrounded grains. Rounded grains were very rare. The ultra-stable minerals show initial to advanced corrosion, especially in tourmaline grains. Apatite is preserved in a form of short subhedral to subrounded grains with incipient signs of corrosion indicating their detrital origin. Cr-rich spinels represent angular to subrounded dark brown, red brown or almost black unaltered fragments. Sporadically preserved minerals such as epidote and chloritoid display advanced signs of corrosion.

### *Chemical composition of garnets*

Almandine-rich garnets with variable grossular, pyrope, and spessartine proportions dominate the examined garnet population in both formations (Fig. 4, Supplementary Tab. S1). Most of the analysed garnets lack inclusions or distinct optical zonation. In few cases inclusions of quartz were observed. The garnet population is slightly more diversified in the Jarmuta-Proč Fm. than in the Malinowa Fm., particularly with more variable grossular molecule proportions (Fig. 4). In the Jarmuta-Proč Fm. the almandine-pyrope garnets with low content of grossular and spessartine ($Alm_{69–85}$ $Prp_{10–25}$ $Grs_{<10}$, $Sps_{<10}$) are the most frequent. These garnets could originate in mica-schists, gneisses metamorphosed under amphibolite or transitional granulite to amphibolite facies conditions. The second group involves almandine-spessartine garnets with low pyrope and grossular molecules ($Alm_{72–77}$ $Sps_{10–40}$ $Prp_{6–14}$ $Grs_{<10}$). Such garnets might come from granitoids (Mange & Morton, 2007). The third group comprises garnets with higher grossular molecule and with variable pyrope and spessartine molecules ($Alm_{55–81}$ $Grs_{11–30}$ $Prp_{1–18}$ $Sps_{1–23}$). Their source rocks might be amphibolites.

In the Malinowa Fm., the almandine-pyrope and almandine-spessartine garnets are the most frequent garnets as well. Here, garnets with higher proportion of grossular can be divided into two groups either with high pyrope and low spessartine ($Alm_{59–73}$ $Grs_{10–20}$ $Prp_{14–27}$ $Sps_{<2}$) or with increased spessartine and low-pyrope molecule ($Alm_{57}$ $Grs_{26}$ $Sps_{12}$ $Prp_5$). The former could originate in more basic metamorphic rocks metamorphosed under higher amphibolite and/or transitional amphibolite to granulite facies conditions, the latter could come from gneisses or amphibolites metamorphosed under lower amphibolite facies conditions.

### *Chemical composition of tourmalines*

Analysed tourmalines display complex optical zoning (Fig. 5). Altogether 74 analyses, representing spot analyses placed in distinct optical zones were carried out to reveal possible changes in chemical compositions indicative of their evolution (Supplementary Tab. S2). Any obvious distinction in chemical compositions between the studied formations has been observed. Based on the dominant occupancy of the X site most of the tourmalines belong to the X-vacant group, less to the alkali group and few tourmalines belong to the calcic group (Fig. 6A). The X-vacant tourmalines have moderate number of vacancies and display magnesio-foititic to foititic compositions (Fig. 6B). The alkaline tourmalines have dravitic-schorlitic compositions (Fig. 6B, Supplementary Tab. S2). Two

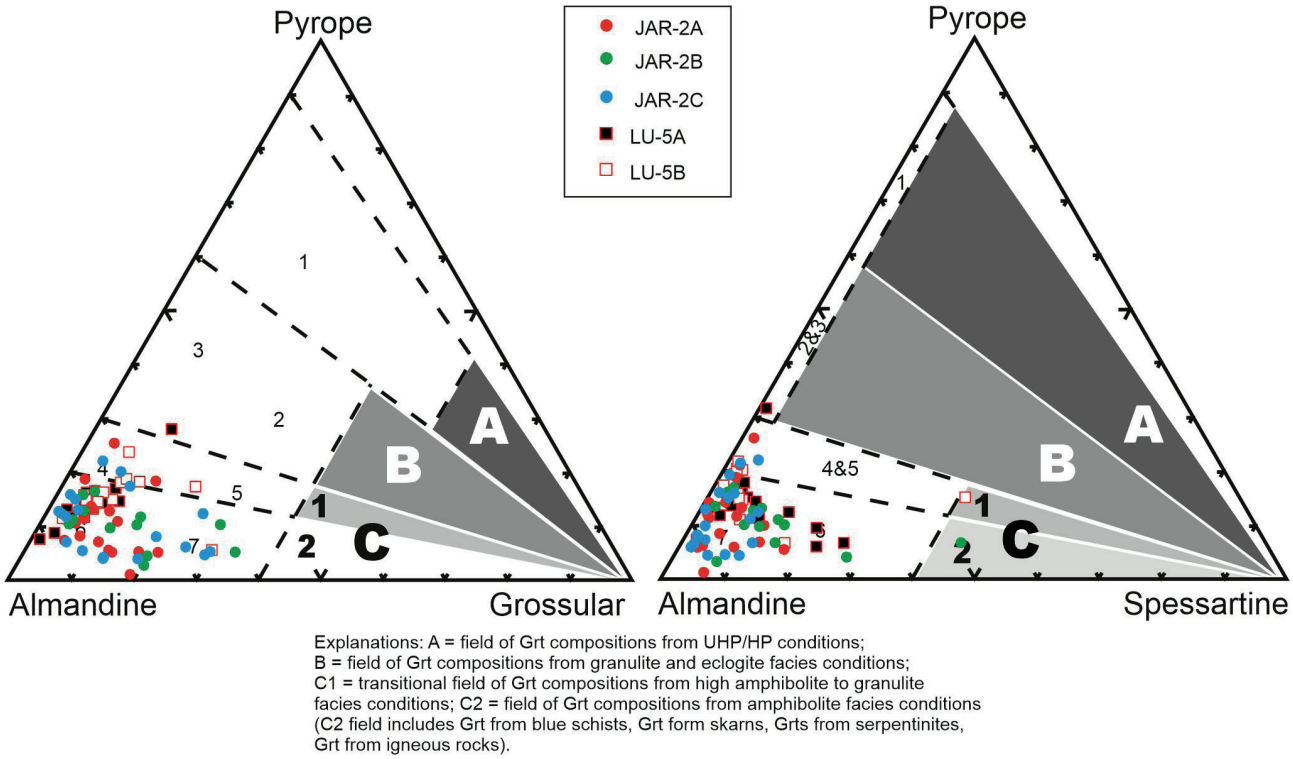


**Fig. 4.** Triangular pyrope-almandine-grossular and pyrope-almandine-spessartine discrimination diagrams for garnets (after Méres, 2008; Aubrecht et al., 2009)

calcic tourmalines show uvite to feruvite compositions (Fig. 6C). The magnesio-foititic and foititic tourmalines forms either cores of grains, oscillatory zones or optically distinct complex zones and rims (Fig. 5A, B, C, D, G). Some grains or zones of dravitic-schorlitic composition show fine complex intergrowths with quartz, which often overgrow the cores or zones of magnesio-foititic to foititic tourmalines (Fig. 5B, D, E). Zones of dravitic-schorlitic compositions contain abundant mineral inclusions represented by quartz, rutile, zircon, monazite, ilmenite, apatite, allanite, albite and Fe-oxides (Fig. 5B, D, E). Some of the tourmaline grains with distinct optical zonations do not show compositional variations (Fig. 5F, G).

Sources of the analysed tourmalines represent mostly metasedimentary rocks both coexisting and not coexisting with Al-saturation phase and iron-rich quartz-tourmaline, calc-silicate rocks and metapelites (Fig. 7A). Lesser number of tourmalines could originate also in Li-poor granitoids and associated pegmatites and aplites. In the $Fe_{tot}$-Mg-Ca diagram (Henry & Guidotti, 1985) the analysed tourmalines plot mostly in the fields of Ca-poor metasedimentary rocks, less in the field of Li-poor granitoids and related pegmatites and aplites (Fig. 7B).

### *Chemical composition of Cr-rich spinels*

In total, 26 detrital Cr-rich spinels were analysed (Supplementary Tab. S3). The analysed Cr-rich spinels do not show signs of alteration or zonation (Fig. 5). The $Al_2O_3$ content vary in the samples from the Jarmuta-Proč Fm. in the narrow range 22.31 to 26.87 wt % and $TiO_2$ content is very low < 0.11 wt % (Fig. 8A). In the samples from the Malinowa Fm., the $Al_2O_3$ and $TiO_2$ contents are more variable in the range 6.04 to 39.10 and < 0.41 wt %, respectively (Fig. 8A). Only few spinel grains from the Malinowa Fm. have the $TiO_2$ concentrations higher than 0.2 wt % (Fig. 8A), which point to their origin in volcanic rocks (Lenaz et al., 2000; Kamenetsky et al., 2001). The volcanic spinels correspond mostly to the compositions of arc and/or back-arc basin basalts (Fig. 8A). Rare inclusions observed in the volcanic spinels consist of clinopyroxene with diopside composition (Supplementary Tab. S4).

Almost all analysed Cr-rich spinels in both formations have the $Fe^{2+}/Fe^{3+}$ ratio higher than 4, what is characteristic for mantle peridotites (Lenaz et al., 2000; Kamenetsky et al., 2001). Analysis of occasional mineral inclusions in the Cr-rich spinels from peridotites showed that they consist of orthopyroxene with composition of Mg-rich enstatite end-member (Supplementary Tab. S4). The Cr# and Mg# in the samples from the Jarmuta-Proč Fm. were ~0.5 and ~0.6, respectively. In the Malinowa Fm., the Cr# and Mg# vary between 0.32 to 0.87 and 0.35 to 0.69, respectively. In the Cr# vs. Mg# diagram (Pober & Faupl, 1988), the analysed Cr-rich spinels best match the harzburgite field and/or podiform chromitite field (Fig. 8B).

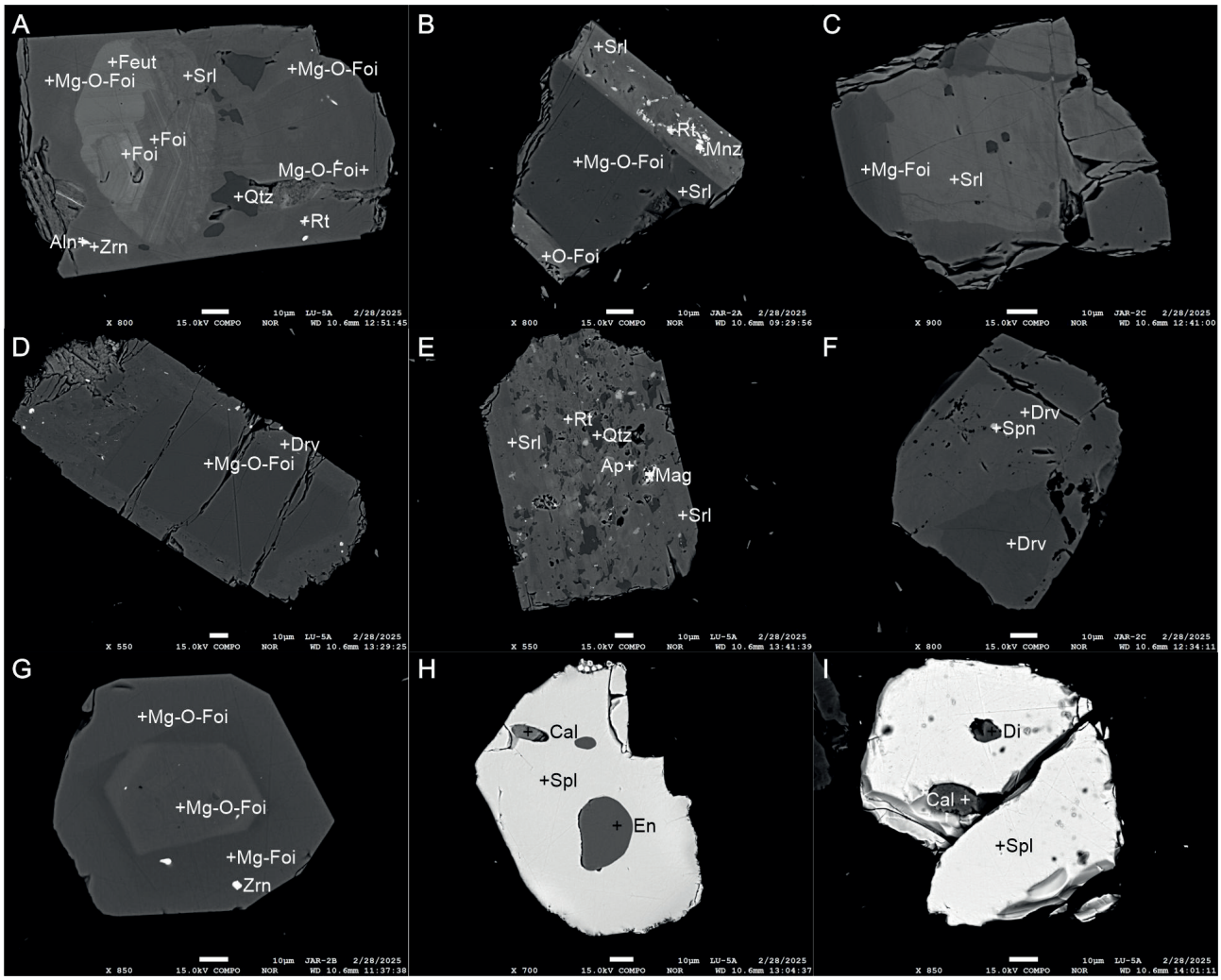


**Fig. 5.** BSE images of the analysed detrital tourmalines (A – G) and Cr-rich spinels (H, I). The tourmalines show distinct optical zoning often with contrasting chemistry. The Cr-rich spinels, either of peridotitic (H) or volcanic origin (I), show no signs of alteration or zonations. Abbreviations after (Whitney & Evans, 2010) except for tourmaline species where: Foi – foitite, Feut – feruvite; Mg-O-Foi – "magnesio-oxy-foitite"; Fe-O-Foi – "oxy-foitite"

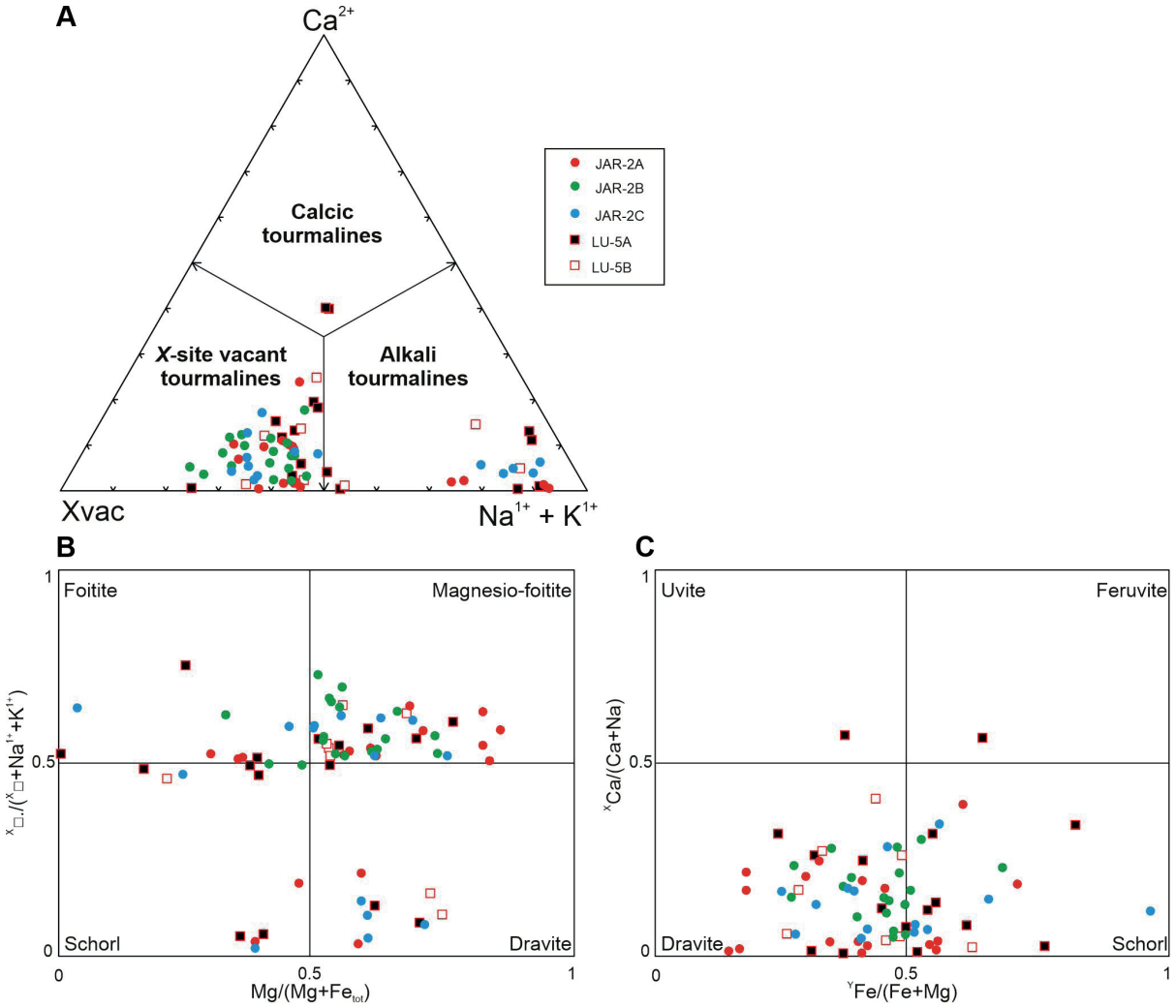


**Fig. 6.** A) Ternary system for the primary tourmaline groups based on the dominant occupancy of the X site; B) binary classification diagram for establishing the appropriate tourmaline subgroups in the alkali and X-vacant groups; C) binary classification diagram for establishing the appropriate tourmaline subgroups in the calcic group (according to Henry et al., 2011)

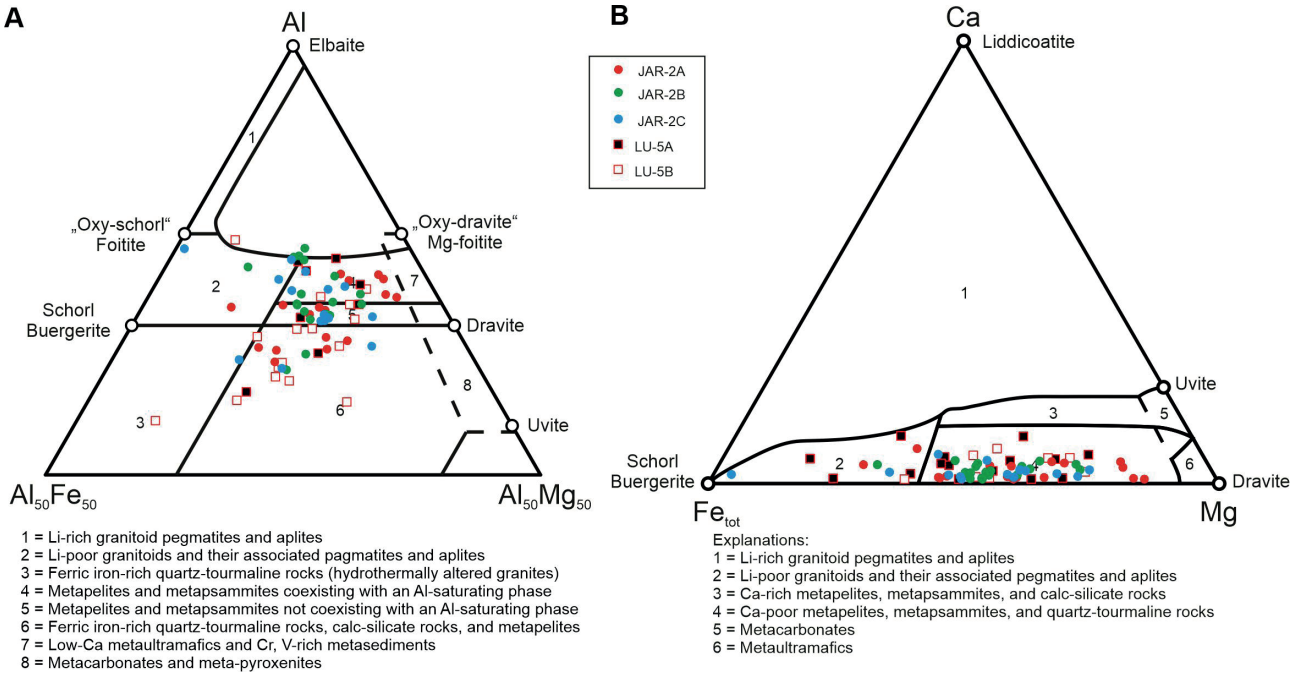


**Fig. 7.** Triangular Al-$Al_{50}Fe_{50}$-$Al_{50}Mg_{50}$ diagram in A) and Ca-$Fe_{tot}$-Mg diagram in B) (in molar proportions) discriminating tourmalines originated in various rock types (after Henry & Guidotti, 1985)

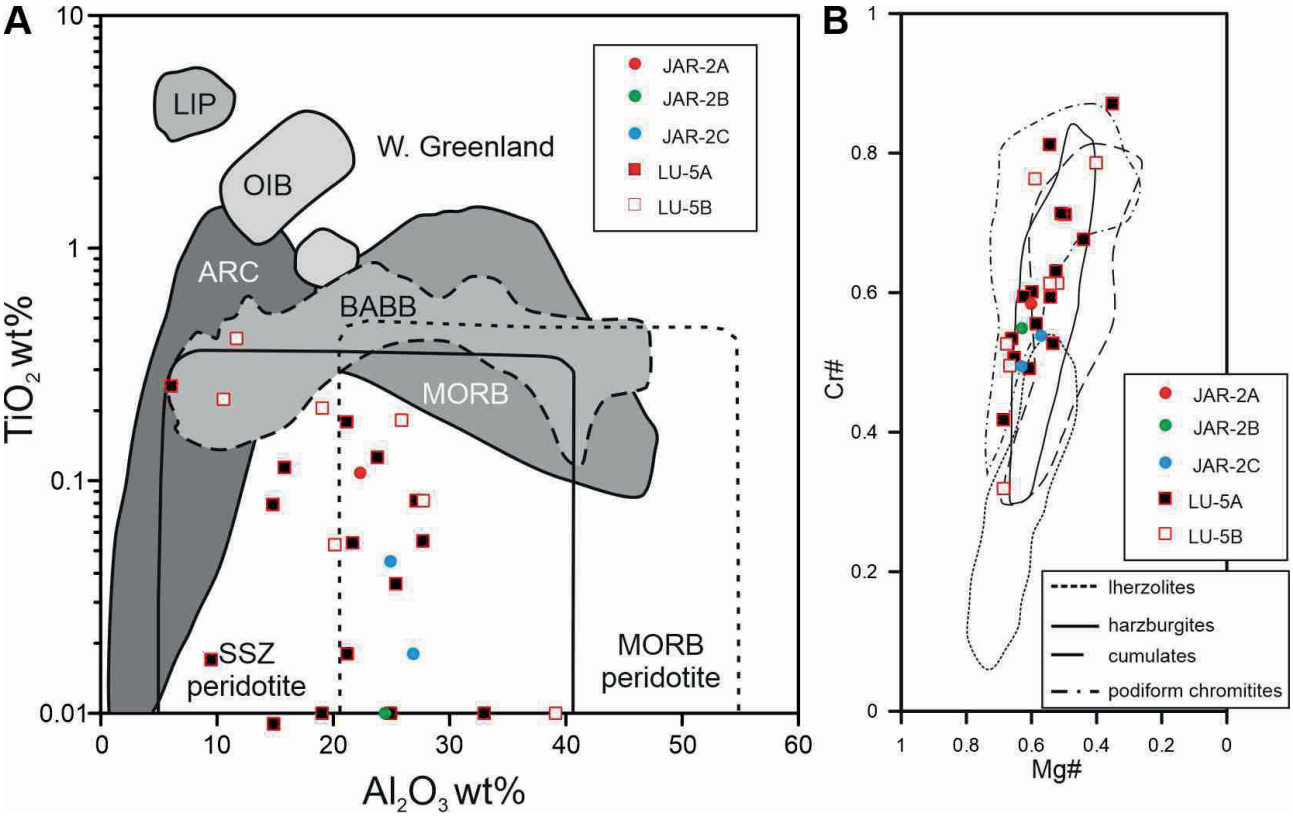


**Fig. 8.** A) The $Al_2O_3$ vs. $TiO_2$ diagram with Cr-rich spinel discrimination fields (after Kamenetsky et al., 2001). Explanations: SSZ = supra-subduction zone, MORB = mid-ocean ridge basalts, BABB = back-arc basin basalts, ARC = island-arc magmas, OIB = ocean-island basalts, LIP = large igneous province. B) The Cr# versus Mg# diagram for Cr-rich spinels (Pober & Faupl, 1988)

## Discussion

### *Provenance of garnets*

Garnet is the most frequent heavy mineral in both studied formations (Tab. 2). It fits the reported increasing garnet contents in the Upper Cretaceous to Lower Eocene synorogenic deposits of the PKB (Salata, 2004; Oszczypko & Salata, 2005; Aubrecht et al., 2009, 2020a, 2021; Bónová et al., 2018; Madzin et al., 2019). The increasing trend has been attributed to a new influx of garnets and associated heavy minerals, especially apatite and rutile, from continental metamorphic and magmatic rocks (Aubrecht et al., 2021). Chemical analyses of detrital garnets showed that almandine-rich garnets prevail. The garnet population is slightly more diverse in the Jarmuta-Proč Fm. than in the Malinowa Fm., which might indeed reflect the new input of garnets from medium-grade basic metamorphic rocks during the latest Cretaceous. Almandine is the most frequent garnet type observed in the Upper Cretaceous to Lower Eocene clastic formations throughout the PKB (Salata, 2004; Oszczypko & Salata, 2005; Aubrecht et al., 2009, 2020a, 2021; Bónová et al., 2018; Madzin et al., 2019). Garnets with high content of pyrope molecule ($Prp_{>30}$), derived from eclogites or mafic granulites, reported from the Jarmuta-Proč Fm. of the more eastern part of the PKB (Madzin et al., 2019) or from the Turonian Snežnica Fm. of the Kysuca (Pieniny) Unit of the Orava sector (Aubrecht et al., 2021) were not observed in our examined material. The analysed garnets were derived mostly from low- to mid-/high-grade polymetamorphic terrains. Some of the almandine-rich garnets could also come from granitoid rocks (cf. Oszczypko & Salata, 2005; Bónová et al., 2018; Madzin et al., 2019).

The almandine garnets with the low pyrope, higher grossular and variable spessartine molecule proportions ($Alm_{>55}$ $Grs_{12–30}Prp_{<5}Sps_{1–24}$) are similar to almandine-dominated garnets described recently from a blueschist-facies metabasite pebble of the Albian-Cenomanian exotics-bearing conglomerates of the Peri-Klippen Klape Unit and from the HP/LT metamorphosed Bôrka Nappe of the Meliata Unit (Putiš et al., 2023). The dating revealed their almost identical Late Jurassic Lu-Hf garnet ages of 152.1 ± 1.5 Ma and 153.95 ± 0.69 Ma, respectively, and comparable P-T metamorphic conditions (Putiš et al., 2023). Accordingly, a part of the detrital garnets might have been derived from the Meliata Unit originally deposited in mid-Cretaceous flysch of the Fatric Klape or analogous units and then resedimented into the Upper Cretaceous to Eocene Jarmuta-Proč Fm. (see e.g., Plašienka et al., 2019).

### *Provenance of tourmalines*

Detrital tourmalines represent one of the most frequent transparent heavy minerals in the Upper Cretaceous to Lower Eocene flysch deposits of the PKB and neighbouring Peri-Klippen Zone (Oszczypko & Salata, 2005; Bellová et al., 2018; Bónová et al., 2018; Madzin et al., 2019; Aubrecht et al., 2020a, 2020b, 2021; Madzin & Plašienka, 2022). The presented chemical compositions of detrital tourmalines from the Malinowa and Jarmuta-Proč Fms. reveal their derivation mostly from low- to medium-grade metamorphic rocks and to a lesser extent also from granitoid rocks (Fig. 7). Distinct optical zoning with very often contrasting chemistry points to a complex polymetamorphic history of the analysed tourmalines. Recently, heavy mineral analyses of the mid- to Late Cretaceous exotics-bearing formations of the Central Western Carpathians (CWC) and PKB revealed considerable amounts of complex-zoned tourmalines that could have been derived from decompressed (exhumed) HP/LT ultramafic rocks of the Meliata ophiolite-bearing complexes (Bellová et al., 2018; Plašienka et al., 2019; Aubrecht et al., 2020a, 2020b, 2021). The poikiloblastic "mosaic" tourmalines with obvious bosiite trend (Bačík et al., 2018; Aubrecht et al., 2020b) have not been observed in our sampled material, but similar complex-zoned magnesio-foititic to foititic and schorlitic-dravitic tourmalines with fine intergrowth with quartz and abundant mineral inclusions represent the dominant types in the deposits studied (Fig. 5). Such magnesio-foititic to foititic tourmalines have not been detected in the previous heavy mineral studies of the Jarmuta-Proč Fm., where optically zoned tourmalines show only dravitic-schorlitic compositions (Oszczypko & Salata, 2005; Madzin et al., 2019). Similar magnesio-foititic to foititic tourmalines were recently found also in the Upper Cretaceous-Paleocene turbiditic deposits of the Pupov Fm. from the Peri-Klippen Zone of the Kysuca sector of the PKB (Madzin & Plašienka, 2022). The magnesio-foititic to foititic tourmalines are quite unusual, however their primary occurrences have already been described from the CWC in alpine-type hydrothermal veins cutting the crystalline basement rocks of the Tatric (Uher et al., 2009) and Gemeric units (Bačík et al., 2017, 2018). The distribution of the hydrothermal veins has been, however, considered to be limited as an important regional source for the complex-zoned tourmalines (Aubrecht et al., 2020a, 2020b). More probably, the complex-zoned tourmalines might come from the HP/LT ultramafic rocks of the Meliata ophiolite-bearing complexes (Bellová et al., 2018; Aubrecht et al., 2020a, 2020b; Plašienka et al., 2019). The apparent controversy related to their presence in the flysch formations deposited on the other (external) side of the orogenic belt and their derivation from the distant southern Western Carpathian zones can be explained by a multiple recycling model as proposed for the derivation of ophiolitic debris in the Cretaceous to Paleogene flysch formations of the CWC and PKB (Plašienka, 2012a and references therein). The Meliata

ophiolite-bearing complexes were exposed to erosion during the Lower Cretaceous in the southern Western Carpathian zones and the ophiolitic debris together with the "exotic" pebble material was primarily deposited in the Albian-Cenomanian flysch deposits of the Poruba Fm. in the Fatric Zliechov Basin (Plašienka, 1995a, 1995b, 1996; Plašienka, 2012a). The Poruba Fm. was, as a part of the Fatric nappe system, emplaced during the Late Turonian into a false accretionary wedge position behind the outer Tatric margin, thereby becoming a part of the Klape Unit in the Peri-Klippen Zone (Plašienka, 1995a, 1995b, 1996, 2012a; Prokešová et al., 2012; Plašienka et al., 2019). In such way, the mid-Cretaceous flysch formations of the Klape Unit, already incorporated into the developing accretionary wedge, could form the "proximal" source of ophiolitic debris and complex-zoned tourmalines for still younger synorogenic deposits in the foredeep basins of the PKB and adjoining zones (Plašienka, 2012a; Plašienka & Soták, 2015; Plašienka et al., 2019; Madzin & Plašienka, 2022). The poor roundness of tourmaline grains may intuitively look contradictory to their supposed recycled origin in the parental Klape/Poruba flysch formations. However, tourmaline represents one of the ultra-high stable minerals, which can survive multiple sedimentary cycles (Hubert, 1962; Morton & Hallsworth, 1999, 2007), and unlike to pebbles in gravel, which are prone to rounding, abrasion of psammitic fraction is a very slow and ineffective process during transport in aqueous conditions (e.g., Garzanti, 2017).

### *Provenance of Cr-rich spinels*

Significant amounts of Cr-rich spinels with decreasing-upward trend were found in the Upper Cretaceous to Lower Eocene flysch deposits of the PKB (Winkler & Ślączka, 1992, 1994; Salata, 2004; Oszczypko & Salata, 2005; Bónová et al., 2018; Madzin et al., 2019; Aubrecht et al., 2009, 2020a, 2021). Comparison of Cr-rich spinel contents between the Turonian-Campanian Malinowa Fm. of the Šariš Unit and contemporaneous Turonian-Santonian Snežnica and Sromowce Fms. of the Kysuca (Pieniny) Unit (Aubrecht et al., 2021) shows the obvious depletion of ophiolitic debris in the former. It might be attributed to a more distal position of the Šariš Basin, where the Malinowa Fm. was deposited, compared to a proximal position of the Pieniny Basin, where turbiditic sandstones and conglomerates of the Snežnica and Sromowce Fms. received large amounts of ophiolitic debris and polymict pebble material during the Late Cretaceous (cf. Plašienka, 2012a).

The chemical compositions of the analysed Cr-rich spinels point to their origin predominantly in supra-subduction zone peridotites of harzburgitic composition and sporadically also in volcanic rocks (cf. Oszczypko & Salata, 2005; Aubrecht et al., 2009, 2020a, 2021; Bónová et al., 2018; Madzin et al., 2019). The source of the ophiolitic detritus in the Upper Cretaceous clastic deposits of the PKB has been generally considered to be the same as for the material of the exotics-bearing Albian-Cenomanian conglomerates of the Klape Unit (Mišík & Marschalko, 1988; Dal Piaz et al., 1995; Kissová et al., 2005; Aubrecht et al., 2009; Plašienka, 2012a). Although, the origin, paleogeographic position and interpretation of the Klape Unit is a subject of decades-lasting debates, there exists a consensus, that the ophiolitic detritus comes from the Neotethyan Meliata ophiolite-bearing complexes situated in the southern Western Carpathian zones (for comprehensive review see recent works by Aubrecht et al., 2009; Plašienka, 2012a; Bellová et al., 2018; Plašienka et al., 2019; Aubrecht, et al., 2020a, 2020b, 2021). Interestingly, Cr-rich spinels from serpentinized peridotite bodies of the Meliata ophiolite-bearing complexes show mostly lherzolitic composition (Mikuš & Spišiak, 2007). In contrast, detrital Cr-rich spinels from harzburgitic sources dominate in the Upper Jurassic to Cretaceous synorogenic formations throughout the whole Alpine-Carpathian-Dinaridic orogenic system (Pober & Faupl, 1988; Mikes et al., 2008; Lužar-Oberiter et al., 2009; Gawlick et al., 2015; Bellová et al., 2018; Aubrecht et al., 2020a). The source of harzburgitic Cr-rich spinels has been interpreted to be in obducted Jurassic Neotethyan ophiolites predominantly of harzburgitic composition (Gawlick et al., 2015, 2020), situated in a higher nappe position over the older almost completely subducted Triassic Neotethyan ocean floor predominantly of lherzolitic composition (e.g., Bortolotti et al., 2013). The ophiolitic nappe stack is however missing in the Western Carpathians and its existence may be witnessed only in polygenetic ophiolite-bearing mélanges (Plašienka et al., 2019; Molčan Matejová et al., 2025), while pure ophiolitic mélanges below overriding ophiolite nappes are well-preserved in the Dinaric-Hellenic orogenic belt (e.g., Gawlick & Missoni, 2019 and references therein).

The original concept assumed the source of the exotic material in an exotic ridge, known as the Pieniny or the Andrusov Ridge (Mišík & Sýkora, 1981; Birkenmajer, 1988; Mišík & Marschalko, 1988). The Andrusov Ridge should have been situated between the Oravic-Vahic sedimentary realm and the CWC domain and was interpreted as an accretionary wedge, formed by the subduction of the South Penninic Vahic Ocean (in sense of Maheľ, 1981, 1989; Birkenmajer, 1988). However, the age and composition of the exotic conglomerates, dominantly of "southern" Meliata-related origin, is inconsistent with the Upper Jurassic to Lower Cretaceous structural, magmatic and sedimentary record from the external Tatric margin (Plašienka, 1995a, 1995b, 1996, 2012a). Consequently, the Klape flysch formations were interpreted to be an analogue to the Albian-Cenomanian

Poruba flysch formations of the Tatric and Fatric units of the CWC, situated in a false accretionary wedge position where they formed the source of ophiolitic debris recycled to younger sediments of the foreland basins of the PKB (as described in *Provenance of tourmalines* section above) (Plašienka, 1995a, 1995b, 1996, 2012a; Plašienka et al., 2019). The high vs low Cr-rich spinel content in proximal vs distal Turonian-Campanian deposits of the Pieniny and Šariš Basins, respectively, might support the multiple recycling model as well.

Another model explaining how the Meliata ophiolite-bearing complexes could become the source for the ophiolitic debris and exotic conglomerates of the PKB (Aubrecht et al., 2009; Bellová et al., 2018; Aubrecht et al., 2020a). In this model, the Oravic crustal segment originally formed a lateral continuation of the CWC, and both units were situated north of the Meliata oceanic realm (e.g., Michalík, 1994; Aubrecht et al., 2009). After the closure of the Meliata Ocean in the Late Jurassic, the Meliata suture zone was welded to the southern (internal) parts of both the CWC and Oravic segment. Later during the Cretaceous, the Meliata ophiolite complex was secondarily doubled by a left-lateral shift of the Oravic crustal segment along the northern (external) margin of the CWC block due to its clockwise rotation (Aubrecht & Túnyi, 2001). A long-lived elevation, the Andrusov Ridge, formed within a complex shear zone between the two rotated crustal segments (e.g., Rakús & Marschalko, 1997; Marschalko & Rakús, 1997). In this way, the Andrusov Ridge could feed the Cretaceous clastic formations of both the CWC and PKB units with pebble material and ophiolitic detritus for a long time (Aubrecht et al., 2009, 2020a; Bellová et al., 2018). However, structural arguments for such movements of the Oravic segment have not yet been presented and the new paleomagnetic data proved that the large clockwise rotation of the CWC block is younger than the Late Turonian-Santonian (Grabowski, 2000; Márton et al., 2020; Madzin et al., 2026).

## Conclusions

The heavy mineral analysis and detrital garnet, tourmaline and Cr-rich spinel chemical compositions from fine-grained turbiditic sandstones of the Maastrichtian-Ypresian Jarmuta-Proč Fm. (samples from the borehole Jar-2) and from fine-grained sandstones of the hemipelagic Turonian-Campanian Malinowa Fm. (samples from outcrop) of the Šariš Unit of the Pieniny Klippen Belt in eastern Slovakia showed that:

1. Almandine-rich garnets with variable grossular, pyrope, and spessartine proportions dominate the examined garnet population in both formations. The analysed garnets were derived mostly from low- to medium/high-grade polymetamorphic terrains. The slightly more diverse garnet population of the Jarmuta-Proč Fm. might reflect a new input of garnets from medium-grade, prevailingly basic metamorphic rocks during the latest Cretaceous. Some of the almandine-rich garnets could come from granitoid rocks.
2. Distinct optical zoning with very often contrasting chemistry point to a complex polymetamorphic history of the analysed tourmalines. The unusual complex-zoned tourmalines are represented mostly by X-vacant magnesio-foititic to foititic and schorlitic-dravitic tourmalines with fine intergrowths with quartz and abundant mineral inclusions.
3. Most of the analysed Cr-rich spinels in both studied formations show chemistry typical for supra-subduction zone peridotites. Sporadic volcanic spinels correspond to the compositions of arc and/or back-arc basin basalts.
4. The chemistry of the Cr-rich spinels and complex-zoned tourmalines supports their common provenance in the Meliata ophiolite-bearing complexes of the internal Western Carpathian zones.
5. The decreasing-upward Cr-rich spinel contents in the Upper Cretaceous to Lower Eocene flysch deposits of the PKB is evident. A multiple recycling model in which the Klape flysch formations situated in a false accretionary wedge position formed the "proximal" source of ophiolitic debris recycled to the younger flysch formations of the foreland basins is advocated.

**Acknowledgements**

This study was financially supported by projects APVV-20-0079, 21-0281, Vega 2/0013/20, 2/0171/24, 2/0012/24, 1/0021/25. Tomáš Mikuš and Sergii Kurylo are appreciated for their help during EMPA analyses. The authors are grateful to reviewers and the editor for comments and suggestions, which helped to improve the paper.

## References

Aubrecht, R. & Túnyi, I., 2001: Original orientation of neptunian dykes in the Pieniny Klippen Belt (Western Carpathians): the first results. *Contributions to Geophysics and Geodesy*, 31, 3, 557–578.

Aubrecht, R., Méres, Š., Sýkora, M. & Mikuš, T., 2009: Provenance of the detrital garnets and spinels from the Albian sediments of the Czorsztyn Unit (Pieniny Klippen Belt, Western Carpathians, Slovakia*). Geologica Carpathica*, 60, 463–483.

Aubrecht, R., Bellová, S. & Mikuš, T., 2020a: Provenance of Albian to Cenomanian exotics-bearing turbidites in the Western Carpathians: a heavy mineral analysis. *Geological Quarterly*, 64, 3, 658–680.

Aubrecht, R., Bačík, P., Mikuš, T. & Bellová, S., 2020b: Detritic tourmalines with complex zonation in the Cretaceous

exotic flysches of the Western Carpathians: Where did they come from? *Lithos*, 362–363, 105443.

Aubrecht, R., Mikuš, T. & Holický, I., 2021: Heavy mineral analysis of the Turonian to Maastrichtian exotics-bearing deposits in the Western Carpathians: What has changed after the Albian and Cenomanian? *Geologica Carpathica*, 72, 505–528.

Bačík, P., Dikej, J., Fridrichová, J., Miglierini, M. & Števko, M., 2017: Chemical composition and evolution of tourmaline-supergroup minerals from the Sb hydrothermal veins in Rožňava area, Western Carpathians. Slovakia. *Mineralogy and Petrology*, 111, 609–624.

Bačík, P., Uher, P., Dikej, J. & Puškelová, Ľ., 2018: Tourmalines from the siderite-quartz-sulphide hydrothermal veins, Gemeric unit, western Carpathians, Slovakia: crystal chemistry and evolution. *Mineralogy and Petrology*, 112, 45–63.

Bellová, S., Aubrecht, R. & Mikuš, T., 2018: First results of systematic provenance analysis of the heavy mineral assemblages from the Albian to Cenomanian exotic flysch deposits of the Klape Unit, Tatricum, Fatricum and some adjacent units. *Acta Geologica Slovaca*, 10, 1, 45–64.

Birkenmajer, K., 1977: Jurassic and Cretaceous lithostratigraphic units of the Pieniny Klippen Belt, Carpathians, Poland. *Studia Geologica Polonica*, 45, 1–158.

Birkenmajer, K., 1986: Stages of structural evolution of the Pieniny Klippen Belt, Carpathians. *Studia Geologica Polonica*, 88, 7–32.

Birkenmajer, K., 1988: Exotic Andrusov Ridge: its role in plate--tectonic evolution of the West Carpathian foldbelt. *Studia Geologica Polonica,* 41, 7–37.

Bortolotti, V., Chiari, M., Marroni, M., Pandolfi, L., Principi, G. & Saccani, E., 2013: Geodynamic evolution of ophiolites from Albania and Greece (Dinaric-Hellenic belt): one, two, or more oceanic basins? *International Journal of Earth Sciences*, 102, 783–811. https://doi.org/10.1007/s00531-012-0835-7.

Bónová, K., Mikuš, T. & Bóna, J., 2018: Is Cr-spinel geochemistry enough for solving the provenance dilemma? Case study from the Palaeogene sandstones of the Western Carpathians (eastern Slovakia). *Minerals*, 8, 543. https://doi.org/10.3390/min8120543.

Dal Piaz, G. V., Martin, S., Villa, M. I., Gosso, G. & Marschalko, R., 1995: Late Jurassic blueschist pebbles from the Western Carpathian orogenic wedge and paleostructural implications for Western Tethys evolution. *Tectonics*, 14, 4, 8974–885.

Galehouse, J. S., 1971: Point counting. In: Carver, R. E. (ed.): Procedures in Sedimentary Petrology. *New York, Wiley InterScience*, 385–407.

Garzanti, E., 2017: The maturity myth in sedimentology and provenance analysis. *Journal of Sedimentary Research*, 87, 353–365. https://doi.org/10.2110/jsr.2017.17.

Gawlick, H.-J. & Missoni, S., 2019: Middle-Late Jurassic sedimentary mélange formation related to ophiolite obduction in the Alpine-Carpathian-Dinaridic Mountain Range. *Gondwana Research*, 74, 144–172. https://doi.org/10.1016/j.gr.2019.03.003.

Gawlick, H.-J., Aubrecht, R., Schlagintweit, F., Missoni, S. & Plašienka, D., 2015: Ophiolitic detritus in Kimmeridgian resedimented limestones and its provenance from an eroded obducted ophiolitic nappe stack south of the Northern Calcareous Alps (Austria). *Geologica Carpathica*, 66, 6, 473–487.

Gawlick, H.-J., Sudar, M., Missoni, S., Aubrecht, R., Schlagintweit, F., Jovanović, D. & Mikuš, T., 2020: Formation of a Late Jurassic carbonate platform on top of the obducted Dinaridic ophiolites deduced from the analysis of carbonate pebbles and ophiolitic detritus in southwestern Serbia. *International Journal of Earth Sciences*, 109, 2023–2048. https://doi.org/10.1007/s00531-020-01886-w.

Golonka, J., Krobicki, M., Waśkowska, A., Cieszkowski, M. & Ślączka, A., 2015: Olistostromes of the Pieniny Klippen Belt, Northern Carpathians. *Geological Magazine*, 152, 269–86.

Grabowski, J., 2000: Palaeo- and rock magnetism of Mesozoic carbonate rocks in the Sub-Tatric series (Central West Carpathians) – palaeotectonic implications. *Polish Geological Institute, Special Papers*, 5, 1–88.

Henry, D. J. & Guidotti, C. V., 1985: Tourmaline as a petrogenetic indicator mineral: an example from the staurolite-grade metapelites of NW Maine. *American Mineralogist*, 70, 1–15.

Henry, D. J., Novák, M., Hawthorne, F. C., Ertl, A., Dutrow, B. L., Uher, P. & Pezzotta, F., 2011: Nomenclature of the tourmaline-supergroup minerals. *American Mineralogist*, 96, 895–913.

Hubert, F. J., 1962: A zircon-tourmaline-rutile maturity index and the interdependence of the composition of heavy mineral assemblages with the gross composition and texture of sandstones. *Journal of Sedimentary Petrology*, 32, 3, 440–450.

Jurewicz, E., 1997: The contact between the Pieniny Klippen Belt and Magura Unit (the Małe Pieniny Mts.). *Geological Quarterly*, 41, 315–326.

Jurewicz, E., 2005: Geodynamic evolution of the Tatra Mts. and the Pieniny Klippen Belt (Western Carpathians): problems and comments. *Acta Geologica Polonica*, 55, 295–338.

Jurewicz, E., 2018: The Šariš Transitional Zone, revealing interactions between Pieniny Klippen Belt, Outer Carpathians and European platform. *Swiss Journal of Geosciences*, 111, 245–267.

Kamenetsky, V. S., Crawford, A. J. & Meffre, S., 2001: Factors controlling chemistry of magmatic spinel: an empirical study of associated olivine, Cr-spinel and melt inclusion from primitive rocks. *Journal of Petrology*, 42, 655–671.

Kissová, D., Dunkl, I., Plašienka, D., Frisch, W. & Marschalko, R., 2005: The Pieninic exotic cordillera (Andrusov Ridge) revisited: new zircon FT ages of granite pebbles from Cretaceous conglomerates of the Pieniny Klippen Belt (Western Carpathians, Slovakia). *Slovak Geological Magazine*, 11, 17–28.

Kováč, P. & Hók, J., 1996: Tertiary development of the western part of Klippen Belt. *Slovak Geological Magazine*, 2, 136–149.

Lenaz, D., Kamenetsky, V. S., Crawford, A. J. & Princivalle, F., 2000: Melt inclusion in detrital spinel from the SE Alps (Italy–Slovenia): a new approach to provenance studies

of sedimentary basins. *Contributions to Mineralogy and Petrology*, 139, 748–758. https://doi.org/10.1007/s004100000170.

Ludwiniak, M., 2018: Miocene transpression effects at the boundary of Central Carpathian Paleogene Basin and Pieniny Klippen Belt: examples from Polish-Slovakian borderland. *Geology Geophysics and Environment*, 44, 91–110. https://doi.org/10.7494/geol.2018.44.1.91.

Lužar-Oberiter, B., Mikes, T., von Eynatten, H. & Babić, L., 2009: Ophiolitic detritus in Cretaceous clastic formations of the Dinarides (NW Croatia): evidence from Cr-spinel chemistry. *International Journal of Earth Sciences*, 98, 1097–1108. https://doi.org/10.1007/s00531-008-0306-3.

Madzin, J. & Plašienka, D., 2022: Petrographic and heavy mineral analysis of the Upper Cretaceous – Paleocene turbiditic deposits of the Pupov Formation (Western Carpathians, Pieniny Klippen Belt, Terchová-Zázrivá area). *Acta Geologica Slovaca*, 14, 2, 115–130.

Madzin, J., Plašienka, D. & Méres, Š., 2019: Provenance of synorogenic deposits of the Upper Cretaceous-Lower Palaeogene Jarmuta-Proč Formation (Pieniny Klippen Belt, Western Carpathians). *Geologica Carpathica*, 70, 1, 15–34. https://doi.org/ 10.2478/geoca-2019-0002.

Madzin, J., Márton, E., Plašienka, D. & Imre, G., 2026: A large post-Santonian clockwise rotation of the Central Carpathian nappe stack constrained by new and published paleomagnetic results. *Journal of Geodynamics*, 167, 102135. https://doi.org/10.1016/j.jog.2026.102135.

Maheľ, M., 1981: Island character of the Klippen Belt: Vahicum-continuation of the southern Penninicum in the Western Carpathians. *Geologický Zborník – Geologica Carpathica*, 32, 3, 293–305.

Maheľ, M., 1986: Geological structure of the Czechoslovak Carpathians, Paleoalpine units 1. *Bratislava, Veda,* SAS, 1–503 (in Slovak).

Maheľ, M., 1989: Pieniny Klippen belt from the geodynamic model aspect. *Mineralia Slovaca*, 21, 99–108.

Mange, M. A. & Morton, A. C., 2007: Geochemistry of heavy minerals. In: Mange, M. A. & Wright, D. T. (eds.): Heavy Minerals in Use. Developments in Sedimentology. *Amsterdam, Elsevier*, 345–391.

Marschalko, R., 1986: Development and geotectonic importance of Cretaceous Flysch of the Klippen Belt. *Bratislava, Veda, SAS*, 1–137 (in Slovak with English summary).

Marschalko, R. & Rakús, M., 1997: Development of the Cretaceous flysch in the Klape unit and the recyclicity problem of the clastic material. In: Plašienka, D., Hók, J., Vozár, J. & Elečko, M. (eds.): Alpine Evolution of the Western Carpathians and Related areas. International Conference. Abstracts & Introductory Articles to the Excursion. *Bratislava, Geological Survey of Slovak Republic*, 71–78.

Márton, E., Madzin, J., Plašienka, D., Grabowski, J., Bučová, J., Aubrecht, R. & Putiš, M., 2020: New paleomagnetic constraints for the large-scale displacement of the Hronic nappe system of the Central Western Carpathians. *Journal of Geodynamics*, 1141–142, 101796. https://doi.org/10.1016/j.jog.2020.101796.

Méres, Š., 2008: Garnets – an important information resource about source area and parent rocks of siliciclastic sedimentary rocks. In: Jurkovič, Ľ. (ed.): Conference "Cambelove dni 2008", Abstract Book. *Bratislava, Comenius University*, 37–43 (in Slovak with English Summary).

Michalík, J., 1994: Notes on the Paleogeography and Paleotectonics of the Western Carpathian area during the Mesozoic. *Mitteilungen Österreichischen Geologischen Gessellschaft*, 86, 101–110.

Mikes, T., Christ, D., Petri, R., Dunkl, I., Frei, D., Báldi-Beke, M., Reitner, J., Wemmer, K., Hrvatović, H. & von Eynatten, H., 2008: Provenance of the Bosnian Flysch. *Swiss Journal of Geosciences*, 101, S31–S54. https://doi.org/10.1007/s00015-008-1291-z.

Mikuš, T. & Spišiak, J., 2007: Chemical composition and alteration of Cr-spinels from Meliata and Penninic serpentinized peridotites (Western Carpathians and Eastern Alps). *Geological Quarterly*, 51, 257–270.

Mišík, M., 1997: The Slovak part of the Pieniny Klippen Belt after the pioneering works of D. Andrusov. *Geologica Carpathica*, 48, 4, 209–220.

Mišík, M. & Marschalko, R., 1988: Exotic conglomerates in flysch sequences: Examples from the West Carpathians. In: Rakús, M., Dercourt, J. & Nairn, E. M. A. (eds.): Evolution of the northern margin of Tethys, Vol. 1. *Mémoires de la Société géologique de France, Paris, Nouvelle Série*, 154, 95–113.

Mišík, M. & Sýkora, M., 1981: Pieniny exotic ridge reconstructed from pebbles of carbonate rocks of Cretaceous conglomerates of the Pieniny Klippen Belt and Manín Unit. *Západné Karpaty, Séria Geológia*, 7, 7–111 (in Slovak with English summary).

Molčan Matejová, M., Potočný, T., Plašienka, D. & Aubrecht, R., 2025: Palaeoenvironmental interpretation of chaotic complexes of the Meliata Unit (Western Carpathians, Slovakia): new data from biochronology, lithostratigraphy and geochemistry. *Ofioliti*, 50, 1, 17–36. https://doi.org/10.4454/ofioliti.v50i1.576.

Morton, A. C. & Hallsworth, C. R., 1999: Processes controlling the composition of heavy mineral assemblages in sandstones. *Sedimentary Geology*, 124, 3–29.

Morton, A. C. & Hallsworth, C. R., 2007: Stability of detrital heavy minerals during burial diagenesis. In: Mange, M. A. & Wright, D. T. (eds.): Heavy Minerals in Use. Developments in Sedimentology. *Amsterdam, Elsevier*, 215–245.

Nemčok, M. & Nemčok, J., 1994: Late Cretaceous deformation of the Pieniny Klippen Belt, West Carpathians. *Tectonophysics*, 290, 137–167. https://doi.org/10.1016/0040-1951(94)90109-0.

Nemčok, J., Kullmanová, A. & Ďurkovič, T., 1989: Development and stratigraphic position of the Gregorianka Breccia of the Klippen Belt in eastern Slovakia. *Geologické práce, Správy*, 89, 11–37 (in Slovak).

Oszczypko, N. & Salata, D., 2005: Provenance analyses of the Late Cretaceous-Palaeocene deposits of the Magura basin (Polish Western Carpathians) – evidence from a study of heavy minerals. *Acta Geologica Polonica*, 55, 3, 237–267.

Oszczypko, N., Oszczypko-Clowes, M., Golonka, J. & Marko, F., 2005: Oligocene – Lower Miocene sequences of the Pieniny Klippen Belt and adjacent Magura Nappe between Jarabina and the Poprad River (East Slovakia and

South Poland): their tectonic position and palaeogeographic implications. *Geological Quarterly*, 49, 379–402.

Plašienka, D., 1995a: Passive and active margin history of the northern Tatricum (Western Carpathians, Slovakia). *Geologische Rundschau*, 84, 748–760.

Plašienka, D., 1995b: Mesozoic evolution of Tatric units in the Malé Karpaty and Považský Inovec Mts.: implications for the position of the Klape and related units in Western Slovakia. *Geologica Carpathica*, 46, 2, 101–112.

Plašienka, D., 1996: Cryptic ridges or collision orogenic belts? *Mineralia Slovaca*, 28, 1, 75–79 (in Slovak).

Plašienka, D., 2012a: Jurassic syn-rift and Cretaceous syn-orogenic, coarse-grained deposits related to opening and closure of the Vahic (South Penninic) Ocean in the Western Carpathians – an overview. *Geological Quarterly*, 56, 4, 601–628.

Plašienka, D., 2012b: Early stages of structural evolution of the Carpathian Klippen Belt (Slovakian Pieniny sector). *Mineralia Slovaca*, 44, 1–16.

Plašienka, D., 2018: The Carpathian Klippen Belt and types of its klippen – an attempt at a genetic classification. *Mineralia Slovaca*, 50, 1–24.

Plašienka, D. & Mikuš, V., 2010: Geological setting of the Pieniny and Šariš sectors of the Klippen Belt between Litmanová and Drienica villages in eastern Slovakia. *Mineralia Slovaca*, 42, 2, 155–178 (in Slovak with English Summary).

Plašienka, D. & Soták, J., 2015: Evolution of Late Cretaceous--Palaeogene synorogenic basins in the Pieniny Klippen Belt and adjacent zones (Western Carpathians, Slovakia): Tectonic controls over a growing orogenic wedge. *Annales Societatis Geologorum Poloniae*, 85, 43–76.

Plašienka, D., Soták, J., Jamrichová, M., Halásová, E., Pivko, D., Józsa, Š, Madzin, J. & Mikuš, V., 2012: Structure and evolution of the Pieniny Klippen Belt demonstrated along a section between Jarabina and Litmanová villages in Eastern Slovakia. *Mineralia Slovaca*, 44, 1, 17–39.

Plašienka, D., Józsa, Š, Gedl, P. & Madzin, J., 2013: Fault contact of the Pieniny Klippen Belt with the Central Carpathian Paleogene Basin (Western Carpathians): new data from a unique temporary exposure in Ľutina village (Eastern Slovakia). *Geologica Carpathica*, 64, 165–168.

Plašienka, D., Méres, Š., Ivan, P., Sýkora, M., Soták, J., Lačný, A., Aubrecht, R., Bellová, S. & Potočný, T., 2019: Meliatic blueschists and their detritus in Cretaceous sediments: New data constraining tectonic evolution of the West Carpathians. *Swiss Journal of Geosciences*, 112, 1, 55–81. https://doi.org/10.1007/s00015-018-0330-7.

Plašienka, D., Bučová, J. & Šimonová, V., 2020: Variable structural styles and tectonic evolution of an ancient backstop boundary: the Pieniny Klippen Belt of the Western Carpathians. *International Journal of Earth Sciences*, 109, 4, 1355–1376.

Pober, E. & Faupl, P., 1988: The chemistry of detrital spinels and its application for the geodynamic evolution of the Eastern Alps. *Geologische Rundschau*, 77, 641–670. https://doi.org/10.1007/BF01830175.

Prokešová, R., Plašienka, D. & Milovský, R., 2012: Structural pattern and emplacement mechanisms of the Krížna cover nappe (Western Carpathians, Slovakia). *Geologica Carpathica*, 63, 13–32.

Putiš, M., Scherer, E. E., Nemec, O., Ackerman, L. & Ružička, P., 2023: Geochemistry, Lu–Hf garnet ages, and P–T conditions of blueschists from the Meliatic and Fatric nappes, Western Carpathians: Indicators of Neotethyan subduction. *Geosystems and Geoenvironment*, 2, 100150. https://doi.org/10.1016/j.geogeo.2022.100150.

Rakús, M. & Marschalko, R., 1997: Position of the Manín, Drietoma and Klape units at the boundary of the Central and Outer Carpathians. In: Plašienka, D., Hók, J., Vozár J. & Elečko, M. (eds.): Alpine Evolution of the Western Carpathians and Related areas. International Conference. Abstracts & Introductory Articles to the Excursion. *Bratislava, Geological Survey of Slovak Republic*, 79–97.

Ratschbacher, L., Frisch, W., Linzer, H.-G., Sperner, B., Meschede, M., Decker, K., Nemčok, M., Nemčok, J. & Grygar, R., 1993: The Pieniny Klippen Belt in the Western Carpathians of northeastern Slovakia: structural evidence for transpression. *Tectonophysics*, 226, 471–483. https://doi.org/10.1016/0040-1951(93)90133-5.

Salata, D., 2004: Detrital garnets from the Upper Cretaceous--Palaeogene sandstones of the Polish part of the Magura Nappe and the Pieniny Klippen Belt: chemical constrains. *Annales Societatis Geologorum Poloniae*, 74, 351–364.

Schmid, M. S., Bernoulli, D., Fügenshuh, B., Matenco, L., Schefer, S., Schuster, R., Tichler, M. & Ustaszewski, K., 2008: The Alpine-Carpathian-Dinaridic orogenic system: correlation and evolution of tectonic units. *Swiss Journal of Geosciences*, 101, 139–183. https://doi.org/10.1007/s00015-008-1247-3.

Starek, D., Aubrecht, R., Sliva, Ľ. & Józsa, Š., 2010: Sedimentary analysis of the Cretaceous flysch sequences at the Zemianska Dedina locality (Nižná Unit, Pieniny Klippen Belt, northern Slovakia). *Mineralia Slovaca*, 42, 179–188.

Tomek, Č., 1993: Deep crustal structure beneath the central and inner West Carpathians. Tectonophysics, 226, 417–431. https://doi.org/10.1016/0040-1951(93)90130-C.

Uher, P., Bačík, P. & Ozdín, D., 2009: Tourmaline (magnesiofoitite and dravite) in quartz vein near Limbach, Malé Karpaty Mts. (Slovakia). *Mineralia Slovaca*, 41, 445–456 (in Slovak with English Summary).

Whitney, L. D. & Evans, W. B., 2010: Abbreviations for names of rock-forming minerals. *American Mineralogist*, 95, 185–187. https://doi.org/10.2138/am.2010.3371.

Winkler, Z. & Ślączka, A., 1992: Sediment dispersal and provenance in the Silesian, Dukla and Magura nappes (Outer Carpathians, Poland). *Geologische Rundschau*, 2, 371–382.

Winkler, Z. & Ślączka, A., 1994: A late Cretaceous to Palaeogene geodynamic model for the Western Carpathians in Poland. *Geologica Carpathica*, 45, 2, 71–82.

# Analýza ťažkých minerálov vrchnokriedových až spodnoeocénnych synorogenetických sedimentov pieninského bradlového pásma (šarišská jednotka, východné Slovensko): nové údaje z vrtu Jar-2 (jarmutsko-pročské s.) a odkryvov (malinowské s.)

Článok prezentuje nové výsledky analýzy ťažkých minerálov a chemické zloženie detritických granátov, turmalínov a Cr-spinelov z jadrového vrtného materiálu štruktúrneho vrtu Jar-2, ktorý prenikol cez turbiditné pieskovce mástrichtsko-spodnoeocénneho jarmutsko-pročského súvrstvia, a z jemnozrnných pieskovcov hemipelagického turónsko-kampánskeho malinowského súvrstvia (vzorky z odkryvu) šarišskej jednotky pieninského bradlového pásma (PBP) na východnom Slovensku. V asociáciách ťažkých minerálov jarmutsko-pročského súvrstvia dominujú granát, apatit a turmalín. O niečo menej zastúpené sú rutil a zirkón. Sporadicky sa vyskytuje Cr-spinel. V malinowskom súvrství sú dominantné granát a rutil, menej zirkón a turmalín. Cr-spinel sa vyskytuje častejšie, pričom najmenej zastúpený ťažký minerál je tu apatit.

V oboch súvrstviach dominujú almandínové granáty s rôznym pomerom grosuláru, pyropu a spessartínu. Analyzované granáty boli derivované prevažne z nízko-, stredno- až vysokostupňových polymetamorfovaných komplexov. O niečo pestrejšia populácia granátov v jarmutsko-pročskom súvrství môže odrážať nový prínos granátov zo stredne metamorfovaných bázickejších zdrojov počas najvrchnejšej kriedy. Niektoré z almandínových granátov môžu pochádzať aj z granitoidných hornín. Časť analyzovaných almandínových granátov s nízkym obsahom pyropu, vyšším obsahom grosulárovej molekuly a variabilným obsahom spessartínu je podobná granátom z obliakov metabazitov v albsko-cenomanských zlepencoch klapskej jednotky a vysokotlakovo a nízkoteplotne metamorfovaného príkrovu Bôrky (Putiš et al., 2023). Môže to indikovať ich pôvod v meliatiku.

Analyzované detritické turmalíny vykazujú zložitú optickú zonalitu. Na základe bodových analýz z odlišných optických zón najčastejším typom turmalínov sú X-vakantné turmalíny. Menej časté sú alkalické turmalíny a zriedkavo zastúpené sú vápenaté turmalíny. X-vakantné turmalíny majú stredný obsah vakancií a zložením zodpovedajú magneziofoititu až foititu. Alkalické turmalíny chemickým zložením zodpovedajú skorylu-dravitu. Vápenaté turmalíny zodpovedajú uvitu a feruvitu. Magneziofoitity až foitity tvoria buď jadrá zŕn, oscilačné zóny, alebo opticky zložité zóny a okraje zŕn. Niektoré zrná alebo zóny so skorylovo-dravitovým zložením sú charakteristické jemným prerastaním s kremeňom a početnými minerálnymi inklúziami. Minerálne inklúzie tvoria kremeň, rutil, zirkón, monazit, titanit, ilmenit, apatit, allanit, albit a oxidy železa. Významný obsah podobných komplexne zonálnych detritických turmalínov bol nedávno objavený v kriedových súvrstviach s „exotickými“ zlepencami z centrálnych Západných Karpát (CZK) a PBP (Bellová et al., 2018; Plašienka et al., 2019; Aubrecht et al., 2020a, 2020b, 2021). Komplexne zonálne turmalíny môžu pochádzať z exhumovaných vysokotlakovo-nízkoteplotných ofiolitových komplexov meliatika (l. c.). Zdanlivý paradox ich výskytu vo flyšových súvrstviach uložených na opačnej (externej) strane orogénneho pásma a ich derivácia z „južných“ (interných) západokarpatských zón sa dá vysvetliť viacfázovou recykláciou, ako sa predpokladá aj pri derivácii ofiolitového detritu s harzburgitovým zložením v kriedových až paleogénnych flyšových súvrstviach CZK a PBP (Plašienka, 2012a a tamojšie citácie). Ofiolitové komplexy meliatika boli počas spodnej kriedy vystavené erózii v interných západokarpatských zónach. Ofiolitový detrit a „exotický“ obliakový materiál bol uložený najprv vo flyšových sedimentoch albsko-cenomanského porubského súvrstvia v zliechovskej panve fatrika. Porubské súvrstvie ako súčasť príkrovového systému fatrika bolo počas vrchného turónu presunuté do pozície falošného akrečného klina za tatrickým externým okrajom. Tam sa stalo súčasťou klapskej jednotky pribradlovej zóny (Plašienka, 1995a, 1995b, 1996, 2012a; Prokešová et al., 2012; Plašienka et al., 2019). Albsko-cenomanské flyšové súvrstvia klapskej jednotky, už kompletne zahrnuté do rastúceho akrečného klina, mohli takýmto spôsobom tvoriť „proximálny“ zdroj ofiolitového detritu aj komplexne zonálnych turmalínov pre čoraz mladšie synorogenetické súvrstvia v čelných panvách PBP a priľahlých zón (Plašienka, 2012a; Plašienka & Soták, 2015; Plašienka et al., 2019; Madzin & Plašienka, 2022).

Analyzované Cr-spinely nevykazujú žiadne znaky premeny alebo zonality. Takmer všetky študované Cr-spinely oboch súvrství majú pomer $Fe^{2+}/Fe^{3+}$ vyšší ako 4, čo je charakteristické pre spinely plášťových peridotitov (Lenaz et al., 2000; Kamenetsky et al., 2001). Analyzované Cr-spinely najlepšie zodpovedajú harzburgitom alebo podiformným chromititom (Pober & Faupl, 1988). Iba niekoľko Cr-spinelov z malinowského súvrstvia vykazuje koncentráciu $TiO_2$ vyššiu ako 0,2 hm. %, čo naznačuje ich pôvod vo vulkanických horninách. Vulkanické spinely svojím zložením zodpovedajú bazaltom vulkanických

oblúkov alebo zaoblúkových paniev (Lenaz et al., 2000; Kamenetsky et al., 2001).

Zdroj ofiolitového detritu vo vrchnokriedových klastických súvrstviach PBP sa všeobecne považuje za rovnaký ako zdroj „exotických" zlepencov klapskej jednotky. Hoci pôvod, paleogeografická pozícia a interpretácia klapskej jednotky sú predmetom desaťročia trvajúcej diskusie, v poslednom čase panuje konsenzus, že ofiolitový detrit pochádza z ofiolitových komplexov meliatika v interných západokarpatských zónach (Aubrecht et al., 2009; Plašienka, 2012a; Bellová et al., 2018; Plašienka et al., 2019; Aubrecht et al., 2020a, 2020b, 2021; Putiš et al., 2023). Chemické zloženie Cr-spinelov a komplexne zonálnych turmalínov analyzovaných v tejto práci túto predstavu podporuje. Vysoký verzus nízky obsah Cr-spinelov v proximálnych verzus distálnych turónsko-kampánskych sedimentoch pieninskej a šarišskej jednotky a smerom nahor sa znižujúci obsah Cr-spinelov vo vrchnokriedových až spodnoeocénnych flyšových sedimentoch PBP je v súlade s konceptom viacnásobnej recyklácie ofiolitového detritu z klapskej jednotky.

Doručené / Recieved: 31. 12. 2025
Prijaté na publikovanie / Accepted: 10. 3. 2026

## Supplementary Table S1

Representative microprobe analyses of detrital garnets from Upper Cretaceous to Paleocene deposits of the Jarmuta-Proč Fm., structural drill JAR-2, Pieniny sector of the PKB, Western Carpathians, Slovakia

| Locality | Jarabina JAR-2 | Jarabina JAR-2 | Jarabina JAR-2 | Jarabina JAR-2 | Jarabina JAR-2 | Jarabina JAR-2 | Jarabina JAR-2 | Jarabina JAR-2 | Jarabina JAR-2 | Jarabina JAR-2 | Jarabina JAR-2 | Jarabina JAR-2 | Jarabina JAR-2 | Jarabina JAR-2 |
|---|---|---|---|---|---|---|---|---|---|---|---|---|---|---|
| Formation | Jarmuta-Proč Fm. | Jarmuta-Proč Fm. | Jarmuta-Proč Fm. | Jarmuta-Proč Fm. | Jarmuta-Proč Fm. | Jarmuta-Proč Fm. | Jarmuta-Proč Fm. | Jarmuta-Proč Fm. | Jarmuta-Proč Fm. | Jarmuta-Proč Fm. | Jarmuta-Proč Fm. | Jarmuta-Proč Fm. | Jarmuta-Proč Fm. | Jarmuta-Proč Fm. |
| Age | Maastrichtian–Middle Eocene | Maastrichtian–Middle Eocene | Maastrichtian–Middle Eocene | Maastrichtian–Middle Eocene | Maastrichtian–Middle Eocene | Maastrichtian–Middle Eocene | Maastrichtian–Middle Eocene | Maastrichtian–Middle Eocene | Maastrichtian–Middle Eocene | Maastrichtian–Middle Eocene | Maastrichtian–Middle Eocene | Maastrichtian–Middle Eocene | Maastrichtian–Middle Eocene | Maastrichtian–Middle Eocene |
| Unit | Šariš U. | Šariš U. | Šariš U. | Šariš U. | Šariš U. | Šariš U. | Šariš U. | Šariš U. | Šariš U. | Šariš U. | Šariš U. | Šariš U. | Šariš U. | Šariš U. |
| Sample | JAR-2A | JAR-2A | JAR-2A | JAR-2A | JAR-2A | JAR-2A | JAR-2A | JAR-2A | JAR-2A | JAR-2A | JAR-2A | JAR-2A | JAR-2A | JAR-2A |
| Point | an5 | an8 | an14 | an15 | an16 | an17 | an18 | an19 | an20 | an21 | an22 | an23 | an24 | an25 |
| $SiO_2$ | 37.21 | 37.26 | 37.44 | 37.50 | 36.89 | 38.36 | 37.72 | 36.91 | 37.01 | 37.11 | 37.30 | 37.86 | 37.25 | 37.59 |
| $TiO_2$ | 0.04 | 0.18 | 0.02 | 0.00 | 0.06 | 0.02 | 0.01 | 0.04 | 0.10 | 0.00 | 0.09 | 0.06 | 0.11 | 0.06 |
| $Al_2O_3$ | 21.32 | 21.25 | 21.07 | 21.59 | 21.35 | 22.03 | 21.05 | 20.97 | 21.18 | 21.05 | 21.06 | 21.74 | 21.08 | 21.35 |
| $Cr_2O_3$ | 0.03 | 0.02 | 0.00 | 0.00 | 0.00 | 0.02 | 0.00 | 0.00 | 0.00 | 0.04 | 0.00 | 0.04 | 0.04 | 0.00 |
| $Fe_2O_3^*$ | 0.00 | 0.00 | 0.00 | 0.00 | 0.00 | 0.00 | 0.00 | 0.07 | 0.00 | 0.10 | 0.00 | 0.00 | 0.00 | 0.00 |
| FeO | 34.08 | 28.25 | 35.66 | 32.70 | 36.87 | 31.30 | 33.39 | 33.75 | 31.51 | 33.37 | 35.39 | 30.07 | 34.23 | 34.35 |
| MnO | 1.25 | 6.00 | 0.47 | 2.39 | 0.74 | 0.71 | 2.50 | 2.13 | 3.09 | 4.70 | 0.56 | 0.72 | 0.99 | 1.04 |
| MgO | 3.33 | 1.13 | 2.82 | 2.61 | 2.70 | 6.43 | 3.10 | 0.27 | 1.24 | 2.36 | 1.76 | 4.60 | 1.27 | 4.63 |
| NiO | 0.00 | 0.00 | 0.00 | 0.00 | 0.00 | 0.00 | 0.00 | 0.00 | 0.00 | 0.00 | 0.00 | 0.00 | 0.00 | 0.00 |
| ZnO | 0.00 | 0.00 | 0.00 | 0.00 | 0.00 | 0.00 | 0.00 | 0.00 | 0.00 | 0.00 | 0.00 | 0.00 | 0.00 | 0.00 |
| CaO | 2.13 | 6.39 | 2.16 | 3.94 | 1.57 | 1.48 | 2.25 | 6.22 | 5.81 | 1.78 | 3.64 | 5.01 | 4.67 | 0.94 |
| Total | 99.38 | 100.47 | 99.64 | 100.72 | 100.17 | 100.35 | 100.02 | 100.34 | 99.93 | 100.51 | 99.79 | 100.10 | 99.63 | 99.96 |
| | | | | | | | | | | | | | | |
| Formulae based on 12 oxygens and with $Fe^{2+}/Fe^{3+}$ calculated assuming full occupancy | | | | | | | | | | | | | | |
| Si | 2.99 | 2.99 | 3.01 | 2.98 | 2.97 | 2.99 | 3.02 | 2.99 | 2.99 | 2.99 | 3.01 | 2.98 | 3.00 | 2.99 |
| Al iv | 0.01 | 0.01 | 0.00 | 0.02 | 0.03 | 0.01 | 0.00 | 0.01 | 0.01 | 0.01 | 0.00 | 0.02 | 0.00 | 0.01 |
| | | | | | | | | | | | | | | |
| Al vi | 2.01 | 1.99 | 2.00 | 2.01 | 2.00 | 2.02 | 1.99 | 1.99 | 2.00 | 1.99 | 2.01 | 2.00 | 2.01 | 2.00 |
| Ti | 0.00 | 0.01 | 0.00 | 0.00 | 0.00 | 0.00 | 0.00 | 0.00 | 0.01 | 0.00 | 0.01 | 0.00 | 0.01 | 0.00 |
| Cr | 0.00 | 0.00 | 0.00 | 0.00 | 0.00 | 0.00 | 0.00 | 0.00 | 0.00 | 0.00 | 0.00 | 0.00 | 0.00 | 0.00 |
| $Fe^{3+}$ | 0.00 | 0.00 | 0.00 | 0.00 | 0.00 | 0.00 | 0.00 | 0.00 | 0.00 | 0.01 | 0.00 | 0.00 | 0.00 | 0.00 |
| | | | | | | | | | | | | | | |
| $Fe^{2+}$ | 2.32 | 1.90 | 2.42 | 2.19 | 2.49 | 2.07 | 2.25 | 2.29 | 2.13 | 2.25 | 2.41 | 1.99 | 2.34 | 2.30 |
| Mn | 0.08 | 0.41 | 0.03 | 0.16 | 0.05 | 0.05 | 0.17 | 0.15 | 0.21 | 0.32 | 0.04 | 0.05 | 0.07 | 0.07 |
| Mg | 0.40 | 0.14 | 0.34 | 0.31 | 0.32 | 0.75 | 0.37 | 0.03 | 0.15 | 0.28 | 0.21 | 0.54 | 0.15 | 0.55 |
| Ni | 0.00 | 0.00 | 0.00 | 0.00 | 0.00 | 0.00 | 0.00 | 0.00 | 0.00 | 0.00 | 0.00 | 0.00 | 0.00 | 0.00 |
| Zn | 0.00 | 0.00 | 0.00 | 0.00 | 0.00 | 0.00 | 0.00 | 0.00 | 0.00 | 0.00 | 0.00 | 0.00 | 0.00 | 0.00 |
| Ca | 0.18 | 0.55 | 0.19 | 0.34 | 0.14 | 0.12 | 0.19 | 0.54 | 0.50 | 0.15 | 0.31 | 0.42 | 0.40 | 0.08 |
| Total | 8.00 | 8.00 | 7.99 | 8.01 | 8.01 | 8.00 | 7.99 | 8.00 | 8.00 | 8.01 | 7.99 | 8.01 | 7.99 | 8.00 |
| | | | | | | | | | | | | | | |
| End members | | | | | | | | | | | | | | |
| Almandine | 77.65 | 63.44 | 81.29 | 72.97 | 82.85 | 69.27 | 75.40 | 75.97 | 71.14 | 74.66 | 81.03 | 66.08 | 78.97 | 76.62 |
| Andradite | 0.00 | 0.00 | 0.00 | 0.00 | 0.00 | 0.00 | 0.00 | 0.21 | 0.00 | 0.31 | 0.00 | 0.00 | 0.00 | 0.00 |
| Grossular | 6.06 | 18.33 | 6.26 | 11.26 | 4.55 | 4.06 | 6.48 | 17.84 | 16.81 | 4.71 | 10.57 | 14.04 | 13.50 | 2.69 |
| Pyrope | 13.36 | 4.53 | 11.38 | 10.37 | 10.89 | 25.04 | 12.42 | 1.08 | 4.97 | 9.47 | 7.10 | 18.13 | 5.14 | 18.36 |
| Spessartine | 2.84 | 13.65 | 1.08 | 5.40 | 1.71 | 1.56 | 5.69 | 4.90 | 7.07 | 10.72 | 1.30 | 1.61 | 2.28 | 2.34 |
| Uvarovite | 0.09 | 0.06 | 0.00 | 0.00 | 0.00 | 0.07 | 0.00 | 0.00 | 0.00 | 0.12 | 0.00 | 0.14 | 0.12 | 0.00 |
| % cations | 99.45 | 99.55 | 99.36 | 99.39 | 99.00 | 99.44 | 99.49 | 99.62 | 99.49 | 99.61 | 99.27 | 99.31 | 99.05 | 99.84 |
| *calculated | | | | | | | | | | | | | | |

**Supplementary Table S1** – continuation

| Locality | Jarabina JAR-2 | Jarabina JAR-2 | Jarabina JAR-2 | Jarabina JAR-2 | Jarabina JAR-2 | Jarabina JAR-2 | Jarabina JAR-2 | Jarabina JAR-2 | Jarabina JAR-2 | Jarabina JAR-2 | Jarabina JAR-2 | Jarabina JAR-2 | Jarabina JAR-2 | Jarabina JAR-2 |
|---|---|---|---|---|---|---|---|---|---|---|---|---|---|---|
| Formation | Jarmuta-Proč Fm. | Jarmuta-Proč Fm. | Jarmuta-Proč Fm. | Jarmuta-Proč Fm. | Jarmuta-Proč Fm. | Jarmuta-Proč Fm. | Jarmuta-Proč Fm. | Jarmuta-Proč Fm. | Jarmuta-Proč Fm. | Jarmuta-Proč Fm. | Jarmuta-Proč Fm. | Jarmuta-Proč Fm. | Jarmuta-Proč Fm. | Jarmuta-Proč Fm. |
| Age | Maastrichtian–Middle Eocene | Maastrichtian–Middle Eocene | Maastrichtian–Middle Eocene | Maastrichtian–Middle Eocene | Maastrichtian–Middle Eocene | Maastrichtian–Middle Eocene | Maastrichtian–Middle Eocene | Maastrichtian–Middle Eocene | Maastrichtian–Middle Eocene | Maastrichtian–Middle Eocene | Maastrichtian–Middle Eocene | Maastrichtian–Middle Eocene | Maastrichtian–Middle Eocene | Maastrichtian–Middle Eocene |
| Unit | Šariš U. | Šariš U. | Šariš U. | Šariš U. | Šariš U. | Šariš U. | Šariš U. | Šariš U. | Šariš U. | Šariš U. | Šariš U. | Šariš U. | Šariš U. | Šariš U. |
| Sample | JAR-2A | JAR-2A | JAR-2A | JAR-2A | JAR-2B | JAR-2B | JAR-2B | JAR-2B | JAR-2B | JAR-2B | JAR-2B | JAR-2B | JAR-2B | JAR-2B |
| Point | an26 | an27 | an28 | an29 | an1 | an2 | an3 | an6 | an7 | an13 | an14 | an15 | an16 | an17 |
| $SiO_2$ | 36.98 | 37.24 | 37.62 | 37.14 | 37.25 | 37.32 | 37.09 | 36.86 | 37.19 | 37.08 | 37.46 | 37.88 | 36.90 | 37.39 |
| $TiO_2$ | 0.02 | 0.04 | 0.07 | 0.06 | 0.07 | 0.06 | 0.00 | 0.06 | 0.00 | 0.06 | 0.04 | 0.06 | 0.11 | 0.08 |
| $Al_2O_3$ | 21.25 | 21.02 | 21.30 | 21.13 | 21.15 | 21.29 | 21.17 | 20.82 | 21.07 | 20.90 | 21.72 | 21.42 | 20.34 | 20.91 |
| $Cr_2O_3$ | 0.01 | 0.01 | 0.01 | 0.03 | 0.05 | 0.02 | 0.01 | 0.02 | 0.00 | 0.00 | 0.00 | 0.03 | 0.04 | 0.00 |
| $Fe_2O_3$* | 0.00 | 0.00 | 0.00 | 0.00 | 0.00 | 0.00 | 0.00 | 0.00 | 0.00 | 0.08 | 0.00 | 0.00 | 0.46 | 0.09 |
| FeO | 35.46 | 34.62 | 34.44 | 33.64 | 31.82 | 34.57 | 33.01 | 31.78 | 31.72 | 25.70 | 34.13 | 24.96 | 19.48 | 30.23 |
| MnO | 2.01 | 1.27 | 0.15 | 5.02 | 3.14 | 1.02 | 5.60 | 2.48 | 6.08 | 10.15 | 1.24 | 3.01 | 17.15 | 3.08 |
| MgO | 1.96 | 1.36 | 3.23 | 1.63 | 2.24 | 3.88 | 2.69 | 0.66 | 2.40 | 0.87 | 4.04 | 2.42 | 1.49 | 2.72 |
| NiO | 0.00 | 0.00 | 0.00 | 0.00 | 0.00 | 0.00 | 0.00 | 0.00 | 0.00 | 0.00 | 0.00 | 0.00 | 0.00 | 0.00 |
| ZnO | 0.00 | 0.00 | 0.00 | 0.00 | 0.00 | 0.00 | 0.00 | 0.00 | 0.00 | 0.00 | 0.00 | 0.00 | 0.00 | 0.00 |
| CaO | 2.39 | 4.39 | 3.37 | 1.59 | 3.65 | 1.34 | 0.69 | 6.54 | 1.36 | 5.34 | 1.85 | 9.35 | 3.59 | 4.96 |
| Total | 100.08 | 99.94 | 100.19 | 100.24 | 99.36 | 99.50 | 100.25 | 99.22 | 99.82 | 100.18 | 100.48 | 99.13 | 99.55 | 99.45 |
| | | | | | | | | | | | | | | |
| Formulae based on 12 oxygens and with $Fe^{2+}/Fe^{3+}$ calculated assuming full occupancy | | | | | | | | | | | | | | |
| Si | 2.99 | 3.01 | 3.00 | 3.00 | 3.00 | 2.99 | 2.99 | 3.00 | 3.00 | 3.00 | 2.97 | 3.01 | 3.00 | 3.01 |
| Al iv | 0.01 | 0.00 | 0.00 | 0.00 | 0.00 | 0.01 | 0.01 | 0.00 | 0.00 | 0.00 | 0.03 | 0.00 | 0.00 | 0.00 |
| | | | | | | | | | | | | | | |
| Al vi | 2.01 | 2.00 | 2.00 | 2.01 | 2.01 | 2.01 | 2.00 | 2.00 | 2.01 | 1.99 | 2.01 | 2.01 | 1.95 | 1.98 |
| Ti | 0.00 | 0.00 | 0.00 | 0.00 | 0.00 | 0.00 | 0.00 | 0.00 | 0.00 | 0.00 | 0.00 | 0.00 | 0.01 | 0.00 |
| Cr | 0.00 | 0.00 | 0.00 | 0.00 | 0.00 | 0.00 | 0.00 | 0.00 | 0.00 | 0.00 | 0.00 | 0.00 | 0.00 | 0.00 |
| $Fe^{3+}$ | 0.00 | 0.00 | 0.00 | 0.00 | 0.00 | 0.00 | 0.00 | 0.00 | 0.00 | 0.00 | 0.00 | 0.00 | 0.03 | 0.01 |
| | | | | | | | | | | | | | | |
| $Fe^{2+}$ | 2.41 | 2.35 | 2.31 | 2.30 | 2.17 | 2.34 | 2.23 | 2.17 | 2.16 | 1.74 | 2.28 | 1.69 | 1.33 | 2.03 |
| Mn | 0.14 | 0.09 | 0.01 | 0.34 | 0.21 | 0.07 | 0.38 | 0.17 | 0.42 | 0.70 | 0.08 | 0.20 | 1.18 | 0.21 |
| Mg | 0.24 | 0.16 | 0.38 | 0.20 | 0.27 | 0.46 | 0.32 | 0.08 | 0.29 | 0.10 | 0.48 | 0.29 | 0.18 | 0.33 |
| Ni | 0.00 | 0.00 | 0.00 | 0.00 | 0.00 | 0.00 | 0.00 | 0.00 | 0.00 | 0.00 | 0.00 | 0.00 | 0.00 | 0.00 |
| Zn | 0.00 | 0.00 | 0.00 | 0.00 | 0.00 | 0.00 | 0.00 | 0.00 | 0.00 | 0.00 | 0.00 | 0.00 | 0.00 | 0.00 |
| Ca | 0.21 | 0.38 | 0.29 | 0.14 | 0.32 | 0.12 | 0.06 | 0.57 | 0.12 | 0.46 | 0.16 | 0.80 | 0.31 | 0.43 |
| Total | 8.00 | 7.99 | 8.00 | 8.00 | 7.99 | 8.00 | 8.00 | 8.00 | 8.00 | 8.00 | 8.01 | 7.99 | 8.00 | 8.00 |
| | | | | | | | | | | | | | | |
| End members | | | | | | | | | | | | | | |
| Almandine | 80.59 | 78.88 | 77.18 | 77.24 | 73.14 | 78.28 | 74.40 | 72.53 | 72.41 | 57.86 | 75.83 | 56.74 | 43.64 | 67.69 |
| Andradite | 0.00 | 0.00 | 0.00 | 0.00 | 0.00 | 0.00 | 0.00 | 0.00 | 0.00 | 0.24 | 0.00 | 0.00 | 1.42 | 0.27 |
| Grossular | 6.87 | 12.72 | 9.60 | 4.53 | 10.47 | 3.82 | 1.95 | 19.01 | 3.95 | 15.19 | 5.30 | 26.71 | 8.99 | 14.08 |
| Pyrope | 7.89 | 5.47 | 12.84 | 6.60 | 9.05 | 15.52 | 10.83 | 2.68 | 9.70 | 3.50 | 16.07 | 9.66 | 6.07 | 10.93 |
| Spessartine | 4.61 | 2.91 | 0.34 | 11.55 | 7.20 | 2.33 | 12.79 | 5.72 | 13.94 | 23.20 | 2.81 | 6.82 | 39.76 | 7.03 |
| Uvarovite | 0.04 | 0.02 | 0.04 | 0.09 | 0.15 | 0.05 | 0.03 | 0.06 | 0.00 | 0.01 | 0.00 | 0.08 | 0.13 | 0.00 |
| % cations | 99.50 | 99.52 | 99.70 | 99.29 | 99.20 | 99.56 | 99.66 | 99.79 | 99.52 | 99.87 | 99.02 | 99.17 | 99.19 | 99.44 |
| *calculated | | | | | | | | | | | | | | |

**Supplementary Table S1** – continuation

| Locality | Jarabina JAR-2 | Jarabina JAR-2 | Jarabina JAR-2 | Jarabina JAR-2 | Jarabina JAR-2 | Jarabina JAR-2 | Jarabina JAR-2 | Jarabina JAR-2 | Jarabina JAR-2 | Jarabina JAR-2 | Jarabina JAR-2 | Jarabina JAR-2 | Jarabina JAR-2 | Jarabina JAR-2 |
|---|---|---|---|---|---|---|---|---|---|---|---|---|---|---|
| Formation | Jarmuta-Proč Fm. | Jarmuta-Proč Fm. | Jarmuta-Proč Fm. | Jarmuta-Proč Fm. | Jarmuta-Proč Fm. | Jarmuta-Proč Fm. | Jarmuta-Proč Fm. | Jarmuta-Proč Fm. | Jarmuta-Proč Fm. | Jarmuta-Proč Fm. | Jarmuta-Proč Fm. | Jarmuta-Proč Fm. | Jarmuta-Proč Fm. | Jarmuta-Proč Fm. |
| Age | Maastrichtian–Middle Eocene | Maastrichtian–Middle Eocene | Maastrichtian–Middle Eocene | Maastrichtian–Middle Eocene | Maastrichtian–Middle Eocene | Maastrichtian–Middle Eocene | Maastrichtian–Middle Eocene | Maastrichtian–Middle Eocene | Maastrichtian–Middle Eocene | Maastrichtian–Middle Eocene | Maastrichtian–Middle Eocene | Maastrichtian–Middle Eocene | Maastrichtian–Middle Eocene | Maastrichtian–Middle Eocene |
| Unit | Šariš U. | Šariš U. | Šariš U. | Šariš U. | Šariš U. | Šariš U. | Šariš U. | Šariš U. | Šariš U. | Šariš U. | Šariš U. | Šariš U. | Šariš U. | Šariš U. |
| Sample | JAR-2B | JAR-2B | JAR-2B | JAR-2C | JAR-2C | JAR-2C | JAR-2C | JAR-2C | JAR-2C | JAR-2C | JAR-2C | JAR-2C | JAR-2C | JAR-2C |
| Point | an19 | an21 | an29 | an2 | an4 | an5 | an6 | an9 | an10 | an16 | an17 | an19 | an20 | an21 |
| $SiO_2$ | 36.83 | 37.20 | 37.84 | 37.40 | 37.84 | 37.26 | 37.63 | 37.77 | 37.38 | 37.72 | 37.92 | 37.62 | 37.88 | 38.45 |
| $TiO_2$ | 0.00 | 0.00 | 0.11 | 0.05 | 0.13 | 0.04 | 0.02 | 0.09 | 0.05 | 0.03 | 0.03 | 0.04 | 0.06 | 0.04 |
| $Al_2O_3$ | 21.29 | 21.39 | 21.41 | 21.28 | 21.40 | 21.03 | 21.43 | 21.33 | 21.18 | 21.50 | 21.46 | 21.55 | 21.57 | 21.60 |
| $Cr_2O_3$ | 0.00 | 0.00 | 0.05 | 0.01 | 0.00 | 0.02 | 0.00 | 0.00 | 0.02 | 0.03 | 0.00 | 0.03 | 0.03 | 0.00 |
| $Fe_2O_3^*$ | 0.00 | 0.00 | 0.00 | 0.00 | 0.00 | 0.00 | 0.00 | 0.00 | 0.00 | 0.00 | 0.00 | 0.00 | 0.00 | 0.00 |
| FeO | 33.57 | 35.36 | 24.77 | 32.96 | 27.03 | 36.52 | 33.03 | 28.88 | 34.46 | 34.96 | 31.80 | 31.61 | 30.42 | 31.75 |
| MnO | 4.46 | 0.73 | 4.57 | 3.90 | 3.59 | 0.64 | 3.84 | 0.57 | 3.62 | 1.29 | 0.45 | 0.68 | 0.51 | 0.73 |
| MgO | 2.32 | 3.18 | 1.20 | 0.97 | 1.25 | 1.35 | 2.99 | 1.18 | 2.72 | 3.67 | 4.37 | 2.02 | 1.56 | 5.05 |
| NiO | 0.00 | 0.00 | 0.00 | 0.00 | 0.00 | 0.00 | 0.00 | 0.00 | 0.00 | 0.00 | 0.00 | 0.00 | 0.00 | 0.00 |
| ZnO | 0.00 | 0.00 | 0.00 | 0.00 | 0.00 | 0.00 | 0.00 | 0.00 | 0.00 | 0.00 | 0.00 | 0.00 | 0.00 | 0.00 |
| CaO | 1.35 | 1.89 | 10.69 | 4.10 | 9.60 | 3.05 | 1.42 | 9.98 | 1.02 | 1.06 | 3.70 | 6.76 | 8.82 | 2.73 |
| Total | 99.82 | 99.75 | 100.66 | 100.67 | 100.84 | 99.90 | 100.35 | 99.80 | 100.45 | 100.25 | 99.73 | 100.31 | 100.85 | 100.35 |
| | | | | | | | | | | | | | | |
| Formulae based on 12 oxygens and with $Fe^{2+}/Fe^{3+}$ calculated assuming full occupancy | | | | | | | | | | | | | | |
| Si | 2.98 | 2.99 | 2.99 | 3.00 | 3.00 | 3.01 | 3.00 | 3.01 | 3.00 | 3.00 | 3.00 | 2.99 | 2.99 | 3.01 |
| Al iv | 0.02 | 0.01 | 0.01 | 0.00 | 0.00 | 0.00 | 0.00 | 0.00 | 0.00 | 0.00 | 0.00 | 0.01 | 0.01 | 0.00 |
| | | | | | | | | | | | | | | |
| Al vi | 2.01 | 2.02 | 1.99 | 2.02 | 1.99 | 2.01 | 2.02 | 2.01 | 2.01 | 2.02 | 2.01 | 2.01 | 2.00 | 2.00 |
| Ti | 0.00 | 0.00 | 0.01 | 0.00 | 0.01 | 0.00 | 0.00 | 0.01 | 0.00 | 0.00 | 0.00 | 0.00 | 0.00 | 0.00 |
| Cr | 0.00 | 0.00 | 0.00 | 0.00 | 0.00 | 0.00 | 0.00 | 0.00 | 0.00 | 0.00 | 0.00 | 0.00 | 0.00 | 0.00 |
| $Fe^{3+}$ | 0.00 | 0.00 | 0.00 | 0.00 | 0.00 | 0.00 | 0.00 | 0.00 | 0.00 | 0.00 | 0.00 | 0.00 | 0.00 | 0.00 |
| | | | | | | | | | | | | | | |
| $Fe^{2+}$ | 2.29 | 2.40 | 1.64 | 2.24 | 1.79 | 2.50 | 2.23 | 1.94 | 2.33 | 2.36 | 2.12 | 2.12 | 2.02 | 2.10 |
| Mn | 0.31 | 0.05 | 0.31 | 0.26 | 0.24 | 0.04 | 0.26 | 0.04 | 0.25 | 0.09 | 0.03 | 0.05 | 0.03 | 0.05 |
| Mg | 0.28 | 0.38 | 0.14 | 0.12 | 0.15 | 0.16 | 0.36 | 0.14 | 0.33 | 0.43 | 0.52 | 0.24 | 0.18 | 0.59 |
| Ni | 0.00 | 0.00 | 0.00 | 0.00 | 0.00 | 0.00 | 0.00 | 0.00 | 0.00 | 0.00 | 0.00 | 0.00 | 0.00 | 0.00 |
| Zn | 0.00 | 0.00 | 0.00 | 0.00 | 0.00 | 0.00 | 0.00 | 0.00 | 0.00 | 0.00 | 0.00 | 0.00 | 0.00 | 0.00 |
| Ca | 0.12 | 0.16 | 0.91 | 0.35 | 0.81 | 0.26 | 0.12 | 0.85 | 0.09 | 0.09 | 0.31 | 0.58 | 0.75 | 0.23 |
| Total | 8.01 | 8.00 | 8.00 | 7.99 | 8.00 | 7.99 | 7.99 | 7.99 | 8.00 | 8.00 | 8.00 | 8.00 | 8.00 | 7.99 |
| | | | | | | | | | | | | | | |
| End members | | | | | | | | | | | | | | |
| Almandine | 76.43 | 80.15 | 54.76 | 75.33 | 59.84 | 84.18 | 75.23 | 65.39 | 77.93 | 79.39 | 71.16 | 71.17 | 67.73 | 70.79 |
| Andradite | 0.00 | 0.00 | 0.00 | 0.00 | 0.00 | 0.00 | 0.00 | 0.00 | 0.00 | 0.00 | 0.00 | 0.00 | 0.00 | 0.00 |
| Grossular | 3.92 | 5.43 | 30.13 | 11.81 | 27.18 | 8.83 | 4.08 | 28.60 | 2.88 | 2.96 | 10.52 | 19.20 | 24.89 | 7.71 |
| Pyrope | 9.41 | 12.74 | 4.73 | 3.92 | 4.93 | 5.46 | 11.96 | 4.71 | 10.89 | 14.64 | 17.30 | 8.00 | 6.16 | 19.85 |
| Spessartine | 10.25 | 1.66 | 10.24 | 8.91 | 8.04 | 1.46 | 8.73 | 1.29 | 8.24 | 2.92 | 1.01 | 1.54 | 1.14 | 1.64 |
| Uvarovite | 0.00 | 0.01 | 0.15 | 0.04 | 0.00 | 0.07 | 0.00 | 0.00 | 0.06 | 0.08 | 0.01 | 0.09 | 0.08 | 0.01 |
| % cations | 99.29 | 99.57 | 99.84 | 99.24 | 99.89 | 99.10 | 99.17 | 99.30 | 99.61 | 99.14 | 99.53 | 99.51 | 99.67 | 99.26 |
| *calculated | | | | | | | | | | | | | | |

**Supplementary Table S1** – continuation

| Locality | Jarabina JAR-2 | Jarabina JAR-2 | Jarabina JAR-2 | Ľutina | Ľutina | Ľutina | Ľutina | Ľutina | Ľutina | Ľutina | Ľutina | Ľutina | Ľutina | Ľutina |
|---|---|---|---|---|---|---|---|---|---|---|---|---|---|---|
| Formation | Jarmuta-Proč Fm. | Jarmuta-Proč Fm. | Jarmuta-Proč Fm. | Malinowa Fm. | Malinowa Fm. | Malinowa Fm. | Malinowa Fm. | Malinowa Fm. | Malinowa Fm. | Malinowa Fm. | Malinowa Fm. | Malinowa Fm. | Malinowa Fm. | Malinowa Fm. |
| Age | Maastrichtian–Middle Eocene | Maastrichtian–Middle Eocene | Maastrichtian–Middle Eocene | Turonian–Campanian | Turonian–Campanian | Turonian–Campanian | Turonian–Campanian | Turonian–Campanian | Turonian–Campanian | Turonian–Campanian | Turonian–Campanian | Turonian–Campanian | Turonian–Campanian | Turonian–Campanian |
| Unit | Šariš U. | Šariš U. | Šariš U. | Šariš U. | Šariš U. | Šariš U. | Šariš U. | Šariš U. | Šariš U. | Šariš U. | Šariš U. | Šariš U. | Šariš U. | Šariš U. |
| Sample | JAR-2C | JAR-2C | JAR-2C | LU-5A | LU-5A | LU-5A | LU-5A | LU-5A | LU-5A | LU-5A | LU-5A | LU-5A | LU-5A | LU-5A |
| Point | an22 | an23 | an24 | an12 | an14 | an22 | an23 | an24 | an31 | an32 | an33 | an39 | an40 | an41 |
| $SiO_2$ | 36.98 | 38.13 | 37.57 | 37.82 | 38.81 | 37.57 | 36.80 | 37.52 | 36.57 | 37.16 | 37.20 | 37.61 | 37.33 | 37.54 |
| $TiO_2$ | 0.03 | 0.04 | 0.10 | 0.01 | 0.05 | 0.03 | 0.00 | 0.02 | 0.00 | 0.06 | 0.05 | 0.00 | 0.00 | 0.02 |
| $Al_2O_3$ | 20.98 | 21.74 | 21.09 | 21.56 | 22.29 | 21.30 | 21.12 | 21.51 | 21.04 | 21.01 | 21.13 | 21.19 | 21.00 | 21.35 |
| $Cr_2O_3$ | 0.01 | 0.10 | 0.02 | 0.01 | 0.05 | 0.01 | 0.03 | 0.00 | 0.02 | 0.00 | 0.04 | 0.04 | 0.04 | 0.01 |
| $Fe_2O_3^*$ | 0.24 | 0.00 | 0.00 | 0.00 | 0.00 | 0.00 | 0.00 | 0.00 | 0.00 | 0.20 | 0.00 | 0.00 | 0.00 | 0.00 |
| FeO | 37.54 | 31.48 | 31.88 | 31.31 | 27.16 | 33.17 | 29.70 | 33.28 | 31.06 | 33.15 | 35.69 | 32.11 | 34.07 | 32.39 |
| MnO | 1.31 | 1.87 | 2.81 | 5.96 | 0.34 | 1.61 | 8.39 | 1.96 | 9.26 | 4.05 | 1.38 | 2.45 | 1.75 | 0.97 |
| MgO | 1.71 | 5.37 | 0.95 | 3.00 | 7.23 | 3.59 | 2.28 | 3.90 | 1.48 | 2.65 | 2.82 | 3.50 | 3.18 | 3.60 |
| NiO | 0.00 | 0.00 | 0.00 | 0.00 | 0.00 | 0.00 | 0.00 | 0.00 | 0.00 | 0.00 | 0.00 | 0.00 | 0.00 | 0.00 |
| ZnO | 0.00 | 0.00 | 0.00 | 0.00 | 0.00 | 0.00 | 0.00 | 0.00 | 0.00 | 0.00 | 0.00 | 0.00 | 0.00 | 0.00 |
| CaO | 2.11 | 1.45 | 6.06 | 1.58 | 4.36 | 2.57 | 1.05 | 1.40 | 0.30 | 2.13 | 1.39 | 2.74 | 2.31 | 3.51 |
| Total | 100.90 | 100.17 | 100.48 | 101.25 | 100.29 | 99.84 | 99.36 | 99.59 | 99.71 | 100.41 | 99.70 | 99.63 | 99.67 | 99.39 |
| | | | | | | | | | | | | | | |
| Formulae based on 12 oxygens and with $Fe^{2+}/Fe^{3+}$ calculated assuming full occupancy | | | | | | | | | | | | | | |
| Si | 2.98 | 3.00 | 3.01 | 3.00 | 2.99 | 3.00 | 2.99 | 2.99 | 2.99 | 2.99 | 3.00 | 3.01 | 3.01 | 3.00 |
| Al iv | 0.02 | 0.00 | 0.00 | 0.00 | 0.01 | 0.00 | 0.01 | 0.01 | 0.01 | 0.01 | 0.00 | 0.00 | 0.00 | 0.00 |
| | | | | | | | | | | | | | | |
| Al vi | 1.98 | 2.01 | 1.99 | 2.01 | 2.01 | 2.01 | 2.02 | 2.02 | 2.01 | 1.98 | 2.01 | 2.00 | 1.99 | 2.01 |
| Ti | 0.00 | 0.00 | 0.01 | 0.00 | 0.00 | 0.00 | 0.00 | 0.00 | 0.00 | 0.00 | 0.00 | 0.00 | 0.00 | 0.00 |
| Cr | 0.00 | 0.01 | 0.00 | 0.00 | 0.00 | 0.00 | 0.00 | 0.00 | 0.00 | 0.00 | 0.00 | 0.00 | 0.00 | 0.00 |
| $Fe^{3+}$ | 0.01 | 0.00 | 0.00 | 0.00 | 0.00 | 0.00 | 0.00 | 0.00 | 0.00 | 0.01 | 0.00 | 0.00 | 0.00 | 0.00 |
| | | | | | | | | | | | | | | |
| $Fe^{2+}$ | 2.53 | 2.10 | 2.15 | 2.09 | 1.77 | 2.23 | 2.04 | 2.26 | 2.14 | 2.23 | 2.43 | 2.16 | 2.30 | 2.19 |
| Mn | 0.09 | 0.12 | 0.19 | 0.40 | 0.02 | 0.11 | 0.58 | 0.13 | 0.64 | 0.28 | 0.09 | 0.17 | 0.12 | 0.07 |
| Mg | 0.21 | 0.63 | 0.11 | 0.35 | 0.83 | 0.43 | 0.28 | 0.46 | 0.18 | 0.32 | 0.34 | 0.42 | 0.38 | 0.43 |
| Ni | 0.00 | 0.00 | 0.00 | 0.00 | 0.00 | 0.00 | 0.00 | 0.00 | 0.00 | 0.00 | 0.00 | 0.00 | 0.00 | 0.00 |
| Zn | 0.00 | 0.00 | 0.00 | 0.00 | 0.00 | 0.00 | 0.00 | 0.00 | 0.00 | 0.00 | 0.00 | 0.00 | 0.00 | 0.00 |
| Ca | 0.18 | 0.12 | 0.52 | 0.13 | 0.36 | 0.22 | 0.09 | 0.12 | 0.03 | 0.18 | 0.12 | 0.24 | 0.20 | 0.30 |
| Total | 8.01 | 8.00 | 7.99 | 8.00 | 8.00 | 8.00 | 8.00 | 8.00 | 8.00 | 8.01 | 8.00 | 7.99 | 8.00 | 8.00 |
| | | | | | | | | | | | | | | |
| End members | | | | | | | | | | | | | | |
| Almandine | 84.00 | 70.56 | 72.33 | 70.21 | 59.39 | 74.68 | 68.36 | 75.90 | 71.65 | 74.01 | 81.42 | 72.57 | 76.63 | 73.33 |
| Andradite | 0.74 | 0.00 | 0.00 | 0.00 | 0.00 | 0.00 | 0.00 | 0.00 | 0.00 | 0.60 | 0.00 | 0.00 | 0.00 | 0.00 |
| Grossular | 5.35 | 3.77 | 17.39 | 4.48 | 11.92 | 7.32 | 2.96 | 4.03 | 0.82 | 5.53 | 3.91 | 7.78 | 6.53 | 10.06 |
| Pyrope | 6.90 | 21.16 | 3.79 | 11.87 | 27.81 | 14.31 | 9.25 | 15.61 | 6.04 | 10.62 | 11.38 | 13.98 | 12.74 | 14.38 |
| Spessartine | 2.99 | 4.19 | 6.41 | 13.41 | 0.74 | 3.65 | 19.33 | 4.45 | 21.44 | 9.24 | 3.17 | 5.56 | 3.99 | 2.20 |
| Uvarovite | 0.02 | 0.33 | 0.07 | 0.02 | 0.14 | 0.04 | 0.09 | 0.00 | 0.05 | 0.00 | 0.12 | 0.11 | 0.12 | 0.03 |
| % cations | 99.37 | 99.24 | 99.39 | 99.51 | 99.49 | 99.60 | 99.52 | 99.16 | 99.53 | 99.60 | 99.44 | 99.50 | 99.81 | 99.44 |
| *calculated | | | | | | | | | | | | | | |

**Supplementary Table S1** – continuation

| Locality | Ľutina | Ľutina | Ľutina | Ľutina | Ľutina | Ľutina | Ľutina | Ľutina | Ľutina | Ľutina | Ľutina | Ľutina | Ľutina | Ľutina | Ľutina | Ľutina |
|---|---|---|---|---|---|---|---|---|---|---|---|---|---|---|---|---|
| Formation | Malinowa Fm. | Malinowa Fm. | Malinowa Fm. | Malinowa Fm. | Malinowa Fm. | Malinowa Fm. | Malinowa Fm. | Malinowa Fm. | Malinowa Fm. | Malinowa Fm. | Malinowa Fm. | Malinowa Fm. | Malinowa Fm. | Malinowa Fm. | Malinowa Fm. | Malinowa Fm. |
| Age | Turonian–Campanian | Turonian–Campanian | Turonian–Campanian | Turonian–Campanian | Turonian–Campanian | Turonian–Campanian | Turonian–Campanian | Turonian–Campanian | Turonian–Campanian | Turonian–Campanian | Turonian–Campanian | Turonian–Campanian | Turonian–Campanian | Turonian–Campanian | Turonian–Campanian | Turonian–Campanian |
| Unit | Šariš U. | Šariš U. | Šariš U. | Šariš U. | Šariš U. | Šariš U. | Šariš U. | Šariš U. | Šariš U. | Šariš U. | Šariš U. | Šariš U. | Šariš U. | Šariš U. | Šariš U. | Šariš U. |
| Sample | LU-5A | LU-5A | LU-5A | LU-5B | LU-5B | LU-5B | LU-5B | LU-5B | LU-5B | LU-5B | LU-5B | LU-5B | LU-5B | LU-5B | LU-5B | LU-5B |
| Point | an43 | an44 | an52 | an1 | an2 | an3 | an4 | an5 | an8 | an9 | an10 | an11 | an13 | an17 | an19 | an21 |
| $SiO_2$ | 37.81 | 37.30 | 36.34 | 38.00 | 37.31 | 37.58 | 38.01 | 37.77 | 37.50 | 37.64 | 38.08 | 37.81 | 37.80 | 37.68 | 37.77 | 37.76 |
| $TiO_2$ | 0.05 | 0.01 | 0.10 | 0.08 | 0.00 | 0.00 | 0.01 | 0.00 | 0.00 | 0.00 | 0.00 | 0.01 | 0.06 | 0.02 | 0.12 | 0.03 |
| $Al_2O_3$ | 21.68 | 21.30 | 20.87 | 21.55 | 21.26 | 21.58 | 21.25 | 21.40 | 21.45 | 21.40 | 21.82 | 21.51 | 21.37 | 21.53 | 21.27 | 21.34 |
| $Cr_2O_3$ | 0.02 | 0.00 | 0.00 | 0.00 | 0.02 | 0.03 | 0.00 | 0.01 | 0.02 | 0.02 | 0.01 | 0.01 | 0.04 | 0.00 | 0.00 | 0.00 |
| $Fe_2O_3^*$ | 0.00 | 0.00 | 0.00 | 0.00 | 0.00 | 0.00 | 0.00 | 0.00 | 0.00 | 0.00 | 0.00 | 0.00 | 0.15 | 0.00 | 0.00 | 0.43 |
| FeO | 31.92 | 31.53 | 28.83 | 31.22 | 34.81 | 32.94 | 33.85 | 32.53 | 33.39 | 34.01 | 32.35 | 31.45 | 31.17 | 34.26 | 25.36 | 19.23 |
| MnO | 1.71 | 3.16 | 10.78 | 0.89 | 2.93 | 1.17 | 0.47 | 2.26 | 1.97 | 1.78 | 0.77 | 1.10 | 0.68 | 2.03 | 5.31 | 17.20 |
| MgO | 4.16 | 3.31 | 1.61 | 4.57 | 2.67 | 3.68 | 4.08 | 3.42 | 3.51 | 3.81 | 4.56 | 4.65 | 4.55 | 3.61 | 1.26 | 3.63 |
| NiO | 0.00 | 0.00 | 0.00 | 0.00 | 0.00 | 0.00 | 0.00 | 0.00 | 0.00 | 0.00 | 0.00 | 0.00 | 0.00 | 0.00 | 0.00 | 0.00 |
| ZnO | 0.00 | 0.00 | 0.00 | 0.00 | 0.00 | 0.00 | 0.00 | 0.00 | 0.00 | 0.00 | 0.00 | 0.00 | 0.00 | 0.00 | 0.00 | 0.00 |
| CaO | 2.91 | 2.49 | 0.73 | 3.23 | 0.92 | 3.11 | 2.40 | 2.30 | 2.34 | 1.39 | 3.07 | 3.23 | 4.27 | 1.63 | 9.15 | 2.00 |
| Total | 100.26 | 99.10 | 99.26 | 99.54 | 99.92 | 100.09 | 100.07 | 99.69 | 100.19 | 100.05 | 100.66 | 99.78 | 100.10 | 100.76 | 100.24 | 101.61 |
| | | | | | | | | | | | | | | | | |
| Formulae based on 12 oxygens and with $Fe^{2+}/Fe^{3+}$ calculated assuming full occupancy | | | | | | | | | | | | | | | | |
| Si | 2.99 | 3.00 | 2.98 | 3.00 | 3.00 | 2.99 | 3.02 | 3.01 | 2.99 | 3.00 | 2.99 | 3.00 | 2.99 | 2.99 | 3.00 | 2.98 |
| Al iv | 0.01 | 0.00 | 0.02 | 0.00 | 0.00 | 0.01 | 0.00 | 0.00 | 0.01 | 0.00 | 0.01 | 0.00 | 0.01 | 0.01 | 0.00 | 0.02 |
| | | | | | | | | | | | | | | | | |
| Al vi | 2.01 | 2.02 | 2.00 | 2.01 | 2.02 | 2.01 | 1.99 | 2.02 | 2.01 | 2.01 | 2.01 | 2.01 | 1.98 | 2.01 | 2.00 | 1.97 |
| Ti | 0.00 | 0.00 | 0.01 | 0.00 | 0.00 | 0.00 | 0.00 | 0.00 | 0.00 | 0.00 | 0.00 | 0.00 | 0.00 | 0.00 | 0.01 | 0.00 |
| Cr | 0.00 | 0.00 | 0.00 | 0.00 | 0.00 | 0.00 | 0.00 | 0.00 | 0.00 | 0.00 | 0.00 | 0.00 | 0.00 | 0.00 | 0.00 | 0.00 |
| $Fe^{3+}$ | 0.00 | 0.00 | 0.00 | 0.00 | 0.00 | 0.00 | 0.00 | 0.00 | 0.00 | 0.00 | 0.00 | 0.00 | 0.01 | 0.00 | 0.00 | 0.03 |
| | | | | | | | | | | | | | | | | |
| $Fe^{2+}$ | 2.13 | 2.15 | 1.99 | 2.10 | 2.37 | 2.21 | 2.26 | 2.21 | 2.24 | 2.29 | 2.14 | 2.09 | 2.06 | 2.29 | 1.70 | 1.27 |
| Mn | 0.11 | 0.22 | 0.75 | 0.06 | 0.20 | 0.08 | 0.03 | 0.15 | 0.13 | 0.12 | 0.05 | 0.07 | 0.05 | 0.14 | 0.36 | 1.15 |
| Mg | 0.49 | 0.40 | 0.20 | 0.54 | 0.32 | 0.44 | 0.48 | 0.41 | 0.42 | 0.45 | 0.53 | 0.55 | 0.54 | 0.43 | 0.15 | 0.43 |
| Ni | 0.00 | 0.00 | 0.00 | 0.00 | 0.00 | 0.00 | 0.00 | 0.00 | 0.00 | 0.00 | 0.00 | 0.00 | 0.00 | 0.00 | 0.00 | 0.00 |
| Zn | 0.00 | 0.00 | 0.00 | 0.00 | 0.00 | 0.00 | 0.00 | 0.00 | 0.00 | 0.00 | 0.00 | 0.00 | 0.00 | 0.00 | 0.00 | 0.00 |
| Ca | 0.25 | 0.21 | 0.06 | 0.27 | 0.08 | 0.27 | 0.20 | 0.20 | 0.20 | 0.12 | 0.26 | 0.27 | 0.36 | 0.14 | 0.78 | 0.17 |
| Total | 8.00 | 8.00 | 8.01 | 7.99 | 8.00 | 8.00 | 7.99 | 7.99 | 8.00 | 8.00 | 8.00 | 8.00 | 8.00 | 8.00 | 7.99 | 8.01 |
| | | | | | | | | | | | | | | | | |
| End members | | | | | | | | | | | | | | | | |
| Almandine | 71.49 | 72.23 | 66.12 | 70.60 | 79.85 | 73.88 | 75.90 | 74.49 | 74.91 | 76.79 | 71.78 | 69.98 | 68.43 | 76.53 | 56.89 | 41.42 |
| Andradite | 0.00 | 0.00 | 0.00 | 0.00 | 0.00 | 0.00 | 0.00 | 0.00 | 0.00 | 0.00 | 0.00 | 0.00 | 0.46 | 0.00 | 0.00 | 1.28 |
| Grossular | 8.18 | 7.21 | 2.13 | 9.23 | 2.60 | 8.79 | 6.85 | 6.62 | 6.61 | 3.91 | 8.63 | 9.16 | 11.51 | 4.63 | 26.12 | 4.40 |
| Pyrope | 16.43 | 13.34 | 6.62 | 18.17 | 10.77 | 14.61 | 16.19 | 13.73 | 13.95 | 15.20 | 17.85 | 18.37 | 17.93 | 14.27 | 4.99 | 14.32 |
| Spessartine | 3.83 | 7.23 | 25.13 | 2.00 | 6.71 | 2.63 | 1.05 | 5.14 | 4.46 | 4.03 | 1.71 | 2.47 | 1.52 | 4.57 | 11.99 | 38.58 |
| Uvarovite | 0.07 | 0.00 | 0.01 | 0.00 | 0.07 | 0.09 | 0.00 | 0.02 | 0.06 | 0.08 | 0.02 | 0.02 | 0.13 | 0.00 | 0.00 | 0.00 |
| % cations | 99.50 | 99.27 | 99.34 | 99.11 | 99.19 | 99.57 | 99.47 | 98.93 | 99.69 | 99.44 | 99.60 | 99.78 | 99.62 | 99.71 | 99.60 | 99.24 |
| *calculated | | | | | | | | | | | | | | | | |

## Supplementary Table S2

Representative microprobe analyses of detrital tourmalines from Upper Cretaceous to Paleocene deposits of the Jarmuta-Proč Fm., structural drill JAR-2, Pieniny sector of the PKB, Western Carpathians, Slovakia

| Locality | Jarabina JAR-2 | Jarabina JAR-2 | Jarabina JAR-2 | Jarabina JAR-2 | Jarabina JAR-2 | Jarabina JAR-2 | Jarabina JAR-2 | Jarabina JAR-2 | Jarabina JAR-2 | Jarabina JAR-2 | Jarabina JAR-2 | Jarabina JAR-2 | Jarabina JAR-2 | Jarabina JAR-2 |
|---|---|---|---|---|---|---|---|---|---|---|---|---|---|---|
| Formation | Jarmuta-Proč Fm. | Jarmuta-Proč Fm. | Jarmuta-Proč Fm. | Jarmuta-Proč Fm. | Jarmuta-Proč Fm. | Jarmuta-Proč Fm. | Jarmuta-Proč Fm. | Jarmuta-Proč Fm. | Jarmuta-Proč Fm. | Jarmuta-Proč Fm. | Jarmuta-Proč Fm. | Jarmuta-Proč Fm. | Jarmuta-Proč Fm. | Jarmuta-Proč Fm. |
| Age | Maastrichtian–Middle Eocene | Maastrichtian–Middle Eocene | Maastrichtian–Middle Eocene | Maastrichtian–Middle Eocene | Maastrichtian–Middle Eocene | Maastrichtian–Middle Eocene | Maastrichtian–Middle Eocene | Maastrichtian–Middle Eocene | Maastrichtian–Middle Eocene | Maastrichtian–Middle Eocene | Maastrichtian–Middle Eocene | Maastrichtian–Middle Eocene | Maastrichtian–Middle Eocene | Maastrichtian–Middle Eocene |
| Unit | Šariš U. | Šariš U. | Šariš U. | Šariš U. | Šariš U. | Šariš U. | Šariš U. | Šariš U. | Šariš U. | Šariš U. | Šariš U. | Šariš U. | Šariš U. | Šariš U. |
| Sample | JAR-2A | JAR-2A | JAR-2A | JAR-2A | JAR-2A | JAR-2A | JAR-2A | JAR-2A | JAR-2A | JAR-2A | JAR-2A | JAR-2A | JAR-2A | JAR-2A |
| Point | an1 | an2 | an3 | an4 | an7 | an9 | an10 | an12 | an13 | an30 | an31 | an32 | an33 | an34 |
| Mineral | Srl | Foi | Mg-Foi | Vac-Mg-O root | Foi | Vac-Mg-O root | Vac-Mg-O root | Mg-Foi | Vac-Mg-O root | Mg-Foi | Drv | Vac-Mg-O root | Vac-Mg-O root | Drv |
| $SiO_2$ | 36.27 | 35.14 | 36.27 | 36.34 | 35.48 | 37.53 | 37.62 | 37.14 | 37.02 | 36.53 | 36.56 | 37.05 | 38.22 | 36.62 |
| $TiO_2$ | 0.67 | 0.68 | 0.96 | 0.61 | 0.22 | 0.10 | 0.19 | 0.45 | 0.58 | 0.38 | 0.91 | 0.56 | 0.49 | 0.08 |
| $Al_2O_3$ | 31.48 | 28.35 | 30.88 | 33.70 | 30.93 | 33.24 | 34.02 | 33.00 | 33.51 | 29.49 | 31.37 | 31.72 | 29.04 | 30.01 |
| $V_2O_3$ | 0.03 | 0.03 | 0.02 | 0.05 | 0.04 | 0.02 | 0.00 | 0.02 | 0.05 | 0.07 | 0.01 | 0.05 | 0.06 | 0.03 |
| $Cr_2O_3$ | 0.03 | 0.00 | 0.05 | 0.01 | 0.00 | 0.02 | 0.00 | 0.01 | 0.02 | 0.03 | 0.04 | 0.02 | 0.00 | 0.00 |
| FeO | 10.23 | 12.95 | 8.84 | 5.48 | 13.44 | 2.77 | 2.92 | 3.36 | 5.21 | 9.14 | 8.00 | 7.85 | 7.28 | 8.73 |
| MnO | 0.03 | 0.04 | 0.02 | 0.00 | 0.10 | 0.00 | 0.00 | 0.00 | 0.05 | 0.16 | 0.04 | 0.02 | 0.00 | 0.05 |
| ZnO | 0.04 | 0.05 | 0.00 | 0.00 | 0.21 | 0.08 | 0.00 | 0.07 | 0.13 | 0.00 | 0.02 | 0.00 | 0.05 | 0.01 |
| CuO | 0.00 | 0.00 | 0.00 | 0.01 | 0.00 | 0.00 | 0.00 | 0.02 | 0.03 | 0.00 | 0.03 | 0.00 | 0.03 | 0.07 |
| MgO | 5.01 | 4.86 | 6.15 | 6.57 | 3.15 | 9.32 | 8.38 | 8.75 | 7.04 | 7.60 | 6.37 | 6.75 | 7.92 | 7.29 |
| CaO | 0.12 | 1.29 | 0.51 | 0.58 | 0.53 | 0.02 | 0.05 | 0.63 | 0.55 | 0.57 | 0.11 | 0.09 | 0.09 | 0.03 |
| BaO | 0.00 | 0.03 | 0.00 | 0.00 | 0.00 | 0.05 | 0.00 | 0.00 | 0.07 | 0.00 | 0.01 | 0.00 | 0.08 | 0.00 |
| $Na_2O$ | 2.45 | 1.08 | 1.34 | 0.99 | 1.27 | 1.31 | 1.56 | 1.25 | 1.17 | 1.29 | 2.39 | 1.42 | 1.47 | 2.99 |
| $K_2O$ | 0.01 | 0.06 | 0.01 | 0.01 | 0.06 | 0.01 | 0.01 | 0.05 | 0.02 | 0.03 | 0.01 | 0.02 | 0.01 | 0.01 |
| F | 0.13 | 0.09 | 0.00 | 0.09 | 0.29 | 0.01 | 0.00 | 0.05 | 0.04 | 0.06 | 0.20 | 0.17 | 0.24 | 0.00 |
| Cl | 0.01 | 0.01 | 0.00 | 0.01 | 0.01 | 0.01 | 0.00 | 0.01 | 0.01 | 0.00 | 0.01 | 0.01 | 0.04 | 0.02 |
| $H_2O^*$ | 3.37 | 3.10 | 3.17 | 3.07 | 2.97 | 3.17 | 3.24 | 3.22 | 3.18 | 3.17 | 3.33 | 3.09 | 3.05 | 3.58 |
| $B_2O_3^*$ | 10.43 | 10.108 | 10.428 | 10.537 | 10.233 | 10.786 | 10.752 | 10.695 | 10.661 | 10.515 | 10.487 | 10.607 | 10.522 | 10.468 |
| O = F | 0.06 | 0.04 | 0.00 | 0.04 | 0.12 | 0.01 | 0.00 | 0.02 | 0.02 | 0.02 | 0.08 | 0.07 | 0.10 | 0.00 |
| Total [%] | 100.26 | 97.83 | 98.63 | 97.99 | 98.82 | 98.44 | 98.75 | 98.69 | 99.31 | 99.01 | 99.79 | 99.34 | 98.46 | 99.98 |
| Si | 6.04 | 6.04 | 6.04 | 5.99 | 6.03 | 6.05 | 6.08 | 6.04 | 6.04 | 6.04 | 6.06 | 6.07 | 6.31 | 6.08 |
| Al | 0.00 | 0.00 | 0.00 | 0.01 | 0.00 | 0.00 | 0.00 | 0.00 | 0.00 | 0.00 | 0.00 | 0.00 | 0.00 | 0.00 |
| T-sum | 6.044 | 6.042 | 6.044 | 6 | 6.026 | 6.048 | 6.082 | 6.035 | 6.035 | 6.037 | 6.059 | 6.07 | 6.313 | 6.08 |
| B | 3.00 | 3.00 | 3.00 | 3.00 | 3.00 | 3.00 | 3.00 | 3.00 | 3.00 | 3.00 | 3.00 | 3.00 | 3.00 | 3.00 |
| Al | 6.00 | 5.74 | 6.00 | 6.00 | 6.00 | 6.00 | 6.00 | 6.00 | 6.00 | 5.74 | 6.00 | 6.00 | 5.65 | 5.87 |
| Cr | 0.00 | 0.00 | 0.00 | 0.00 | 0.00 | 0.00 | 0.00 | 0.00 | 0.00 | 0.00 | 0.00 | 0.00 | 0.00 | 0.00 |
| Mg | 0 | 0.252 | 0 | 0 | 0 | 0 | 0 | 0 | 0 | 0.243 | 0 | 0 | 0.338 | 0.123 |
| $Fe^{3+}$ | 0.00 | 0.00 | 0.00 | 0.00 | 0.00 | 0.00 | 0.00 | 0.00 | 0.00 | 0.00 | 0.00 | 0.00 | 0.00 | 0.00 |
| Z-sum | 6.00 | 6.00 | 6.00 | 6.00 | 6.00 | 6.00 | 6.00 | 6.00 | 6.00 | 6.00 | 6.00 | 6.00 | 6.00 | 6.00 |
| Al | 0.18 | 0.00 | 0.07 | 0.55 | 0.19 | 0.31 | 0.48 | 0.32 | 0.44 | 0.00 | 0.13 | 0.12 | 0.00 | 0.00 |
| Ti | 0.08 | 0.09 | 0.12 | 0.08 | 0.03 | 0.01 | 0.02 | 0.05 | 0.07 | 0.05 | 0.11 | 0.07 | 0.06 | 0.01 |
| $Fe^{3+}$ | 0.00 | 0.00 | 0.00 | 0.00 | 0.00 | 0.00 | 0.00 | 0.00 | 0.00 | 0.00 | 0.00 | 0.00 | 0.00 | 0.00 |
| $Fe^{2+}$ | 1.43 | 1.86 | 1.23 | 0.76 | 1.91 | 0.37 | 0.40 | 0.46 | 0.71 | 1.26 | 1.11 | 1.08 | 1.01 | 1.21 |
| $Mn^{2+}$ | 0.01 | 0.01 | 0.00 | 0.00 | 0.02 | 0.00 | 0.00 | 0.00 | 0.01 | 0.02 | 0.01 | 0.00 | 0.00 | 0.01 |
| Mg | 1.246 | 0.995 | 1.527 | 1.614 | 0.799 | 2.24 | 2.019 | 2.119 | 1.71 | 1.63 | 1.574 | 1.649 | 1.612 | 1.68 |
| Y-sum | 2.96 | 2.96 | 2.96 | 3.00 | 2.97 | 2.95 | 2.92 | 2.97 | 2.97 | 2.96 | 2.94 | 2.93 | 2.69 | 2.92 |
| Ca | 0.02 | 0.24 | 0.09 | 0.10 | 0.10 | 0.00 | 0.01 | 0.11 | 0.10 | 0.10 | 0.02 | 0.02 | 0.02 | 0.01 |
| Na | 0.79 | 0.36 | 0.43 | 0.32 | 0.42 | 0.41 | 0.49 | 0.39 | 0.37 | 0.42 | 0.77 | 0.45 | 0.47 | 0.96 |
| K | 0.00 | 0.01 | 0.00 | 0.00 | 0.01 | 0.00 | 0.00 | 0.01 | 0.01 | 0.01 | 0.00 | 0.00 | 0.00 | 0.00 |
| X-vacancy | 0.19 | 0.39 | 0.47 | 0.58 | 0.47 | 0.58 | 0.50 | 0.49 | 0.53 | 0.48 | 0.21 | 0.53 | 0.51 | 0.03 |
| X-sum | 1.00 | 1.00 | 1.00 | 1.00 | 1.00 | 1.00 | 1.00 | 1.00 | 1.00 | 1.00 | 1.00 | 1.00 | 1.00 | 1.00 |
| OH | 3.74 | 3.56 | 3.53 | 3.37 | 3.37 | 3.41 | 3.50 | 3.49 | 3.45 | 3.49 | 3.69 | 3.38 | 3.36 | 3.96 |
| O | 0.19 | 0.39 | 0.47 | 0.58 | 0.47 | 0.58 | 0.50 | 0.49 | 0.53 | 0.48 | 0.21 | 0.53 | 0.51 | 0.03 |
| V + W | 4.00 | 4.00 | 4.00 | 4.00 | 4.00 | 4.00 | 4.00 | 4.00 | 4.00 | 4.00 | 4.00 | 4.00 | 4.00 | 4.00 |
| *calculated | | | | | | | | | | | | | | |

**Supplementary Table S2** – continuation

| Locality | Jarabina JAR-2 | Jarabina JAR-2 | Jarabina JAR-2 | Jarabina JAR-2 | Jarabina JAR-2 | Jarabina JAR-2 | Jarabina JAR-2 | Jarabina JAR-2 | Jarabina JAR-2 | Jarabina JAR-2 | Jarabina JAR-2 | Jarabina JAR-2 | Jarabina JAR-2 | Jarabina JAR-2 |
|---|---|---|---|---|---|---|---|---|---|---|---|---|---|---|
| Formation | Jarmuta-Proč Fm. | Jarmuta-Proč Fm. | Jarmuta-Proč Fm. | Jarmuta-Proč Fm. | Jarmuta-Proč Fm. | Jarmuta-Proč Fm. | Jarmuta-Proč Fm. | Jarmuta-Proč Fm. | Jarmuta-Proč Fm. | Jarmuta-Proč Fm. | Jarmuta-Proč Fm. | Jarmuta-Proč Fm. | Jarmuta-Proč Fm. | Jarmuta-Proč Fm. |
| Age | Maastrichtian–Middle Eocene | Maastrichtian–Middle Eocene | Maastrichtian–Middle Eocene | Maastrichtian–Middle Eocene | Maastrichtian–Middle Eocene | Maastrichtian–Middle Eocene | Maastrichtian–Middle Eocene | Maastrichtian–Middle Eocene | Maastrichtian–Middle Eocene | Maastrichtian–Middle Eocene | Maastrichtian–Middle Eocene | Maastrichtian–Middle Eocene | Maastrichtian–Middle Eocene | Maastrichtian–Middle Eocene |
| Unit | Šariš U. | Šariš U. | Šariš U. | Šariš U. | Šariš U. | Šariš U. | Šariš U. | Šariš U. | Šariš U. | Šariš U. | Šariš U. | Šariš U. | Šariš U. | Šariš U. |
| Sample | JAR-2A | JAR-2A | JAR-2A | JAR-2B | JAR-2B | JAR-2B | JAR-2B | JAR-2B | JAR-2B | JAR-2B | JAR-2B | JAR-2B | JAR-2B | JAR-2B |
| Point | an36 | an37 | an38 | an4 | an5 | an8 | an9 | an10 | an11 | an18 | an20 | an22 | an23 | an24 |
| Mineral | Vac-Mg-O root | Vac-Mg-O root | Srl | Vac-Mg-O root | Srl | Vac-Mg-O root | Srl | Mg-Foi | Vac-Mg-O root | Vac-Mg-O root | Vac-Mg-O root | Vac-Mg-O root | Vac-Mg-O root | Vac-Mg-O root |
| $SiO_2$ | 36.97 | 34.31 | 36.51 | 36.35 | 35.47 | 36.48 | 36.35 | 36.03 | 36.13 | 36.89 | 36.84 | 36.54 | 36.64 | 36.67 |
| $TiO_2$ | 0.58 | 1.22 | 0.41 | 0.59 | 0.15 | 0.28 | 0.82 | 0.80 | 0.28 | 0.67 | 0.91 | 0.36 | 0.31 | 0.32 |
| $Al_2O_3$ | 34.31 | 26.50 | 28.16 | 31.41 | 27.77 | 32.06 | 28.23 | 30.43 | 32.44 | 32.06 | 30.91 | 34.76 | 34.43 | 31.51 |
| $V_2O_3$ | 0.16 | 0.04 | 0.04 | 0.06 | 0.07 | 0.00 | 0.05 | 0.00 | 0.04 | 0.01 | 0.04 | 0.00 | 0.13 | 0.01 |
| $Cr_2O_3$ | 0.32 | 0.01 | 0.02 | 0.04 | 0.00 | 0.04 | 0.02 | 0.00 | 0.03 | 0.01 | 0.04 | 0.00 | 0.04 | 0.02 |
| FeO | 3.10 | 11.96 | 11.92 | 9.30 | 12.27 | 9.45 | 10.34 | 8.92 | 7.11 | 5.25 | 7.77 | 7.94 | 7.34 | 9.21 |
| MnO | 0.01 | 0.00 | 0.05 | 0.00 | 0.03 | 0.02 | 0.00 | 0.07 | 0.05 | 0.05 | 0.01 | 0.00 | 0.07 | 0.05 |
| ZnO | 0.08 | 0.06 | 0.04 | 0.00 | 0.00 | 0.03 | 0.07 | 0.04 | 0.01 | 0.08 | 0.07 | 0.05 | 0.04 | 0.00 |
| CuO | 0.00 | 0.04 | 0.00 | 0.00 | 0.00 | 0.01 | 0.00 | 0.00 | 0.04 | 0.01 | 0.02 | 0.00 | 0.00 | 0.06 |
| MgO | 8.11 | 5.49 | 5.53 | 5.51 | 6.42 | 5.58 | 6.70 | 6.24 | 6.92 | 7.95 | 6.74 | 4.51 | 4.92 | 5.99 |
| CaO | 0.40 | 0.09 | 0.07 | 0.34 | 0.97 | 0.13 | 0.18 | 0.43 | 0.49 | 0.65 | 0.28 | 0.29 | 0.31 | 0.13 |
| BaO | 0.00 | 0.01 | 0.01 | 0.00 | 0.00 | 0.10 | 0.00 | 0.00 | 0.04 | 0.00 | 0.00 | 0.10 | 0.12 | 0.00 |
| $Na_2O$ | 1.06 | 1.37 | 2.63 | 1.24 | 1.24 | 1.33 | 1.49 | 1.35 | 1.21 | 1.19 | 1.39 | 0.80 | 1.03 | 1.44 |
| $K_2O$ | 0.04 | 0.03 | 0.39 | 0.01 | 0.01 | 0.02 | 0.02 | 0.02 | 0.06 | 0.01 | 0.01 | 0.01 | 0.01 | 0.02 |
| F | 0.08 | 0.00 | 0.00 | 0.05 | 0.00 | 0.02 | 0.00 | 0.00 | 0.26 | 0.13 | 0.15 | 0.00 | 0.00 | 0.12 |
| Cl | 0.01 | 0.02 | 0.02 | 0.00 | 0.01 | 0.00 | 0.00 | 0.00 | 0.00 | 0.00 | 0.01 | 0.01 | 0.00 | 0.00 |
| $H_2O^*$ | 3.13 | 2.96 | 3.50 | 3.09 | 3.16 | 3.13 | 3.13 | 3.14 | 3.05 | 3.14 | 3.10 | 3.02 | 3.09 | 3.11 |
| $B_2O_3^*$ | 10.774 | 9.821 | 10.237 | 10.414 | 10.223 | 10.518 | 10.31 | 10.352 | 10.541 | 10.609 | 10.5 | 10.565 | 10.56 | 10.517 |
| O = F | 0.04 | 0.00 | 0.00 | 0.02 | 0.00 | 0.01 | 0.00 | 0.00 | 0.11 | 0.06 | 0.06 | 0.00 | 0.00 | 0.05 |
| Total [%] | 99.11 | 93.92 | 99.53 | 98.39 | 97.80 | 99.18 | 97.70 | 97.82 | 98.59 | 98.68 | 98.69 | 98.95 | 99.04 | 99.10 |
| Si | 5.96 | 6.07 | 6.20 | 6.07 | 6.03 | 6.03 | 6.13 | 6.05 | 5.96 | 6.04 | 6.10 | 6.01 | 6.03 | 6.06 |
| Al | 0.04 | 0.00 | 0.00 | 0.00 | 0.00 | 0.00 | 0.00 | 0.00 | 0.04 | 0.00 | 0.00 | 0.00 | 0.00 | 0.00 |
| T-sum | 6 | 6.072 | 6.199 | 6.067 | 6.031 | 6.028 | 6.127 | 6.048 | 6 | 6.044 | 6.097 | 6.011 | 6.029 | 6.059 |
| B | 3.00 | 3.00 | 3.00 | 3.00 | 3.00 | 3.00 | 3.00 | 3.00 | 3.00 | 3.00 | 3.00 | 3.00 | 3.00 | 3.00 |
| Al | 6.00 | 5.53 | 5.64 | 6.00 | 5.57 | 6.00 | 5.61 | 6.00 | 6.00 | 6.00 | 6.00 | 6.00 | 6.00 | 6.00 |
| Cr | 0.00 | 0.00 | 0.00 | 0.00 | 0.00 | 0.00 | 0.00 | 0.00 | 0.00 | 0.00 | 0.00 | 0.00 | 0.00 | 0.00 |
| Mg | 0 | 0.465 | 0.357 | 0 | 0.425 | 0 | 0.381 | 0 | 0 | 0 | 0 | 0 | 0 | 0 |
| $Fe^{3+}$ | 0.00 | 0.00 | 0.00 | 0.00 | 0.00 | 0.00 | 0.00 | 0.00 | 0.00 | 0.00 | 0.00 | 0.00 | 0.00 | 0.00 |
| Z-sum | 6.00 | 6.00 | 6.00 | 6.00 | 6.00 | 6.00 | 6.00 | 6.00 | 6.00 | 6.00 | 6.00 | 6.00 | 6.00 | 6.00 |
| Al | 0.49 | 0.00 | 0.00 | 0.18 | 0.00 | 0.24 | 0.00 | 0.02 | 0.27 | 0.19 | 0.03 | 0.74 | 0.68 | 0.14 |
| Ti | 0.07 | 0.16 | 0.05 | 0.08 | 0.02 | 0.03 | 0.10 | 0.10 | 0.03 | 0.08 | 0.11 | 0.04 | 0.04 | 0.04 |
| $Fe^{3+}$ | 0.00 | 0.00 | 0.00 | 0.00 | 0.00 | 0.00 | 0.00 | 0.00 | 0.00 | 0.00 | 0.00 | 0.00 | 0.00 | 0.00 |
| $Fe^{2+}$ | 0.42 | 1.77 | 1.69 | 1.30 | 1.74 | 1.31 | 1.46 | 1.25 | 0.98 | 0.72 | 1.08 | 1.09 | 1.01 | 1.27 |
| $Mn^{2+}$ | 0.00 | 0.00 | 0.01 | 0.00 | 0.00 | 0.00 | 0.00 | 0.01 | 0.01 | 0.01 | 0.00 | 0.00 | 0.01 | 0.01 |
| Mg | 1.951 | 0.983 | 1.043 | 1.372 | 1.201 | 1.375 | 1.302 | 1.561 | 1.7 | 1.943 | 1.662 | 1.106 | 1.208 | 1.475 |
| Y-sum | 3.00 | 2.93 | 2.80 | 2.93 | 2.97 | 2.97 | 2.87 | 2.95 | 3.01 | 2.96 | 2.90 | 2.99 | 2.97 | 2.94 |
| Ca | 0.07 | 0.02 | 0.01 | 0.06 | 0.18 | 0.02 | 0.03 | 0.08 | 0.09 | 0.12 | 0.05 | 0.05 | 0.05 | 0.02 |
| Na | 0.33 | 0.47 | 0.86 | 0.40 | 0.41 | 0.43 | 0.49 | 0.44 | 0.39 | 0.38 | 0.45 | 0.25 | 0.33 | 0.46 |
| K | 0.01 | 0.01 | 0.09 | 0.00 | 0.00 | 0.00 | 0.00 | 0.00 | 0.01 | 0.00 | 0.00 | 0.00 | 0.00 | 0.00 |
| X-vacancy | 0.59 | 0.51 | 0.04 | 0.53 | 0.41 | 0.54 | 0.48 | 0.48 | 0.51 | 0.51 | 0.50 | 0.69 | 0.61 | 0.51 |
| X-sum | 1.00 | 1.00 | 1.00 | 1.00 | 1.00 | 1.00 | 1.00 | 1.00 | 1.00 | 1.00 | 1.00 | 1.00 | 1.00 | 1.00 |
| OH | 3.37 | 3.49 | 3.96 | 3.44 | 3.59 | 3.45 | 3.52 | 3.52 | 3.36 | 3.43 | 3.42 | 3.31 | 3.39 | 3.43 |
| O | 0.59 | 0.51 | 0.04 | 0.53 | 0.41 | 0.54 | 0.48 | 0.48 | 0.51 | 0.51 | 0.50 | 0.69 | 0.61 | 0.51 |
| V + W | 4.00 | 4.00 | 4.00 | 4.00 | 4.00 | 4.00 | 4.00 | 4.00 | 4.00 | 4.00 | 4.00 | 4.00 | 4.00 | 4.00 |
| *calculated | | | | | | | | | | | | | | |

**Supplementary Table S2** – continuation

| Locality | Jarabina JAR-2 | Jarabina JAR-2 | Jarabina JAR-2 | Jarabina JAR-2 | Jarabina JAR-2 | Jarabina JAR-2 | Jarabina JAR-2 | Jarabina JAR-2 | Jarabina JAR-2 | Jarabina JAR-2 | Jarabina JAR-2 | Jarabina JAR-2 | Jarabina JAR-2 | Jarabina JAR-2 |
|---|---|---|---|---|---|---|---|---|---|---|---|---|---|---|
| Formation | Jarmuta-Proč Fm. | Jarmuta-Proč Fm. | Jarmuta-Proč Fm. | Jarmuta-Proč Fm. | Jarmuta-Proč Fm. | Jarmuta-Proč Fm. | Jarmuta-Proč Fm. | Jarmuta-Proč Fm. | Jarmuta-Proč Fm. | Jarmuta-Proč Fm. | Jarmuta-Proč Fm. | Jarmuta-Proč Fm. | Jarmuta-Proč Fm. | Jarmuta-Proč Fm. |
| Age | Maastrichtian–Middle Eocene | Maastrichtian–Middle Eocene | Maastrichtian–Middle Eocene | Maastrichtian–Middle Eocene | Maastrichtian–Middle Eocene | Maastrichtian–Middle Eocene | Maastrichtian–Middle Eocene | Maastrichtian–Middle Eocene | Maastrichtian–Middle Eocene | Maastrichtian–Middle Eocene | Maastrichtian–Middle Eocene | Maastrichtian–Middle Eocene | Maastrichtian–Middle Eocene | Maastrichtian–Middle Eocene |
| Unit | Šariš U. | Šariš U. | Šariš U. | Šariš U. | Šariš U. | Šariš U. | Šariš U. | Šariš U. | Šariš U. | Šariš U. | Šariš U. | Šariš U. | Šariš U. | Šariš U. |
| Sample | JAR-2B | JAR-2B | JAR-2B | JAR-2B | JAR-2B | JAR-2B | JAR-2B | JAR-2C | JAR-2C | JAR-2C | JAR-2C | JAR-2C | JAR-2C | JAR-2C |
| Point | an25 | an27 | an28 | an30 | an31 | an32 | an33 | an7 | an11 | an12 | an13 | an14 | an15 | an25 |
| Mineral | Vac-Mg-O root | Vac-Mg-O root | Mg-Foi | Vac-Mg-O root | Vac-Mg-O root | Vac-Mg-O root | Mg-Foi | Drv | Vac-Fe-O root | Vac-Mg-O root | Vac-Fe-O root | Drv | Srl | Foi |
| $SiO_2$ | 36.34 | 34.78 | 36.98 | 36.29 | 36.20 | 36.73 | 36.45 | 36.62 | 36.76 | 36.74 | 34.43 | 36.85 | 35.85 | 35.36 |
| $TiO_2$ | 0.88 | 0.60 | 0.97 | 0.90 | 0.87 | 0.30 | 0.75 | 1.19 | 0.34 | 0.86 | 0.15 | 0.00 | 0.54 | 0.52 |
| $Al_2O_3$ | 32.57 | 34.02 | 31.20 | 34.16 | 34.85 | 35.29 | 32.37 | 30.97 | 32.74 | 32.77 | 34.48 | 31.73 | 27.57 | 33.33 |
| $V_2O_3$ | 0.05 | 0.00 | 0.03 | 0.01 | 0.07 | 0.03 | 0.02 | 0.10 | 0.00 | 0.04 | 0.00 | 0.03 | 0.08 | 0.03 |
| $Cr_2O_3$ | 0.01 | 0.02 | 0.04 | 0.04 | 0.11 | 0.06 | 0.04 | 0.04 | 0.00 | 0.03 | 0.01 | 0.00 | 0.00 | 0.00 |
| FeO | 8.79 | 11.24 | 7.67 | 6.05 | 7.55 | 6.90 | 4.91 | 8.49 | 9.27 | 5.63 | 14.49 | 8.14 | 12.37 | 9.70 |
| MnO | 0.05 | 0.05 | 0.02 | 0.09 | 0.00 | 0.00 | 0.10 | 0.03 | 0.07 | 0.00 | 0.19 | 0.04 | 0.05 | 0.02 |
| ZnO | 0.05 | 0.10 | 0.02 | 0.06 | 0.00 | 0.07 | 0.03 | 0.00 | 0.05 | 0.03 | 0.15 | 0.04 | 0.00 | 0.16 |
| CuO | 0.00 | 0.00 | 0.00 | 0.00 | 0.02 | 0.00 | 0.00 | 0.00 | 0.00 | 0.00 | 0.01 | 0.00 | 0.00 | 0.00 |
| MgO | 5.53 | 3.02 | 6.97 | 6.50 | 4.68 | 4.73 | 7.65 | 6.78 | 5.11 | 6.92 | 0.30 | 6.85 | 6.16 | 4.40 |
| CaO | 0.66 | 0.55 | 0.60 | 0.70 | 0.47 | 0.21 | 0.44 | 0.33 | 0.14 | 0.31 | 0.24 | 0.23 | 0.35 | 0.96 |
| BaO | 0.03 | 0.00 | 0.00 | 0.00 | 0.00 | 0.00 | 0.00 | 0.03 | 0.01 | 0.01 | 0.00 | 0.00 | 0.00 | 0.03 |
| $Na_2O$ | 0.94 | 1.01 | 1.30 | 1.00 | 0.95 | 0.91 | 1.36 | 2.52 | 1.22 | 1.14 | 1.01 | 2.86 | 2.76 | 1.00 |
| $K_2O$ | 0.01 | 0.05 | 0.01 | 0.02 | 0.01 | 0.01 | 0.02 | 0.01 | 0.01 | 0.01 | 0.04 | 0.03 | 0.03 | 0.05 |
| F | 0.12 | 0.24 | 0.00 | 0.07 | 0.00 | 0.00 | 0.02 | 0.13 | 0.05 | 0.10 | 0.00 | 0.00 | 0.02 | 0.00 |
| Cl | 0.00 | 0.01 | 0.00 | 0.01 | 0.01 | 0.01 | 0.01 | 0.00 | 0.01 | 0.00 | 0.00 | 0.01 | 0.01 | 0.00 |
| $H_2O^*$ | 3.06 | 2.96 | 3.21 | 3.14 | 3.09 | 3.04 | 3.18 | 3.47 | 3.08 | 3.07 | 2.98 | 3.61 | 3.51 | 3.15 |
| $B_2O_3^*$ | 10.557 | 10.356 | 10.587 | 10.675 | 10.587 | 10.602 | 10.522 | 10.585 | 10.552 | 10.555 | 10.201 | 10.585 | 10.241 | 10.413 |
| O = F | 0.05 | 0.10 | 0.00 | 0.03 | 0.00 | 0.00 | 0.01 | 0.06 | 0.02 | 0.04 | 0.00 | 0.00 | 0.01 | 0.00 |
| Total [%] | 99.60 | 98.91 | 99.61 | 99.68 | 99.46 | 98.89 | 97.83 | 101.23 | 99.40 | 98.16 | 98.68 | 100.99 | 99.54 | 99.13 |
| Si | 5.98 | 5.84 | 6.07 | 5.91 | 5.94 | 6.02 | 6.02 | 6.01 | 6.06 | 6.05 | 5.87 | 6.05 | 6.09 | 5.90 |
| Al | 0.02 | 0.16 | 0.00 | 0.09 | 0.06 | 0.00 | 0.00 | 0.00 | 0.00 | 0.00 | 0.13 | 0.00 | 0.00 | 0.10 |
| T-sum | 6 | 6 | 6.071 | 6 | 6 | 6.022 | 6.02 | 6.013 | 6.055 | 6.049 | 6 | 6.05 | 6.085 | 6 |
| B | 3.00 | 3.00 | 3.00 | 3.00 | 3.00 | 3.00 | 3.00 | 3.00 | 3.00 | 3.00 | 3.00 | 3.00 | 3.00 | 3.00 |
| Al | 6.00 | 6.00 | 6.00 | 6.00 | 6.00 | 6.00 | 6.00 | 5.99 | 6.00 | 6.00 | 6.00 | 6.00 | 5.51 | 6.00 |
| Cr | 0.00 | 0.00 | 0.00 | 0.00 | 0.00 | 0.00 | 0.00 | 0.01 | 0.00 | 0.00 | 0.00 | 0.00 | 0.00 | 0.00 |
| Mg | 0 | 0 | 0 | 0 | 0 | 0 | 0 | 0 | 0 | 0 | 0 | 0 | 0.475 | 0 |
| $Fe^{3+}$ | 0.00 | 0.00 | 0.00 | 0.00 | 0.00 | 0.00 | 0.00 | 0.00 | 0.00 | 0.00 | 0.00 | 0.00 | 0.00 | 0.00 |
| Z-sum | 6.00 | 6.00 | 6.00 | 6.00 | 6.00 | 6.00 | 6.00 | 6.00 | 6.00 | 6.00 | 6.00 | 6.00 | 6.00 | 6.00 |
| Al | 0.30 | 0.57 | 0.04 | 0.46 | 0.69 | 0.82 | 0.30 | 0.00 | 0.36 | 0.36 | 0.79 | 0.14 | 0.00 | 0.46 |
| Ti | 0.11 | 0.08 | 0.12 | 0.11 | 0.11 | 0.04 | 0.09 | 0.15 | 0.04 | 0.11 | 0.02 | 0.00 | 0.07 | 0.07 |
| $Fe^{3+}$ | 0.00 | 0.00 | 0.00 | 0.00 | 0.00 | 0.00 | 0.00 | 0.00 | 0.00 | 0.00 | 0.00 | 0.00 | 0.00 | 0.00 |
| $Fe^{2+}$ | 1.21 | 1.58 | 1.05 | 0.82 | 1.04 | 0.95 | 0.68 | 1.17 | 1.28 | 0.78 | 2.06 | 1.12 | 1.76 | 1.35 |
| $Mn^{2+}$ | 0.01 | 0.01 | 0.00 | 0.01 | 0.00 | 0.00 | 0.01 | 0.00 | 0.01 | 0.00 | 0.03 | 0.01 | 0.01 | 0.00 |
| Mg | 1.358 | 0.755 | 1.706 | 1.577 | 1.145 | 1.157 | 1.883 | 1.659 | 1.255 | 1.699 | 0.077 | 1.677 | 1.083 | 1.094 |
| Y-sum | 3.00 | 3.00 | 2.93 | 3.00 | 3.00 | 2.98 | 2.98 | 2.99 | 2.95 | 2.95 | 3.00 | 2.95 | 2.92 | 3.00 |
| Ca | 0.12 | 0.10 | 0.11 | 0.12 | 0.08 | 0.04 | 0.08 | 0.06 | 0.03 | 0.06 | 0.04 | 0.04 | 0.06 | 0.17 |
| Na | 0.30 | 0.33 | 0.41 | 0.32 | 0.30 | 0.29 | 0.43 | 0.80 | 0.39 | 0.37 | 0.33 | 0.91 | 0.91 | 0.32 |
| K | 0.00 | 0.01 | 0.00 | 0.01 | 0.00 | 0.00 | 0.00 | 0.00 | 0.00 | 0.00 | 0.01 | 0.01 | 0.01 | 0.01 |
| X-vacancy | 0.58 | 0.56 | 0.48 | 0.56 | 0.61 | 0.67 | 0.49 | 0.14 | 0.58 | 0.58 | 0.62 | 0.05 | 0.02 | 0.49 |
| X-sum | 1.00 | 1.00 | 1.00 | 1.00 | 1.00 | 1.00 | 1.00 | 1.00 | 1.00 | 1.00 | 1.00 | 1.00 | 1.00 | 1.00 |
| OH | 3.36 | 3.31 | 3.52 | 3.41 | 3.39 | 3.33 | 3.51 | 3.80 | 3.39 | 3.37 | 3.38 | 3.95 | 3.97 | 3.51 |
| O | 0.58 | 0.56 | 0.48 | 0.56 | 0.61 | 0.67 | 0.49 | 0.14 | 0.58 | 0.58 | 0.62 | 0.05 | 0.02 | 0.49 |
| V + W | 4.00 | 4.00 | 4.00 | 4.00 | 4.00 | 4.00 | 4.00 | 4.00 | 4.00 | 4.00 | 4.00 | 4.00 | 4.00 | 4.00 |
| *calculated | | | | | | | | | | | | | | |

**Supplementary Table S2** – continuation

| Locality | Ľutina | Ľutina | Ľutina | Ľutina | Ľutina | Ľutina | Ľutina | Ľutina | Ľutina | Ľutina | Ľutina | Ľutina | Ľutina | Ľutina |
|---|---|---|---|---|---|---|---|---|---|---|---|---|---|---|
| Formation | Malinowa Fm. | Malinowa Fm. | Malinowa Fm. | Malinowa Fm. | Malinowa Fm. | Malinowa Fm. | Malinowa Fm. | Malinowa Fm. | Malinowa Fm. | Malinowa Fm. | Malinowa Fm. | Malinowa Fm. | Malinowa Fm. | Malinowa Fm. |
| Age | Turonian–Campanian | Turonian–Campanian | Turonian–Campanian | Turonian–Campanian | Turonian–Campanian | Turonian–Campanian | Turonian–Campanian | Turonian–Campanian | Turonian–Campanian | Turonian–Campanian | Turonian–Campanian | Turonian–Campanian | Turonian–Campanian | Turonian–Campanian |
| Unit | Šariš U. | Šariš U. | Šariš U. | Šariš U. | Šariš U. | Šariš U. | Šariš U. | Šariš U. | Šariš U. | Šariš U. | Šariš U. | Šariš U. | Šariš U. | Šariš U. |
| Sample | JAR-2C | JAR-2C | JAR-2C | JAR-2C | JAR-2C | JAR-2C | JAR-2C | JAR-2C | LU-5A | LU-5A | LU-5A | LU-5A | LU-5A | LU-5A |
| Point | an26 | an27 | an28 | an30 | an31 | an32 | an33 | an34 | an1 | an2 | an3 | an4 | an5 | an6 |
| Mineral | Vac-Mg-O root | Drv | Drv | Mg-Foi | Srl | Vac-Mg-O root | Mg-Foi | Vac-Fe-O root | Vac-Mg-O root | Feruvi | Foi | Foi | Srl | Vac-Mg-O root |
| $SiO_2$ | 36.80 | 36.47 | 36.80 | 36.65 | 35.48 | 36.11 | 36.88 | 36.18 | 36.28 | 35.07 | 34.23 | 35.79 | 35.90 | 36.06 |
| $TiO_2$ | 0.23 | 0.57 | 0.22 | 0.77 | 1.22 | 0.98 | 0.90 | 0.71 | 1.06 | 0.92 | 0.39 | 0.15 | 0.34 | 0.56 |
| $Al_2O_3$ | 33.04 | 30.70 | 30.10 | 30.53 | 27.24 | 33.74 | 31.00 | 34.22 | 29.74 | 24.90 | 24.03 | 27.91 | 29.35 | 29.87 |
| $V_2O_3$ | 0.03 | 0.06 | 0.01 | 0.07 | 0.04 | 0.06 | 0.06 | 0.03 | 0.02 | 0.02 | 0.03 | 0.00 | 0.08 | 0.04 |
| $Cr_2O_3$ | 0.05 | 0.06 | 0.04 | 0.01 | 0.00 | 0.07 | 0.02 | 0.03 | 0.09 | 0.00 | 0.01 | 0.00 | 0.01 | 0.00 |
| FeO | 6.91 | 8.15 | 6.22 | 7.72 | 14.34 | 7.65 | 4.95 | 8.09 | 9.08 | 15.71 | 21.45 | 12.69 | 12.84 | 10.11 |
| MnO | 0.00 | 0.04 | 0.11 | 0.09 | 0.07 | 0.00 | 0.00 | 0.17 | 0.01 | 0.02 | 0.00 | 0.05 | 0.00 | 0.02 |
| ZnO | 0.00 | 0.08 | 0.00 | 0.04 | 0.00 | 0.03 | 0.04 | 0.00 | 0.00 | 0.05 | 0.08 | 0.04 | 0.04 | 0.03 |
| CuO | 0.00 | 0.00 | 0.00 | 0.04 | 0.00 | 0.00 | 0.00 | 0.08 | 0.28 | 0.02 | 0.04 | 0.04 | 0.00 | 0.01 |
| MgO | 6.45 | 6.84 | 9.31 | 6.87 | 4.36 | 5.21 | 8.51 | 4.42 | 6.45 | 5.02 | 2.67 | 6.07 | 4.67 | 5.95 |
| CaO | 0.42 | 0.22 | 0.28 | 0.49 | 0.45 | 0.73 | 0.49 | 0.19 | 0.33 | 2.13 | 1.03 | 1.00 | 0.22 | 0.19 |
| BaO | 0.00 | 0.01 | 0.00 | 0.02 | 0.00 | 0.00 | 0.00 | 0.00 | 0.00 | 0.00 | 0.00 | 0.05 | 0.02 | 0.00 |
| $Na_2O$ | 1.10 | 2.66 | 2.74 | 1.35 | 1.43 | 1.01 | 1.35 | 1.20 | 1.30 | 0.88 | 1.07 | 1.18 | 1.46 | 1.29 |
| $K_2O$ | 0.03 | 0.01 | 0.02 | 0.00 | 0.04 | 0.03 | 0.04 | 0.04 | 0.02 | 0.04 | 0.08 | 0.03 | 0.03 | 0.01 |
| F | 0.11 | 0.10 | 0.00 | 0.06 | 0.00 | 0.14 | 0.07 | 0.04 | 0.17 | 0.00 | 0.00 | 0.04 | 0.07 | 0.04 |
| Cl | 0.00 | 0.01 | 0.01 | 0.01 | 0.00 | 0.00 | 0.00 | 0.00 | 0.00 | 0.02 | 0.00 | 0.00 | 0.00 | 0.00 |
| $H_2O^*$ | 3.08 | 3.47 | 3.59 | 3.15 | 3.10 | 3.08 | 3.17 | 3.09 | 3.04 | 3.18 | 3.04 | 3.15 | 3.09 | 3.06 |
| $B_2O_3^*$ | 10.588 | 10.46 | 10.621 | 10.44 | 10.088 | 10.532 | 10.546 | 10.505 | 10.385 | 9.944 | 9.836 | 10.261 | 10.26 | 10.322 |
| O = F | 0.05 | 0.04 | 0.00 | 0.03 | 0.00 | 0.06 | 0.03 | 0.02 | 0.07 | 0.00 | 0.00 | 0.02 | 0.03 | 0.02 |
| Total [%] | 98.80 | 99.85 | 100.08 | 98.28 | 97.84 | 99.29 | 98.01 | 98.99 | 98.18 | 97.93 | 97.98 | 98.44 | 98.34 | 97.53 |
| Si | 6.04 | 6.06 | 6.02 | 6.10 | 6.11 | 5.96 | 6.08 | 5.99 | 6.07 | 6.13 | 6.05 | 6.06 | 6.08 | 6.07 |
| Al | 0.00 | 0.00 | 0.00 | 0.00 | 0.00 | 0.04 | 0.00 | 0.01 | 0.00 | 0.00 | 0.00 | 0.00 | 0.00 | 0.00 |
| T-sum | 6.04 | 6.059 | 6.023 | 6.101 | 6.112 | 6 | 6.078 | 6 | 6.071 | 6.13 | 6.048 | 6.062 | 6.081 | 6.072 |
| B | 3.00 | 3.00 | 3.00 | 3.00 | 3.00 | 3.00 | 3.00 | 3.00 | 3.00 | 3.00 | 3.00 | 3.00 | 3.00 | 3.00 |
| Al | 6.00 | 6.00 | 5.81 | 5.99 | 5.53 | 6.00 | 6.00 | 6.00 | 5.87 | 5.13 | 5.01 | 5.57 | 5.86 | 5.93 |
| Cr | 0.00 | 0.00 | 0.01 | 0.00 | 0.00 | 0.00 | 0.00 | 0.00 | 0.01 | 0.00 | 0.00 | 0.00 | 0.00 | 0.00 |
| Mg | 0 | 0 | 0.187 | 0 | 0.464 | 0 | 0 | 0 | 0.119 | 0.867 | 0.704 | 0.428 | 0.128 | 0.068 |
| $Fe^{3+}$ | 0.00 | 0.00 | 0.00 | 0.00 | 0.00 | 0.00 | 0.00 | 0.00 | 0.00 | 0.00 | 0.00 | 0.00 | 0.00 | 0.00 |
| Z-sum | 6.00 | 6.00 | 6.00 | 6.00 | 6.00 | 6.00 | 6.00 | 6.00 | 6.00 | 6.00 | 6.00 | 6.00 | 6.00 | 6.00 |
| Al | 0.39 | 0.01 | 0.00 | 0.00 | 0.00 | 0.52 | 0.02 | 0.66 | 0.00 | 0.00 | 0.00 | 0.00 | 0.00 | 0.00 |
| Ti | 0.03 | 0.07 | 0.03 | 0.10 | 0.16 | 0.12 | 0.11 | 0.09 | 0.13 | 0.12 | 0.05 | 0.02 | 0.04 | 0.07 |
| $Fe^{3+}$ | 0.00 | 0.00 | 0.00 | 0.00 | 0.00 | 0.00 | 0.00 | 0.00 | 0.00 | 0.00 | 0.00 | 0.00 | 0.00 | 0.00 |
| $Fe^{2+}$ | 0.95 | 1.13 | 0.85 | 1.08 | 2.07 | 1.06 | 0.68 | 1.12 | 1.27 | 2.30 | 2.89 | 1.80 | 1.82 | 1.42 |
| $Mn^{2+}$ | 0.00 | 0.01 | 0.02 | 0.01 | 0.01 | 0.00 | 0.00 | 0.02 | 0.00 | 0.00 | 0.00 | 0.01 | 0.00 | 0.00 |
| Mg | 1.579 | 1.695 | 2.083 | 1.705 | 0.655 | 1.282 | 2.091 | 1.091 | 1.489 | 0.44 | 0 | 1.105 | 1.053 | 1.425 |
| Y-sum | 2.96 | 2.94 | 2.98 | 2.90 | 2.89 | 3.00 | 2.92 | 3.00 | 2.93 | 2.87 | 2.95 | 2.94 | 2.92 | 2.93 |
| Ca | 0.07 | 0.04 | 0.05 | 0.09 | 0.08 | 0.13 | 0.09 | 0.03 | 0.06 | 0.40 | 0.20 | 0.18 | 0.04 | 0.03 |
| Na | 0.35 | 0.86 | 0.87 | 0.44 | 0.48 | 0.32 | 0.43 | 0.39 | 0.42 | 0.30 | 0.37 | 0.39 | 0.48 | 0.42 |
| K | 0.01 | 0.00 | 0.00 | 0.00 | 0.01 | 0.01 | 0.01 | 0.01 | 0.01 | 0.01 | 0.02 | 0.01 | 0.01 | 0.00 |
| X-vacancy | 0.57 | 0.10 | 0.08 | 0.47 | 0.43 | 0.54 | 0.47 | 0.57 | 0.51 | 0.29 | 0.42 | 0.42 | 0.47 | 0.54 |
| X-sum | 1.00 | 1.00 | 1.00 | 1.00 | 1.00 | 1.00 | 1.00 | 1.00 | 1.00 | 1.00 | 1.00 | 1.00 | 1.00 | 1.00 |
| OH | 3.37 | 3.84 | 3.92 | 3.49 | 3.57 | 3.39 | 3.49 | 3.41 | 3.40 | 3.70 | 3.58 | 3.56 | 3.49 | 3.44 |
| O | 0.57 | 0.10 | 0.08 | 0.47 | 0.43 | 0.54 | 0.47 | 0.57 | 0.51 | 0.29 | 0.42 | 0.42 | 0.47 | 0.54 |
| V + W | 4.00 | 4.00 | 4.00 | 4.00 | 4.00 | 4.00 | 4.00 | 4.00 | 4.00 | 4.00 | 4.00 | 4.00 | 4.00 | 4.00 |
| *calculated | | | | | | | | | | | | | | |

**Supplementary Table S2** – continuation

| Locality | Ľutina | Ľutina | Ľutina | Ľutina | Ľutina | Ľutina | Ľutina | Ľutina | Ľutina | Ľutina | Ľutina | Ľutina |
|---|---|---|---|---|---|---|---|---|---|---|---|---|
| Formation | Malinowa Fm. | Malinowa Fm. | Malinowa Fm. | Malinowa Fm. | Malinowa Fm. | Malinowa Fm. | Malinowa Fm. | Malinowa Fm. | Malinowa Fm. | Malinowa Fm. | Malinowa Fm. | Malinowa Fm. |
| Age | Turonian–Campanian | Turonian–Campanian | Turonian–Campanian | Turonian–Campanian | Turonian–Campanian | Turonian–Campanian | Turonian–Campanian | Turonian–Campanian | Turonian–Campanian | Turonian–Campanian | Turonian–Campanian | Turonian–Campanian |
| Unit | Šariš U. | Šariš U. | Šariš U. | Šariš U. | Šariš U. | Šariš U. | Šariš U. | Šariš U. | Šariš U. | Šariš U. | Šariš U. | Šariš U. |
| Sample | LU-5A | LU-5A | LU-5A | LU-5A | LU-5A | LU-5A | LU-5A | LU-5A | LU-5A | LU-5A | LU-5B | LU-5B |
| Point | an7 | an19 | an20 | an25 | an26 | an35 | an36 | an37 | an38 | an42 | an6 | an7 |
| Mineral | Vac-Mg-O root | Mg-Foi | Uvi | Vac-Mg-O root | Drv | Drv | Srl | Srl | Srl | Vac-Fe-O root | Vac-Mg-O root | Vac-Mg-O root |
| $SiO_2$ | 36.03 | 36.75 | 35.43 | 36.56 | 37.06 | 36.90 | 35.76 | 36.30 | 35.98 | 35.90 | 36.23 | 36.35 |
| $TiO_2$ | 0.60 | 0.44 | 1.55 | 0.96 | 0.25 | 0.19 | 0.44 | 0.34 | 0.41 | 0.17 | 1.31 | 0.48 |
| $Al_2O_3$ | 31.91 | 32.31 | 25.94 | 33.34 | 31.53 | 30.05 | 26.96 | 28.16 | 27.29 | 35.23 | 30.55 | 35.11 |
| $V_2O_3$ | 0.04 | 0.01 | 0.14 | 0.08 | 0.02 | 0.04 | 0.00 | 0.04 | 0.05 | 0.03 | 0.04 | 0.07 |
| $Cr_2O_3$ | 0.08 | 0.00 | 0.01 | 0.09 | 0.06 | 0.00 | 0.02 | 0.01 | 0.03 | 0.00 | 0.00 | 0.08 |
| FeO | 7.50 | 6.08 | 9.56 | 4.43 | 6.31 | 8.33 | 12.39 | 12.28 | 13.16 | 10.98 | 9.50 | 5.30 |
| MnO | 0.04 | 0.01 | 0.00 | 0.03 | 0.00 | 0.03 | 0.00 | 0.00 | 0.09 | 0.06 | 0.00 | 0.07 |
| ZnO | 0.04 | 0.07 | 0.00 | 0.07 | 0.05 | 0.11 | 0.02 | 0.05 | 0.05 | 0.08 | 0.00 | 0.06 |
| CuO | 0.00 | 0.00 | 0.03 | 0.00 | 0.00 | 0.00 | 0.00 | 0.01 | 0.00 | 0.04 | 0.02 | 0.07 |
| MgO | 6.20 | 7.59 | 9.16 | 7.93 | 8.09 | 8.09 | 6.68 | 6.12 | 6.14 | 1.96 | 5.87 | 6.17 |
| CaO | 0.66 | 0.76 | 2.21 | 0.88 | 0.06 | 0.02 | 0.02 | 0.62 | 0.72 | 0.03 | 0.13 | 0.69 |
| BaO | 0.00 | 0.00 | 0.10 | 0.05 | 0.00 | 0.00 | 0.00 | 0.02 | 0.07 | 0.00 | 0.00 | 0.04 |
| $Na_2O$ | 1.11 | 1.17 | 0.87 | 1.03 | 2.85 | 2.71 | 1.57 | 2.55 | 2.48 | 0.74 | 1.39 | 1.01 |
| $K_2O$ | 0.00 | 0.03 | 0.08 | 0.03 | 0.01 | 0.03 | 0.06 | 0.03 | 0.04 | 0.03 | 0.01 | 0.04 |
| F | 0.01 | 0.10 | 0.06 | 0.03 | 0.00 | 0.02 | 0.03 | 0.00 | 0.00 | 0.12 | 0.18 | 0.12 |
| Cl | 0.01 | 0.00 | 0.01 | 0.00 | 0.00 | 0.00 | 0.01 | 0.00 | 0.00 | 0.00 | 0.00 | 0.01 |
| $H_2O^*$ | 3.11 | 3.17 | 3.28 | 3.20 | 3.59 | 3.53 | 3.10 | 3.52 | 3.51 | 2.86 | 3.04 | 3.11 |
| $B_2O_3^*$ | 10.401 | 10.618 | 10.308 | 10.694 | 10.642 | 10.615 | 10.221 | 10.34 | 10.29 | 10.41 | 10.43 | 10.66 |
| O = F | 0.00 | 0.04 | 0.03 | 0.01 | 0.00 | 0.01 | 0.01 | 0.00 | 0.00 | 0.05 | 0.08 | 0.05 |
| Total [%] | 97.75 | 99.07 | 98.70 | 99.38 | 100.52 | 100.65 | 97.26 | 100.36 | 100.30 | 98.59 | 98.63 | 99.36 |
| Si | 6.02 | 6.02 | 5.97 | 5.94 | 6.05 | 6.04 | 6.08 | 6.10 | 6.08 | 6.00 | 6.04 | 5.93 |
| Al | 0.00 | 0.00 | 0.01 | 0.06 | 0.00 | 0.00 | 0.00 | 0.00 | 0.00 | 0.01 | 0.00 | 0.07 |
| T-sum | 6.021 | 6.016 | 6 | 6 | 6.052 | 6.041 | 6.08 | 6.104 | 6.079 | 6 | 6.04 | 6 |
| B | 3.00 | 3.00 | 3.00 | 3.00 | 3.00 | 3.00 | 3.00 | 3.00 | 3.00 | 3.00 | 3.00 | 3.00 |
| Al | 6.00 | 6.00 | 5.15 | 6.00 | 6.00 | 5.80 | 5.40 | 5.58 | 5.43 | 6.00 | 6.00 | 6.00 |
| Cr | 0.00 | 0.00 | 0.00 | 0.00 | 0.00 | 0.00 | 0.00 | 0.00 | 0.00 | 0.00 | 0.00 | 0.00 |
| Mg | 0 | 0 | 0.832 | 0 | 0 | 0.197 | 0.594 | 0.414 | 0.555 | 0 | 0 | 0 |
| $Fe^{3+}$ | 0.00 | 0.00 | 0.00 | 0.00 | 0.00 | 0.00 | 0.00 | 0.00 | 0.00 | 0.00 | 0.00 | 0.00 |
| Z-sum | 6.00 | 6.00 | 6.00 | 6.00 | 6.00 | 6.00 | 6.00 | 6.00 | 6.00 | 6.00 | 6.00 | 6.00 |
| Al | 0.28 | 0.23 | 0.00 | 0.33 | 0.07 | 0.00 | 0.00 | 0.00 | 0.00 | 0.93 | 0.00 | 0.67 |
| Ti | 0.08 | 0.05 | 0.20 | 0.12 | 0.03 | 0.02 | 0.06 | 0.04 | 0.05 | 0.02 | 0.16 | 0.06 |
| $Fe^{3+}$ | 0.00 | 0.00 | 0.00 | 0.00 | 0.00 | 0.00 | 0.00 | 0.00 | 0.00 | 0.00 | 0.00 | 0.00 |
| $Fe^{2+}$ | 1.05 | 0.83 | 1.35 | 0.60 | 0.86 | 1.14 | 1.76 | 1.73 | 1.86 | 1.53 | 1.33 | 0.72 |
| $Mn^{2+}$ | 0.01 | 0.00 | 0.00 | 0.00 | 0.00 | 0.00 | 0.00 | 0.00 | 0.01 | 0.01 | 0.00 | 0.01 |
| Mg | 1.545 | 1.853 | 1.471 | 1.92 | 1.971 | 1.777 | 1.1 | 1.119 | 0.991 | 0.489 | 1.458 | 1.501 |
| Y-sum | 2.98 | 2.98 | 3.02 | 3.00 | 2.95 | 2.96 | 2.92 | 2.90 | 2.92 | 3.00 | 2.96 | 3.00 |
| Ca | 0.12 | 0.13 | 0.40 | 0.15 | 0.01 | 0.00 | 0.00 | 0.11 | 0.13 | 0.01 | 0.02 | 0.12 |
| Na | 0.36 | 0.37 | 0.28 | 0.33 | 0.90 | 0.86 | 0.52 | 0.83 | 0.81 | 0.24 | 0.45 | 0.32 |
| K | 0.00 | 0.01 | 0.02 | 0.01 | 0.00 | 0.01 | 0.01 | 0.01 | 0.01 | 0.01 | 0.00 | 0.01 |
| X-vacancy | 0.52 | 0.49 | 0.29 | 0.51 | 0.09 | 0.13 | 0.47 | 0.05 | 0.05 | 0.75 | 0.53 | 0.55 |
| X-sum | 1.00 | 1.00 | 1.00 | 1.00 | 1.00 | 1.00 | 1.00 | 1.00 | 1.00 | 1.00 | 1.00 | 1.00 |
| OH | 3.47 | 3.46 | 3.69 | 3.47 | 3.91 | 3.86 | 3.52 | 3.95 | 3.95 | 3.19 | 3.38 | 3.39 |
| O | 0.52 | 0.49 | 0.27 | 0.51 | 0.09 | 0.13 | 0.47 | 0.05 | 0.05 | 0.75 | 0.53 | 0.55 |
| V + W | 4.00 | 4.00 | 4.00 | 4.00 | 4.00 | 4.00 | 4.00 | 4.00 | 4.00 | 4.00 | 4.00 | 4.00 |
| *calculated | | | | | | | | | | | | |

**Supplementary Table S2** – continuation

| Locality | Ľutina | Ľutina | Ľutina | Ľutina | Ľutina | Ľutina |
|---|---|---|---|---|---|---|
| Formation | Malinowa Fm. | Malinowa Fm. | Malinowa Fm. | Malinowa Fm. | Malinowa Fm. | Malinowa Fm. |
| Age | Turonian–Campanian | Turonian–Campanian | Turonian–Campanian | Turonian–Campanian | Turonian–Campanian | Turonian–Campanian |
| Unit | Šariš U. | Šariš U. | Šariš U. | Šariš U. | Šariš U. | Šariš U. |
| Sample | LU-5B | LU-5B | LU-5B | LU-5B | LU-5B | LU-5B |
| Point | an14 | an15 | an16 | an22 | an23 | an29 |
| Mineral | Drv | Mg-Foi | Srl | Mg-Foi | Drv | Vac-Mg-O root |
| $SiO_2$ | 37.26 | 35.50 | 35.57 | 36.06 | 36.79 | 36.97 |
| $TiO_2$ | 0.88 | 1.22 | 0.73 | 0.60 | 1.07 | 0.64 |
| $Al_2O_3$ | 33.74 | 34.23 | 25.68 | 28.84 | 32.12 | 33.69 |
| $V_2O_3$ | 0.16 | 0.25 | 0.01 | 0.14 | 0.03 | 0.08 |
| $Cr_2O_3$ | 0.13 | 0.23 | 0.00 | 0.01 | 0.07 | 0.03 |
| FeO | 4.69 | 7.78 | 15.10 | 9.73 | 5.46 | 7.58 |
| MnO | 0.00 | 0.00 | 0.01 | 0.06 | 0.00 | 0.08 |
| ZnO | 0.04 | 0.09 | 0.00 | 0.00 | 0.03 | 0.00 |
| CuO | 0.01 | 0.05 | 0.00 | 0.00 | 0.00 | 0.01 |
| MgO | 7.65 | 4.73 | 5.26 | 7.27 | 7.90 | 5.22 |
| CaO | 0.29 | 0.77 | 0.06 | 1.38 | 0.83 | 0.08 |
| BaO | 0.00 | 0.03 | 0.14 | 0.00 | 0.02 | 0.00 |
| $Na_2O$ | 2.66 | 1.18 | 1.55 | 1.07 | 2.23 | 1.08 |
| K2O | 0.09 | 0.06 | 0.05 | 0.07 | 0.03 | 0.01 |
| F | 0.02 | 0.08 | 0.00 | 0.00 | 0.06 | 0.12 |
| Cl | 0.00 | 0.01 | 0.00 | 0.00 | 0.00 | 0.01 |
| $H_2O^*$ | 3.62 | 3.16 | 3.08 | 3.23 | 3.52 | 3.01 |
| $B_2O_3^*$ | 10.81 | 10.52 | 10.07 | 10.39 | 10.65 | 10.59 |
| O = F | 0.01 | 0.03 | 0.00 | 0.00 | 0.02 | 0.05 |
| Total [%] | 102.04 | 99.82 | 97.29 | 98.85 | 100.77 | 99.13 |
| Si | 5.99 | 5.87 | 6.14 | 6.04 | 6.01 | 6.07 |
| Al | 0.01 | 0.14 | 0.00 | 0.00 | 0.00 | 0.00 |
| T-sum | 6 | 6 | 6.142 | 6.035 | 6.006 | 6.066 |
| B | 3.00 | 3.00 | 3.00 | 3.00 | 3.00 | 3.00 |
| Al | 6.00 | 6.00 | 5.23 | 5.69 | 6.00 | 6.00 |
| Cr | 0.00 | 0.00 | 0.00 | 0.00 | 0.00 | 0.00 |
| Mg | 0 | 0 | 0.773 | 0.293 | 0 | 0 |
| $Fe^{3+}$ | 0.00 | 0.00 | 0.00 | 0.00 | 0.00 | 0.00 |
| Z-sum | 6.00 | 6.00 | 6.00 | 6.00 | 6.00 | 6.00 |
| Al | 0.39 | 0.53 | 0.00 | 0.00 | 0.18 | 0.51 |
| Ti | 0.11 | 0.15 | 0.10 | 0.08 | 0.13 | 0.08 |
| $Fe^{3+}$ | 0.00 | 0.00 | 0.00 | 0.00 | 0.00 | 0.00 |
| $Fe^{2+}$ | 0.63 | 1.08 | 2.18 | 1.36 | 0.75 | 1.04 |
| $Mn^{2+}$ | 0.00 | 0.00 | 0.00 | 0.01 | 0.00 | 0.01 |
| Mg | 1.835 | 1.165 | 0.581 | 1.519 | 1.922 | 1.276 |
| Y-sum | 3.00 | 3.00 | 2.86 | 2.97 | 2.99 | 2.93 |
| Ca | 0.05 | 0.14 | 0.01 | 0.25 | 0.15 | 0.01 |
| Na | 0.83 | 0.38 | 0.52 | 0.35 | 0.71 | 0.34 |
| K | 0.02 | 0.01 | 0.01 | 0.01 | 0.01 | 0.00 |
| X-vacancy | 0.10 | 0.48 | 0.45 | 0.39 | 0.14 | 0.64 |
| X-sum | 1.00 | 1.00 | 1.00 | 1.00 | 1.00 | 1.00 |
| OH | 3.89 | 3.48 | 3.55 | 3.61 | 3.83 | 3.29 |
| O | 0.10 | 0.48 | 0.45 | 0.39 | 0.14 | 0.64 |
| V + W | 4.00 | 4.00 | 4.00 | 4.00 | 4.00 | 4.00 |
| *calculated | | | | | | |

## Supplementary Table S3

Representative microprobe analyses of detrital chromian spinels from Upper Cretaceous to Paleocene deposits of the Jarmuta-Proč Fm., structural drill JAR-2, Pieniny sector of the PKB, Western Carpathians, Slovakia

| Locality | Jarabina JAR-2 | Jarabina JAR-2 | Ľutina | Ľutina | Ľutina | Ľutina | Ľutina | Ľutina | Ľutina | Ľutina | Ľutina | Ľutina | Ľutina | Ľutina |
|---|---|---|---|---|---|---|---|---|---|---|---|---|---|---|
| Formation | Jarmuta-Proč Fm. | Jarmuta-Proč Fm. | Malinowa Fm. | Malinowa Fm. | Malinowa Fm. | Malinowa Fm. | Malinowa Fm. | Malinowa Fm. | Malinowa Fm. | Malinowa Fm. | Malinowa Fm. | Malinowa Fm. | Malinowa Fm. | Malinowa Fm. |
| Age | Maastrichtian–Middle Eocene | Maastrichtian–Middle Eocene | Turonian–Campanian | Turonian–Campanian | Turonian–Campanian | Turonian–Campanian | Turonian–Campanian | Turonian–Campanian | Turonian–Campanian | Turonian–Campanian | Turonian–Campanian | Turonian–Campanian | Turonian–Campanian | Turonian–Campanian |
| Unit | Šariš U. | Šariš U. | Šariš U. | Šariš U. | Šariš U. | Šariš U. | Šariš U. | Šariš U. | Šariš U. | Šariš U. | Šariš U. | Šariš U. | Šariš U. | Šariš U. |
| Sample | JAR-2A | JAR-2B | JAR-2C | JAR-2C | LU-5A | LU-5A | LU-5A | LU-5A | LU-5A | LU-5A | LU-5A | LU-5A | LU-5A | LU-5A |
| Point | an35 | an12 | an29 | an35 | an8 | an11 | an15 | an16 | an17 | an18 | an21 | an28 | an29 | an45 |
| $SiO_2$ | 0.04 | 0.00 | 0.01 | 0.02 | 0.01 | 0.03 | 0.00 | 0.02 | 0.02 | 0.04 | 0.02 | 0.02 | 0.04 | 0.03 |
| $TiO_2$ | 0.11 | 0.00 | 0.02 | 0.05 | 0.00 | 0.02 | 0.13 | 0.06 | 0.18 | 0.08 | 0.01 | 0.04 | 0.02 | 0.08 |
| $Al_2O_3$ | 22.31 | 24.43 | 26.87 | 24.91 | 24.92 | 9.48 | 23.77 | 27.69 | 21.15 | 14.79 | 14.86 | 25.36 | 21.19 | 27.11 |
| $Cr_2O_3$ | 46.65 | 44.34 | 39.17 | 43.27 | 41.45 | 61.17 | 44.23 | 39.86 | 46.04 | 54.55 | 55.11 | 43.36 | 47.63 | 41.54 |
| FeO | 15.19 | 14.15 | 14.15 | 16.43 | 17.62 | 16.07 | 15.70 | 15.21 | 17.07 | 17.76 | 17.61 | 13.09 | 15.15 | 13.41 |
| $Fe_2O_3^*$ | 1.49 | 0.80 | 3.16 | 1.49 | 2.96 | 0.19 | 1.59 | 1.68 | 2.30 | 0.00 | 0.00 | 1.27 | 1.43 | 0.79 |
| MnO | 0.24 | 0.22 | 0.24 | 0.27 | 0.31 | 0.28 | 0.28 | 0.20 | 0.26 | 0.29 | 0.29 | 0.18 | 0.23 | 0.21 |
| MgO | 12.84 | 13.47 | 13.54 | 12.23 | 11.36 | 10.79 | 12.46 | 13.18 | 11.35 | 9.84 | 10.23 | 14.31 | 12.69 | 14.19 |
| NiO | 0.08 | 0.06 | 0.13 | 0.06 | 0.09 | 0.08 | 0.13 | 0.13 | 0.10 | 0.05 | 0.07 | 0.13 | 0.08 | 0.11 |
| ZnO | 0.14 | 0.12 | 0.25 | 0.17 | 0.24 | 0.06 | 0.15 | 0.13 | 0.14 | 0.31 | 0.11 | 0.07 | 0.05 | 0.14 |
| $V_2O_5$ | 0.19 | 0.15 | 0.13 | 0.18 | 0.13 | 0.24 | 0.24 | 0.21 | 0.23 | 0.22 | 0.26 | 0.20 | 0.22 | 0.24 |
| Total | 99.27 | 97.71 | 97.67 | 99.06 | 99.09 | 98.40 | 98.66 | 98.35 | 98.83 | 97.93 | 98.55 | 98.02 | 98.73 | 97.86 |
| | | | | | | | | | | | | | | |
| Formulae based on 3 cations. 4 O anions and iron valence calculation | | | | | | | | | | | | | | |
| Si | 0.00 | 0.00 | 0.00 | 0.00 | 0.00 | 0.00 | 0.00 | 0.00 | 0.00 | 0.00 | 0.00 | 0.00 | 0.00 | 0.00 |
| Ti | 0.00 | 0.00 | 0.00 | 0.00 | 0.00 | 0.00 | 0.00 | 0.00 | 0.00 | 0.00 | 0.00 | 0.00 | 0.00 | 0.00 |
| Al | 0.82 | 0.82 | 0.82 | 0.82 | 0.82 | 0.82 | 0.82 | 0.82 | 0.82 | 0.82 | 0.82 | 0.82 | 0.82 | 0.82 |
| Cr | 1.14 | 1.14 | 1.14 | 1.14 | 1.14 | 1.14 | 1.14 | 1.14 | 1.14 | 1.14 | 1.14 | 1.14 | 1.14 | 1.14 |
| $Fe^{3+*}$ | 0.03 | 0.03 | 0.03 | 0.03 | 0.03 | 0.03 | 0.03 | 0.03 | 0.03 | 0.03 | 0.03 | 0.03 | 0.03 | 0.03 |
| $Fe^{2+}$ | 0.39 | 0.39 | 0.39 | 0.39 | 0.39 | 0.39 | 0.39 | 0.39 | 0.39 | 0.39 | 0.39 | 0.39 | 0.39 | 0.39 |
| Mn | 0.01 | 0.01 | 0.01 | 0.01 | 0.01 | 0.01 | 0.01 | 0.01 | 0.01 | 0.01 | 0.01 | 0.01 | 0.01 | 0.01 |
| Mg | 0.59 | 0.59 | 0.59 | 0.59 | 0.59 | 0.59 | 0.59 | 0.59 | 0.59 | 0.59 | 0.59 | 0.59 | 0.59 | 0.59 |
| Ni | 0.00 | 0.00 | 0.00 | 0.00 | 0.00 | 0.00 | 0.00 | 0.00 | 0.00 | 0.00 | 0.00 | 0.00 | 0.00 | 0.00 |
| Zn | 0.00 | 0.00 | 0.00 | 0.00 | 0.00 | 0.00 | 0.00 | 0.00 | 0.00 | 0.00 | 0.00 | 0.00 | 0.00 | 0.00 |
| V | 0.00 | 0.00 | 0.00 | 0.00 | 0.00 | 0.00 | 0.00 | 0.00 | 0.00 | 0.00 | 0.00 | 0.00 | 0.00 | 0.00 |
| Total | 3.000 | 3.000 | 3.000 | 3.000 | 3.000 | 3.000 | 3.000 | 3.000 | 3.000 | 3.000 | 3.000 | 3.000 | 3.000 | 3.000 |
| | | | | | | | | | | | | | | |
| Cr# | 0.58 | 0.55 | 0.49 | 0.54 | 0.53 | 0.81 | 0.56 | 0.49 | 0.59 | 0.71 | 0.71 | 0.53 | 0.60 | 0.51 |
| Mg# | 0.60 | 0.63 | 0.63 | 0.57 | 0.53 | 0.54 | 0.59 | 0.61 | 0.54 | 0.50 | 0.51 | 0.66 | 0.60 | 0.65 |
| $Fe^{2+}/Fe^{3+}$ | 11.35 | 19.73 | 4.97 | 12.27 | 6.62 | 93.74 | 10.99 | 10.08 | 8.26 | – | – | 11.45 | 11.74 | 18.75 |
| $FeO/Fe_2O_3$ | 10.21 | 17.75 | 4.47 | 11.04 | 5.96 | 84.35 | 9.89 | 9.07 | 7.43 | – | – | 10.30 | 10.56 | 16.87 |
| *calculated | | | | | | | | | | | | | | |

**Supplementary Table S3** – continuation

| Locality | Ľutina | Ľutina | Ľutina | Ľutina | Ľutina | Ľutina | Ľutina | Ľutina | Ľutina | Ľutina | Ľutina | Ľutina |
|---|---|---|---|---|---|---|---|---|---|---|---|---|
| Formation | Malinowa Fm. | Malinowa Fm. | Malinowa Fm. | Malinowa Fm. | Malinowa Fm. | Malinowa Fm. | Malinowa Fm. | Malinowa Fm. | Malinowa Fm. | Malinowa Fm. | Malinowa Fm. | Malinowa Fm. |
| Age | Turonian–Campanian | Turonian–Campanian | Turonian–Campanian | Turonian–Campanian | Turonian–Campanian | Turonian–Campanian | Turonian–Campanian | Turonian–Campanian | Turonian–Campanian | Turonian–Campanian | Turonian–Campanian | Turonian–Campanian |
| Unit | Šariš U. | Šariš U. | Šariš U. | Šariš U. | Šariš U. | Šariš U. | Šariš U. | Šariš U. | Šariš U. | Šariš U. | Šariš U. | Šariš U. |
| Sample | LU-5A | LU-5A | LU-5A | LU-5A | LU-5A | LU-5B | LU-5B | LU-5B | LU-5B | LU-5B | LU-5B | LU-5B |
| Point | an46 | an47 | an48 | an49 | an50 | an12 | an18 | an24 | an25 | an26 | an27 | an28 |
| $SiO_2$ | 0.00 | 0.05 | 0.01 | 0.00 | 0.02 | 0.04 | 0.00 | 0.02 | 0.06 | 0.02 | 0.00 | 0.02 |
| $TiO_2$ | 0.11 | 0.00 | 0.00 | 0.05 | 0.26 | 0.41 | 0.00 | 0.22 | 0.21 | 0.08 | 0.05 | 0.18 |
| $Al_2O_3$ | 15.79 | 19.02 | 32.96 | 21.65 | 6.04 | 11.67 | 39.11 | 10.54 | 19.04 | 27.72 | 20.12 | 25.86 |
| $Cr_2O_3$ | 49.20 | 48.50 | 35.27 | 47.35 | 60.85 | 56.05 | 27.34 | 57.71 | 45.07 | 40.56 | 47.52 | 42.88 |
| FeO | 19.80 | 17.45 | 12.56 | 14.29 | 21.87 | 14.83 | 12.85 | 20.28 | 17.68 | 12.91 | 16.83 | 12.53 |
| $Fe_2O_3^*$ | 3.60 | 2.07 | 1.22 | 1.33 | 2.78 | 3.57 | 2.13 | 0.00 | 5.38 | 0.68 | 1.76 | 1.32 |
| MnO | 0.35 | 0.29 | 0.19 | 0.20 | 0.45 | 0.27 | 0.15 | 0.37 | 0.27 | 0.21 | 0.30 | 0.20 |
| MgO | 8.74 | 10.83 | 15.44 | 13.26 | 6.67 | 11.94 | 15.78 | 7.63 | 10.73 | 14.48 | 11.24 | 14.69 |
| NiO | 0.08 | 0.08 | 0.09 | 0.08 | 0.08 | 0.12 | 0.17 | 0.02 | 0.14 | 0.10 | 0.13 | 0.13 |
| ZnO | 0.27 | 0.19 | 0.11 | 0.05 | 0.13 | 0.04 | 0.17 | 0.23 | 0.06 | 0.04 | 0.19 | 0.15 |
| $V_2O_5$ | 0.33 | 0.30 | 0.12 | 0.20 | 0.24 | 0.15 | 0.17 | 0.20 | 0.25 | 0.22 | 0.14 | 0.13 |
| Total | 98.27 | 98.77 | 97.97 | 98.47 | 99.39 | 99.08 | 97.86 | 97.24 | 98.88 | 97.01 | 98.27 | 98.10 |
| | | | | | | | | | | | | |
| Formulae based on 3 cations. 4 O anions and iron valence calculation | | | | | | | | | | | | |
| Si | 0.00 | 0.00 | 0.00 | 0.00 | 0.00 | 0.00 | 0.00 | 0.00 | 0.00 | 0.00 | 0.00 | 0.00 |
| Ti | 0.00 | 0.00 | 0.00 | 0.00 | 0.00 | 0.00 | 0.00 | 0.00 | 0.00 | 0.00 | 0.00 | 0.00 |
| Al | 0.82 | 0.82 | 0.82 | 0.82 | 0.82 | 0.82 | 0.82 | 0.82 | 0.82 | 0.82 | 0.82 | 0.82 |
| Cr | 1.14 | 1.14 | 1.14 | 1.14 | 1.14 | 1.14 | 1.14 | 1.14 | 1.14 | 1.14 | 1.14 | 1.14 |
| $Fe^{3+*}$ | 0.03 | 0.03 | 0.03 | 0.03 | 0.03 | 0.03 | 0.03 | 0.03 | 0.03 | 0.03 | 0.03 | 0.03 |
| $Fe^{2+}$ | 0.39 | 0.39 | 0.39 | 0.39 | 0.39 | 0.39 | 0.39 | 0.39 | 0.39 | 0.39 | 0.39 | 0.39 |
| Mn | 0.01 | 0.01 | 0.01 | 0.01 | 0.01 | 0.01 | 0.01 | 0.01 | 0.01 | 0.01 | 0.01 | 0.01 |
| Mg | 0.59 | 0.59 | 0.59 | 0.59 | 0.59 | 0.59 | 0.59 | 0.59 | 0.59 | 0.59 | 0.59 | 0.59 |
| Ni | 0.00 | 0.00 | 0.00 | 0.00 | 0.00 | 0.00 | 0.00 | 0.00 | 0.00 | 0.00 | 0.00 | 0.00 |
| Zn | 0.00 | 0.00 | 0.00 | 0.00 | 0.00 | 0.00 | 0.00 | 0.00 | 0.00 | 0.00 | 0.00 | 0.00 |
| V | 0.00 | 0.00 | 0.00 | 0.00 | 0.00 | 0.00 | 0.00 | 0.00 | 0.00 | 0.00 | 0.00 | 0.00 |
| Total | 3.000 | 3.000 | 3.000 | 3.000 | 3.000 | 3.000 | 3.000 | 3.000 | 3.000 | 3.000 | 3.000 | 3.000 |
| | | | | | | | | | | | | |
| Cr# | 0.68 | 0.63 | 0.42 | 0.595 | 0.871 | 0.763 | 0.319 | 0.786 | 0.614 | 0.495 | 0.613 | 0.527 |
| Mg# | 0.44 | 0.53 | 0.69 | 0.62 | 0.35 | 0.59 | 0.69 | 0.40 | 0.52 | 0.67 | 0.54 | 0.68 |
| $Fe^{2+}/Fe^{3+}$ | 6.11 | 9.38 | 11.44 | 11.98 | 8.75 | 4.61 | 6.70 | – | 3.65 | 21.09 | 10.63 | 10.55 |
| $FeO/Fe_2O_3$ | 5.50 | 8.44 | 10.30 | 10.78 | 7.87 | 4.15 | 6.03 | – | 3.29 | 18.97 | 9.57 | 9.49 |
| *calculated | | | | | | | | | | | | |

**Supplementary Table S4**

Representative microprobe analyses of pyroxene inclusions in detrital chromian spinels from Upper Cretaceous to Paleocene deposits of the Jarmuta-Proč Fm., structural drill JAR-2, Pieniny sector of the PKB, Western Carpathians, Slovakia

| Locality | Ľutina | Ľutina | Ľutina |
|---|---|---|---|
| Formation | Malinowa Fm. | Malinowa Fm. | Malinowa Fm. |
| Age | Turonian–Campanian | Turonian–Campanian | Turonian–Campanian |
| Unit | Šariš U. | Šariš U. | Šariš U. |
| Sample | LU-5A | LU-5A | LU-5A |
| Point | an9 | an10 | an51 |
| $SiO_2$ | 55.78 | 55.84 | 54.51 |
| $TiO_2$ | 0.08 | 0.06 | 0.01 |
| $Al_2O_3$ | 1.34 | 1.43 | 0.29 |
| $Cr_2O_3$ | 0.92 | 0.95 | 1.64 |
| $Fe_2O_3$ | 0.00 | 0.00 | |
| FeO | 5.12 | 5.46 | 1.68 |
| MnO | 0.14 | 0.15 | 0.04 |
| MgO | 34.51 | 34.49 | 17.67 |
| CaO | 0.44 | 0.39 | 24.32 |
| $Na_2O$ | 0.00 | 0.00 | 0.23 |
| Total | 98.40 | 98.85 | 100.49 |
| | | | |
| Formulae normalized to 6 oxygens. | | | |
| Si | 1.95 | 1.94 | 1.98 |
| Ti | 0.00 | 0.00 | 0.00 |
| Al | 0.06 | 0.06 | 0.01 |
| Cr | 0.03 | 0.03 | 0.05 |
| $Fe^{3+}$ | 0.02 | 0.02 | 0.00 |
| $Fe^{2+}$ | 0.13 | 0.14 | 0.05 |
| Mn | 0.00 | 0.00 | 0.00 |
| Mg | 1.80 | 1.79 | 0.96 |
| Ca | 0.02 | 0.01 | 0.95 |
| Na | 0.00 | 0.00 | 0.00 |
| Total | 4 | 4 | 4.00 |
| | | | |
| End members | | | |
| Wo | 0.83 | 0.75 | 48.43 |
| En | 91.55 | 91.16 | 48.96 |
| Fs | 7.62 | 8.09 | 2.61 |

*Mineralia Slovaca, Web ISSN 1338-3523, ISSN 0369-2086, https://doi.org/10.56623/ms.2025.57.2.3*
*57, 2 (2025), 145 – 158, © Authors 2025. CC BY 4.0*

# Brief review of the history and characteristics of the acid tar-contaminated site Predajná I and the potential application of electrochemical oxidation for the remediation of surface waters from uncapped lagoons

DANIEL KUPKA[1]*, CLAUDIA ČIČÁKOVÁ[1], DÁVID JÁGER[1], EVA MAČINGOVÁ[1], PETER SEKULA[2], MIROSLAV BAČÍK[2], PETER SEKULA JR.[2], MIROSLAVA VÁCLAVÍKOVÁ[1] and LUCIA IVANIČOVÁ[1]

[1] Institute of Geotechnics of the Slovak Academy of Sciences, Watsonova 45, 040 01 Košice, Slovak Republic; *
*corresponding author, dankup@saske.sk
[2] Environcentrum, s. r. o., Rastislavova 58, 040 01 Košice, Slovak Republic

**Abstract:** Historical disposal of acid tars from Petrochema refinery operations has resulted in persistent environmental hazards arising from the open acid-tar lagoons. These lagoons accumulate strongly acidic, highly contaminated waters enriched with organic compounds and heavy metals, posing significant risks of overflow and contamination of surrounding soils and groundwater. To mitigate these risks, electrochemical advanced oxidation using boron-doped diamond electrodes (BDD) was investigated as a treatment method for the contaminated surface water. Laboratory experiments demonstrated progressive degradation of organic pollutants, with chemical oxidation demand (COD) and total organic carbon (TOC) reductions of up to 94 % after four hours. Sulfonated compounds were oxidatively cleaved, releasing sulfate ions, while oxalate formed as a transient intermediate before complete conversion to $CO_2$ and water. Instantaneous current efficiencies reached ~90 % and specific energy consumption 25 kWh per kg of COD removed in the initial current-limited stage, decreasing at higher currents due to mass transport limitations and side reactions. These results highlight the potential of electrochemical oxidation to achieve near-complete mineralization of persistent organics, and provide a sustainable solution for the remediation of acid-tar-contaminated waters at legacy industrial sites.

**Key words:** acid tar lagoons, electrochemical oxidation, boron-doped diamond BDD

**Graphical abstract**

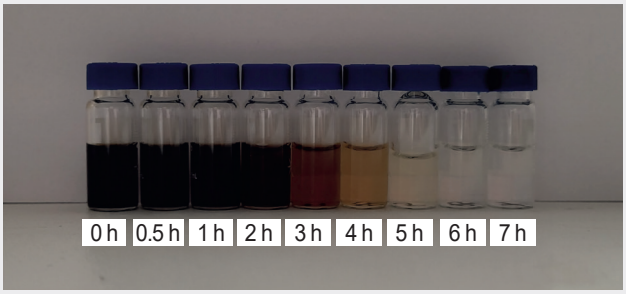


**Highlights**

- Acid-tar lagoons at Predajná site contain highly acidic, organic- and metal-rich waters, posing ongoing environmental risks.
- Electrochemical oxidation using a boron-doped diamond (BDD) anode achieved up to 99.6 % COD reduction and near-complete mineralization of persistent organics.
- The proposed treatment offers a sustainable, waste-free, and environmentally friendly solution for continuous remediation of contaminated lagoon waters.

## Introduction

Acid tars are black- to brown-colored, highly viscous residues produced during crude-oil processing and are characterized by extremely low pH (approx. pH 0.8–2) and a strong, acrid odor. They arise as by-products of three major industrial operations: benzole refining, oil re-refining, and white-oil production, all of which historically relied on concentrated sulfuric acid for feedstock purification (Milne et al., 1986; Nancarrow et al., 2001; Speight, 2014). The treatment of petroleum products with strong acids has been practiced for decades in petroleum chemistry. However, the management of the resulting spent acid sludge remains a significant environmental and operational challenge, prompting ongoing efforts toward its recovery, treatment, and reuse (Hadadi & Moradi, 2019; Leonard & Stegemann, 2010). Throughout the 20th century, waste acid tars were commonly disposed of in unengineered pits

or natural depressions near production sites. They were often mixed with other wastes and left without treatment or isolation. This practice created acid-tar lagoons that remain a lasting environmental burden.

Apart from the co-disposed waste, acid tars typically comprise water, sulfuric acid and a broad spectrum of organic compounds that remain soluble in concentrated sulfuric acid. These residues contain numerous toxic and environmentally relevant constituents, including saturated and unsaturated aliphatic and cyclic hydrocarbons, polycyclic aromatic hydrocarbons (PAHs), organic acids such as sulfonic, carboxylic, and aromatic acids, as well as trace to moderate concentrations of heavy metals (Leonard et al., 2010; Milne et al., 1986).

The physical properties of acid tars further complicate their management. Their viscosity is strongly temperature-dependent: at elevated temperatures acid tars become more fluid and mobile, whereas at lower temperatures they can solidify. Reported bulk densities typically range from 1,020 to 1,430 $kg \cdot m^{-3}$ (Hao & Smith, 2005; Nichol, 2000) exceeding those of typical coal tars (approximately 1,140–1,250 $kg \cdot m^{-3}$ (PubChem, 2025), primarily due to their high sulfuric acid content (density of 98 % $H_2SO_4$ = 1,840 $kg \cdot m^{-3}$).

At uncapped acid-tar lagoons, an overlying aqueous phase that is highly acidic and enriched in sulfate ions is frequently observed, as reported for the contaminated Predajná site in Slovakia. This surface water layer is formed primarily through atmospheric precipitation and is sustained by the low permeability of the underlying acid tar matrix, which restricts infiltration and drainage (Adzimová et al., 2023; Knapcová & Samešová, 2017). The partial solubility of acid tars in water is attributed, to the presence of sulfonic acids and other polar sulfur-containing compounds, such as sodium dodecyl sulfate (SDS) that exhibit surfactant-like properties, thereby enhancing the transfer of organic constituents into the aqueous phase (Bhoi et al., 2015).

### *Production and Disposal of Acid Tars in Petrochema plant*

The petroleum refinery in the municipality of Dubová, located in the Banská Bystrica Region of central Slovakia, was established in 1938 as a state-owned enterprise and later operated under the name Petrochema (Ďurigová, 2001). The facility was initially designed to process crude oil of Slovak and Czech origin. During the Second World War, the refinery suffered extensive damage as a result of aerial bombing (Šumichrast, 2014).

At the Petrochema plant, acid tars were generated as by-products of treating petroleum fractions with concentrated sulfuric acid. This refining step was employed to remove unsaturated hydrocarbons and heterocyclic compounds from heavy lubricating-oil fractions, enabling the production of white oils used in medicinal, cosmetic, and specialized lubrication applications. In addition, sulfonation technology was particularly applied for the synthesis of alkyl-sulfonate detergents (Hrušková et al., 2013; Samešová et al., 2007).

Chemical production waste from Petrochema rafinery was deposited in two lagoons situated within the rafinery premises. The larger lagoon occupies an area of 8,680 $m^2$, while the smaller covers 2,440 $m^2$, together providing an estimated storage capacity of approximately 100,000 $m^3$. Two additional acid-tar disposal sites are situated approximately 3.5 km east of the refinery, near the municipality of Predajná. The Predajná I landfill was constructed in 1963, currently covering an area of 10,577 $m^2$ and containing an estimated 100,000 $m^3$ of acid waste. The Predajná II landfill, built in 1973, occupies an area of 5,700 $m^2$ and stores approximately 50,000 $m^3$ of acid tar (Adzimová et al., 2023; Paluchová et al., 2008). A location of acid-tar deposits in relation to the municipality Predajná is provided in Fig. 1. Documentation of the current landfill conditions is shown in Fig. 2a.

### *Environmental risks and hydrogeological context*

The tar dumps are situated on Middle Triassic dolomites of the Choč Nappe (Ostrolucký et al., 1982). The surrounding and underlying bedrock consists predominantly of sedimentary carbonate rocks, chiefly dolomite and dolomitic limestone, with an estimated thickness of several tens of meters (Polák et al., 2003a; Polák et al., 2003b). The deposition of acid tars and other chemical wastes directly into carbonate bedrock without bottom sealing poses a significant environmental risk. Hydrodynamic tests indicate that the permeability of the bedrock beneath the tar dumps is low to very low (Pirman & Potyš, 1997). Nevertheless, the hydrogeological environment is highly heterogeneous, with preferential groundwater flow occurring along open fractures, caverns, and karst channels associated with zones of karstification and tectonic disturbance (Ostrolucký & Gálisová, 1986). Historical records indicate that during landfill filling, acid tar infiltrated the heterogeneous bedrock and migrated through the dam body, resulting in contamination of the surrounding groundwater (Auxt et al., 2020; Jánová, 2019).

After landfill closure in 1976, the lagoons remained exposed to surface water infiltration, leading to the formation of a persistent water layer within the landfill. This contaminated water exhibits seasonal fluctuations driven by precipitation, snowmelt, and runoff from surrounding slopes, increasing the risk of overflow from

the landfill margins and subsequent contamination of surface and groundwater, soils, and other environmental compartments (Adzimová et al., 2023; Jánová, 2019). The uncontrolled disposal of hazardous materials at these sites underscores the severe environmental challenges associated with historical refinery operations. Notably, both Predajná landfills are situated within the protection zone of the Low Tatras National Park (Knapcová et al., 2017).

### *Geological survey and remediation efforts*

The Predajná I and II landfills are classified as confirmed, high-priority environmental burdens due to persistent contamination: *BR (015) Predajná – skládka PO Predajná I (SK/EZ/BR/73) and BR (016) Predajná – skládka PO Predajná II (SK/EZ/BR/74)*.

Since 2016, the State Geological Institute of Dionýz Štúr (SGIDŠ) has been conducting monitoring of Predajná I and II landfill sites as part of the project Geological

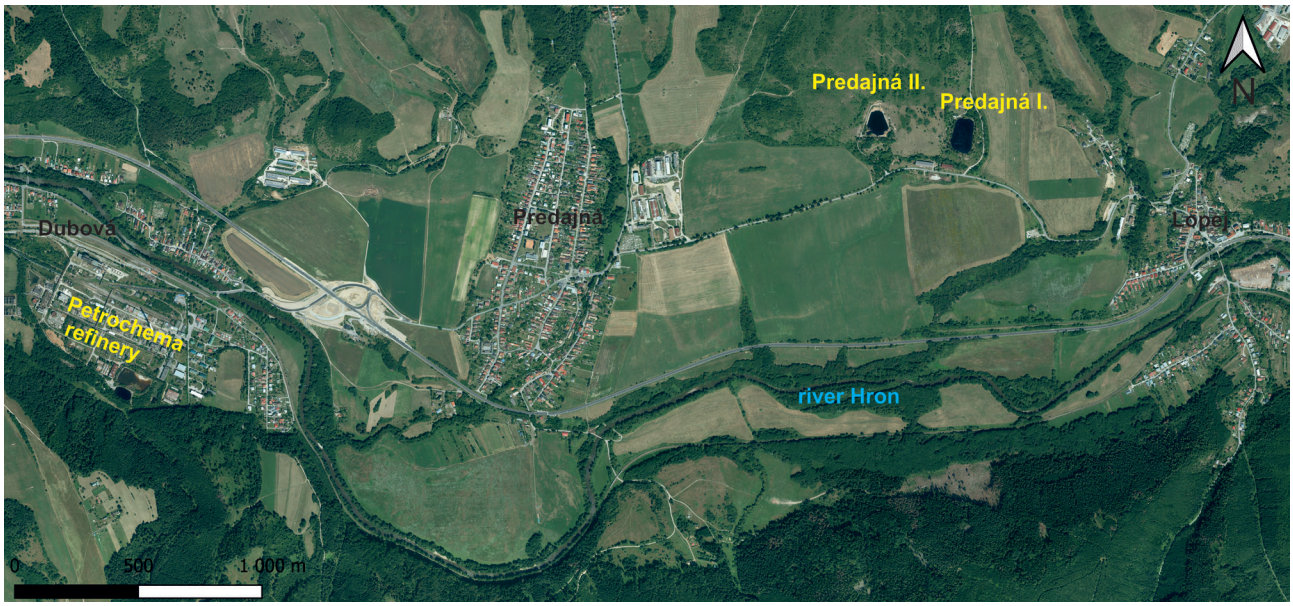


**Fig. 1.** Location of acid tars lagoons in relation to the municipality of Predajná and former Petrochema Dubová plant

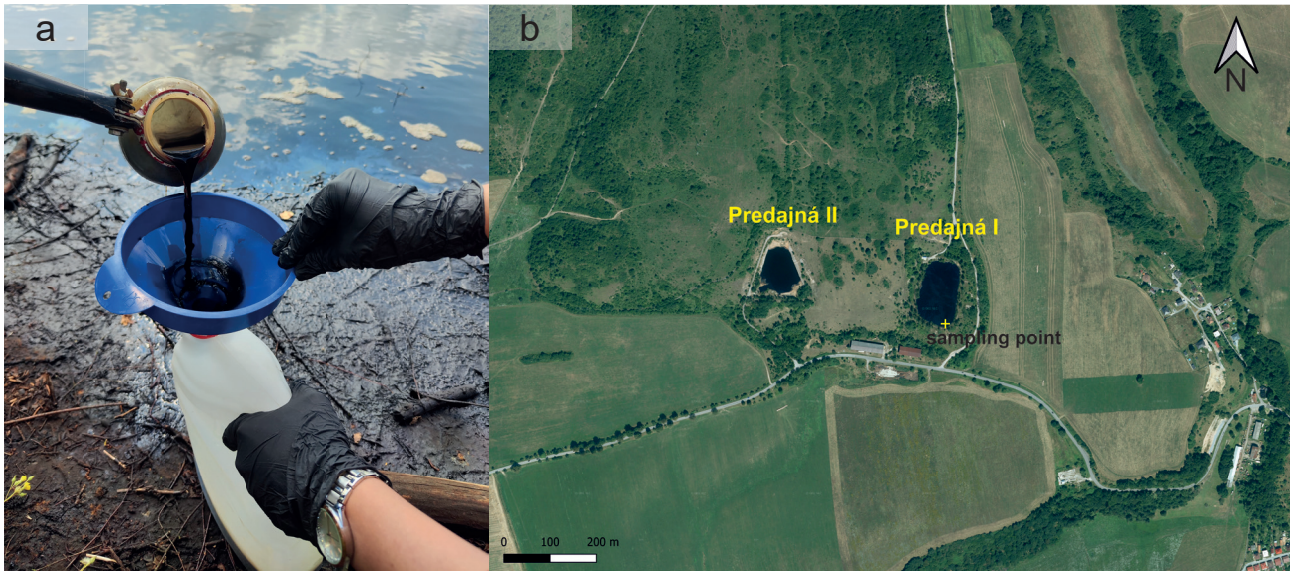


**Fig. 2.** Sampling of the acid-tar surface water (a), sampling point location (b)

survey of selected environmental burdens in Slovakia (Kordík et al., 2023). Between 2021 and 2023, an additional comprehensive geological survey was carried out at both sites, following up the results of previous works, with the aim of ensuring a detailed survey of both landfills and assessing the risks of these environmental burdens (Adzimová et al., 2023). As part of this survey, surface water samples were collected from the water body present at the Predajná I landfill. This water, representing a mixture of landfill leachate and rainwater, is characterized by a brownish coloration and a pronounced organic or petroleum-like odor. Chemical analyses revealed several characteristic properties (Adzimová et al., 2023). Extremely low pH values (1.0–1.9), high specific electrical conductivity (average 1,710 $mS \cdot m^{-1}$), very high TOC concentrations, reaching up to 5,457 $mg \cdot L^{-1}$ elevated concentrations of metals were confirmed, including Al, Fe, Mn, As, Sb, Cd, and V, along with high sulfate concentrations and high surfactant concentrations reaching (1,130 $mg \cdot L^{-1}$). Significant petroleum-derived substances were identified as NEL UV (614 $mg \cdot L^{-1}$), along with elevated concentrations of dichlorobenzene.

These results confirm that the surface water within the landfill exhibits extreme acidity, a high organic load and elevated levels of both inorganic and organic contaminants, emphasizing the ongoing environmental risks associated with uncontrolled leachate accumulation.

In September 2021, Vodohospodárska výstavba, š. p., State-owned Enterprise, acting under the authority of the Ministry of the Environment of the Slovak Republic, prepared a Technical and Safety Supervision Program for the Dubová water structures, including the Predajná I and II tar lagoons (Kasana et al., 2021). As part of this program, the Slovak Hydrometeorological Institute (SHMÚ) monitors the water levels in both lagoons continuously. In spring 2022, at the Ministry's request, the company deployed a mobile facility to pump and treat top water from Predajná I, representing a critical intervention to reduce immediate environmental risks (TASR, 2022a).

The applied technology combined on-site chemical treatment with subsequent biological treatment at a municipal wastewater treatment plant. Approximately 800,000 liters of highly acidic, tar-contaminated water were successfully removed and treated, temporarily mitigating the risk of dam overflow.

The treatment process involved several sequential steps: extraction of contaminated water by pumping, chemical neutralization and coagulation, separation of generated sludge by flotation and sedimentation, and transfer of pre-treated water to the municipal wastewater treatment plant. The resulting non-hazardous sludge was disposed of at an authorized landfill (TASR, 2022b).

This treatment technology relies on separation processes that remove pollutants from the aqueous matrix without substantial chemical modification. However, the approach inevitably produces waste sludge that must be handled safely or landfilled. The sludge still contains both the extracted contaminants and the chemical agents used to induce precipitation and coagulation. Even after stabilization, such sludge may retain substantial amounts of toxic substances and therefore represents a potential long-term environmental risk.

### *Advanced electrochemical oxidation*

This work focuses on developing a continuous treatment technology for tar-lagoon surface water to reduce the volume of contaminated water and thereby minimize the risk of overflow from containment dams. Given the complexity, toxicity, and persistence of the contaminants present, electrochemical advanced oxidation processes (EAOPs) were selected as the primary treatment method (Chaplin, 2014)

In an electrochemical cell, strong oxidizing agents are generated both at the electrode surfaces and within the bulk solution from species naturally present in the electrolyte. These oxidants include reactive oxygen species (hydroxyl radicals •OH, with $E^0 = 2.73$ V), active chlorine species and other highly reactive intermediates formed through the electrolytic decomposition of water molecules or dissolved ions (Ferro et al., 2000). Due to their high oxidative potential, hydroxyl radicals readily attack organic contaminants, facilitating their transformation and ultimately promoting complete mineralization to carbon dioxide and inorganic end products (Martínez-Huitle et al., 2015).

The performance of various electrode materials for electrochemical water treatment has been extensively investigated (Comninellis, 1994; Kraft, 2007; Martínez-Huitle, 2014). In EAOPs, an effective anode material should exhibit a low overpotential for the oxidation of the target pollutant while maintaining a high overpotential for undesired side reactions, thereby minimizing energy losses and maximizing degradation efficiency (Martínez-Huitle et al., 2015; Panizza & Cerisola, 2005). Boron-doped diamond (BDD) is an exceptional electrode material that exhibits the widest electrochemical potential window reported for any known electrode, defined as the potential range that can be applied before the onset of electrolyte oxidation or reduction at the electrode surface (Martínez-Huitle et al., 2015).

Electrochemical treatment enables the degradation and mineralization of organic contaminants without the addition of chemical reagents, as oxidation reactions are driven solely by electrical energy. Consequently, electrochemical processes are widely regarded as environmentally friendly

technologies, with the electron itself functioning as a clean, safe, and highly efficient reagent (Comninellis, 1994; Comninellis et al., 2014; Comninellis et al., 2008; Muff, 2014).

## Materials and Methods

### *Sampling*

A surface-water sample was collected in June 2025 by point sampling near the shoreline from the upper water layer formed within the landfill lagoon Predajná I (Fig. 2a, b). The water level in the lagoon was stirred and mixed over a range of approximately 5 m to ensure a homogeneous sample collection as much as possible. The composition of the surface water in the lagoon varies throughout the year in response to seasonal factors. Thus, the sample collected for laboratory-scale experiments represents the composition of surface water in the summer, or warmer period. Sampling was conducted with permission and under the supervision of a Petrochema refinery officer. Field parameters, including temperature, pH, oxidation-reduction potential (ORP), and electrical conductivity (EC), were measured in situ using calibrated portable instruments in accordance with standard field sampling protocols (STN-ISO-5667-4 2018).

### *Chemical analyses*

Total organic carbon (TOC) in both the untreated and electrochemically treated samples was determined by the combustion method using a Vario TOC Cube analyzer (Analysensysteme GmbH, Germany).

Chemical oxygen demand ($COD_{Cr}$) was determined using LCK400 test kits (Hach Lange GmbH). Samples were digested with a solution of $K_2Cr_2O_7$ and $H_2SO_4$ at 150 °C for 120 min. COD concentrations were subsequently measured using a Hach Lange DR 3900 spectrometer.

Anion and cation concentrations were determined by ion chromatography using a Dionex ICS-5000 system (Thermo Fisher Scientific, Sunnyvale, CA, USA) equipped with electrolytic eluent generators, suppressed conductivity detection, and UV detection.

Metal and metalloid concentrations were analyzed using flame and graphite furnace atomic absorption spectrometry (FAAS and GFAAS; Varian AA240FS and AA240Z).

Polycyclic aromatic hydrocarbons (PAHs) were extracted from 20 mL water samples using CHROMABOND® Easy solid-phase extraction (SPE) columns (Macherey-Nagel). The analytes were eluted sequentially with 2 mL of methanol followed by 2 mL of acetone. The combined eluates were evaporated by nitrogen gas stream, and the resulting residue was reconstituted in acetonitrile prior to chromatographic analysis. Quantitative and qualitative analyses of PAHs were performed using a Dionex UltiMate 3000 RS liquid chromatograph (Thermo Fisher Scientific) equipped with a diode array detector (DAD 3000-RS) and a fluorescence detector (FLD 3400-RS). HPLC separation was achieved on a Nucleosil 100-5 C18 PAH column (250 × 3 mm, 5 µm, 100 Å; Macherey-Nagel).

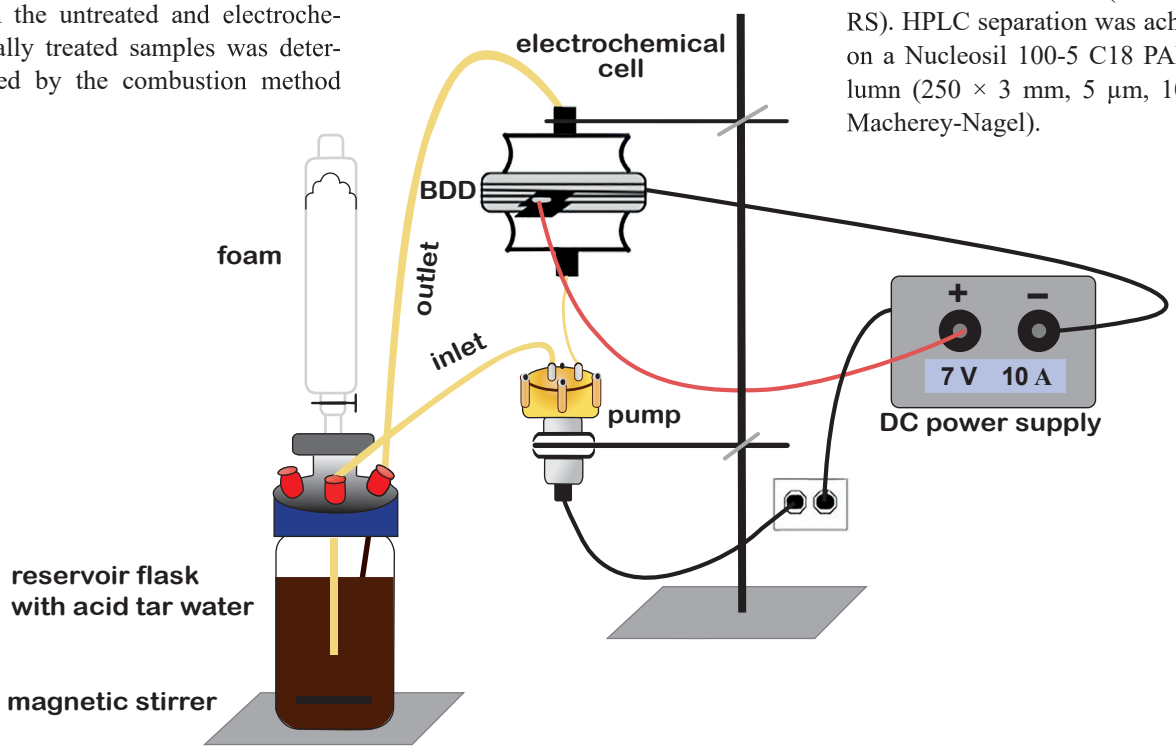


**Fig. 3.** Schematic representation of the experimental setup used for electrochemical treatment

Additional organic compounds were analyzed using a Bruker Q-TOF Compact mass spectrometer (Bruker Daltonics GmbH, Germany), either by direct injection or following SPE and ultra-high-performance liquid chromatography (UHPLC) separation.

***Electrochemical treatment***

Electrochemical treatment was carried out in batch mode with continuous recirculation of wastewater through the electrochemical reactor (Fig. 3). Wastewater was pumped upward from a thermostated reservoir through the non-divided electrochemical cell and subsequently returned to the reservoir, forming a closed-loop system. The reactor consisted of a four-electrode stack comprising two BDD anodes and two BDD cathodes arranged alternately. Each electrode was circular, with a diameter of 5 cm, corresponding to a geometric surface area of 19.635 $cm^2$. Wastewater flowed directly through the electrode apertures and inter-electrode gaps, maximizing fluid-electrode contact and enhancing mass transfer efficiency. The process was conducted at a constant temperature of 25 °C, and a flow rate of 3 $L \cdot min^{-1}$. The system was powered by a regulated DC supply operating under galvanostatic control, with real-time monitoring of current and voltage via an ammeter and voltmeter. Laboratory tests were performed in accordance with the experimental conditions specified in Table 1.

**Tab. 1**

Experimental conditions for laboratory tests

| Name of the test | Time [h] | Voltage [V] | Current [A] |
|---|---|---|---|
| T-01 | 4 | 6 | 10 |
| T-02 | 7 | 9 | 12 |

**Tab. 2**

Selected chemical parameters of surface water sampled from the Predajná I lagoon

| COD [$mg.L^{-1}$] | TOC [$mg.L^{-1}$] | pH | $Na^+$ [$mg.L^{-1}$] | $NH_4^+$ [$mg.L^{-1}$] | $K^+$ [$mg.L^{-1}$] | $Mg^{2+}$ [$mg.L^{-1}$] | $Ca^{2+}$ [$mg.L^{-1}$] | $Cl^-$ [$mg.L^{-1}$] | $SO_4^{2-}$ [$mg.L^{-1}$] | $NO_2^-$ [$mg.L^{-1}$] | $NO_3^-$ [$mg.L^{-1}$] |
|---|---|---|---|---|---|---|---|---|---|---|---|
| 19,300 | 5,588 | 1.04 | 125.6 | 19.53 | 25.65 | 170.3 | 175.9 | 34.8 | 8,133 | 0.32 | 3.87 |

**Tab. 3**

Concentrations of metals and metalloids in surface water from the Predajná I lagoon

| Fe [$mg.L^{-1}$] | Al [$mg.L^{-1}$] | Mn [$mg.L^{-1}$] | Zn [$mg.L^{-1}$] | Cu [$mg.L^{-1}$] | Pb [$\mu g.L^{-1}$] | Cr [$\mu g.L^{-1}$] | As [$\mu g.L^{-1}$] | Ni [$\mu g.L^{-1}$] | Sb [$\mu g.L^{-1}$] | Co [$\mu g.L^{-1}$] | Cd [$\mu g.L^{-1}$] |
|---|---|---|---|---|---|---|---|---|---|---|---|
| 72.4 | 37.1 | 2.13 | 1.70 | 1.22 | 446.3 | 221 | 82.3 | 69.7 | 54.8 | 16.4 | 5.60 |

**Tab. 4**

Concentrations of polycyclic aromatic hydrocarbons (PAHs) in Predajná I lagoon surface water: native sample, sample after 4 h of electrochemical treatment at 10 A, and after 7 h at 12 A. Indication (ID) and intervention (IT) criteria according the Directive of the Ministry of the Environment of the Slovak Republic 1/2015-7.Values represent mean ± standard deviation (SD), calculated from four independent experimental measurements (n = 4).

| Sample | | Fluorene | Phenanthrene | Fluoranthene | Pyrene | Chrysene |
|---|---|---|---|---|---|---|
| | unit | [$\mu g.L^{-1}$] | [$\mu g.L^{-1}$] | [$\mu g.L^{-1}$] | [$\mu g.L^{-1}$] | [$\mu g.L^{-1}$] |
| **Native sample** | average | 4.53 | **81.73** | 4.35 | 19.75 | **12.01** |
| | SD | 0.87 | 5.55 | 0.33 | 0.13 | 1.19 |
| **After 4 h** | average | 0.95 | 8.70 | 0.50 | 0.50 | **0.35** |
| | SD | 0.07 | 0.42 | 0.00 | 0.00 | 0.07 |
| **After 7 h** | average | 0.55 | 3.70 | 0.25 | 0.15 | 0.15 |
| | SD | 0.07 | 0.57 | 0.07 | 0.07 | 0.21 |
| **ID** | | – | 5 | 25 | 25 | 0.1 |
| **IT** | | **–** | **10** | **50** | **50** | 0.2 |

## Results

Surface water collected from the Predajná I lagoon, consisting of a mixture of landfill leachate and rainwater, exhibited a brownish coloration and a pronounced petroleum-like odor. The analytical results for the sampled water are summarized in Tables 2–4.

Electrochemical treatment of the surface water sample was carried out by continuous recirculation through the reactor using the experimental setup shown in Fig. 4. This configuration ensured multiple passes and repeated contact of the wastewater with the electrode surfaces. The electrodes were stable under both anodic and cathodic conditions, allowing periodic polarity reversal during each experimental run. For each experiment, 0.5 L of real wastewater was recirculated through the electrolytic cell using a pump operating at a constant flow rate of 3 $L \cdot min^{-1}$. During electrochemical treatment, pronounced foam formation was observed, resulting from the high concentration of alkyl sulfonate surfactants present in the water (Fig. 4b). Foaming was most intense during the initial stage of the process, and gradually diminished with prolonged electrolysis as the surface-active compounds were progressively degraded and removed from the solution.

Hydroxyl radicals, generated at the anode are among the strongest oxidizing species known after fluorine and are widely employed in EAOPs for water treatment (Martínez-Huitle et al., 2015). These radicals react non-selectively with organic compounds in "R" aqueous media through hydroxylation, dehydrogenation, and electron-transfer mechanisms, resulting in the cleavage of aromatic rings, rupture of C–C bonds, and ultimately complete mineralization to $CO_2$ and inorganic products.

$$BDD + H_2O \rightarrow BDD(\bullet OH) + H_+ + e^- \quad [1]$$

$$BDD(\bullet OH) + R \rightarrow BDD + \text{mineralization products} + e^- \quad [2]$$

Parameters such as TOC and COD are commonly used as group indicators to evaluate the overall organic load in wastewater, particularly for complex matrices with unknown composition. During electrochemical treatment at applied currents of 10 A and 12 A, both COD and TOC exhibited progressive decreases, indicating efficient oxidation of organic compounds (Figs. 5a, b). In the initial two hours of treatment, COD declined almost linearly, reflecting a current-limited regime in which the rate of organic oxidation is controlled primarily by the applied

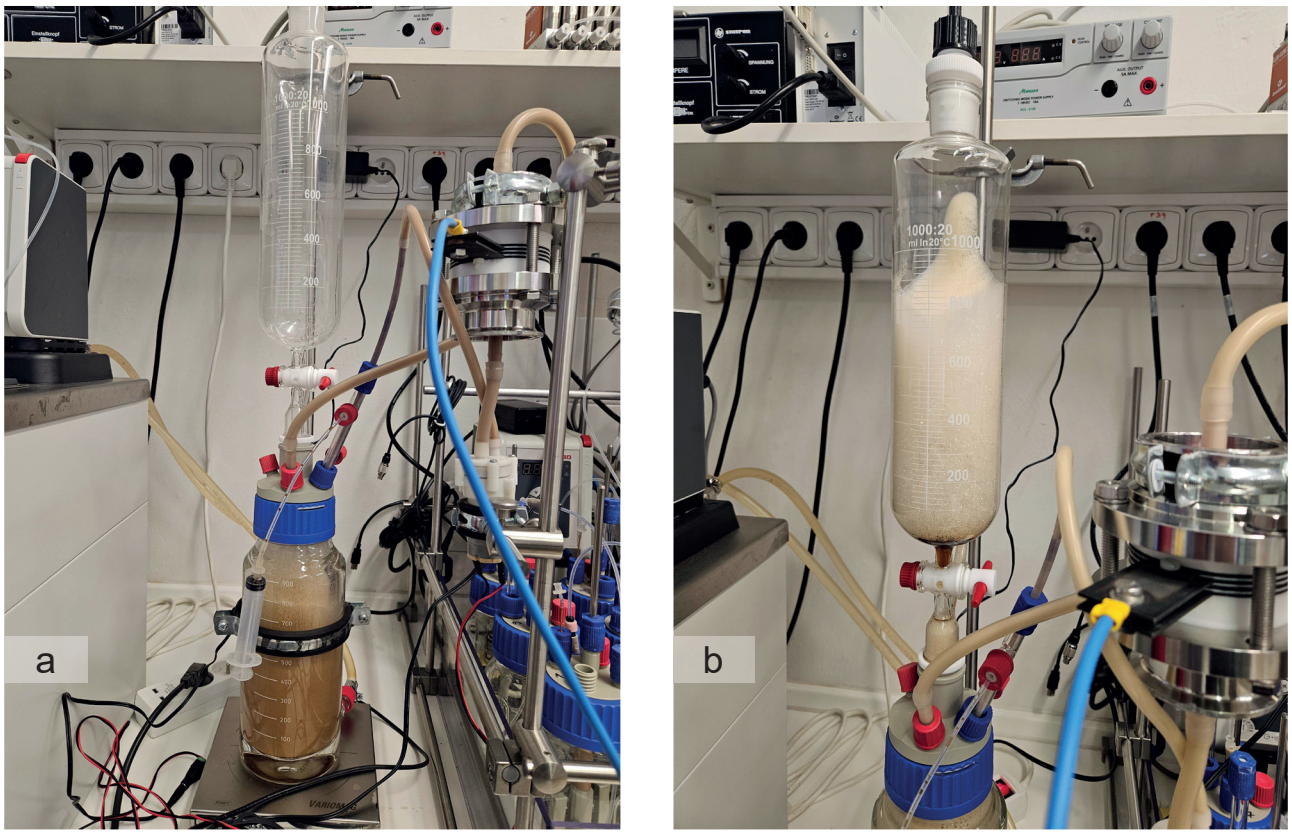


**Fig. 4.** Experimental setup for the electrochemical treatment (a). Foam formation observed during electrochemical treatment (b).

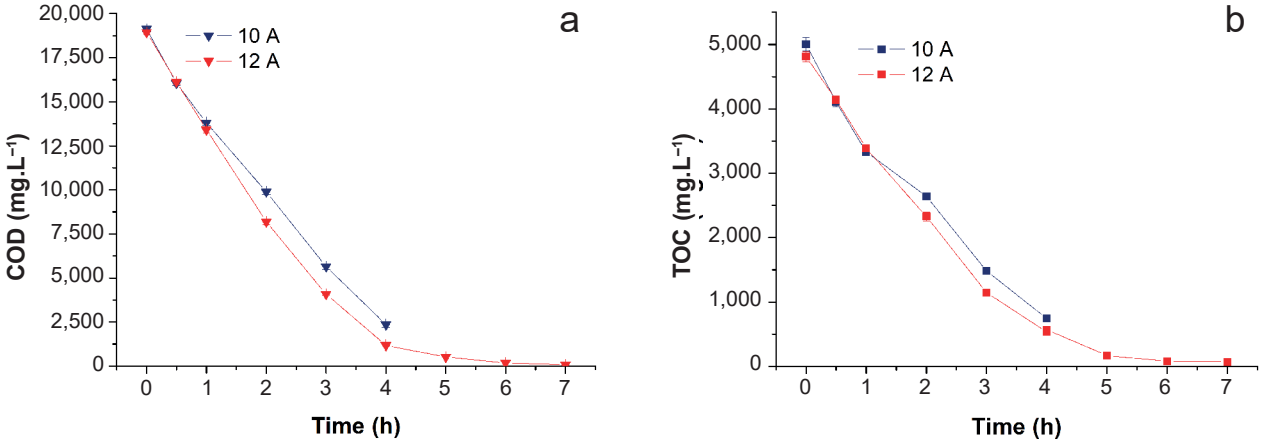


**Fig. 5.** Time evolution of (a) chemical oxygen demand (COD) and (b) total organic carbon (TOC) during electrochemical treatment at applied currents of 10 A and 12 A

current rather than mass transport. The COD degradation rates were 5,300 mg·L$^{-1}$·h$^{-1}$, and 5,500 mg·L$^{-1}$·h$^{-1}$, at 10 A and 12 A, respectively, with the instantaneous current efficiencies of approximately 90 % and 80 % (Fig. 6a). These results highlight the high effectiveness of BDD-based electrochemical oxidation for mineralizing organic pollutants, with slightly reduced efficiency at higher applied current due to enhanced side reactions.

In the subsequent stage, the degradation rates of both COD and TOC slowed, indicating the onset of mass transfer limitations as the concentration of readily oxidizable organic compounds declined and their transport to the electrode surface became the rate-limiting factor. After four hours of treatment, COD and TOC parameters were reduced by 87.7 % and 85.1 % at 10 A and by 93.9 % and 88.7 % and at 12 A, respectively, demonstrating the strong influence of applied current on degradation rates.

The electrochemical treatment also achieved substantial elimination of polycyclic aromatic hydrocarbons, with fluorene reduced by 79 % at 10 A and 88 % at 12 A, and other PAHs showing 90–99 % decreases (Tab. 4). Residual concentrations of monitored PAHs were generally below the indication criteria (ID) established by the Directive of the Ministry of the Environment of the Slovak Republic 1/2015-7, with the exception of chrysene, which remained at 0.15 µg.L$^{-1}$. These results indicate that EAOPs not only oxidize bulk organic matter, as reflected in COD and TOC removal, but also generate highly reactive radicals capable of breaking down recalcitrant and toxic compounds such as PAHs.

An important factor influencing the kinetics of electrochemical reactions is the transport of target compounds to the electrode surface, where the reactions take place. Current efficiency (CE) and specific energy consumption (EC) are key performance indicators for evaluating the effectiveness of electrochemical treatment processes for COD removal. CE reflects the fraction of the applied electrical current that is effectively utilized for target contaminant oxidation, while EC represents the electrical energy required per unit mass of COD removed (Muff, 2014). High CE values are generally associated with selective oxidation pathways (Zöllig et al., 2017) and limited parasitic reactions, whereas increased EC often indicates energy losses due to side reactions such as oxygen evolution (Panizza et al., 2008). Optimizing operating conditions to maximize CE while minimizing EC is therefore essential for improving the overall energy efficiency and practical feasibility of electrochemical COD removal.

Numerous studies (Aquino et al., 2014; Fóti et al., 1999; Panizza & Cerisola, 2005; Rodrigo et al., 2001; Xing et al., 2018) have reported near-complete mineralization of organic pollutants with current efficiencies approaching theoretical maxima under conditions where mass transport is not limiting. However, as electrochemical treatment progresses and organic concentrations decline, the instantaneous current efficiency (ICE) generally diminishes due to mass transport limitations and the increasing contribution of side reactions, such as oxygen and chlorine evolution (Kapałka et al., 2010). Under such conditions, diffusion of residual organics to the electrode surface becomes rate-limiting, and the probability of charge consumption in non-productive processes increases (Figs. 6a, b).

The instantaneous current efficiency (ICE) can be defined as the part of the current directly used for the oxidation of organic compounds. ICE during electrolysis can be performed from the decrease of COD by the means of the following eq. 3 (Muff, 2014; Panizza & Cerisola, 2009; Tsantaki et al., 2012):

$$ICE = FV \frac{COD_t - COD_{t+\Delta t}}{8I\,\Delta t} \quad [3]$$

where $F$ is the Faraday constant (96,487 C mol$^{-1}$) $V$ is the treated volume (m$^3$), $I$ is the applied current (A), $t$ is the treatment time (h), COD is the chemical oxygen demand (kg·m$^{-3}$).

The specific energy consumption (EC), expressed as kWh per kg of COD removed, was calculated according to the following eq. 4:

$$EC = \frac{Ult}{(COD_0 - COD)\,V} \quad [4]$$

where $U$ is the average cell voltage (V), $I$ is the applied current (A), $t$ is the treatment time (h), COD is the chemical oxygen demand (kg·m$^{-3}$), and $V$ is the treated volume (m$^3$).

In aqueous solutions containing chlorides and sulfates, which are commonly present in natural waters and wastewaters, additional indirect oxidation pathways can occur. Chloride ions can be anodically converted into hypochlorous species, which act as secondary oxidants with relatively long lifetimes in solution. During treatment with BDD anodes, hypochlorite can be further oxidized to chlorate and perchlorate. Notably, BDD anodes exhibit a perchlorate formation potential that is approximately three orders of magnitude higher than that of other electrode materials tested (Bergmann et al., 2015; Kupka et al., 2017).

Sulfate may be electrochemically activated to sulfate radicals ($SO_4^{\bullet-}$) and subsequently generate persulfate ($S_2O_8^{2-}$) under certain current densities (Saha et al., 2022; Zuo et al., 2023). The formation of such highly oxidized species can enhance pollutant degradation (Saien & Jafari, 2022) but also contributes to anodic charge consumption that does not directly mineralize the target compounds, further reducing ICE at advanced treatment stages.

Sulfonated compounds constitute a major fraction of acid tars, including sulfonic acids and other sulfonated organic molecules such as aromatic sulfonates, sulfonated phenols, and thiophenes. Polyaromatic and heteroaromatic sulfonates are primarily formed during petroleum refining, where concentrated sulfuric acid reacts with unsaturated hydrocarbons, aromatic compounds and heterocycles (Speight, 2014). This sulfonation reaction introduces the sulfonic acid functional group (–$SO_3H$) into the organic molecules, producing stable sulfonated compounds that are resistant to conventional chemical or biological degradation (Lin et al., 1999; Martins et al., 2011).

During electrochemical treatment, sulfonated compounds undergo oxidative cleavage by radicals generated at the anode, breaking the C–S bonds and releasing sulfate ions ($SO_4^{2-}$) into the solution (dos Santos et al., 2024; Lai et al., 2025; Lu et al., 2022).

The formation of sulfate reflects the mineralization of sulfonated organics and serves as a direct indicator of the treatment efficiency for this class of persistent pollutants. Sulfate concentrations increased steadily during the first three hours of treatment (Fig. 7a), confirming the progressive degradation of sulfonated compounds and the effective conversion of these highly stable organosulfur species into inorganic products. After three hours, the sulfate concentration in the electrolyte reached a plateau, indicating that the bulk of the sulfonated compounds had been destroyed. In the subsequent phase, a slight decrease in sulfate concentration was observed, likely due to its further conversion into persulfates under the strongly oxidizing conditions within the reactor. The ability to mineralize sulfonated compounds is particularly significant, as these

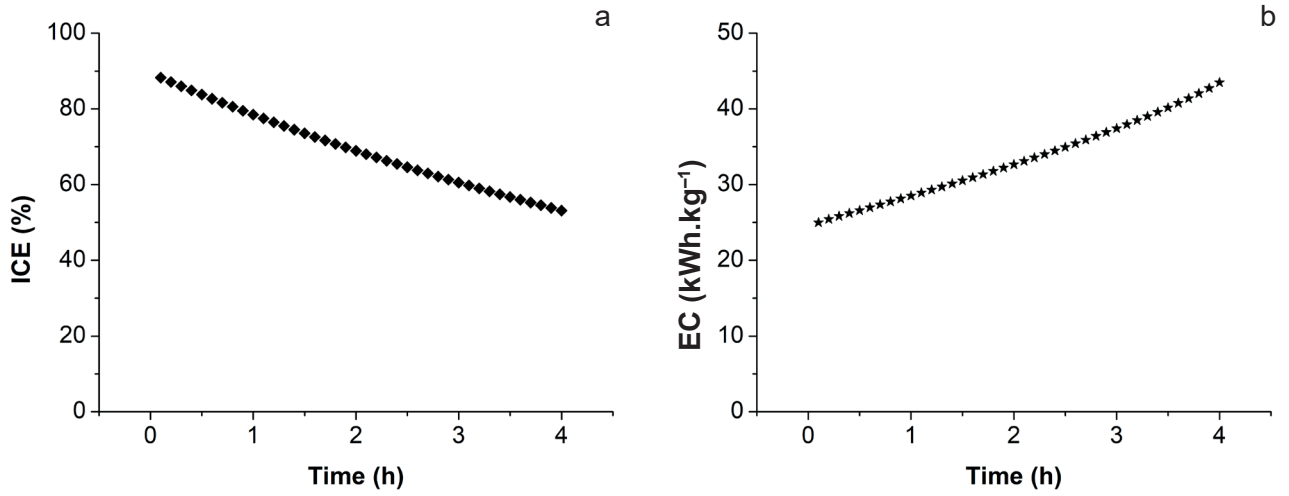


**Fig. 6.** Time evolution of (a) instantaneous current efficiency and (b) specific energy consumption (kWh per kg of COD removed) during electrochemical treatment of wastewater at an applied current of 10 A.

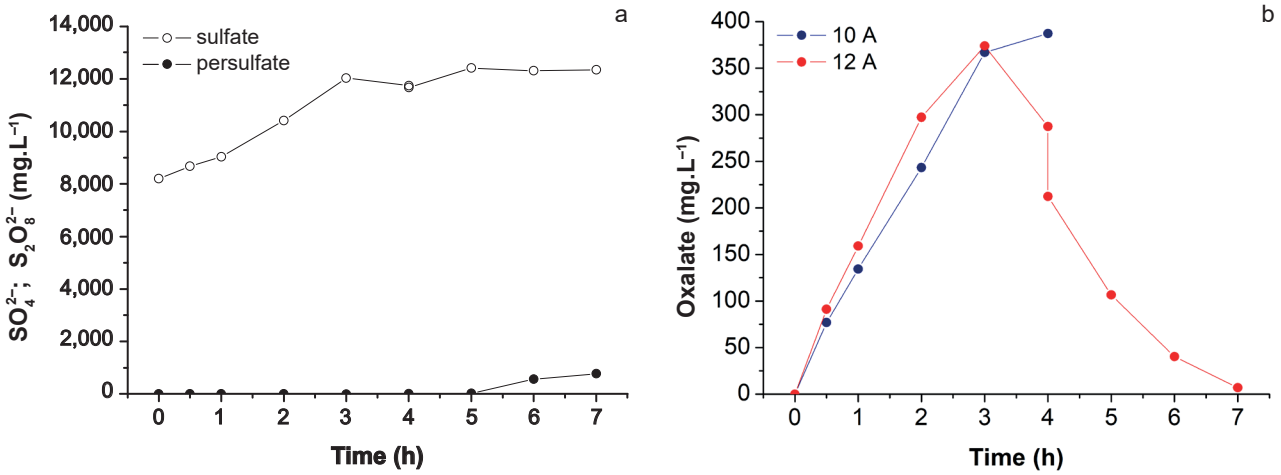


**Fig. 7.** Time evolution of (a) sulfate and persulfate anion concentrations during electrochemical treatment at an applied current of 12 A, and (b) oxalate concentration during electrochemical treatment at applied currents of 10 A and 12 A.

species are otherwise resistant to conventional wastewater treatment, highlighting the advantage of electrochemical advanced oxidation processes for the remediation of acid tar-contaminated water.

EAOPs can attain complete mineralization of contaminants to $CO_2$ given sufficient contact time, during which strong oxidants are continuously generated at non-active anodes (Panizza et al., 2008). The oxidation of aromatic compounds tends to yield short-chain carboxylic acids that are non-toxic and can easily be biodegraded (Brillas et al., 2000). Figure 6b illustrates the concentration profile of oxalate during electrochemical treatment. During the first three hours, oxalate concentration increased reaching a maximum of approximately 375 mg·L$^{-1}$, indicating its accumulation in the electrolyte. Oxalic acid is frequently observed as the main and final intermediate for the catalytic and electrochemical oxidation of a wide range of organic compounds (Martínez-Huitle et al., 2004; Scialdone et al., 2009a; Scialdone et al., 2009b).

Oxalic acid (HOOC–COOH) is a low-molecular-weight dicarboxylic acid that commonly forms as an intermediate during the oxidative degradation of complex organic matter, including carbohydrates, lignin, humic substances, and petroleum-derived organics. Its formation is observed in both biological and chemical oxidation processes (Gadd et al., 2014).

During the oxidative breakdown of complex organics, such as phenolic compounds, aromatic hydrocarbons and sulfonated organics, oxalic acid is relatively stable due to its small molecular size and resistance to mild chemical oxidation. Consequently, it often accumulates transiently in advanced oxidation treatment systems, including ozonation, photocatalysis, Fenton oxidation, and electrochemical advanced oxidation processes (Nakagawa & Yamaguchi, 2012). Oxalate is frequently observed as the final intermediate during anodic oxidation of a wide range of organic compounds on DSA electrodes (Scialdone et al., 2009a).

If the electrooxidation process is maintained for a sufficient duration, oxalate is further oxidized to carbon dioxide and water, achieving complete mineralization. This is evidenced by the gradual decrease in oxalate concentration observed after more than three hours of treatment at 12 A (Fig. 7b). In aqueous media, oxalic acid can also combine with cations such as sodium, calcium, magnesium, ferrous iron, or potassium to form oxalate salts, which are sparingly soluble. The combined trends in COD, TOC, PAHs, sulfate, and oxalate demonstrate the effectiveness of BDD-based electrochemical advanced oxidation in achieving near-complete mineralization of complex organic pollutants in acid tar-contaminated waters.

## Conclusions

Acid-tar lagoons from historical Petrochema refinery operations represent a persistent environmental hazard due to the accumulation of highly acidic, organic- and metal-rich leachates. Surface water from the Predajná I landfill exhibited extreme acidity, elevated TOC and COD, as well as high concentrations of sulfate, metals, and sulfonated organics, confirming the ongoing environmental risks associated with uncontrolled leachate accumulation.

Previous immediate mitigation via on-site chemical neutralization and coagulation successfully removed a substantial fraction of contaminants from the aqueous phase, producing stabilized sludge for safe disposal (Vodohospodársky podnik, š. p.). However, such type of sludge still contains toxic substances and represents hazardous waste. Therefore, this approach does not achieve complete

mineralization and generates secondary waste that requires careful handling.

Electrochemical advanced oxidation using BDD electrodes proved highly effective for the mineralization of complex and persistent organic compounds in lagoon water. Laboratory tests showed a reduction in total organic carbon and chemical oxygen demand of 88.7 % and 94 %, respectively, after four hours of electrolysis, and 98.5 % and 99.6 %, after seven hours, respectively. The strong correlation between bulk organic load reduction and PAH degradation suggests that EAOPs can effectively target complex mixtures of dissolved organics, combining generalized oxidation with effective destruction of persistent pollutants.

Sulfonated compounds were efficiently converted to sulfate, while oxalate, formed as an intermediate, was further oxidized to $CO_2$ and water during extended treatment. The observed trends in TOC, COD, sulfate, and oxalate provide insights into reaction kinetics, mass transport limitations, and intermediate dynamics, highlighting the ability of BDD-based EAOPs to overcome the limitations of conventional chemical treatments. Overall, electrochemical treatment represents an essentially waste-free and environmentally friendly approach for the continuous remediation of contaminated lagoon water, offering a safer and more sustainable alternative to conventional physicochemical methods. Pilot experiments will be the subject of further study. It is potentially possible to consider some flow-through or batch systems using alternative energy sources directly on site, without the need for electricity.

**Acknowledgment**

This work was supported by the EU NextGenerationEU through the Recovery and Resilience Plan for Slovakia under the project No. 09I03-03-V03-00083.

## References

Adzimová, K., Kotuč, J., Olšavský, M., Pelech, O., Marcin, D., Malík, P., Kordík, J., Jelínek, R., Šottník, P., Bahnová, N., Jajčišinová, S., Dugovič, R., Pavlanská, L., Németh, Z., Grexová, S., Siska, M., Pijáková, R., Zeman, I., Surový, M., Vizi, L. & Ostrolucký, J., 2023: Geologický prieskum vybraných environmentálnych záťaží 4 – ŠGÚDŠ. *Manuscript. Bratislava, Archive of St. Geol. Inst. of D. Štúr* (arch. no. 103754), 239 pp.

Aquino, J. M., Rocha-Filho, R. C., Sáez, C. Cañizares, P. & Rodrigo, M. A., 2014: High efficiencies in the electrochemical oxidation of an anthraquinonic dye with conductive-diamond anodes. *Environmental Science and Pollution Research*, 21, 14, 8442–8450. https://doi.org/10.1007/s11356-014-2784-0.

Auxt, A., Tupý, P., Červeňan, M., Ferianc, P., Filo, J., Brngálová, K. & Hrubý, V., 2020: Eliminácia rizika pretečenia hrádze znížením hladiny vody nad uloženými gudrónmi, *Manuscript. Banská Bystrica, ENVIGEO – HES-COMGEO*, 244 pp.

Bergmann, M. E. H., Iourtchouk, T., Schmidt, W., Hartmann, J., Fischer, M., Nüsske, G. & Gerngross, D., 2015: Laboratory- and technical-scale comparison of chlorate and perchlorate formation during drinking water electrolysis: a field study. *Journal of Applied Electrochemistry*, 45, 7, 765–778. https://doi.org/10.1007/s10800-015-0826-z.

Bhoi, P. R., Huhnke, R. L., Singarapu, K., Kumar, A. & Payton, M. E., 2015: Solubility enhancement of producer gas tar compounds in water using sodium dodecyl sulfate as a surfactant. *Fuel Processing Technology,* 133, 75–79. https://doi.org/10.1016/j.fuproc.2015.01.008.

Brillas, E., Calpe, J. C. & Casado, J., 2000: Mineralization of 2,4-D by advanced electrochemical oxidation processes. *Water Research*, 34, 8, 2253–2262. https://doi.org/10.1016/S0043-1354(99)00396-6.

Chaplin, B. P., 2014: Critical review of electrochemical advanced oxidation processes for water treatment applications. *Environmental Science: Processes & Impacts*, 16, 6, 1182–1203. https://doi.org/10.1039/c3em00679d.

Comninellis, C., 1994: Electrocatalysis in the electrochemical conversion/combustion of organic pollutants for waste water treatment. *Electrochimica Acta*, 39, 11, 1857–1862. https://doi.org/10.1016/0013-4686(94)85175-1.

Comninellis, C., Kapałka, A., Fierro, S., Fóti, G., Michaud, P.-A. & Dimitriou-Christidis, P., 2014: Organic Pollutants, Direct Electrochemical Oxidation. In: Kreysa, G., K.-i. Ota & R. F. Savinell (eds.): Encyclopedia of Applied Electrochemistry. *New York, Springer*, 1428–1435.

Comninellis, C., Kapalka, A., Malato, S., Parsons, I., Poulios, S. A. & Mantzavinos, D. 2008: Advanced oxidation processes for water treatment: advances and trends for R&D. *Journal of Chemical Technology and Biotechnology*, 83, 6, 769–776.

dos Santos, A. J., Shen, H., Lanza, M. R. V., Li, Q. & Garcia-Segura, S., 2024: Electrochemical oxidation of surfactants as an essential step to enable greywater reuse. *Environmental Technology & Innovation*, 34, 103563. https://doi.org/10.1016/j.eti.2024.103563.

Ďurigová, I., 2001: Výstavba Štátnej rafinérie minerálnych olejov v Dubovej a spracovanie gbelskej nafty. In: Z dejín ťažby ropy a zemného plynu na Slovensku, Gbely, 24. – 25. október 2001.

Ferro, S., De Battisti, A., Duo, I., Comninellis, C., Haenni, W. & Perret, A., 2000: Chlorine Evolution at Highly Boron-Doped Diamond Electrodes. *Journal of the Electrochemical Society*, 147, 7, 2614–2619.

Fóti, G., Gandini, D., Comninellis, C., Perret, A. & Haenni, W., 1999: Oxidation of organics by intermediates of water discharge on $IrO_2$ and synthetic diamond anodes. *Electrochemical and solid-state letters*, 2, 5, 228–230.

Gadd, G. M., Bahri-Esfahani, J., Li, Q., Rhee, Y. J., Wei, Z., Fomina, M. & Liang, X., 2014: Oxalate production by fungi: significance in geomycology, biodeterioration and bioremediation. *Fungal Biology Reviews*, 28, 2, 36–55. https://doi.org/10.1016/j.fbr.2014.05.001.

Hadadi, V. & Moradi, A., 2019: A novel method for refining of acidic sludge and mixing with vacuum bottom to improve bitumen properties. *Petroleum Science and Technology*, 37, 13, 1529–1538. https://doi.org/10.1080/10916466.2019.1573258.

Hao, X. & Smith, C., 2005: Physical and chemical properties of acid tars. Consoil 2005, 9th International FZK / TNO Conference on Soil-Water Systems. *Bordeaux Convention Center, Bordeaux, France.*

Hrušková, L., Daučík, P., Hadvinová, M., Hájeková, E., Hudec, P. & Rosevák, M., 2013: Sauer Sludges – Origination, Deposits, Properties and Characterization. In: *Proceedings of the 46th International Conference on Petroleum Processing*, June 7, 2013, Bratislava, Slovak Republic.

Jánová, V., 2019: Plán prác na odstránenie environmentálnej záťaže BR (015) / Predajná – Skládka PO Predajná I. *Bratislava, Ministerstvo životného prostredia SR*, 35 pp.

Kapałka, A., Fóti, G. & Comninellis, C., 2010: Basic Principles of the Electrochemical Mineralization of Organic Pollutants for Wastewater Treatment. In: Comninellis, C. & Chen, G. (eds.): *Electrochemistry for the Environment. New York, Springer*, 1–23. https://doi.org/10.1007/978-0-387-68318-8_1.

Kasana, A., Hammel, B. & Hudec, R., 2021: Vodná stavba odkalisko Dubová (Nádrže gudrónov Predajná I a Predajná II). Program Technicko-bezpečnostného dohľadu. *Bratislava, Vodohospodárska výstavba.*

Knapcová, I., Fialová, J., Hybská, H. & Samešová, D., 2017: Environmental burden in the Protection zone of Low Tatras. In: Miklós, L. & Diviaková, A. (eds.): Proceedings of the Conference Sustainable development goals target of the integrated environmental management. Zvolen, Slovak Republic. *Zvolen, Technická univerzita vo Zvolene*, 85–94.

Knapcová, I. & Samešová, D., 2017: Problematika odpadových kyslých dechtov (gudrónov). *Acta Facultatis Ecologiae Zvolen*, 36, 29–37.

Kordík, J., Slaninka, I., Bahnová, N., Benková, K., Bodiš, D., Bottlik, F., Dananaj, I., Demko, R., Dénes, D., Dodoková, Z., Fordinál, K., Fričovská, J., Fričovský, B., Gazdačko, Ľ., Gluch, A., Gonda, S., Gurinová, E., Györög, I., Hlodák, M., Husár, M., Iglárová, Ľ., Jankulár, M., Jelínek, R., Kotuč, J., Kubač, A., Kúšik, A., Lenhardtová, E., Mašlár, E., Mašlárová, I., Mikušová, J., Olšavský, M., Ondrášiková, B., Pijaková, E., Pramuka, S., Siska, M., Stašik, Ľ., Stríček, I., Šefčík, P., Ševčíková, P., Mackových, D., Repková, R., Vabcová, J., Kovalčíková, A., Nováková, J., Uhrinová, K., Michalko, J., Nováčková, M. & Pešta, I., 2023: Zabezpečenie monitorovania environmentálnych záťaží Slovenska – 1. časť. Final report. *Manuscript. Bratislava, Archive of St. Geol. Inst. of D. Štúr* (arch. no. 102803), 162 s. (in Slovak).

Kraft, A., 2007: Doped Diamond: A Compact Review on a New, Versatile Electrode Material. *International Journal of Electrochemical Science*, 2, 355–385. https://doi.org/10.1016/S1452-3981(23)17080-5.

Kupka, D., Václavíková, M., Bártová, Z., Ivaničová, L., Jáger, D. & Gallios, G., 2017: Elimination of Oxo-Chlorine By-Products Generated During Electrolytic Treatment. Paper presented at the In: INESS: Abstracts Book International Conference on Nanomaterials and Advanced Energy Storage Systems & 4th Workshop on Water and Soil Clean-up from Mixed Contaminants. *Astana, Kazakhstan, Nazarbayev University.*

Lai, D., Schaefer, T., Zhang, Y., Li, Y. J., Herrmann, H. & Chan, M. N., 2025: Oxidation Kinetics of Alkyl Sulfates and Sulfonates by Sulfate Radical ($SO_4^{\bullet-}$) in the Aqueous Phase: Deactivating Role of Sulfur Functional Groups. *ACS Earth and Space Chemistry*, 9, 1, 158–168. https://doi.org/10.1021/acsearthspacechem.4c00313.

Leonard, S. A. & Stegemann, J. A., 2010: Contaminant Leaching from Stabilized/Solidified Acid Tars. *Journal of Environmental Engineering*, 136, 12, 1369–1378. https://doi.org/10.1061/(ASCE)EE.1943-7870.0000282.

Leonard, S. A., Stegemann, J. A. & Roy, A., 2010: Characterization of acid tars. *Journal of Hazardous Materials*, 175, 1, 382–392. https://doi.org/10.1016/j.jhazmat.2009.10.015.

Lin, S. H., Lin, C. M. & Leu, H. G., 1999: Operating characteristics and kinetic studies of surfactant wastewater treatment by Fenton oxidation. *Water Research*, 33, 7, 1735–1741. https://doi.org/10.1016/S0043-1354(98)00403-5.

Lu, J., R. Hou, Y., Wang, Zhou, L. & Yuan, Y., 2022: Surfactant-sodium dodecyl sulfate enhanced degradation of polystyrene microplastics with an energy-saving electrochemical advanced oxidation process (EAOP) strategy. *Water Research*, 226, 119277. https://doi.org/10.1016/j.watres.2022.119277.

Martínez-Huitle, C. A., 2014. Organic Pollutants in Water Using BDD, Direct and Indirect Electrochemical Oxidation. In: Kreysa, G., Ota, K.-i. & Savinell, R. F. (eds.): Encyclopedia of Applied Electrochemistry. *New York, Springer*, 1402–1407.

Martínez-Huitle, C. A., Ferro, S. & De Battisti, A., 2004: Electrochemical incineration of oxalic acid: Role of electrode material. *Electrochimica Acta*, 49, 22, 4027–4034. https://doi.org/10.1016/j.electacta.2004.01.083.

Martínez-Huitle, C. A., Rodrigo, M. A., Sirés, I. & Scialdone, O., 2015: Single and Coupled Electrochemical Processes and Reactors for the Abatement of Organic Water Pollutants: A Critical Review. *Chemical Reviews*, 115, 24, 13362–13407. https://doi.org/10.1021/acs.chemrev.5b00361.

Martins, R. C., Silva, A. M. T., Castro-Silva, S., Garção-Nunes, P. & Quinta-Ferreira, R. M., 2011: Advanced oxidation processes for treatment of effluents from a detergent industry. *Environmental Technology*, 32, 9, 1031–1041. https://doi.org/10.1080/09593330.2010.523439.

Milne, D. D., Clark, A. I. & Perry, R., 1986: Acid tars: their production, treatment and disposal in the U.K. *Waste Management & Research*, 4, 4, 407–418.

Muff, J., 2014. Chapter 3 – Electrochemical Oxidation – A Versatile Technique for Aqueous Organic Contaminant Degradation A2 – Søgaard, Erik G Chemistry of Advanced Environmental Purification Processes of Water. *Amsterdam, Elsevier*, 75–134.

Nakagawa, H. & Yamaguchi, E., 2012: Influence of oxalic acid formed on the degradation of phenol by Fenton reagent.

*Chemosphere*, 88, 2, 183–187. https://doi.org/10.1016/j.chemosphere.2012.02.082.

Nancarrow, D. J., Slade, N. J. & Steeds, J. E., 2001: Land Contamination: Technical Guidance on Special Sites: Acid Tar Lagoons. Environment Agency R&D, Technical Report P5-042/TR/04, ISBN 185-705- 583-7, 11–50.

Nichol, D., 2000: Geo-engineering problems at Hoole Bank acid tar lagoon, Cheshire, UK. *Land Contamination & Reclamation*, 8, 167–173.

Ostrolucký, J. & Gálisová, M., 1986: Predajná II. – Sledovanie zmien znečistenia podzemnej vody. *Manuscript. Bratislava, Archive of State Geological Institute of Dionýz Štúr* (arch. no. 74401), 57 pp.

Ostrolucký, J., Gálisová, M., Biely, A., Kullman, E., Gazda, S. & Višňovský, D.,1982: Predajná II. – Skládka gudrónov, vyhľadávací HGP. *Manuscript. Bratislava, Archive of State Geological Institute of Dionýz Štúr* (arch. no. 54280), 84 pp.

Paluchová, K., Auxt, A., Bruchániková, A., Helma, J., Schwarz, J. & Pacola, E., 2008: Systematic identification of environmental burdens of the Slovak Republic, final report. *Manuscript. Bratislava, Archive of State Geological Institute of Dionýz Štúr* (arch. no. 89101), 154 pp.

Panizza, M., Brillas, E. & Comninellis, C., 2008: Application of boron-doped diamond electrodes for wastewater treatment. *J. Environ. Eng. Management,* 18, 3, 139–153.

Panizza, M. & Cerisola, G., 2005: Application of diamond electrodes to electrochemical processes. *Electrochimica Acta*, 51, 2, 191–199. https://doi.org/10.1016/j.electacta.2005.04.023.

Panizza, M. & Cerisola, G., 2009: Direct And Mediated Anodic Oxidation of Organic Pollutants. *Chemical Reviews*, 109, 12, 6541–6569. https://doi.org/10.1021/cr9001319.

Pirman, I. & Potyš, Z., 1997: Skládky gudrónov Predajná I a II – Hydrogeologický prieskum. *Manuscript. Bratislava, Archive of State Geological Institute of Dionýz Štúr* (arch. no. 80981), 7 pp.

Polák, M., Filo, I., Havrila, M., Bezák, V., Kohút, M. & Kováč, P., 2003a: Vysvetlivky ku geologickej mape Starohorských vrchov, Čierťaže a severnej časti Zvolenskej kotliny 1 : 50 000. Bratislava, Štátny geologický ústav Dionýza Štúra, 218 pp., ISBN 80-88974-45-3.

Polák, M. Filo, I., Havrila, M., Bezák, V., Kohút, M., Kováč, P., Vozár, J., Mello, J., Maglay, J., Elečko, M., Olšavský, M., Pristaš, J., Siman, P., Bučeк, S., Hók, J., Rakús, M., Lexa, J. & Šimon, L., 2003b: Geologická mapa Starohorských vrchov, Čierťaže a severnej časti Zvolenskej kotliny 1 : 50 000. Bratislava, Štátny geologický ústav Dionýza Štúra, ISBN 80-88974-44-5.

PubChem, 2025: National Center for Biotechnology Information. "PubChem Compound Summary for Coal Tar" PubChem, https://pubchem.ncbi.nlm.nih.gov/compound/Coal-Tar. Accessed 17 December, 2025.

Rodrigo, M. A., Michaud, P. A., Duo, I., Panizza, M., Cerisola, G. & Comninellis, C., 2001: Oxidation of 4-Chlorophenol at Boron-Doped Diamond Electrode for Wastewater Treatment. *Journal of The Electrochemical Society*, 148, 5, D60. https://doi.org/10.1149/1.1362545.

Saha, P., Wang, J., Zhou, Y., Carlucci, L., Jeremiasse, A. W., Rijnaarts, H. H. M. & Bruning, H., 2022: Effect of electrolyte composition on electrochemical oxidation: Active sulfate formation, benzotriazole degradation, and chlorinated by-products distribution. *Environmental Research*, 211, 113057. https://doi.org/10.1016/j.envres.2022.113057.

Saien, J. & Jafari, F., 2022: Methods of Persulfate Activation for the Degradation of Pollutants: Fundamentals and Influencing Parameters. In: Zhu, M., Bian, Z. & Zhao, C. (eds.): Persulfate-based Oxidation Processes in Environmental Remediation. *The Royal Society of Chemistry*, 364 pp.

Samešová, D., Ladomerský, J. & Hroncová, E., 2007: Príspevok k posudzovaniu vplyvov gudrónových odpadov na životné prostredie (Contribution to Assessment of Goudron Wastes Impact on the Environment). *Acta Facultatis Ecologiae*, 15, 49–53.

Scialdone, O., Randazzo, S., Galia, A. & Filardo, G., 2009a: Electrochemical oxidation of organics at metal oxide electrodes: The incineration of oxalic acid at $IrO_2$–$Ta_2O_5$ (DSA-$O_2$) anode. *Electrochimica Acta*, 54, 4, 1210–1217. https://doi.org/10.1016/j.electacta.2008.08.064.

Scialdone, O., Randazzo, S., Galia, A. & Silvestri, G., 2009b: Electrochemical oxidation of organics in water: Role of operative parameters in the absence and in the presence of NaCl. *Water Research*, 43, 8, 2260–2272. https://doi.org/10.1016/j.watres.2009.02.014.

Speight, J. G., 2014: The Chemistry and Technology of Petroleum, Fifth Edition. *Boca Raton, CRC Press, Taylor & Francis.*

STN-ISO-5667-4, 2018: Water quality. Sampling. Part 4: Guidance on sampling from lakes, natural and man-made. Slovak Technical Norm, June 2018.

Šumichrast, P., 2014: 70. výročie leteckého náletu na Dubovú. Vojenský historický ústav. https://www.vhu.sk/70-vyrocie-leteckeho-naletu-na-dubovu/.

TASR, 2022a: Technicko-bezpečnostný dohľad gudrónových jám. Spravodajský portál Tlačovej agentúry Slovenskej republiky. 22. januára 2022, 15:16. https://www.teraz.sk/slovensko/vv-vykonava-odborny-technicko-bezpecn/606386-clanok.html?utm_source=teraz&utm_medium=organic&utm_campaign=click&utm_content=.%253Bsearch.

TASR, 2022b: V Predajnej pokračujú v čistení vody z toxických gudrónových jám. Spravodajský portál Tlačovej agentúry Slovenskej republiky. 12. júna 2022, 20:07. https://www.teraz.sk/regiony/v-predajnej-pokracuju-prace-na-ciste/640244-clanok.html.

Tsantaki, E., Velegraki, T., Katsaounis, A. & Mantzavinos, D., 2012: Anodic oxidation of textile dyehouse effluents on boron-doped diamond electrode. *Journal of Hazardous Materials*, 207–208, 91–96. https://doi.org/10.1016/j.jhazmat.2011.03.107.

Xing, X., Ni, J., Zhu, X., Jiang, Y. & Xia, J., 2018: Maximization of current efficiency for organic pollutants oxidation at BDD, Ti/$SnO_2$-Sb/$PbO_2$, and Ti/$SnO_2$-Sb anodes. *Chemosphere*, 205, 361–368. https://doi.org/10.1016/j.chemosphere.2018.04.090.

Zöllig, H., Remmele, A., Morgenroth, E. & Udert, K. M., 2017: Removal rates and energy demand of the electro-

chemical oxidation of ammonia and organic substances in real stored urine. *Environmental Science: Water Research & Technology*, 3, 3, 480–491. https://doi.org/10.1039/C7EW00014F.

Zuo, K., Garcia-Segura, S., Cerrón-Calle, G. A., Chen, F.-Y., Tian, X., Wang, X., Huang, X., Wang, H., Alvarez, P. J. J., Lou, J., Elimelech, M. & Li, Q., 2023: Electrified water treatment: fundamentals and roles of electrode materials. *Nature Reviews Materials*, 8, 7, 472–490. https://doi.org/10.1038/s41578-023-00564-y.

# Stručný prehľad histórie a charakteristika lokality Predajná, kontaminovanej kyslým dechtom, a potenciálne využitie elektrochemickej oxidácie na sanáciu povrchovej vody z otvorených lagún

Kyslé gudrónové smoly sú odpad, ktorý vznikal pri spracovaní ropných frakcií a rafinácii recyklovaných ropných produktov kyselinou sírovou. V areáli bývalého podniku Petrochema Dubová a na súvisiacich skládkach Predajná I a II sa tento odpad ukladal na miesta bez adekvátneho technického zabezpečenia. Skládky gudrónov patria medzi najzávažnejšie environmentálne záťaže, spojené s chemickým priemyslom 20. storočia. Kyslé gudrónové smoly sa vyznačujú vysokou koncentráciou kyseliny sírovej, tenzidov, polycyklických aromatických uhľovodíkov, sulfonovaných organických látok a kovov. V dôsledku atmosférických zrážok sa na povrchu lagún vytvorila silne kyslá vodná fáza obohatená o sulfáty a organické látky, ktorá predstavuje dlhodobý zdroj kontaminácie okolitého prostredia.

Skládky Predajná I a II sa nachádzajú v oblasti s karbonátovým podložím tvoreným dolomitmi a dolomitickými vápencami a sú situované v ochrannom pásme Národného parku Nízke Tatry. Absencia potrebnej izolácie umožnila infiltráciu kontaminovaných výluhov do horninového prostredia a podzemnej vody, čo sa potvrdilo geologickým prieskumom. Sezónne kolísanie hladiny povrchovej vody v lagúnach v závislosti od zrážok a topenia snehu zvyšuje riziko pretečenia hrádzí a šírenia kontaminácie do okolitého prostredia. Tieto aspekty poukazujú na potrebu výskumu účinných sanačných opatrení, zameraných predovšetkým na bezpečné a dlhodobo udržateľné nakladanie s takto kontaminovanou vodnou fázou.

Predmetom tohto článku bolo posúdenie potenciálnej aplikácie a účinnosti elektrochemickej pokročilej oxidačnej metódy založenej na aplikácii elektród z diamantu dopovaného bórom (BDD) na dekontamináciu povrchovej vody z lagúny Predajná I. Experimenty sa realizovali vo vsádzkovom režime s recirkuláciou. Odpadová voda sa zo zásobnej temperovanej nádoby čerpala obehovým čerpadlom do externého okruhu s prietokovým elektrochemickým reaktorom a následne sa vracala späť do zásobnej nádoby. Táto konfigurácia umožňovala kontinuálny prietok odpadovej vody cez reaktor a opakovaný kontakt s povrchom elektród. Výsledky laboratórnych testov preukázali vysokú účinnosť procesu. V priebehu štyroch hodín elektrolýzy sa znížila koncentrácia celkového organického uhlíka (TOC) a hodnota chemickej spotreby kyslíka ($CHSK_{Cr}$) o 88,7 %, resp. 94 % a po siedmich hodinách elektrolýzy o 98,5 %, resp. 99,6 %.

V procese elektrochemickej oxidácie sa štiepili sulfonované organické zlúčeniny a následne sa uvoľňovali sírany. Ako stabilný medziprodukt bol identifikovaný oxalát, ktorý sa pri dlhšom čase pôsobenia elektrochemicky generovaných oxidačných činidiel ďalej mineralizoval na oxid uhličitý a vodu. Ďalšie produkty rozpadu zložitých chemických zlúčenín stále podliehajú laboratórnym testom. Dosiaľ dosiahnuté výsledky potvrdzujú, že elektrochemická oxidácia s využitím elektród z BDD predstavuje perspektívny, environmentálne prijateľný a bezodpadový spôsob využiteľný na sanácie silne kontaminovanej vody aj v gudrónových lagúnach. Na rozdiel od konvenčných chemicko-fyzikálnych postupov, táto technológia umožňuje vysoký stupeň degradácie perzistentných organických látok bez vzniku sekundárneho nebezpečného odpadu. Elektrochemické pokročilé oxidačné prístupy by tak mohli prichádzať do úvahy ako súčasť komplexných sanačných prístupov pri riešení tejto environmentálnej záťaže na Slovensku.

Doručené / Received: 19. 12. 2025
Prijaté na publikovanie / Accepted: 10. 3. 2026

*Mineralia Slovaca, Web ISSN 1338-3523, ISSN 0369-2086, https://doi.org/10.56623/ms.2025.57.2.4*
*57, 2 (2025), 159 – 172, © Authors 2025. CC BY 4.0*

# Environmental burdens in Šurany – groundwater pollution by chlorinated aliphatic hydrocarbons

JURAJ MACEK[1, 2]*, ROMAN TÓTH[1, 2] and ĽUBOMÍR JURKOVIČ[2]

[1] Centre of Environmental Services, Ltd., Kutlíkova 17, 852 50 Bratislava, Slovak Republic,
*corresponding author, macek@cenvis.sk
[2] Comenius University in Bratislava, Faculty of Natural Sciences, Department of Geochemistry,
Ilkovičova 6, 842 15 Bratislava, Slovak Republic

**Abstract:** In the past, the town of Šurany was a local center of industrial production, which resulted in the existence of five environmental burdens. Industry was associated with the intensive use of hazardous substances. In 2022, geological surveys of the environment were carried out on three environmental burdens in the town's cadastral area (the former sugar mill, the former CALEX plant and the municipal solid waste dump). The survey results were processed together with the results of a detailed geological survey of the STS and ELITEX site (2015) and a supplementary survey of the CALEX plant (2023). The aim was to identify various groups of pollutants in the soil and groundwater (petroleum hydrocarbons, PAHs, BTEX, CAHs, metals). Geological work confirmed massive groundwater contamination with chlorinated aliphatic hydrocarbons in the southwestern part of the town. The results show that the main source of contamination is the former STS and ELITEX site, from which the contamination spreads downgradient with groundwater flow. The maximum concentrations of pollution were very high (cis-1,2-dichloroethene 2,810 µg.L$^{-1}$, trichloroethene 2,970 µg.L$^{-1}$, tetrachloroethene 247 µg.L$^{-1}$). Unlike the other sites investigated, vinyl chloride was also present in the groundwater (max 168 µg.L$^{-1}$). High concentrations of CAHs were identified 500 m downgradient the STS and ELITEX sites in groundwater at a municipal solid waste dump (cis-1,2-dichloroethene 469 µg.L$^{-1}$, trichloroethene 842 µg.L$^{-1}$, tetrachloroethene 125 µg.L$^{-1}$).

**Key words:** Groundwater, Contamination, Chlorinated Aliphatic Hydrocarbons, Environmental Burden, Šurany

**Graphical abstract**

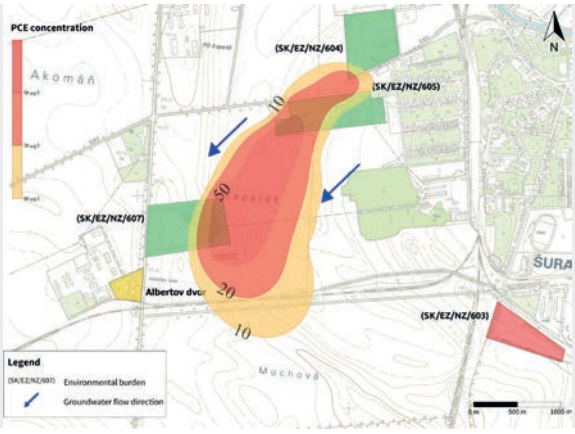


**Highlights**

- Summary interpretation of the results of geological environmental surveys at four environmental burdens in the municipality of Šurany
- The results confirmed groundwater contamination with chlorinated aliphatic hydrocarbons over a large area
- The source of the contamination is the former plant STS and ELITEX

## Introduction

Chlorinated aliphatic hydrocarbons (CAHs) are among the most widespread groundwater pollutants. This is due to their long-term use (since the beginning of the 20th century) and their wide range of applications, particularly in industrial degreasing and dry cleaning of clothing (Booij et al., 1992; Doherty, 2000). CAHs belong to dense non-aqueous phase liquids (DNAPLs), substances with density higher than water (Kram et al., 2001; Pankow & Cherry, 1996). The most commonly used are trichloroethene (TCE) and tetrachloroethene (PCE) (He et al., 2021). The first mention of their negative impact on groundwater quality dates back to 1949 (Lyne & McLachlan, 1949). Dichloroethene (DCE) and PCE isomers are classified as probable carcinogens according to the US EPA, while vinyl chloride (VC) and TCE are classified as confirmed carcinogens (ATSDR, 2019, 2024). DNAPLs migrate vertically through the unsaturated zone in a similar way to light non-aqueous phase liquids from the point of leakage. They gradually descend through the aquifer until they reach an impermeable layer (e.g. clay), where they may accumulate in depressions (Huling & Weaver, 1991; Rubin et al., 1998). CAHs, as water-soluble pollutants can easily spread and contaminate aquifers in large areas (Hyldegaard & Ottosen, 2021). DNAPLs can persist in

groundwater for several decades and act as an perennial source of contamination (Essaid et al., 2015). Remediation is due to their nature complicated and requires a detailed study of bedrock properties.

The aim of the study is to assess the spread of pollution from several possible sources located close to each other in the western part of the town of Šurany. Despite the facilities being shut down for more than 30 years, groundwater pollution persists in high concentrations. Monitoring the development of concentrations in groundwater in space and time is the starting point for the implementation of remediation activities.

## Characteristics of the area

The town of Šurany is located in the Danube Lowland, in the southern part of Slovakia (Nové Zámky District). In the past, the town was a center of industrial and food production, employing people from the wider area. The town was home to the oldest sugar mill in Central Europe (founded in 1854), the ELITEX plant (approx. 2,200–2,600 employees) produced components for cars and later for knitting machines. At the CALEX plant, approx. 300 employees produced parts for refrigeration equipment (Šutka et al., 2008). The entire town of Šurany has approximately 10,000 inhabitants. After the

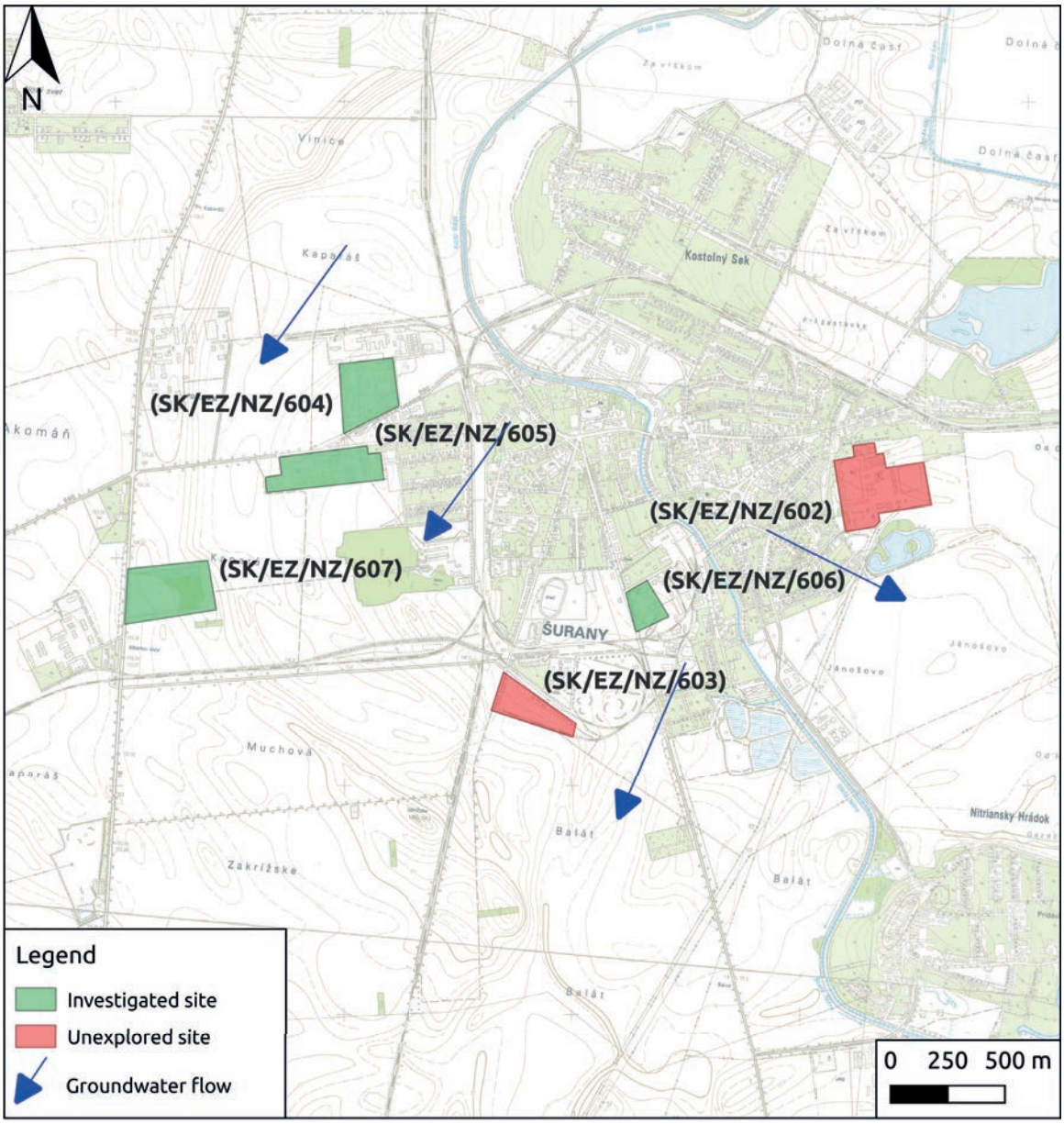


**Fig. 1.** Environmental burdens in Šurany municipality

transition to a market economy in 1989, former socialist companies had problems with sales and gradually ceased operations. Today, the former production facilities are used in a different way. The type of production activity, together with the approach to environmental protection at the time, meant that all of the above-mentioned plants were classified as probable environmental burdens (EB) when the environmental burden information system was created in 2010 (https://envirozataze.enviroportal.sk/). Through several projects implemented by the Ministry of the Environment of the Slovak Republic, probable burdens in the town of Šurany were selected for detailed geological environmental surveys. The first geological survey focused on environmental burdens was carried out in 2015. The results showed massive groundwater contamination by chlorinated aliphatic hydrocarbons in the EB area, as well as their spreading downgradient with groundwater flow (Tupý et al., 2015). Currently, there are 6 probable/verified EBs registered in the cadastre of the municipality of *Šurany*, none of which had been remediated by 2025.

In 2022, according to the Register of EBs, there were 6 sites registered in Šurany in registers A (probable environmental burden) and B (confirmed environmental burden). Their position in relation to the town of Šurany is shown in Figure 1. Four of them were the subject of a detailed geological survey and two were classified as probable environmental burdens without more detailed information on the state of pollution. Detailed geological surveys of the environment constituted an extensive set of works aimed at identifying and evaluating the presence of pollution in soil air, rock environment and groundwater. Given that a significant portion of the pollution (or pollution posing a risk to environmental components) was identified in groundwater, this study focuses on the assessment of this matrix. The authors of the study formed the core of the teams that conducted geological surveys at three sites in 2022 and 2023 – municipal solid waste dump [SK/EZ/NZ/607 (Tupý et al., 2022c)], former sugar mill [SK/EZ/NZ/606 (Tupý et al., 2022b)], former CALEX site [SK/EZ/NZ/604 (Tupý et al., 2022a)]. Due to problems with access to the site, part of the CALEX site was surveyed in 2022 (Tupý et al., 2022a) and the remaining part in 2023 (Macek et al., 2023). The fourth EB – the former ELITEX and STS site (SK/EZ/NZ/605) – was investigated in 2015. The site of the former CALEX plant, located upgradient of the ELITEX and STS EBs, was identified as a possible source of CAHs groundwater contamination (Tupý et al., 2015). The assumption of high concentrations of CAHs was based on an analogy with a similar site – the CALEX plant in Zlaté Moravce. In 2022, the remediation of the main CALEX plant in Zlaté Moravce was completed, where free phase of CAHs was present at the bottom of the aquifer (Auxt et al., 2022). From 2016 to 2023, the State Geological Institute of Dionýz Štúr monitored the quality of groundwater at the site (Kordík et al., 2023).

### *General geological characteristics of the north-east part of Danubian Lowland*

In the north-eastern part of the Danube Lowland, the basement of the Neogene depression is formed by crystalline and Mesozoic rocks. The oldest Neogene formation is the Badenian, whose rocks were identified near Šurany (Lower Badenian). The Badenian marked a fundamental change in the development of the entire Danube Basin, which manifested itself in significant subsidence and volcanic activity. The territory is largely covered by Quaternary – Pleistocene and Holocene sediments (Priechodská et al., 1988). Quaternary sediments dominate the Nitra Hills. They continuously cover the southern, less the central and northern parts of the territory. The thickness of the cover increases from north to south and from the surrounding mountains to the central parts of the hills. Loess and loess-like sediments play a major role, while the second most significant type are fluvial sediments, which fill depressions and hollows. The thickness of Quaternary sediments rarely exceeds 25 m, with a maximum in the southern part on the terraces of the confluence of the Nitra and Váh rivers (Pristaš et al., 2000).

The town of Šurany lies on fluvial sediments linked to the valley of the Nitra River and its larger tributaries. In the flat area around Šurany, they form a continuous layer on a tectonically subsiding territory. At the base, there are gravels and sands belonging to the low terrace. Above them are Holocene clays (sandy to loamy). In the vicinity of Šurany, organic sediments consisting of dark to black clays with a significant proportion of organic matter have been preserved. Overall, the sediments are mostly grey and brownish-grey, with lighter or darker shades in places. A typical feature is the occurrence of carbonates. The total thickness of Holocene fluvial sands is 1–3 m, rarely up to 5 m (Priechodská et al., 1988; Pristaš et al., 2000).

The area is located west and southwest of the town of Šurany (Fig. 2). West of the town, there are Pleistocene fluvial sediments (younger Riss) – sandy gravels of the lower terrace covered with loess and loess loams. The main lower terrace is one of the most widespread terrace levels in the region, protruding significantly mainly on the left bank of the Nitra River. Between Sereď and Nové Zámky, it borders the southwestern edge of the Nitra Hills – the Nitra Plateau – with a wide strip. The width of the terrace reaches 4–5 km in places, or even more. The surface of the terrace is located approximately 8–12 m above the floodplains of the rivers. The terrace is mostly covered by loess and loess loam. The upper layer of the terrace profile in the area west of Šurany contains humus black earth and brown earth soils of the Riss-Würm interglacial period (Pristaš et al., 2000). Southwest of the town, there are Pleistocene fluvial sediments (Würm) – sandy gravel and sand of a low terrace covered with washed-out loess

and marsh loess. The low terrace at a relative height of 4–6 m (maximum 8 m) above the floodplains has the lowest morphological position in the Nitra Valley between the terraces. The surface of the terrace near Šurany is slightly undulating with clear signs of deflation and eolian activity. In the area southwest of Šurany, light yellow to grey, in places brownish to greenish, dusty to fine-sandy calcareous clay – marsh loess – protrudes from the overburden of fluvial clays and sands (Pristaš et al., 2000).

### *Geological characteristics of the area*

In the western part of Šurany, the geological conditions have been verified by several surveys in the past. Neogene sediments have been identified beneath the Quaternary sediments, consisting of gravelly sandy layers with occurrences of sandy clays, but the Quaternary-Neogene boundary is unclear. The interface is reported at a level of 21 m below ground surface (Obuch, 2008). The thickness of the clay layers in the boreholes reached approximately 3 m (Kmeť, 2008). From approximately 3.0 m below ground surface, the first water-bearing horizon of sand or sandy gravel is located. A 55 m deep borehole detected alternating gravel and clay layers from approximately 9.0 m below ground surface (0.0–4.0 m clay; 4.0–9.0 m sand; 9.0–11.0 m gravel; 11.0–14.0 m gravel; 14.0–16.0 m clay; 16.0–23.0 m gravel; 23.0–27.0 m clay; 27.0–29.0 m

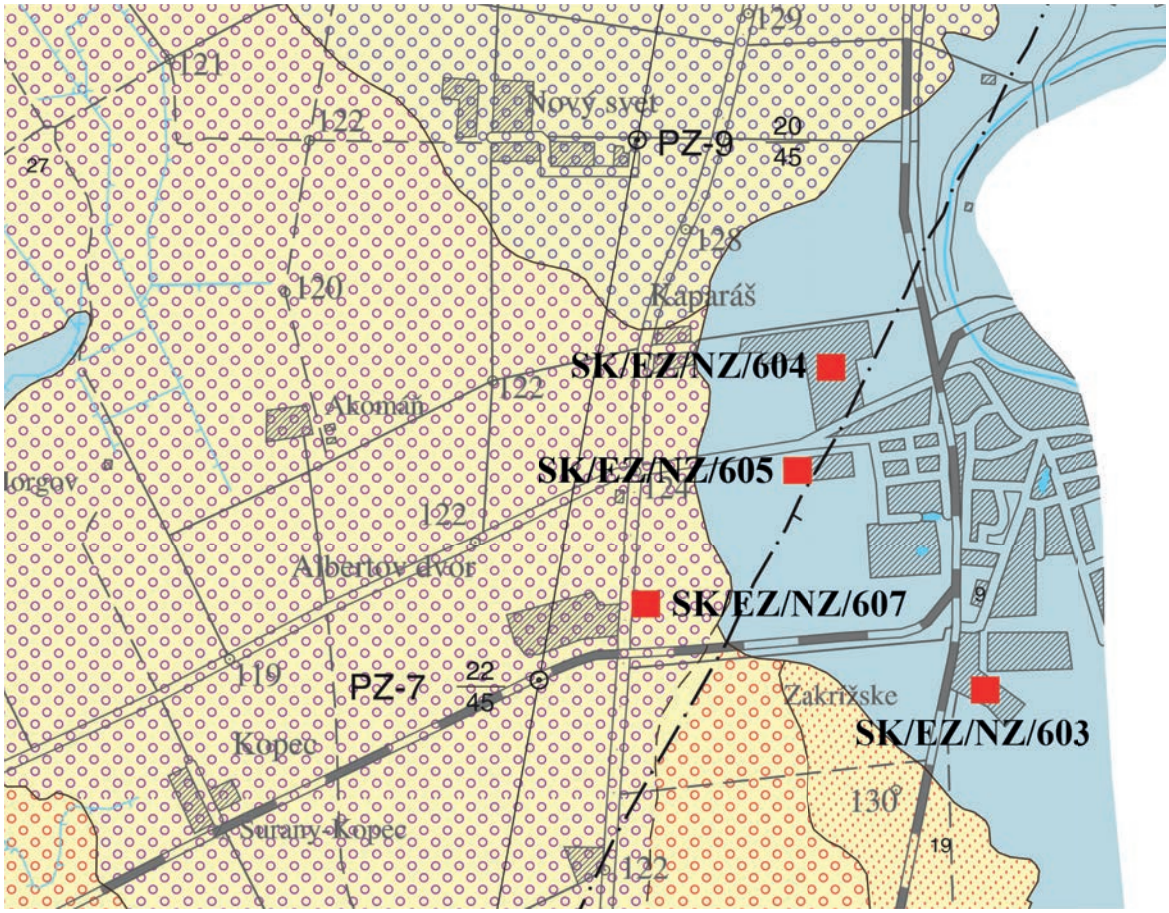


Legend:

| | |
|---|---|
| | Holocene: loams, sandy loams, clays, loamy sands and gravels of river and creek flood plains |
| | Würm, eolian sediments: sands with short eolian transport |
| | Würm, fluvial sediments: sandy gravels and sands of lower terrace with cover of redeposited loesses and swamp loesses |
| | Upper Riss, fluvial sediments: sandy gravels of lower middle terrace with loesses and loess loam covers |
| | Lower Riss, fluvial sediments: sandy gravels of upper middle terrace with loesses cover and cover of run-off loesses |

**Fig. 2.** Šurany area geological setting (Pristaš et al., 2000)

gravel; 29.0–36.0 m clay; 36.0–38.0 m sand; 38.0–44.0 m clay; 44.0–47.0 m gravel; 47.0–48.5 m sand; 48.5–51.0 m clay; 51.0–54.5 m gravel; 54.5–55.0 m clay), which are approximately 2.0 m thick (Obuch, 2008). A similar lithological development was also observed in a 65 m deep borehole drilled near the CALEX site (Kertész et al., 1978). The hydraulic conductivity values, calculated on the basis of pumping test results, were $K = 1.66 \cdot 10^{-4}$ m.s$^{-1}$ (Kertész et al., 1978) and $K = 8.06 \cdot 10^{-4}$ m.s$^{-1}$ (Obuch, 2008). The aquifer is represented by gravelly sand formation and the groundwater flow is characterized by intergranular permeability. The water-saturated bed of poorly graded sand (from approx. 3.5 m below ground level) is highly permeable. The general direction of groundwater flow is on the right side of the Malá Nitra River NE–SW, on the left side NW–SE, and the groundwater is confined.

## Material and methods

Geological surveys were carried out using a uniform methodology in accordance with the Methodological Guide for Geological Surveys of the Environment in Contaminated Areas (Schwarz et al., 2020). After the drilling of new wells, groundwater samples were collected after short pumping. The sampling was combined with measurements of the groundwater level. Field parameters [temperature, oxidation-reduction potential (ORP), pH,

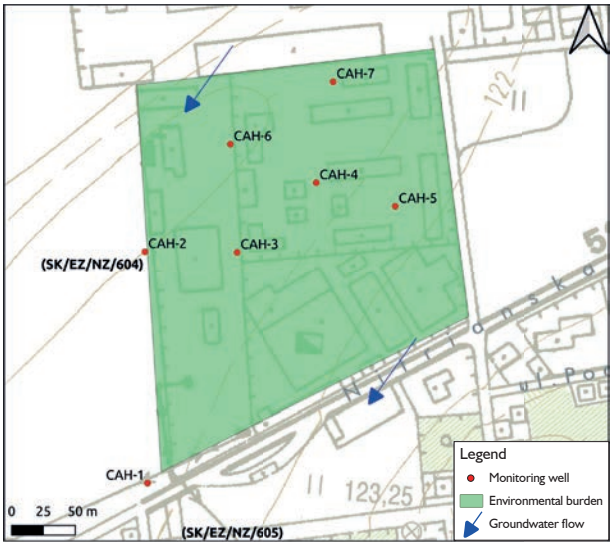


Former CALEX plant (SK/EZ/NZ/604)

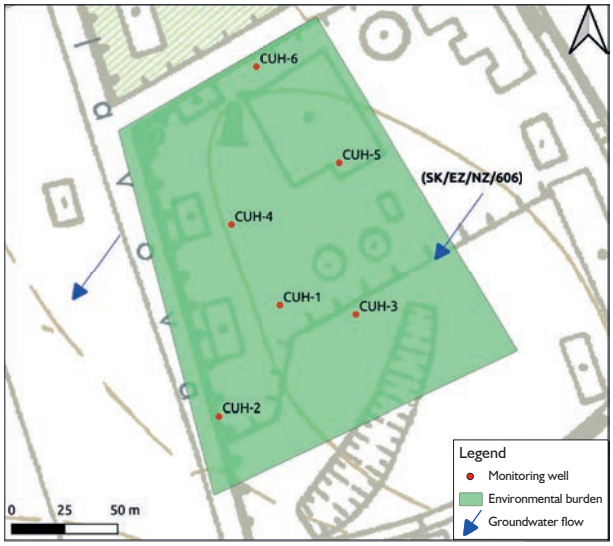


Former sugar mill (SK/EZ/NZ/606)

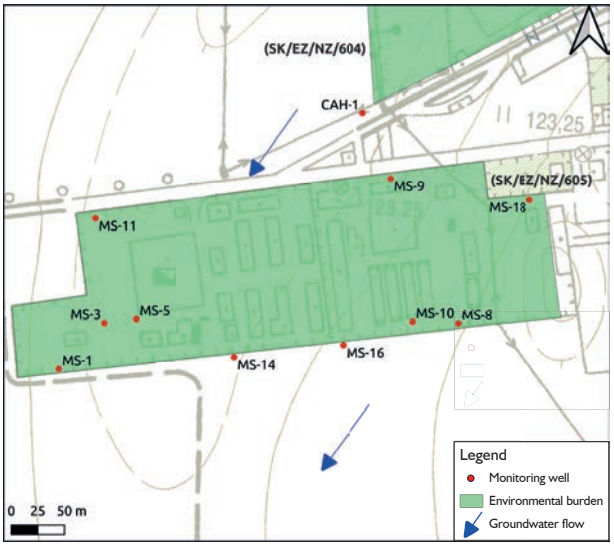


Former ELITEX and STS plants (SK/EZ/NZ/605)

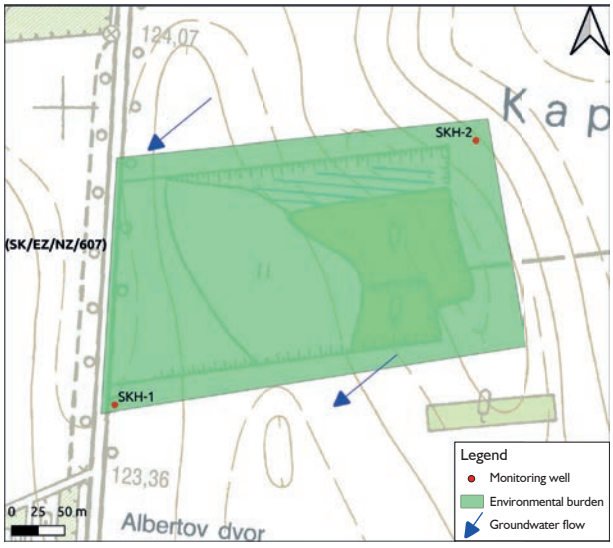


Municipal solid waste dump (SK/EZ/NZ/607)

**Fig. 3.** Depiction of the investigated sites

electrolytic conductivity (EC), dissolved oxygen (DO)] were measured prior to sampling. The measurements were performed with a calibrated Hanna HI98194 multimeter in a flow-through vessel. Groundwater samples were collected using a 12 V Gigant submersible pump (flow rate 0.1 $L.s^{-1}$). After rinsing the sample container (EPA VIAL) with groundwater, it was then filled so that no water bubbled over and no air was present in the filled sample container. Due to the priority pollutants (CAHs), groundwater samples were taken from the lower part of the water column (at the bottom of the performed interval). The filled sample containers were placed in cooled transport bag and immediately transported to an accredited laboratory.

Analytical work was carried out in an accredited laboratory in accordance with internal operating procedures – determination of volatile organic compounds (vinyl chloride, trans-1,2-dichloroethene, cis-1,2-dichloroethene; trichloroethene, tetrachloroethene) using gas chromatography with FID and MS detection and calculation of the sum of volatile organic compounds from the measured values. The analytical methods used corresponded to US EPA 624, US EPA 5021A, US EPA 8260, US EPA 8015. The obtained values were graphically processed by kriging interpolation in Golden Software Surfer 16.0.

The situation of the evaluated environmental burdens within the town of Šurany is shown in Figure 1, and the detailed location of the sampled wells at individual sites is shown in Figure 3.

## Results and discussion

The assessment of groundwater contamination in the area of Šurany was carried out on the basis of the results of surveys conducted in 2022 and 2023, together with the results of monitoring of the ELITEX and STS sites. The content of pollutants in groundwater was assessed in accordance with Directive of the Ministry of the Environment of the Slovak Republic No. 1/2015-7 on the preparation of a risk analysis of contaminated sites (hereinafter referred to as the "Directive"). The results of the first geological survey identified significant contamination of groundwater with CAHs (Tab. 1). The area of contamination, obtained by data interpolation, was in the case of PCE more than 10 hectares (concentrations higher than the Directive indicative criterion value for individual parameters) and more than 7 hectares (concentrations higher than the Directive intervention criterion value). An indicative criterion (ID) is a threshold value for the concentration of a pollutant, the exceeding of which may endanger human health and the environment. An intervention criterion (IT) is a critical value for the concentration of a pollutant, the exceeding of which is likely to endanger human health and the environment.

**Tab. 1**
Maximum concentrations of selected contaminants in 2015, ELITEX and STS (according to Tupý et al., 2015), *IT Criterion from the Directive of Ministry of Environment of the Slovak Republic No. 1/2015-7

| Parameter (Well) | Maximum identified concentration [$\mu g.L^{-1}$] | IT Criterion value* [$\mu g.L^{-1}$] |
|---|---|---|
| VC (VS-4) | 118 | 10 |
| DCE (VS-4) | 2,720 | 50 |
| TCE (MS-4) | 7,010 | 50 |
| PCE (MS-1) | 467 | 20 |

Table 2 shows the results of field parameters measured prior to groundwater sampling. The measurements taken in autumn represent more extensive data sets; measurements at the CALEX site in 2023 were taken during two sampling cycles (March 2023, May 2023). From the municipal solid waste dump (MSWD) site, only the part of the data that represents the properties of the water-saturated gravel layer was selected (there is also a second water-saturated level at the site, located in the body of the landfill).

When evaluating the results of field measurements in the western part of the city, it is clear that the measured values do not differ significantly among individual sites. The median temperatures ranged from 13.5 °C (MSWD) to 14.3 °C (CALEX). The higher water temperature in the CALEX area in 2023 is the result of a change in the season in which the measurements were taken. The deviations from the maximum and minimum values were small. Overall, the measured values roughly correspond to the natural groundwater values at the site and the given season.

Similarly, no significant differences were identified in the measured pH values. The medians of the measured values at the individual sites ranged from 7.11 and 7.33 (CALEX) to 7.31 (MSWD). The deviations from the maximum and minimum values were small. These are natural values for groundwater, which do not show any significant anomalies with regard to the expected presence of pollutants.

The medians of the measured values of specific electrolytic conductivity ranged from 603 $\mu S.cm^{-1}$ (CALEX) to 806 $\mu S.cm^{-1}$ (sugar mill). The values are approximately at the same level. However, the differences between the sites in relation to the measured minimum and maximum values are more significant. Locally high values document anthropogenic influence on groundwater quality. This was most evident at the sugar mill site, where a value of up to 3,876 $\mu S.cm^{-1}$ (CUH-3) was measured. Differences were observed between the values within the site in wells

**Tab. 2**
Results of field measurements at investigated sites

| Parameter | t [°C] | EC [µS.cm$^{-1}$] | DO [mg.L$^{-1}$] | pH | ORP [mV] |
|---|---|---|---|---|---|
| *CALEX – 131 measurements, October–November 2022* | | | | | |
| **Minimum** | 12.1 | 309 | 0 | 6.42 | –551 |
| **Maximum** | 16.2 | 876 | 6.12 | 7.89 | 303 |
| **Average** | 14.1 | 596 | 1.70 | 7.14 | 57 |
| **Median** | 14.3 | 603 | 0.98 | 7.11 | 137 |
| *Sugar mill – 72 measurements, October–November 2022* | | | | | |
| **Minimum** | 13.3 | 236 | 0.05 | 6.79 | –241 |
| **Maximum** | 15.4 | 3,876 | 5.1 | 7.76 | 559 |
| **Average** | 14.0 | 1,314 | 2.31 | 7.21 | 190 |
| **Median** | 14.1 | 806 | 2.55 | 7.15 | 230 |
| *MSWD – 73 measurements, October–November 2022* | | | | | |
| **Minimum** | 11.5 | 455 | 0.29 | 6.99 | –247 |
| **Maximum** | 15.6 | 1.002 | 4.78 | 7.56 | 580 |
| **Average** | 13.7 | 759 | 2.58 | 7.28 | 149 |
| **Median** | 13.5 | 744 | 2.96 | 7.32 | 83 |
| *CALEX – 11 measurements, March – May 2023* | | | | | |
| **Minimum** | 13.2 | 575 | 3.60 | 7.07 | 151 |
| **Maximum** | 16.8 | 1,040 | 5.20 | 7.44 | 208 |
| **Average** | 14.8 | 817 | 4.26 | 7.30 | 189 |
| **Median** | 14.8 | 759 | 4.20 | 7.33 | 193 |

CUH-1 to CUH-3, which are located in the direction of groundwater flow from the presumed source of pollution (fuel oil tanks), and wells in the area against the direction of groundwater flow (CUH-4 to CUH-6). In the former, conductivity values typically ranged around 2,000 µS.cm$^{-1}$, while in the case of well CUH-3, very high values exceeding the IT criterion of the Directive were measured (3,000 µS.cm$^{-1}$). In wells CUH-4 to CUH-6, the conductivity values measured were significantly lower (but probably also anthropogenically influenced), ranging from approximately 500 to 1,000 µS.cm$^{-1}$. Their occurrence mainly in the part where various secondary raw materials (mainly scrap metal) are temporarily stored indicates that they are more likely to be the result of activities carried out at the site at present (secondary raw material collection) than in the past (heavy fuel oil boiler). The median values obtained from measurements at the other two sites do not differ significantly from the values typical for natural conditions. According to Rapant et al. (1996), the median electrolytic conductivity for Quaternary groundwater (fluvial sediments of river plains) is 661 µS.cm$^{-1}$. Common groundwater and surface water conductivity values are 50 to 500 µS.cm$^{-1}$ (Pitter, 2015).

The measured values of DO in groundwater varied widely. At the CALEX site (in 2022), the minimum measured value was 0.0 mg.L$^{-1}$ and the maximum value was 6.12 mg.L$^{-1}$. It is not possible to draw clear conclusions from the measured values that would link changes in DO concentrations to other phenomena [low DO concentrations may indicate increased CAHs concentrations (Oldenhuis et al., 1989)]. Significant differences in the measured values were also observed within a single well – wells marked CAH-XY at the CALEX site were sampled from three depth levels. For example, in the CAH-7 well, which serves as a background well at the site, both low (0.2 mg.L$^{-1}$) and relatively high concentrations (4.78 mg.L$^{-1}$) were measured. The results of measurements at the MSWD and sugar mill sites were similar.

Similar to DO, ORP values also showed a wide range. During the 2022 surveys, values at all three sites ranged

from negative (up to –551 mV, CALEX, indicating the presence of CAHs) to positive (up to 580 mV, MSWD). The medians of the measured ORP values ranged from 83 mV (MSWD) to 230 mV (sugar mill). Measurements in 2023 at the CALEX site form a balanced set of values ranging from 151 to 208 mV. Negative ORP values indicate a reducing environment (ability to transfer electrons). This may be due to limited oxygen access or the decomposition of organic matter by microorganisms. Positive ORP values indicate an oxidative environment (ability to accept electrons). Dissolved oxygen is present in the environment and oxidative reactions are energetically favorable.

Identifying the presence of pollutants is problematic based on the results of measurements of basic groundwater field parameters. At the sugar mill site, the lowest ORP values were measured in well CAH-5, which is located outside the presumed source of pollution. In the other observed wells, located in the direction of groundwater flow from the presumed source of contamination (CUH-1, CUH-2, CUH-3, CUH-4), as well as in the background well CUH-6, the measured ORP values were predominantly positive or ranged between oxidative and reductive conditions (value of 200 mV). The situation at the CALEX site was comparable. The CAH-1 well, in which the highest degree of CAHs contamination was identified, had predominantly positive ORP values, or values ranging between oxidative and reductive conditions (200 mV). Negative or low ORP values were observed in water from wells CAH-6 and CAH-7, which serve as background wells at the site. However, it is possible that there are other factors affecting groundwater quality at the sites under investigation that could not be identified based on the input data.

The work carried out also included measurements of groundwater levels. For the purposes of graphical interpretation of the data, the results from 22nd November 2022 were used. Hydraulic contour lines created on the basis of the data obtained confirmed the general direction of groundwater flow on the right bank of the Malá Nitra stream, which was in the NE-SW direction (Fig. 4).

The direction of groundwater flow affects the spread of pollution further into the area. The source of CAHs is apparently the ELITEX and STS site. From there, the pollution spreads in a SW direction, reaching another EB (MSWD). High-permeability soils (gravels, sands) can comprise heterogeneous and homogeneous layers (Gill et al., 2014; Hansen et al., 2015). The grain sizes in such environments are large, which contributes to higher hydraulic conductivity > $10^{-4}$ m.s$^{-1}$ and further pollution spreading (Appelo & Postma, 2005; Hyldegaard & Ottosen, 2021).

In 2015, high concentrations of CAHs were also identified in domestic wells in the Albertov dvor area, located approximately 80 m southwest of the MSWD (Tupý et al., 2015). Based on the results from 2022, a graphical interpretation of the spread of contamination from the source

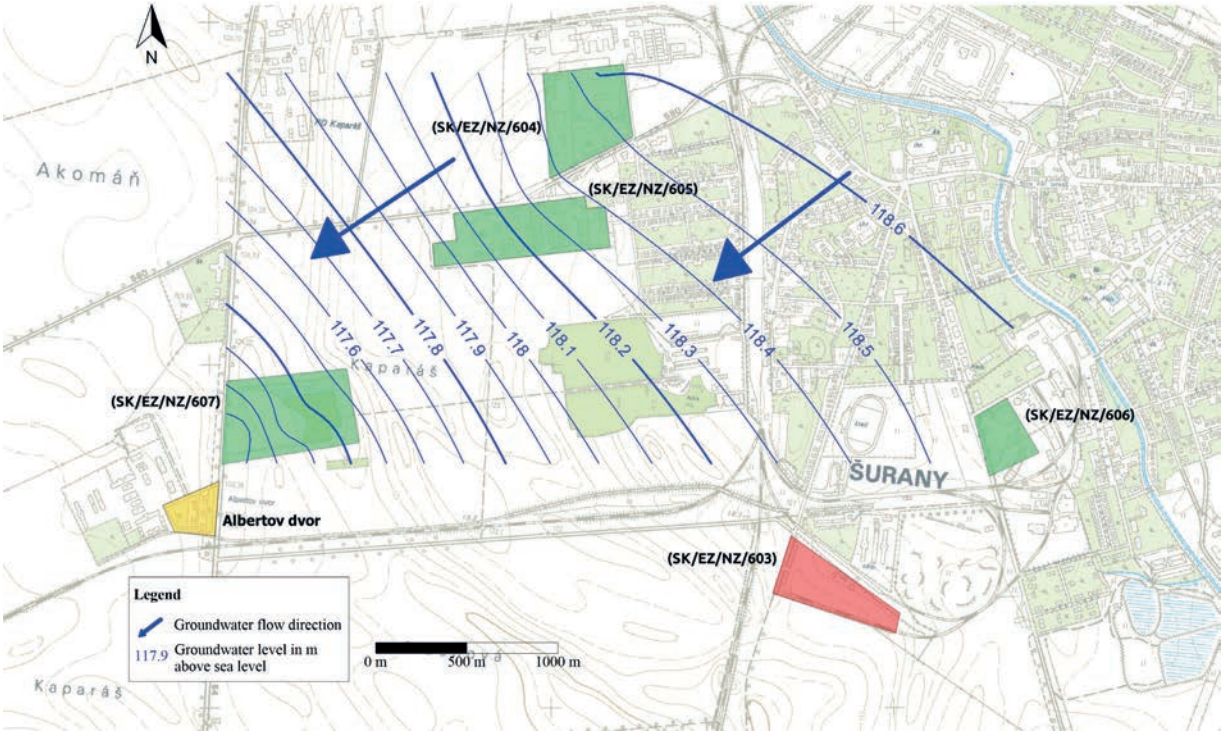


**Fig. 4.** Groundwater flow direction as of 22 November 2022

was prepared (Fig. 5). The contamination plume extends to the landfill, where CAHs concentrations in 14 samples from the SKH-2 well ranged from 291 to 469 µg.L$^{-1}$ (DCE), from 574 to 842 µg.L$^{-1}$ (TCE) and from 63.6 to 125 µg.L$^{-1}$ (PCE). In samples from the MS-1 well, located at the source of pollution (ELITEX and STS), the concentrations in the 8 samples were significantly higher. They ranged from 952 to 2,810 µg.L$^{-1}$ (DCE), 701–2,970 µg.L$^{-1}$ (TCE), 69.5–194 µg.L$^{-1}$ (PCE), and unlike well SKH-2, VC concentrations were also high (37–168 µg.L$^{-1}$). The following table shows the concentration ranges of individual pollutants detected in groundwater samples (Tab. 3).

The following figures (Fig. 6, Fig. 7) show the interpreted development of DCE, TCE and PCE concentrations

**Tab. 3**

Contaminant concentrations in selected wells

| Well | Yearof sampling | Number of samples | DCE [µg.L$^{-1}$] | TCE [µg.L$^{-1}$] | PCE [µg.L$^{-1}$] | VC [µg.L$^{-1}$] | Site |
|---|---|---|---|---|---|---|---|
| MS-1 | 2022 | 8 | 952–2,810 | 701–2,970 | 69.5–194 | 37–168 | SK/EZ/NZ/605 |
| SKH-2 | 2022 | 14 | 291–469 | 574–842 | 63.6–125 | < 1.00 | SK/EZ/NZ/607 |
| MS-3 | 2022 | 2 | 8.8–9.9 | 161–176 | 222–247 | < 1.00 | SK/EZ/NZ/605 |
| CAH-1 | 2022 | 18 | 2.52–4.89 | 4.42–21.3 | 24.1–60.4 | < 1.00 | SK/EZ/NZ/604 |
| CAH-1 | 2023 | 2 | 2.83–4.25 | 3.3–4.4 | 29–42 | < 1.00 | SK/EZ/NZ/604 |

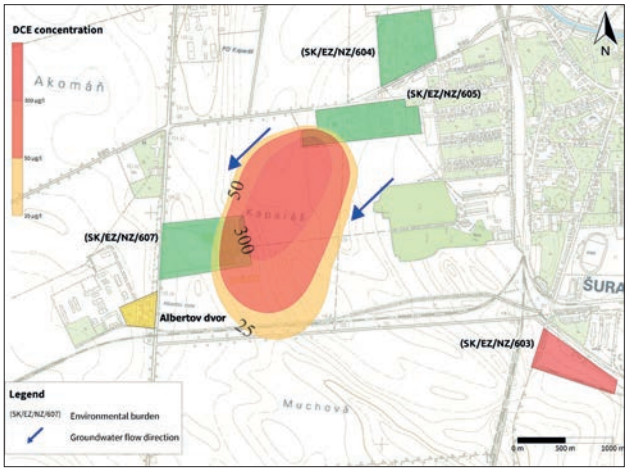


DCE plume

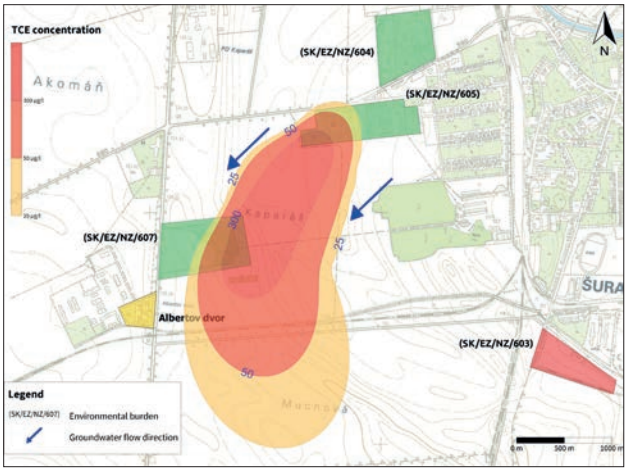


TCE plume

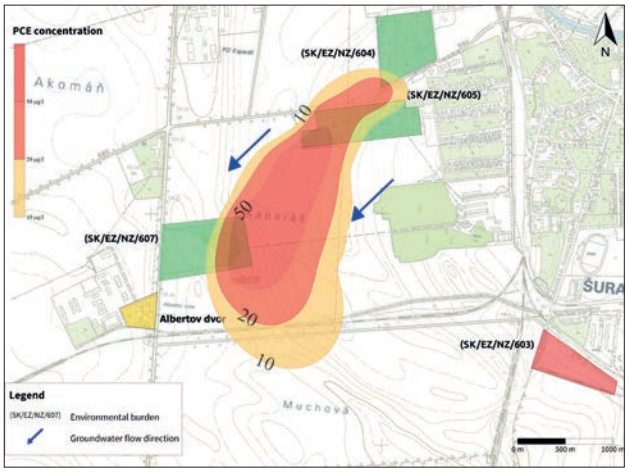


PCE plume

**Fig. 5.** Interpolated contaminant plumes for DCE, TCE and PCE

in samples from well MS-1, together with the development of the groundwater level. The data presented are a synthesis of monitoring and survey results. The concentrations of pollutants are clearly dependent on changes in the groundwater level. When the level rises, pollutant concentrations usually decrease, and vice versa. However, the changes are not a regular seasonal phenomenon, as the maximum and minimum groundwater levels in the monitored period do not correspond to seasonal changes.

More accurate identification of the source of pollution at the ELITEX site is possible thanks to data from 2015 (Tupý et al., 2015) and monitoring results from 2016 to

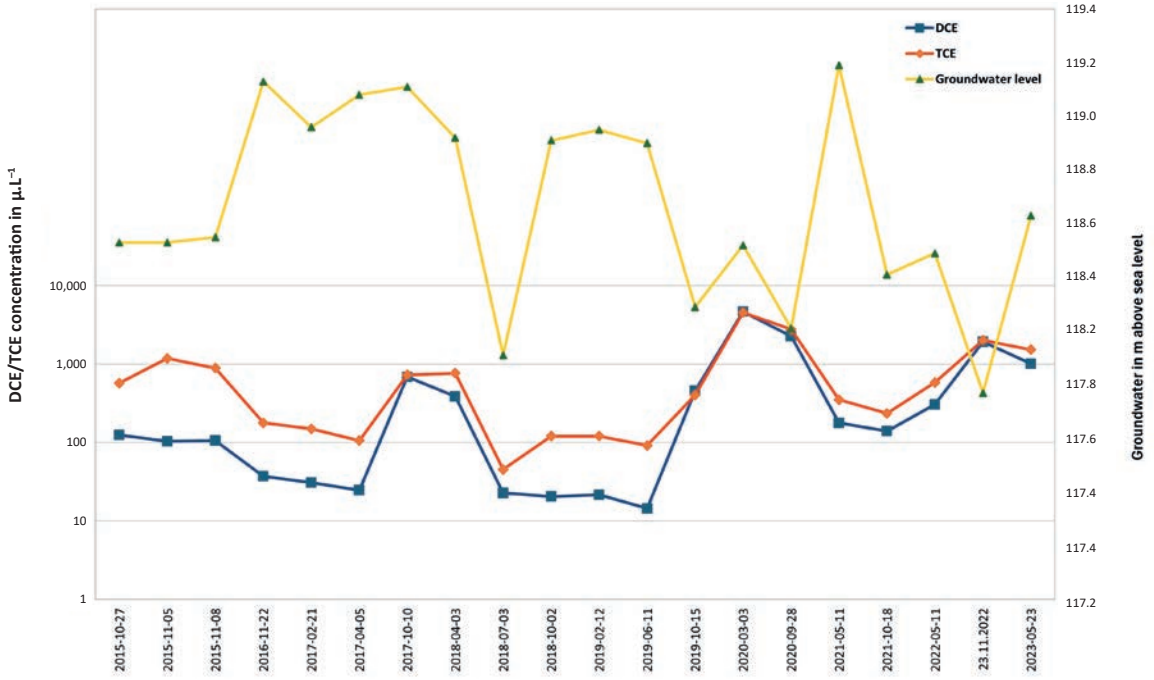


**Fig. 6.** DCE and TCE concentration change in well MS-1 in relation to groundwater level

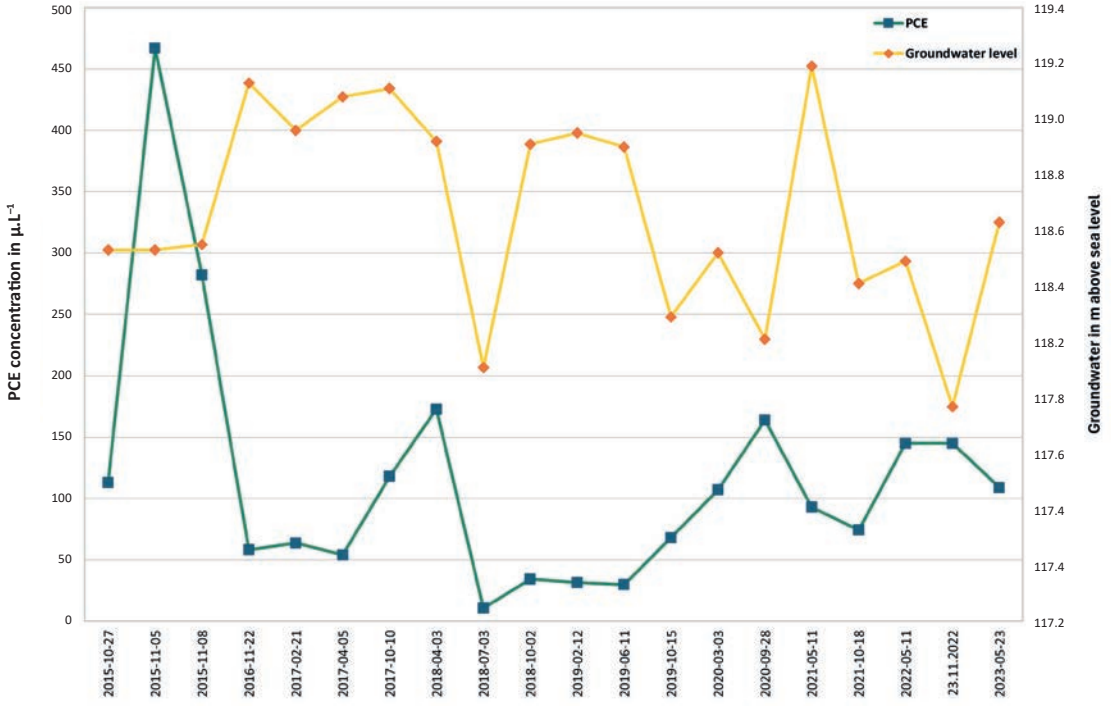


**Fig. 7.** PCE concentration change in well MS-1 in relation to groundwater level

2023 (Kordík et al., 2023). In terms of CAHs concentrations, the monitored wells can be classified into several groups, or, on this basis, sub-areas with varying degrees of contamination can be identified. The MS-1, MS-3 and MS-5 wells, located in the south-western part of the ELITEX site, define the area with the most significant source of contamination. In wells MS-8, MS-10, MS-14 and MS-18, high concentrations of some of the monitored pollutants were identified only in the 2015 sample. In the last three monitored wells, the presence of pollution was rarely recorded, with a time lag (MS-9 in 2015, 2022, MS-11 in 2015, 2017, 2022, MS-16 in 2015, 2022). Wells with low or occasionally high concentrations are located mainly around the perimeter of the EB, so it is possible to more accurately define the source within the site.

The results of the 2023 survey in the CALEX site (Macek et al., 2023) clearly show that the source of contamination (PCE) detected during the 2022 survey (Tupý et al., 2022a) is not located on the site of the former CALEX plant. Low concentrations of CAHs (DCE, TCE, PCE) were identified by both surveys throughout the CALEX site, but only in low concentrations (with the exception of the vicinity of the CAH-5 well, where PCE concentrations exceeded the ID criterion value of the Directive). Given the degree of contamination at the ELITEX site and the characteristics of the geological environment [alternating layers of sandy gravel and sandy clay (Obuch, 2008; Pristaš et al., 2000)], it can be assumed that the contamination in the CAH-1 well is the result of gravitational transport of CAHs through an impermeable layer towards the CALEX site (the well is located approximately 60 m from the ELITEX site). DNAPLs migrating below the water level move downward and laterally under the influence of gravity, capillary, and viscous forces (Conrad & Glass, 2000), and under certain conditions, gravitational forces may prevail over hydraulic forces (Dawson & Roberts, 1997).

The continuous spread of pollution from the ELITEX and STS sites to a large area in the town of Šurany requires remediation. Theoretical background and practical experience from other sites in Slovakia suggest that a suitable solution is to create a reactive barrier, which essentially involves creating reducing conditions by applying aqueous reagents to the contaminated environment (e.g., whey, sulfidized zero-valent iron, etc.). In the process of reductive dechlorination by the action of reagents, reduced forms of the contaminant with less harmful or less dangerous properties are formed in groundwater (transition of PCE to DCE). Remediation can be carried out passively (without the need to pump groundwater). The main source of pollution is well defined, and the technical facilities (wells) needed to create a barrier could be located at the interface between the former ELITEX site and agricultural land (subject to agreement with the landowners). After pilot tests aimed at selecting the most effective agent, the main challenge would remain the sustainability of the project – continuous monitoring of effectiveness and possible changes in the technological processes of groundwater remediation. However, the intensity of the spread of pollution, as well as its volume, pose a significant risk to groundwater quality over a large area. Addressing this situation should be one of the city‘s priorities.

## Conclusions

Based on the results of the surveys and monitoring carried out, it was confirmed that there is widespread contamination with chlorinated aliphatic hydrocarbons in a relatively large area in the western part of the town of Šurany (ca 80 hectares). The secondary source of contamination (CAHs in the rock environment) is still active, meaning that the contamination plume is still growing. A comprehensive assessment of geological tasks carried out in 2022 and 2023, together with the results of ELITEX and STS site monitoring, have enabled a more accurate definition of the source of pollution, as well as modelling of the likely direction and intensity of pollution spread in the direction of groundwater flow.

The identified state of groundwater pollution clearly requires remediation work. Currently, it is possible to choose suitable procedures that have been field-tested with good results. Traditional methods include, for example, pump and clean treatment, using chemical oxidation/reduction and reactive permeable barriers, electrochemical methods as well as bioremediation. To achieve the optimal effect of remediation work, it is recommended to carry out laboratory experiments that simulate the properties of the geological environment and pollutants as accurately as possible.

### Acknowledgements

Data presented in this paper were collected during geological surveys of three environmental burdens, carried out as a part of the project *Geological survey of selected probable environmental burdens (2) – part 3* (implemented with financial support of the European Union from Cohesion Fund in the frame of Operational Programme Quality of Environment. We are also grateful to the Centre of Environmental Services, Ltd. (Bratislava) for taking part in financing this research.

## References

Appelo, C. A. & Postma, D., 2005: Flow and transport. In: *Geochemistry, Groundwater and Pollution* (2nd ed.). *Leiden, CRC Press*, 63–118.

ATSDR, 2019: Toxicological Profile for Trichloroethylene. *Agency for Toxic Substances and Disease Registry, U.S.*

*Department of Health and Human Services, Public Health Service*. https://www.atsdr.cdc.gov/toxprofiles/tp19.pdf.

ATSDR, 2024: Toxicological Profile for Vinyl Chloride. *Agency for Toxic Substances and Disease Registry, U.S. Department of Health and Human Services, Public Health Service*. https://www.atsdr.cdc.gov/toxprofiles/tp20.pdf.

Auxt, A., Klučiar, T., Vetráková, L., Siska, F., Ingár, K., Podhorská, M., Ševčíková, Ľ., Bágelová, A., Scherer, S., Šuchová, M., Jenčko, P., Bauer, K., Polčan, I., Krakovský, D., Sentpetery, M., Miklasová, J., Kovács, T., Filo, J., Máša, B. & Klúz, M., 2022: Sanácia environmentálnej záťaže ZM (013) / Zlaté Moravce – bývalý areál Calexu. Final report. *Manuscript. Bratislava, Archive of St. Geol. Inst. of D. Štúr,* 128 pp. (in Slovak).

Booij, K., Achterberg, E. P. & Sundby, B., 1992: Release rates of chlorinated hydrocarbons from contaminated sediments. *Netherlands Journal of Sea Research, 29, 4,* 297–310.

Conrad, S. H. & Glass, R. J., 2000: Physics of DNAPL Migration and Remediation in the Presence of Heterogeneities (No. EMSP-73812-2000. *Sandia National Laboratories, U.S. Department of Energy, Environmental Management Science Program,* 1–29. https://www.osti.gov/servlets/purl/834598/).

Dawson, H. E. & Roberts, P. V., 1997: Influence of Viscous, Gravitational, and Capillary Forces on DNAPL Saturation. *Groundwater, 35, 2,* 261–269.

Directive of Ministry of Environment of the Slovak Republic No. 1/2015-7 for the elaboration of risk assessment analysis of contaminated sites. *Bratislava, Ministry of Environment of the Slovak Republic*, 96 pp. Available online: https://www.enviroportal.sk/dokument/smernica-1-2015-7-na-vypracovanie-analyzy-rizika-znecisteneho-uzemia (in Slovak).

Doherty, R. E., 2000: A History of the Production and Use of Carbon Tetrachloride, Tetrachloroethylene, Trichloroethylene and 1,1,1-Trichloroethane in the United States: Part 1 – Historical Background; Carbon Tetrachloride and Tetrachloroethylene. *Environmental Forensics, 1, 2,* 69–81.

Essaid, H. I., Bekins, B. A. & Cozzarelli, I. M., 2015: Organic contaminant transport and fate in the subsurface: Evolution of knowledge and understanding. *Water Resources Research, 51, 7,* 4861–4902.

Gill, R. T., Harbottle, M. J., Smith, J. W. N. & Thornton, S. F., 2014: Electrokinetic-enhanced bioremediation of organic contaminants: A review of processes and environmental applications. *Chemosphere, 107,* 31–42.

Hansen, B. H., Nedergaard, L. W., Ottosen, L. M., Riis, C. & Broholm, M. M., 2015: Experimental design for assessment of electrokinetically enhanced delivery of lactate and bacteria in 1,2-cis-dichloroethylene contaminated limestone. *Environmental Technology & Innovation, 4,* 73–81.

He, H., Li, Y., Shen, R., Shim, H., Zeng, Y., Zhao, S., Lu, Q., Mai, B. & Wang, S., 2021: Environmental occurrence and remediation of emerging organohalides: A review. *Environmental Pollution, 290, 118060*.

Huling, S. G. & Weaver, J. W., 1991: Dense Nonaqueous Phase Liquids (Ground Water Issue, EPA/540/4-91-002). *Office of Solid Waste and Emergency Response, US EPA, Washington, D.C.* 21 pp. https://www.epa.gov/sites/default/files/2015-06/documents/dnapl_issue_paper.pdf.

Hyldegaard, B. H. & Ottosen, L. M., 2021: Electrokinetic and Electrochemical Removal of Chlorinated Ethenes: Application in Low- and High-Permeability Saturated Soils. Chapter 21. In: *Electrokinetic Remediation for Environmental Security and Sustainability. John Wiley,* 503–540.

Kertész, A., Šimonovičová, Ľ. & Notlíková, I., 1978: Šurany – vyhľadávací hydrogeologický prieskum. Final report of the hydrogeological survey. *Manuscript. Bratislava, Archive of St. Geol. Inst. of D. Štúr* (arch. no. 42422), 19 pp. (in Slovak).

Kmeť, V., 2008: Vstrekolisovňa SEHWA SK s.r.o. Final report of the engineering geological survey. *Manuscript. Bratislava, Archive of St. Geol. Inst. of D. Štúr* (arch. no. 87551), 21 pp. (in Slovak).

Kordík, J., Slaninka, I., Bahnová, N., Benková, K., Bodiš, D., Bottlik, F., Dananaj, I., Demko, R., Dénes, D., Dodoková, Z., Fordinál, K., Fričovská, J., Fričovský, B., Gazdačko, Ľ., Gluch, A., Gonda, S., Gurinová, E., Györög, I., Hlodák, M., Husár, M., Iglárová, Ľ., Jankulár, M., Jelínek, R., Kotuč, J., Kubač, A., Kúšik, A., Lenhardtová, E., Mašlár, E., Mašlárová, I., Mikušová, J., Olšavský, M., Ondrášiková, B., Pijaková, E., Pramuka, S., Siska, M., Stašik, Ľ., Stríček, I., Šefčík, P., Ševčíková, P., Mackových, D., Repková, R., Vabcová, J., Kovalčíková, A., Nováková, J., Uhrinová, K., Michalko, J., Nováčková, M. & Pešta, I., 2023: Zabezpečenie monitorovania environmentálnych záťaží Slovenska – 1. časť. Final report. *Manuscript. Bratislava, Archive of St. Geol. Inst. of D. Štúr,* (arch. no. 102803), 162 s. (in Slovak).

Kram, M. L., Keller, A. A., Rossabi, J. & Everett, L. G., 2001: DNAPL Characterization Methods and Approaches, Part 1: Performance Comparisons. *Groundwater Monitoring & Remediation, 21, 4,* 109–123.

Lyne, F. A. & McLachlan, T., 1949: Contamination of Water by Tricholroethylene. *The Analyst, 74, 882,* 513.

Macek, J., Malý, V., Tóth, R., Brutenič, M., Kravchenko, D. & Drábik, A., 2023: Geologický prieskum Šurany – bývalý areál CALEX. Záverečná správa s analýzou rizika znečisteného územia. Final report. *Manuscript. Bratislava, Archive of St. Geol. Inst. of D. Štúr* (arch. no. 103296), 1–52 (in Slovak).

Obuch, Š., 2008: ŠURANY – vodný zdroj HŠ – 1. Final report of the hydrogeological survey. *Manuscript. Bratislava, Archive of St. Geol. Inst. of D. Štúr* (arch. no. 87466), 1–18 (in Slovak).

Oldenhuis, R., Vink, R. L., Janssen, D. B. & Witholt, B., 1989: Degradation of chlorinated aliphatic hydrocarbons by *Methylosinus trichosporium* OB3b expressing soluble methane monooxygenase. *Applied and Environmental Microbiology, 55, 11,* 2819–2826.

Pankow, J. F. & Cherry, J. A., 1996: Dense chlorinated solvents and other DNAPLs in groundwater. *Ontario, Waterloo Press,* 538 pp.

Pitter, P., 2015: Hydrochemie (5th ed.). *Praha, VŠCHT,* 792 pp.

Priechodská, Z. & Harčár, J. (eds.), Karolus, K., Karolusová, E., Remšík, A. & Šucha, P., 1988: Vysvetlivky ku geologickej mape severovýchodnej časti Podunajskej nížiny 1 : 50 000. *Bratislava, Geologický ústav Dionýza Štúra,* 114 pp. (in Slovak).

Pristaš, J. (ed.), Elečko, M., Maglay, J., Fordinál, K., Šimon, L., Gross, P., Polák, M., Havrila, M., Ivanička, J., Határ, J., Vozár, J., Tkáčová, H., Tkáč, J., Liščák, P., Jánová, V., Švasta, J., Remšík, A. Žáková, E. & Töröková, I., 2000: Vysvetlivky ku geologickej mape Podunajskej nížiny – Nitrianskej pahorkatiny 1 : 50 000. *Bratislava, Štátny geologický ústav Dionýza Štúra,* 250 pp. (in Slovak).

Rapant, S., Vrana, K., Bodiš, D. et al. (eds.), 1996: Geochemický atlas Slovenska. Časť I: Podzemné vody. *Bratislava, Geologická služba Slovenskej republiky,* 284 pp. (in Slovak).

Rubin, H., Narkis, N. & Carberry, J. (eds.), 1998: Soil and Aquifer Pollution: Non-Aqueous Phase Liquids – Contamination and Reclamation. *Berlin – Heidelberg, Springer,* 414 pp.

Schwarz, J., Mikita, S., Filo, J., Valko, J., Vozár, J., Jasovský, Z., Drahoš, M., Jurkovič, Ľ., Pitoňák, P., Masiar, R. & Nigrínová, J., 2020: Metodická príručka geologického prieskumu životného prostredia v znečistenom území. *Banská Bystrica, Slovenská agentúra životného prostredia,* 1–170. https://www.minzp.sk/files/sekcia-geologie-prirodnych-zdrojov/538_mppp_fin_2021.pdf.

Šutka, J., Várady, I., Tomaškovič, J. & Kolečáni, K., 2008: Šurany v zrkadle dejín. *Šurany, Mestské kultúrne stredisko,* 280 pp.

Tupý, P., Lichý, A., Masiar, R., Tomasch, M. & Mészárosová, Z., 2015: Prieskum pravdepodobnej environmentálnej záťaže NZ (033) / Šurany – bývalý areál Elitexu a STS (SK/EZ/NZ/605). Final report. *Manuscript. Bratislava, Archive of St. Geol. Inst. of D. Štúr* (arch. no. 94695), 122 pp. (in Slovak).

Tupý, P., Macek, J., Malý, V., Tóth, R., Brutenič, M., Kravchenko, D., Jurkovič, Ľ., Drábik, A., Schwarz, J., Lichý, A., Masiar, R., Filo, J. & Jasovský, Z., 2022a: Geologický prieskum pravdepodobnej environmentálnej záťaže NZ (032) / Šurany – bývalý areál CALEX (SK/EZ/NZ/604). Final report. *Manuscript. Bratislava, Archive of St. Geol. Inst. of D. Štúr* (arch. no. 102565), 82 pp. (in Slovak).

Tupý, P., Macek, J., Malý, V., Tóth, R., Brutenič, M., Kravchenko, D., Jurkovič, Ľ., Drábik, A., Schwarz, J., Lichý, A., Masiar, R., Filo, J. & Jasovský, Z., 2022b: Geologický prieskum pravdepodobnej environmentálnej záťaže NZ (034) / Šurany – bývalý cukrovar (SK/EZ/NZ/606). Final report. *Manuscript.* Bratislava, *Archive of St. Geol. Inst. of D. Štúr* (arch. no. 102246), 74 pp. (in Slovak).

Tupý, P., Macek, J., Malý, V., Tóth, R., Brutenič, M., Kravchenko, D., Jurkovič, Ľ., Drábik, A., Schwarz, J., Lichý, A., Masiar, R., Filo, J. & Jasovský, Z., 2022c: Geologický prieskum pravdepodobnej environmentálnej záťaže NZ (035) / Šurany – mestská skládka TKO (SK/EZ/NZ/607). Final report. *Manuscript. Bratislava, Archive of St. Geol. Inst. of D. Štúr* (arch. no. 102703), 98 pp. (in Slovak).

# Environmentálne záťaže v Šuranoch – znečistenie podzemnej vody chlórovanými alifatickými uhľovodíkmi

Cieľom štúdie je hodnotenie šírenia znečistenia z viacerých možných zdrojov, ktoré sa nachádzajú neďaleko od seba v západnej časti intravilánu mesta Šurany. Mesto Šurany leží v Podunajskej nížine, v južnej časti Slovenska. V minulosti bola v meste koncentrovaná priemyselná a potravinárska výroba, ktorá zamestnávala ľudí zo širšieho okolia mesta (výrobné podniky CALEX, ELITEX, STS, cukrovar). Napriek skončeniu aktivity v uvedených prevádzkach pred viac ako 30 rokmi znečistenie podzemnej vody pretrváva vo vysokej koncentrácii. Druh výrobnej činnosti spolu s vtedajším prístupom k ochrane životného prostredia zapríčinili, že všetky uvedené prevádzky boli pri vzniku registra environmentálnych záťaží zaradené ako pravdepodobné environmentálne záťaže. V roku 2022 bolo v Šuranoch podľa uvedeného registra evidovaných 6 lokalít. Štyri z nich boli predmetom podrobného geologického prieskumu [mestská skládka tuhého komunálneho odpadu (SK/EZ/NZ/607); bývalý cukrovar (SK/EZ/NZ/606); bývalý areál CALEX (SK/EZ/NZ/604); bývalý areál ELITEXU a STS (SK/EZ/NZ/605)] a dve ako pravdepodobné environmentálne záťaže bez podrobnejších informácií o stave znečistenia [areál bývalého ELITEXU, Družstevná 5 (SK/EZ/NZ/602); Šurany – areál Kovošrotu (SK/EZ/NZ/603)].

Mesto Šurany leží na fluviálnych sedimentoch viazaných na dolinu toku Nitry a jej väčších prítokov. V rovinnom stupni v okolí Šurian tvoria súvislú vrstvu na tektonicky poklesávajúcom území. Na báze sú štrky až piesky patriace k nízkej terase. V ich nadloží sa nachádzajú holocénne hliny (piesčité až ílové). V západnej časti Šurian boli geologické podmienky v minulosti overené viacerými prieskumami. Pod kvartérnymi uloženinami boli identifikované neogénne sedimenty tvorené štrkopieskovými telesami s výskytom piesčitých ílov, hranica kvartér/neogén je však nejasná. Obuch (2008) uvádza rozhranie na úrovni 21 m p. t. Ílovité vrstvy vo vrtoch dosahovali hrúbku zhruba 3 m (Kmeť, 2008). Približne od 3,0 m p. t. je prvý zvodnený horizont pieskov, resp. piesčitých štrkov. Vrt hlboký 55 m p. t. zhruba od 9,0 m p. t. zachytil striedanie štrkových a ílových vrstiev, ktoré sú hrubé približne 2,0 m (Obuch, 2008). Hodnoty koeficientu filtrácie, vypočítané na základe výsledkov čer-

pacích skúšok, boli $k_f = 1{,}66 \cdot 10^{-4}$ m . $s^{-1}$ (Kertesz, 1978), resp. $k_f = 8{,}06 \cdot 10^{-4}$ m . $s^{-1}$ (Obuch, 2008). Generálny smer prúdenia podzemnej vody na pravej strane toku Malá Nitra je SV – JZ, na ľavej strane SZ – JV, hladina podzemnej vody je napätá.

Hodnotenie znečistenia podzemnej vody v priestore mesta Šurany sa urobilo na základe výsledkov prieskumov vykonaných v rokoch 2022 a 2023 spolu s výsledkami monitorovania lokality ELITEX a STS. V roku 2015 boli ClU vo vysokej koncentrácii identifikované aj v domových studniach v časti Albertov dvor, ktorá sa nachádza vo vzdialenosti asi 80 m jz. smerom od EZ mestská skládka (Tupý et al., 2015). Na základe výsledkov z roku 2022 sme spracovali grafickú interpretáciu šírenia znečistenia od zdroja. Mrak znečistenia siaha až po EZ mestská skládka, kde sa koncentrácia ClU v 14 vzorkách z vrtu SKH-2 pohybovala v rozsahu 291 – 469 µg . $l^{-1}$ (DCE), 574 – 842 µg . $l^{-1}$ (TCE) a 63,6 – 125 µg . $l^{-1}$ (PCE). Vo vzorkách z vrtu MS-1, ktorý sa nachádza v zdroji znečistenia, bola koncentrácia v 8 odobratých vzorkách výrazne vyššia. Pohybovala sa v rozsahu 952 – 2 810 µg . $l^{-1}$ (DCE), 701 – 2 970 µg . $l^{-1}$ (TCE) a 69,5 – 194 µg . $l^{-1}$ (PCE). Na rozdiel od vrtu SKH-2 bola vysoká aj koncentrácia VC (37 – 168 µg . $l^{-1}$).

Presnejšiu identifikáciu zdroja znečistenia v areáli ELITEX umožňujú údaje z roku 2015 (Tupý et al., 2015) a výsledky monitorovania z rokov 2016 – 2023 (ŠGÚDŠ). Vrty MS-1, MS-3 a MS-5, ktoré sú situované v jz. časti areálu ELITEX, vymedzujú územie s najvýraznejším zdrojom znečistenia. Z výsledkov prieskumu v EZ CALEX v roku 2023 (Macek et al., 2023) je zrejmé, že zdroj znečistenia (PCE), ktoré bolo zachytené počas prieskumu v roku 2022 (Tupý et al., 2022a), sa nenachádza v priestore bývalého podniku CALEX. ClU migrujúce pod hladinou podzemnej vody vplyvom gravitácie, kapilárnych a viskóznych síl sa pohybujú smerom nadol a do strán, pričom za istých podmienok môže gravitačé pôsobenie prevažovať nad hydraulickým.

Na základe výsledkov realizovaných prieskumov a monitorovania môžeme konštatovať, že v západnej časti mesta Šurany je plošné znečistenie chlórovanými alifatickými uhľovodíkmi na pomerne rozsiahlej ploche (zhruba 80 hektárov). Sekundárny zdroj znečistenia (ClU v horninovom prostredí) je stále aktívny, čiže mrak znečistenia sa stále zväčšuje. Komplexné hodnotenie geologických úloh realizovaných v rokoch 2022 a 2023 spolu s výsledkami monitorovania EZ ELITEX umožnilo presnejšie vymedzenie zdroja znečistenia, ako aj modelovanie pravdepodobného smeru a intenzity šírenia znečistenia v smere prúdenia podzemnej vody. Identifikovaný stav znečistenia podzemnej vody jednoznačne vyžaduje sanačné práce. V súčasnosti je možné zvoliť vhodné postupy, ktoré boli s dobrými výsledkami overené v praxi. Tradičnými metódami sú napríklad čerpanie a čistenie podzemnej vody, využitie chemickej oxidácie/redukcie a reaktívnych priepustných bariér, elektrochemické metódy a bioremediácia. Na dosiahnutie optimálneho efektu sanačných prác sa odporúča realizovať laboratórne experimenty, pri ktorých sa čo najvernejšie simulujú vlastnosti geologického prostredia a znečisťujúcich látok.

Doručené / Received: 16. 12. 2025
Prijaté na publikovanie / Accepted: 10. 3. 2026

# Inštrukcie autorom

## *www.geology.sk/mineralia položka* ***Inštrukcie autorom***

1. Manuskripty sa do redakcie zasielajú e-mailom (editovateľné súbory formátu .doc, .docx alebo .odt a verzia v PDF formáte) na adresu vedeckého redaktora alebo mineralia.slovaca@geology.sk.
2. **Súčasne s manuskriptom je potrebné redakcii poslať autorské vyhlásenie o originalite textu a obrázkov. Kópie obrázkov z iných publikácií musia byť legalizované získaním práva na publikovanie. Vyhlásenie musí obsahovať meno autora (autorov), akademický titul** a tr**valé bydlisko.** Články sú uverejnené pod licenciou ***Creative Commons Attribution (CC BY)***. Autori článkov majú možnosť požiadať aj o iný typ licencie ***Creative Commons***.
3. Rozsah manuskriptu na publikovanie je štandardne do 40 rukopisných strán (font Times New Roman, veľkosť písmen 12 bodov, riadkovanie 1,5) vrátane literatúry, obrázkov, popisov obrázkov a tabuliek. V prípade veľkého odborného prínosu sú v ojedinelých prípadoch povolené aj dlhšie články. Rozsiahlejšie doplňujúce materiály v prípade potreby je možné publikovať ako prílohu online.
4. Články sú publikované v angličtine, výnimočne aj v slovenčine. Články písané v angličtine musia obsahovať slovenské resumé. Články v slovenčine musia obsahovať anglický preklad názvu, abstraktu, kľúčových slov, resumé a popisov k obrázkom a tabuľkám.

### Text

Úprava textu aj zoznamu literatúry musí korešpondovať so súčasnou úpravou článkov v časopise. Predkladaný manuskript musí spĺňať tieto požiadavky:

1. Text manuskriptu musí mať priebežne číslované riadky.
2. Na začiatku manuskriptu je uvedený názov, ktorý by mal byť stručný a informatívny.
3. Meno a priezvisko autora alebo autorov musí byť uvedené spolu s názvom pracoviska a adresou (mesto, krajina). Korešpondujúci autor musí byť riadne označený a musí byť uvedená jeho e-mailová adresa. Ak je k dispozícii aj ORCID autorov, treba ho uvádzať.
4. V úvode v časti Highlights a v závere príspevku musí autor jasne deklarovať, čím konkrétnym je jeho príspevok prínosný pre rozvoj geovied.
5. Abstrakt stručne sumarizuje článok. Môže mať najviac 200 slov a nemá obsahovať citácie. Počet kľúčových slov je maximálne 6.
6. Text má takéto členenie: úvod, charakteristika (stav) skúmaného problému vrátane prehľadu dôležitých starších výskumov, použitá metodika, nové zistenia (výsledky), ich interpretácia, diskusia, záver, poďakovanie, zoznam literatúry a resumé v slovenskom, resp. anglickom jazyku (pri článku v slovenčine). Východiskové údaje musia byť zreteľne odlíšené od interpretácií. V texte musia byť odvolávky na všetky použité obrázky a tabuľky.
7. V texte je možné použiť maximálne 3 hierarchické úrovne podnadpisov.
8. V texte sa uprednostňuje citácia v zátvorke, napr. (Dubčák, 1987; Hrubý et al., 1988), pred formou napr. podľa Dubčáka (1987).
9. Manuskript odporúčame zasielať s obrázkami vloženými v texte alebo na konci manuskriptu.
10. V texte treba prednostne používať platné jednotky SI, napr. s (sekunda, nie sec), m (meter), kg (kilogram). V oprávnených prípadoch možno použiť aj iné miery zaužívané v odbornej literatúre a v zátvorke uviesť ich ekvivalent v jednotkách SI, napr. 3 kbar (300 MPa, resp. 0,3 GPa), 30 kt, resp. 30 000 t (3,107 kg), 800 K (527 °C), 4,26 Å (4,26 . $10^{-10}$ m).
11. V texte sa môžu používať len názvy minerálov oficiálne schválené Komisiou pre nové minerály a nomenklatúra schválená Medzinárodnou mineralogickou asociáciou (CNMNC IMA). Ich zoznam (inovovaný každé dva mesiace) je prístupný na stránke https://cnmnc.units.it/ (*IMA-CNMNC List of Mineral Names*). Rovnako sa môžu používať len odporúčané skratky minerálov (*Updated list of IMA-CNMNC mineral symbols*). Pokiaľ autori disponujú chemickou analýzou minerálu, treba napísať jeho celý platný názov, napr. fluórapatit (nie apatit), monazit-(Ce) (nie monazit). Neúplné názvy minerálov (napr. apatit, monazit) možno použiť pri petrografickom opise hornín alebo názve metódy (napr. monazitové datovanie). Použitie názvov izomorfných sérií minerálov zaužívaných v geologickej literatúre (napr. biotit, zinnwaldit, olivín) alebo skupinových názvov minerálov (napr. granáty, turmalíny, amfiboly, spinely) je akceptované. V prípade nejasností sa autori môžu písomne obrátiť na redakčnú radu.

### Obrázky, ilustrácie a tabuľky

1. Ilustrácie a tabuľky vysokej kvality bývajú publikované buď **na šírku stĺpca** (81 mm)**, alebo strany (170 mm)**. Optimálna veľkosť písma a čísiel v publikovaných obrázkoch je 2 mm. Články v angličtine majú všetky texty v angličtine. Články v slovenčine musia mať popisy v obrázkoch a tabuľkách v slovenčine, záhlavie tabuliek a texty pod obrázkami a tabuľkami sú v slovenčine a angličtine. **Maximálny rozmer ilustrácie a tabuľky vytlačený v časopise je 170 x 230 mm**. Väčšie (skladané) ilustrácie sú publikované len v ojedinelých prípadoch.
2. Ilustrácie vrátane fotografií musia obsahovať **grafickú mierku** v centimetrovej či metrovej škále, prípadne sa rozmer zobrazených objektov vyjadrí v popise obrázka. Mapy a profily musia mať aj **azimutálnu orientáciu** a jednotné vysvetlivky, ktoré sa uvedú pri prvom obrázku. Zoskupené obrázky, napr. fotografie a diagramy, sa uvádzajú ako jeden obrázok s jednotlivými časťami označenými písmenami (a, b, c atď.).
3. **Ilustrácie, mapy a fotografie je nutné uložiť vo formátoch JPG, PNG alebo TIF v rozlíšení minimálne 600 dpi, vektorovú grafiku vo formátoch EPS, PDF, AI alebo COR.**

**Redakcia si vyhradzuje právo vrátiť autorovi grafické prílohy na opravu po jazykovej úprave, resp. požiadať o ich nahradenie za prílohy v požadovanej kvalite.**

### Literatúra

Zoznam použitej literatúry musí obsahovať iba publikované alebo akceptované práce. Pri jednom autorovi sú práce v zozname zoradené abecedne podľa priezviska autora každého diela. Pri dvoch autoroch sa práce uvádzajú abecedne najprv podľa priezviska prvého autora, potom podľa priezviska spoluautora a potom chronologicky. Pri viac ako dvoch autoroch sa práce zoradia abecedne iba podľa priezviska prvého autora, potom chronologicky. Ak má publikácia DOI, vždy sa uvádza za číslom citovaných strán vo forme https://doi.org/číslo.

### Spôsob uvádzania literatúry v zozname literatúry:

***Knižná publikácia:*** Gazda, L. & Čech, M., 1988: Paleozoikum medzevského príkrovu. Bratislava, Alfa, 155 s.

***Časopis:*** Hók, J. & Olšavský, M., 2023: Vernaricum – regional distribution, lithostratigraphy, tectonics and paleogeography. Mineralia Slovaca, 55, 1, 3 – 12. https://doi.org/10.56623/ms.2023.55.1.1.

***Zborník:*** Návesný, D., 1987: Vysokodraselné ryolity. In: Romanov, V. (ed.): Stratiformné ložiská gemerika. Špec. publ. Košice, Slovenská geologická spoločnosť, 203 – 215.

***Manuskript:*** Tulis, J. & Novotný, L., 1998: Zhodnotenie geologických prác na U rudy v mladšom paleozoiku hronika v severnej časti Nízkych Tatier a Kozích chrbtov. Manuskript. Bratislava, archív Štátny geologický ústav Dionýza Štúra (arch. č. 82752), 144 s.

# Instructions to authors

## *www.geology.sk/mineralia item* ***Instructions to authors***

1. The manuscripts must be sent to Editorial Office by e-mail (editable files in .doc, .docx or .odt format, plus complete preview version in PDF format) to the Scientific Editor or mineralia.slovaca@geology.sk.
2. **Simultaneously with the manuscript the Editorial Office must receive the author´s proclamation that no part of the manuscript was already published and figures and tables are original as well. Copied illustrations from other publications must contain a copyright.** The articles are published under a Creative Commons Attribution (CC BY) license. Authors have the option to apply for other types of Creative Commons licenses.
3. The extent of the manuscript for publishing is limited to 40 manuscript pages (12 points Times New Roman font, line spacing 1.5) including figures, tables, explanations and references. In the case of contribution with a high scientific value, the longer manuscripts for publishing are exceptionally permitted. More extensive supplementary material can be published as an online annex if required.
4. Articles are published in English (preferably) or Slovak languages. The title, abstract, key words, graphical abstract, highlights, shortened text (summary), as well as description to figures and tables in Slovak articles are published also in English. Articles published in English contain Slovak resumé.

### Text

The format of the text and the reference list must correspond to the current format of the papers in the journal. The submitted manuscript must meet the following requirements:

1. The text of the manuscript must have continuously numbered lines.
2. The title at the beginning of the manuscript should be brief and informative.
3. The name and surname of the author(s) must be given together with affiliation(s) to the institutions and the address (city, country). The corresponding author must be properly marked and his/her e-mail address must be given. If the ORCID of the authors is also available, it should be provided.
4. The Highlights section in the beginning of the manuscript and in the conclusions at the end of the paper, must clearly declare main results and importance for the Earth sciences.
5. Abstract briefly summarizing the manuscript is limited to 200 words, no references are allowed. The maximum number of key words is 6.
6. The text must be structured as follows: the introduction, characterization (state) of investigated problem, applied methodology, obtained new findings (results), interpretation, discussion, conclusion, acknowledgements and references. The obtained data must be distinctly separated from interpretations. All applied figures and tables must be referred in the text.
7. A maximum of 3 hierarchical levels of headings may be used in the text.
8. In the case of references in the text the parentheses are preferred, e.g. (Dubčák, 1987; Hrubý et al., 1988). The form “according to Dubčák (1987)” should be used only exceptionally.
9. We recommend submitting the manuscript with figures inserted in the text or at the end of the manuscript.
10. Valid SI units ought to be used in the text, preferably, e.g. s (second, not sec), m (metre), kg (kilogram). Where justified, other units used in the literature may be used and their equivalent in SI units may be given in brackets, e.g. 3 kbar (300 MPa or 0.3 GPa), 30 kt or 30 000 t ($3.10^7$ kg), 800 K (527 °C), 4.26 Å (4.26 . $10^{-10}$ m).
11. Only mineral names officially approved by the Commission for New Minerals and nomenclature approved by the International Mineralogical Association (CNMNC IMA) may be used in the text. A list of these (updated every two months) is available at https://cnmnc.units.it/ (IMA-CNMNC List of Mineral Names). Also, only recommended mineral abbreviations may be used (Updated list of IMA-CNMNC mineral symbols). If the authors have a chemical analysis of the mineral, its full valid name should be written, e.g. fluorapatite (not apatite), monazite-(Ce) (not monazite). Incomplete mineral names (e.g. apatite, monazite) may be used in the petrographic description of the rocks or the name of the method (e.g. monazite dating). The use of isomorphic mineral series names established in the geological literature (e.g. biotite, zinnwaldite, olivine) or mineral group names (e.g. garnets, tourmalines, amphiboles, spinels) is accepted. It is recommended to contact the Editorial Board in unclear cases.

### Figures and tables

1. The high-quality figures and tables can be published either in **maximum width of column (81 mm) or page (170 mm)**. The optimum size of letters and numbers in the printed figure is 2 mm. Manuscripts published in Slovak contain the Slovak descriptions in figures and tables, the tables headings and descriptions beneath figures and tables are in Slovak and English. English manuscripts contain all texts in English. **Maximum dimension of figures and tables in the journal is 170 x 230 mm. Larger (folded)** illustrations are published only exceptionally.
2. Illustrations including photographs must contain graphic (metric) scale, eventually the dimensions of visualized objects have to be stated in the describing text to figure. Maps and profiles must contain also the azimuth orientation; their unified explanations are stated at the first figure. Grouped figures, e.g. photographs and diagrams, are compiled as one figure with separate parts designated by letters (a, b, c, etc.).
3. **Illustrations, maps and photographs must be saved in JPG, PNG or TIFF formats with a resolution of at least 600 dpi, vector graphics in EPS, PDF, AI or COR formats**.

**The editors reserve the right to return illustrations to the author for correction after language editing, or to request their replacement with illustrations of the required quality.**

### References

The list of references used must include only published or accepted works. Single-authored works are listed alphabetically by the surname of the author of each work. For two authors, the works are listed alphabetically first by the surname of the first author, then by the surname of the co-author, and then chronologically. For more than two authors, the works are listed alphabetically only by the surname of the first author, then chronologically. If a publication has a DOI, it is always listed after the citation page number in the form https://doi.org/number.

### References examples:

***Book:*** Gazda, L. & Čech, M., 1988: Paleozoikum medzevského príkrovu [Paleozoic of the Medzev nappe]. Bratislava, Alfa, 155 pp.

***Journal:*** Hók, J. & Olšavský, M., 2023: Vernaricum – regional distribution, lithostratigraphy, tectonics and paleogeography. Mineralia Slovaca, 55, 1, 3 – 12. https://doi.org/10.56623/ms.2023.55.1.1.

***Proceedings contribution:*** Návesný, D., 1987: Vysokodraselné ryolity. In: Romanov, V. (ed.): Stratiformné ložiská gemerika [High-potassium rhyolites. In: Romanov, V. (ed.): Stratiform deposits of Gemericum]. Spec. publ. Košice, Slov. geol. soc., 203 – 215.

***Manuscript:*** Tulis, J. & Novotný, L., 1998: Zhodnotenie geologických prác na U rudy v mladšom paleozoiku hronika v severnej časti Nízkych Tatier a Kozích chrbtov. [Assessment of geological works on U ore in the Late Paleozoic of Hronicum in the northern part of the Nízke Tatry and Kozie chrbty Mts.] Manuscript. Bratislava, Archive of State Geological Institute of Dionýz Štúr (arch. no. 82752), 144 pp. (in Slovak).

**Ďalšie informácie / Further information:** mineralia.slovaca@geology.sk**;** ondrej.pelech@geology.sk

**Indexed / Abstracted / Accessed by SCOPUS, WEB OF SCIENCE and EBSCO**
Indexované / abstraktované / sprístupňované databázami SCOPUS, WEB OF SCIENCE a EBSCO

**www.geology.sk/mineralia**